The University Of Sheffield.

How does environmental variability drive macroecological patterns of diversity in marine and terrestrial systems?

Emma L. John

A thesis submitted in partial fulfilment of the requirements for the degree of Doctor of Philosophy

The University of Sheffield
Faculty of Science
Department of Animal and Plant Sciences

March 2020

Acknowledgements

Firstly, I would like to thank the University of Sheffield Department of Animal and Plant Sciences for 4 years of funding, support and opportunities.

I owe so many thanks to my PhD supervisors: Dr Tom Webb and Dr Beth Scott. Tom, thank you for your constant support, encouragement and for saying yes to every opportunity I wanted to take that had nothing to do with my PhD. Beth, that first week in Aberdeen changed the course of my PhD and I am eternally grateful for it. Thank you for your (immense!) knowledge, your feedback and for welcoming me so warmly into your lab group.

For their expert advice along the way I'd like to thank: Dr Jacqui Tweddle for all of the plankton knowledge; Dr Shaun Coutts and Dr Benjamin Williamson for making spectral frequency understandable to a biologist; Dr Peter Long and David Benz for their help with the terrestrial index methods; and Dr Robert Frouin and Dr Tom Jackson for their advice on remote sensing data.

My lab mates, both in Sheffield and Aberdeen, it's been a pleasure to go on this journey with you. A special shout out has to go to Hayley - 6 years later and we're still modelling! You were the best desk buddy, the best wine, fajitas and Attenborough buddy and I will always be in awe of your ggplot2 skills. To my best friends Amy and Christine. Amy, thank you for making sure that I didn't completely fall off the radar in the first couple of years, for being my European conference holiday buddy and for the many life chats. Christine, thank you for not minding that I fell off the radar in the first couple of years, for your invaluable statistics tutorials and for being my work club companion in the final straight. I love you both, I'm so proud of your achievements and I look forward to seeing where our Doctoring takes us.

To my parents, thank you for your continuous support throughout my university journey, for always being there for me and for helping me to move house more times than can ever be considered reasonable. I couldn't have done it without you!

Andy, thank you for seven years of love, support and belief in me. I am undoubtedly a better person for my time with you. Irene and David, thank you for welcoming me so lovingly into your family and for helping me to move to Nottingham. You are endlessly generous, and I have truly valued your support and kindness during this PhD process.

And finally, to Stack Overflow, without whom no biologist would ever realistically complete a coding-based PhD.

Abstract

The ability to withstand environmental variability is a key component of an ecosystem's stability, and with predictions of continued change in both the mean and variability of environmental conditions, it is of vital importance to understand how ecosystems respond to both existing and unexpected fluctuations in environmental variability. Marine and terrestrial ecosystems will not be affected by these changes in isolation; however, marine and terrestrial ecology are often treated as separate disciplines, slowing the progress of cross-realm research. In this thesis I aim to determine whether an explicit consideration of patterns of environmental variation, and species responses to these, can help to move beyond binary marine-terrestrial distinctions towards a more generalised formulation of ecological responses to environmental change, that hold across marine and terrestrial systems. I adopt a bottom-up approach, initially assessing the effects of environmental variability on primary productivity in marine systems by developing of a new index of marine primary productivity sensitivity relative to environmental variability, from which marine regions of low resilience can be identified (Chapter 2). I then combine this index with an existing index for the terrestrial realm to identify general trends in cross-realm sensitivity to variability (Chapter 3). I also investigate trends in marine and terrestrial community structure across trophic levels along gradients of primary productivity sensitivity to determine if the effects of environmental variability can be tracked through the food web, via changes in resource availability and predictability (Chapter 4). This approach provides a clear path from climate variability to primary productivity and on to higher trophic level species, while also bridging the marine-terrestrial divide. It is hoped that this work will provide a foundation for future cross-realm macroecological studies aimed at understanding the role of environmental variability in shaping ecosystems, and how this is likely to change with our changing climate.

Declaration

The following people were involved in this research project:

Emma L. John

Dr Tom J. Webb

Dr Beth E. Scott

Chapter 2: The Phytoplankton Sensitivity Index: Determining the sensitivity of marine primary productivity to environmental variability

ELJ conceived the idea for the study (with input from BES);

ELJ performed the analyses and wrote the manuscript;

TJW and BES commented on drafts of the manuscript.

Chapter 3: A global picture of sensitivity: Comparing the sensitivity of marine and terrestrial primary productivity to environmental variability

ELJ conceived the idea for the study (with input from TJW);

ELJ performed the analyses and wrote the manuscript;

TJW and BES commented on drafts of the manuscript.

Chapter 4: Temporal trends in Species Abundance Distributions: Comparing marine and terrestrial community structure along gradients of environmental variability

ELJ and TJW conceived the idea for the study;

ELJ performed the analyses and wrote the manuscript;

TJW and BES commented on drafts of the manuscript.

I, the author, confirm that the Thesis is my own work. I am aware of the University's Guidance on the Use of Unfair Means (www.sheffield.ac.uk/ssid/unfair-means). This work has not been previously been presented for an award at this, or any other, university.

Contents

List of Figures

List of Tables

“Wherein differ the sea and the land, that a miracle upon one

is not a miracle upon the other?”

–Melville, *Moby Dick*

1 General Introduction

1.1 The marine-terrestrial divide

Marine and terrestrial ecology have historically been treated as separate disciplines, being taught on separate degree programs, published in separate journals and presented at separate conferences (Chase, 2000; Menge et al., 2009; Rafaelli et al., 2005; Steele, 1991b; Stergiou and Browman, 2005). The separation between the disciplines has also caused the development of two languages and two approaches to what may be very similar topics (Rafaelli et al., 2005). Both marine and terrestrial ecology include the study of population dynamics, trophic structure, food webs and increasingly, responses to environmental change, however differences arise in how hypotheses are developed (Chase, 2000) and where the emphasis is placed on subsequent explanatory processes (Steele, 1991a; Stergiou and Browman, 2005). For example, in terrestrial ecology population structure and persistence are generally considered to be governed by internal dynamics such as predator-prey interactions and density dependence (Steele, 1985, 1991a), whereas in the marine realm the focus is placed on the external dynamics of long-term environmental control, due to tighter coupling between the scales of physical and biological processes (Steele, 1985; Steele and Henderson, 1994; Section 1.1.1).

This separation between the disciplines has occurred due to the existence of 'fundamental differences' between the realms stemming from a water versus air-based medium. In the first instance the majority of marine animals have a 3D environment available to them, compared to a 2D environment for all land animals except birds and a small number of mammals. On top of this, the different viscosities of water versus air (Dawson and Hamner, 2008) and the relative openness of the marine realm (Paine, 2005; Rafaelli *et al.*, 2005) results in large disparities between the realms ranging from dispersal distances to locomotory strategies. Differences are also apparent in the structuring of marine and terrestrial ecosystems. In the marine realm body size and life span typically increase linearly with trophic level from producers to predators (Steele, 1991b) and species can fill multiple trophic levels throughout their lifespan, resulting in size-structured populations (Trebilco *et al.*, 2013). The relationship between the size and lifespan of organisms with trophic level in the terrestrial realm is more complex (Steele, 1991b), as plants and herbivores are typically the longest lived and largest species and both herbivores and predators can cover a large range of sizes and life spans. Terrestrial species however tend to remain within the same trophic level throughout life, resulting in population

structure being classified by trophic level (Trebilco *et al.*, 2013). The existence of these fundamental differences has consistently been viewed as a barrier to comparative study, impeding the advancement of cross-realm communication and integration (Steele, 1991a; Stergiou and Browman, 2005).

1.1.1 John Steele and the importance of scale

In 1985 John Steele published the first of a series of papers examining the differences between the marine and terrestrial realms and advocating the need for increased integration of the disciplines. In his seminal paper, Steele (1985) highlighted the different temporal scales of environmental variance experienced in each realm as a result of a water versus air based medium. In the marine realm, short-term variability is buffered by the thermal capacity of the ocean, and large patterns of ocean circulation are semi-predictable due to the fixed boundaries of landmasses, resulting in environmental variance that increases with the length of time examined (Steele, 1985; Steele *et al.*, 2019). The terrestrial realm on the other hand experiences high environmental variance that remains constant from days to decades due to the lack of barriers to atmospheric circulation (Steele, 1985; Steele *et al.*, 2019). This difference can be better described in terms of the temporal autocorrelation structure of variability and its subsequent position on the colour spectrum (Halley, 1996; Keshner, 1982). The increased environmental predictability and dampened short-term variability exhibited in the marine realm displays positive temporal autocorrelation, where subsequent time points are more correlated within a time series (Rohani, 2004), and is reflective of reddened spectra or 'red noise' on the colour spectrum (Steele, 1985). 'White noise' represents environmental time series that are temporally uncorrelated and highly variable at both short and long temporal scales (Halley, 1996; Rohani, 2004), characteristic of the constant high-frequency variance exhibited in the terrestrial realm (Steele, 1985).

The distinction between marine and terrestrial environments of red and white noise respectively is not a strict dichotomy however, as across coastal areas and in large freshwater bodies a white-red gradient from terrestrial-aquatic environments often occurs (Cyr and Cyr, 2003; Vasseur and Yodzis, 2004) and both realms exhibit flatter spectra at temperate latitudes compared to in polar and equatorial regions (Vasseur and Yodzis, 2004). Recent research also suggests that short term variability in the marine realm driven by local 'weather' rather than large-scale 'climate' is considerably higher than previously thought (Bates *et al.*, 2018). The red-white contrast in spectral colour across realms is predominantly exhibited in abiotic variables (Weber and Talkner, 2001), however population density time series that are usually reddened (Petchey, 2000; Pimm and Redfearn, 1988) have also been shown to differ between

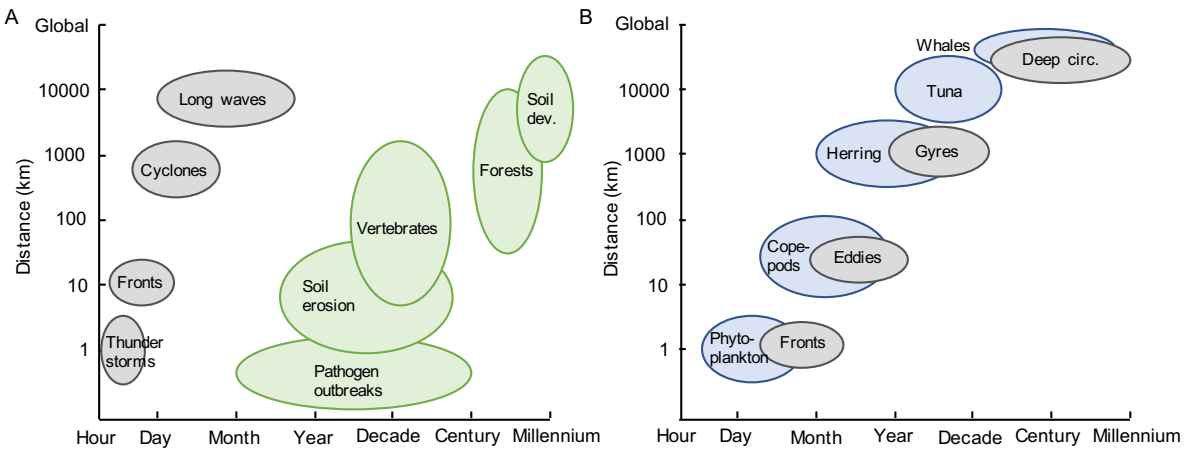

Figure 1.1: Differences in the temporal and spatial scales of the marine and terrestrial realm. Plots showing differences in the temporal and spatial scales of physical and biological processes in the terrestrial (A) and marine (B) realm. Physical processes in the terrestrial realm cover a smaller temporal scale but larger spatial scale than marine equivalents and are uncoupled from biological processes (A). In the marine realm physical and ecological processes are closely coupled due to the long temporal scale of physical processes (B). Adapted from Steele (1991b).

marine and terrestrial environments (Ariño and Pimm, 1995; Steele, 1985). Steele (1985) accurately predicted that these differences in the temporal scales of variability structure would likely lead to different adaptations, with marine and terrestrial populations adapted to long versus short-term environmental variability respectively (Section 1.2.1).

In further papers Steele detailed important differences in both the temporal and spatial scales of physical and biological processes in each realm (Steele, 1991a, 1991b; Steele and Henderson, 1994). For example, the slower transfer of heat and energy in large water bodies results in physical processes such as eddies lasting considerably longer in the marine realm compared to their terrestrial counterparts - for years compared to days (Steele, 1991b). Spatially however, they cover an area an order of magnitude smaller (Figure 1.1; Steele, 1991b). This results in physical and biological processes being tightly coupled in the marine realm due to the large temporal scales of physical processes overlapping with ecological processes (Figure 1.1B; Steele, 1991b; Steele and Henderson, 1994), whereby each life stage of a marine organism can be reliant on a different physical ocean process (Steele, 1991b). In the terrestrial realm, ecological processes have a longer temporal scale and are completely separated from atmospheric processes (Figure 1.1A). It is this disparity in physical and biological coupling which has led to the temporal dynamics of marine populations being attributed to external control compared to internal dynamics in terrestrial systems (Steele and Henderson, 1994).

Considerable differences thus clearly do exist between the marine and terrestrial realms which at times will necessitate a realm-specific approach (Carr *et al.*, 2003), however Steele

maintained that this should not be necessary in all contexts and criticised the restrictive criteria typically imposed in comparative studies which reinforced or did not account for differences in scale, making comparisons unviable (Steele, 1985). Steele argued that differences in scale proved problematic when comparisons were attempted at the same scale in each realm (Steele, 1985, 1991a, 1991b), however if realm-specific spatial and temporal scales were employed then cross-realm comparisons would be possible and could provide more rigorous testing of ecological hypotheses, revealing generalised patterns that hold across realms.

1.1.2 Progress since Steele - Bridging the divide

In the decades since Steele's initial publication, an increasing number of comparative studies have been conducted and cross-fertilisation of ideas is increasing (Webb, 2012). New insights have been gained from examining similar species found in contrasting environmental settings, for example in marine versus terrestrial vertebrate carnivores (Tamburello *et al.*, 2015) and propagule dispersal in macroalgae versus angiosperms (Kinlan and Gaines, 2003); in different species occurring in similar environmental settings such as benthic versus soil ecosystems (Dawson, 2009; Dawson and Hamner, 2008); and by grouping functionally analogous species for comparison irrespective of environment such as cross-realm predator-prey biomass relationships (Cebrian, 2015; Hatton *et al.*, 2015). Reviews of the impacts of large-scale climate patterns now regularly include a cross realm approach (e.g. Ottersen *et al.*, 2001; Stenseth *et al.*, 2002, 2003; Section 1.2) and Dawson and Hamner (2008) have shown that when viewed from a biophysical perspective, both water and air can be quantitatively analysed via fluid dynamics revealing cross-realm differences that are statistical rather than fundamental. Whilst these advances show a promising move in the right direction for the integration of marine and terrestrial ecology, the idea of fundamental differences between the realms has persisted and it has been suggested that some studies are still plagued by a terrestrially oriented viewpoint (Dawson and Hamner, 2008). A special journal issue dedicated to the progress made since Steele concluded that whilst communication has improved, barriers are still in place (Stergiou and Browman, 2005). It is worth noting that this special issue was published in a specialised marine journal. The global scope of the threat of climate change makes the remaining separation increasingly disadvantageous, and the need to determine how both realms will respond to the growing pressures of a changing climate has resulted in an increasing number of studies beginning to explore the benefits of a cross-realm approach to ecology (e.g. Blowes *et al.*, 2019; Burrows *et al.*, 2011; Parmesan and Yohe, 2003; Pinsky *et al.*, 2019; Sunday *et al.*, 2012; Wiens, 2016).

1.2 Life under environmental variability

Confirming Steele's hypothesis regarding appropriate scales for comparison, at long temporal scales coupling between physical and biological processes occurs in both realms (Steele, 1991a) and several large-scale patterns of climate variability such as the El Niño Southern Oscillation (ENSO; Philander, 1990) and the North Atlantic Oscillation (NAO) are now known to have wide-ranging influences across the marine and terrestrial realms (Ottersen *et al.*, 2001; Stenseth *et al.*, 2002, 2003). Through their governance of micro-scale weather conditions these large-scale patterns of climate variability influence the physical and biological processes controlling the phenology, composition, abundance and distribution of organisms across trophic levels in freshwater, terrestrial and marine ecosystems (Blenckner and Hillebrand, 2002; Drinkwater *et al.*, 2003; Henson *et al.*, 2012; Mysterud *et al.*, 2003; Ottersen *et al.*, 2001; Stenseth *et al.*, 2003). For example, NAO-driven warming of sea surface and air temperatures has lengthened the growing season for both phytoplankton (Racault *et al.*, 2012; Reid *et al.*, 1998) and terrestrial plants (Myneni *et al.*, 1997); sea surface temperature (SST) in the Pacific driven by ENSO is a more accurate predictor of maize yield in Africa than terrestrial rainfall (Cane *et al.*, 1994); differences between ENSO warm El Niño and cold La Niña periods can switch the Humboldt Current Eastern Boundary Upwelling System (EBUS) from a sardine to an anchovy dominated ecosystem (Alheit and Niquen, 2004); and North Atlantic SST driven by the Atlantic Multi-decadal Oscillation (AMO) has been correlated with variability in the Indian summer monsoon (Goswami *et al.*, 2006) and precipitation across the majority of the United States, with subsequent effects on river flows (Enfield *et al.*, 2001) and nutrient inputs in coastal areas (Goberville *et al.*, 2010; Harley *et al.*, 2006). Thus, despite emphasis on the role of internal processes in determining terrestrial population dynamics (Section 1.1.1), the role of patterns such as the NAO in the terrestrial realm are now readily accepted (e.g. Blenckner and Hillebrand, 2002; Hurrell and Deser, 2010; Mysterud *et al.*, 2003; Stenseth *et al.*, 2002).

1.2.1 Sensitivity to variability

Despite cross-realm linkages in large scale patterns of variability, the different physical structure of marine and terrestrial environments results in contrasting levels of environmental variability manifesting in each realm (Steele, 1985; Section 1.1.1). As well as determining physical conditions, environmental variability interacts with demographic processes to influence life history traits (Dawson and Hamner, 2008), population dynamics (García-Carreras and Reuman, 2011; Ruokolainen *et al.*, 2009) and extinction risk (Heino and Sabadell, 2003; Mustin *et al.*, 2013; Ripa and Lundberg, 1996; Ruokolainen and Fowler, 2008). Reddened environments are more likely to favour specialist species (Righetti *et al.*, 2019) with persistence

or ‘slow’ life history traits such as late maturity, suited to long runs of predictable conditions (Kindsvater *et al.*, 2016), whereas generalist species are favoured in white environments with greater stochasticity (Righetti *et al.*, 2019; Suryan *et al.*, 2009). These adaptations to variability influence an ecosystem’s ability to withstand anomalous climate fluctuations. The Climatic Variability Hypothesis (Stevens, 1989) demonstrates that populations living in more variable environments have wider environmental tolerances, and combined with being generalists, are more able to absorb fluctuating environmental conditions (Holling, 1973). Species in stable, reddened environments, on the other hand, are typically less well adapted to fluctuating environmental conditions and are less able to absorb climate anomalies (Holling, 1973; Pintor *et al.*, 2015). Furthermore, long runs of poor environmental conditions are more likely to occur with reddened environmental variability, which - combined with specialist species with reduced adaptability - can put populations at risk of extinction (Dawson and Hamner, 2008; Mustin *et al.*, 2013).

The ability to withstand environmental variability is a key component of an ecosystem’s stability (Harrison, 1979a) and with predictions of continued change in both the mean and variability of environmental conditions (Section 1.2.2), it is of vital importance to understand how ecosystems respond to both existing variability and unexpected fluctuations in their governing environmental conditions (Easterling *et al.*, 2000; Harrison, 1979a; Ma *et al.*, 2015). An ecosystem’s ability to persist in its current state in the face of external pressure is a marker of both its resilience and resistance to stress events (Harrison, 1979a; Holling, 1973; Seddon *et al.*, 2016; Webster *et al.*, 1975). Resistance is typically defined in terms of a population or ecosystem’s immediate response to a stress event, with a resistant population showing smaller fluctuations in size and avoiding displacement. Resilience on the other hand is a population or ecosystem’s ability to return to its pre-impact state after the stress period has passed (Webster *et al.*, 1975). ‘Sensitivity’ encapsulates this combination of resistance and resilience and provides a measure of ecosystem health and stability relative to the magnitude of a stress event (Seddon *et al.*, 2016). Healthy ecosystems with high resistance and/or high resilience and therefore low sensitivity, are able to persist for long periods of time in the face of environmental variability, expected or otherwise, by either exhibiting minimal perturbation and absorbing the impact in the first instance (resistance) or by quickly returning to normal post-event (resilience; Holling, 1973). However, many of the world’s ecosystems are currently degraded from decades of anthropogenic exploitation and pollution (Halpern *et al.*, 2008) and are now facing a barrage of new pressures from a changing climate. Increasing pressure on already degraded ecosystems progressively reduces their resilience so that when an unexpected event such as a climate anomaly occurs, their resiliency limits are passed, resulting in a rapid change to a new ecosystem state (Beaugrand *et al.*, 2008; Holling, 1973).

Amplified responses and slowed recovery rates in populations to unexpected climate events are indicative of an ecosystem having low resistance and resilience and being highly sensitive to environmental variability (Scheffer *et al.*, 2009; Smith, 2011a).

1.2.2 Climate change and variability

Environmental variability (IPCC, 2019; Jentsch *et al.*, 2007) and extreme environmental events (Easterling *et al.*, 2000; Ma *et al.*, 2015; Vasseur *et al.*, 2014) are predicted to increase with climate change, with the potential for wide-ranging ecological impacts which are currently far less well understood than responses to changes in mean environmental conditions (Sydeman *et al.*, 2013; Thornton *et al.*, 2014). Evidence already suggests that El Niño years are increasing in frequency (becoming less red; Power *et al.*, 2013) whilst Northern Hemisphere weather systems are experiencing longer 'stalled periods' of the same weather pattern (becoming more reddened), increasing the likelihood of persistent heat and associated extreme weather events (Mann *et al.*, 2017). The Northern Hemisphere has so far experienced the fastest rates of warming in the last century (IPCC, 2007), however it is the Southern Hemisphere and low latitude tropical regions that are predicted to be first affected by weather extremes and increased variability (Beaumont *et al.*, 2011; Diffenbaugh and Giorgi, 2012). The predicted expansion of Hadley cells, which govern sub-tropical atmospheric circulation and winds, could see poleward shifts in both upwelling location and intensity in EBUS (Bakun *et al.*, 2015; Kang and Lu, 2012; Lu *et al.*, 2007; Rykaczewski *et al.*, 2015) causing poleward shifts in primary productivity due to the change in distribution of upwelled nutrients (Thomas *et al.*, 2012), and further desertification of subtropical areas through increasing inland temperatures (Lu *et al.*, 2007). Increased pressure gradients resulting from higher inland temperatures could also cause lateral transfers in marine productivity from increased offshore advection (Bakun *et al.*, 2015). These predicted geographical shifts in marine productivity could result in substantial changes to resource availability with reductions in the tropics and increases at higher latitudes, which combined with changes to inland precipitation (Enfield *et al.*, 2001) could have consequences for coastal ecosystems in both realms. Marine ecosystems subsidise coastal terrestrial environments with particulate matter, detritus and living plant and animal biomass (Heck *et al.*, 2008) and can contribute more energy and biomass to the system than terrestrial primary production (Polis and Hurd, 1996), whilst terrestrial precipitation governs the horizontal transfer of nutrients and freshwater into coastal marine environments through its effects on river flow and run-off (Enfield *et al.*, 2001; Goberville *et al.*, 2010; Harley *et al.*, 2006).

Given the scope of influence of environmental variability on both physical and biological ecosystem processes, considerable concern exists about the ecosystem impacts of it altering with climate change (Easterling *et al.*, 2000; García-Carreras and Reuman, 2011; Wigley *et al.*, 1998). Species responses to environmental variability can vary markedly (Morris *et al.*, 2008; Stenseth *et al.*, 2002; Vasseur *et al.*, 2014) both across space (von Holle *et al.*, 2010) and trophic level (Durant *et al.*, 2007; Thackeray *et al.*, 2010, 2016), and population responses to global change are not guaranteed to be consistent or occur at the same rate across realms (Blowes *et al.*, 2019; Pinsky *et al.*, 2019). This extensive spatial variation in responses to environmental variability makes it necessary to account for the current bias in climate change studies to date focussing largely on temperature effects in northern, temperate latitudes (Harley *et al.*, 2006; Pearce-Higgins *et al.*, 2015). Furthermore, as anomalous environmental conditions could be expected to elicit different responses in marine and terrestrial ecosystems (Section 1.2.1), comparative studies of the responses of organisms to different regimes of environmental variability will be necessary to determine whether general responses to climate change are likely. To date, estimating spectral colour for environmental variables explicitly linked to biotic data using empirical rather than modelled data has rarely been attempted (García-Carreras and Reuman, 2011; Gilljam *et al.*, 2019). Identifying ecosystems in both marine and terrestrial realms exhibiting amplified responses to climate anomalies within the context of their underlying variability structure could therefore help to assess which regions are most at risk from a changing environmental variability regime (Smith, 2011a).

1.3 Is macroecology the answer?

First defined by Brown and Maurer (1989), macroecology identifies statistical relationships between organisms and their environment at large spatial and temporal scales, to reveal generalised patterns explaining the distribution, abundance and diversity of species. The unifying potential of macroecology for marine and terrestrial research was identified by Steele (1991b), who proposed that looking at a macro scale could overcome the challenges posed by the different temporal and spatial scales encountered in marine and terrestrial systems. This is due to the relative simplicity of phenomena which are emergent at large scales compared to the complexity when looking at a community ecology level (Lawton, 1999), resulting in the most general ecological patterns and most fundamental differences becoming apparent in the abiotic and biotic features of marine and terrestrial data at macroecological scales (Dawson and Hamner, 2008; Lawton, 1999; Rafaelli *et al.*, 2005; Webb, 2012). Whilst originally a terrestrially dominated discipline (Rafaelli *et al.*, 2005), increases in marine data availability (Section 1.3.2) have led to a number of classical macroecological patterns being

demonstrated across realms. For example, species abundance distributions (SADs; Gray *et al.*, 2006; Webb, 2012), species-range size relationships (Gaston, 2003), species-area relationships (SAR; Drakare *et al.*, 2006) and latitudinal diversity gradients (Fisher *et al.*, 2010; Hillebrand, 2004) all exhibit similar patterns in both realms. A macroecological approach has also revealed parallels in predator-prey scaling laws in each realm (Cebrian, 2015; Hatton *et al.*, 2015) and instances of realm-independent explanatory processes, for example variation in species' home range size is better explained by shared life history traits than by realm (Tamburello *et al.*, 2015). Differences have also been demonstrated between the realms at a macroecological scale, for example Horne *et al.* (2015) showed that size clines along latitudinal gradients were the opposite in each realm with oxygen being the main limiting factor in the marine realm compared to voltinism (the number of broods produced per year) in terrestrial systems.

1.3.1 A dynamic macroecology for climate change

A macroecological approach has proven to be a useful tool in identifying similarities and differences in the organisational structure of cross-realm environments, however this simplicity of approach can make it difficult to infer the underlying processes behind observed patterns. To further improve the utility of macroecological patterns, a more dynamic, mechanistic approach to macroecology is developing to increase understanding of the underlying processes driving patterns of diversity (Connolly *et al.*, 2017; McGill and Potochnik, 2018), with temporal and spatial data implicitly included in analyses and patterns integrated within ecological frameworks (Beck *et al.*, 2012; Brown and Maurer, 1989; Fisher *et al.*, 2010; McGill, 2010b; McGill *et al.*, 2007; Tyler *et al.*, 2012; Webb, 2012). Climate change presents several opportunities to further develop this new approach to macroecology, as the different scenarios predicted to occur under climate change provide the opportunity for pseudo-experimental testing of macroecological hypotheses (Kerr *et al.*, 2007). Comparative cross-realm analyses will also provide more thorough and novel opportunities to test new and existing hypotheses (Steele, 1985; Webb, 2012). It will also be important to understand and incorporate the influence local processes can have on large scale patterns (Kissling *et al.*, 2010) of climate variability, particularly as some links between the environment and ecology only become apparent at large scales (Webb, 2009).

This improved, process driven macroecology will be invaluable for predicting global responses to climate change (Kerr *et al.*, 2007). The prevalence of cross-realm climatic linkages (Section 1.2) makes it reasonable to assume that variability in macro-scale patterns of climate will affect marine and terrestrial realms in tandem, however the existence of cross-realm

macroecological patterns does not necessarily signify shared causal mechanisms (Webb, 2012) or shared responses to change. Determining whether there are corresponding mechanisms driving patterns and their responses across realms will greatly enhance our ability to predict future change (Fisher *et al.*, 2010). A global, macroecological approach has already been used to reveal differences in the pace of climate change across realms and subsequent effects on species distributions (Burrows *et al.*, 2011, 2014), and to show that the signal of large climate patterns can successfully be detected in changes in macro patterns of species diversity (Fisher *et al.*, 2008). Considering the spatial and temporal scales of environmental variation is another potentially useful way of unifying climate focussed studies across realms, with tighter coupling between physical and biological scales expected in more oceanic compared to more terrestrial systems (Steele, 1991a, 1991b). With increasing levels of change occurring in natural systems reliable measures for effective unification, monitoring and prediction are needed, however environmental variability has yet to be formally incorporated into a macroecological approach that can be used to predict patterns of change and is applicable both across trophic levels and realms.

1.3.2 Data availability for macroecology

Recent advances in remote sensing technologies (Section 1.3.2.1) and the collection, compilation and storage capacity of large-scale ecological data (Section 1.3.2.2) have greatly enhanced the ability to conduct cross-realm macroecological comparisons, and the importance of big data to the future of macroecology in both realms is now widely acknowledged (Beck *et al.*, 2012; Edgar *et al.*, 2016; Keith *et al.*, 2012; Kerr *et al.*, 2007).

1.3.2.1 Remote sensing

Despite being available for over 40 years, remote sensing data has only recently become widely used in studies of ecological change due to previous difficulties in combining datasets recorded by satellites with differing technological capabilities and a lack of clear understanding in, or availability of, their associated uncertainties (Hollmann *et al.*, 2013). Progress on this front has been aided by the designation of essential climate variables (ECVs) by the Global Climate Observing System (GCOS; GCOS, 2010). ECVs, specified for atmospheric, marine and terrestrial systems and covering physical, biological and chemical components, are variables considered essential for monitoring and predicting the impacts of climate change (Bojinski *et al.*, 2014). In response to these designations, agencies around the world have set up initiatives both to collect new satellite data and to synthesise existing data for these variables into single, homogenised datasets. For example, the European Space Agency's (ESA) Climate Change Initiative (CCI) aims to produce easily accessible datasets for 13 ECVs

in collaboration with user needs (Hollmann *et al.*, 2013; Plummer *et al.*, 2017). Crucially these datasets are made freely available, often at a range of processing levels, spatial resolutions and geographic projections to suit the different needs and skillsets of physical versus biological modellers, making the data more accessible to ecologists who may be unused to working with satellite derived data. As a result of these projects we now have ~30 years of consistent, high resolution datasets covering large spatial scales, which can be used to further the identification of macroecological trends of climate impacts.

Remote sensing has proven particularly useful for mapping global primary productivity. In the marine realm both ocean colour (surface chlorophyll-a (Chl-a)) and physical variables necessary for primary productivity (e.g. sea surface temperature) are designated ECVs (Bojinski *et al.*, 2014), ensuring the continued collection and synthesis of new data products such as the ESA's Ocean Colour Climate Change Initiative (OC-CCI; Jackson *et al.*, 2017; Lavender *et al.*, 2015). Remotely sensed measurements of ocean colour provide temporally and spatially explicit measures of Chl-a concentration and have become a common proxy for marine photosynthetic biomass (Blondeau-Patissier *et al.*, 2014; Cullen, 1982; Hirata *et al.*, 2012; McClain, 2009; Sathyendranath and Platt, 1997), expanding the scope of studies beyond the limited availability of physical phytoplankton distribution and abundance data (Hays *et al.*, 2005). Whilst there are too many examples to provide an exhaustive list, satellite derived primary productivity data in the marine realm has been used to determine: decadal trends in Chl-a concentration (Beaulieu *et al.*, 2013; Gregg and Rousseaux, 2014; Marrari *et al.*, 2017); climate impacts on phytoplankton composition (Rousseaux and Gregg 2012; Rousseaux and Gregg 2015) and phenology (Cabré *et al.*, 2016; Friedland *et al.*, 2018; González Taboada and Anadón, 2014; Henson *et al.*, 2013; Racault *et al.*, 2012, 2017); driving mechanisms of phytoplankton variability (Nieto and Mélin, 2017a; Signorini *et al.*, 2015); and signals of climate change (Henson *et al.*, 2010). For terrestrial primary productivity there are two measures related to productivity designated as ECVs (Leaf Area Index and Above-ground biomass; Bojinski *et al.*, 2014), however the most similar in scale and simplicity to ocean colour is the Enhanced Vegetation Index (EVI; Solano *et al.*, 2010) which measures global vegetation canopy 'greenness'. As with marine primary productivity, these datasets have been used to examine large scale trends in terrestrial primary productivity in relation to climate (e.g. Holmgren *et al.*, 2013; Nemani *et al.*, 2003).

Advances in remote sensing have also led to the development of more detailed, nested spatial delineations of the marine and terrestrial realms with both static boundaries, such as Longhurst's biogeographic regions (Longhurst, 1995a, 2007; Sathyendranath *et al.*, 1995), the Pelagic Provinces of the World (Spalding *et al.*, 2012), Marine Ecoregions of the World

(Spalding *et al.*, 2007) and Ecoregions2017 (Dinerstein *et al.*, 2017), and dynamic boundaries accounting for seasonal variation (Reygondeau *et al.*, 2013), all of which better enable hypothesis testing of macroecological patterns at a range of spatial scales.

1.3.2.2 Biological data repositories

As well as advances in remote sensing data, macroecology is also benefiting from the development of large open access database compilations for empirically collected biological data (Edgar *et al.*, 2016). These include the BioTIME database (Dornelas *et al.*, 2014, 2018) for assemblage time series of cross-realm species abundances, the Global Biodiversity Information Facility (GBIF; https://www.gbif.org) for global species observation records, the Ocean Biogeographical Observation System (OBIS; https://www.obis.org) for global ocean biodiversity observations and the COMADRE (Salguero-Gómez *et al.*, 2016) and COMPADRE (Salguero-Gómez *et al.*, 2015) animal and plant matrix population model databases. These databases do require consideration in terms of the different methodologies employed in the individual studies and whether standardisation is required, and the data within them can also be messy and unstructured data (Edgar *et al.*, 2016). Nevertheless, they provide an invaluable resource of temporal, georeferenced records which can be integrated with satellite data for climate variables to investigate global trends across trophic levels. Satellite tagging also provides another important resource of georeferenced species data, particularly for migratory species, and has been used to produce striking records of large-scale species distributions (e.g. Harrison *et al.*, 2018).

1.4 Sensitivity in primary productivity as a unifying approach

Primary productivity provides an ideal foundation for cross-realm macroecological analysis as it can be directly associated with both environmental drivers (e.g. Hays *et al.*, 1993) and higher trophic level responses (e.g. Visser and Holleman, 2001), due to the dependence of primary producers on abiotic forcing and their essential role at the base of marine and terrestrial food webs. Similarities in cross-realm primary productivity responses to environmental change have already been demonstrated for phenology (Section 1.2; Chambers *et al.*, 2013; Parmesan and Yohe, 2003; Root *et al.*, 2003; Thackeray *et al.*, 2010), with warming temperatures causing earlier leaf emergence, flower blooming and lengthened growing seasons in terrestrial systems (Mysterud *et al.*, 2003; Post and Stenseth, 1999), comparable to earlier bloom times observed in marine phytoplankton (Edwards and Richardson, 2004a). Furthermore, whilst terrestrial primary producers are typically not as closely coupled to scales of environmental variability as marine producers (Section 1.1.1; Steele, 1991b), their responses to environmental variation

are similarly variable across space (von Holle *et al.*, 2010) and trophic level (Durant *et al.*, 2007; Thackeray *et al.*, 2010, 2016) as in marine systems, with trophic mismatch and wider ecosystem consequences an inevitable result (Durant *et al.*, 2005; Stenseth and Mysterud, 2002; Toszogyova and Storch, 2019; Visser and Holleman, 2001). Environmental variability can also modify global gradients of primary producer diversity and richness (Righetti *et al.*, 2019) and differentially effect higher trophic level patterns of richness depending on the mean productivity of an area, with high variability and high mean productivity associated with reductions in richness (Toszogyova and Storch, 2019). As a result, primary resource availability and predictability can act as both an explanatory and predictive mechanism for population responses to environmental change.

1.4.1 A Vegetation Sensitivity Index for the terrestrial realm

The publication of a global Vegetation Sensitivity Index (VSI) for terrestrial primary productivity (Seddon *et al.*, 2016) has opened up new avenues for macroecological examinations of environmental variability impacts. Using remote sensing data for canopy greenness and driving climate variables of productivity, Seddon *et al.* (2016) determined the sensitivity of global terrestrial primary productivity relative to variability in temperature, precipitation and cloud cover over a 14-year time series (2000-2013) at high spatial resolution (5 km). By coupling terrestrial primary productivity directly with abiotic variables Seddon *et al.* (2016) identified specific regions and ecosystems in which primary productivity is especially sensitive to current environmental variability (Figure 1.2), whereby high sensitivity indicates an amplified response in primary productivity relative to environmental variability, indicative of an ecosystem having low resilience (Scheffer *et al.*, 2009; Smith, 2011a). The index also makes it possible to extract the contribution each climate variable makes towards driving sensitivity in any given pixel (Figure 1.3). The VSI therefore provides crucial guidance on where wider ecosystem impacts are likely to occur, both now and in the future, as a result of changes in resource availability and predictability due to a changing environmental variability regime, thus focussing future research efforts.

1.4.2 A Phytoplankton Sensitivity Index for the marine realm

Marine phytoplankton are the dominant primary producers of the oceans and are likely to be the first indicators of a marine ecosystem's changing sensitivity to environmental variability (Dutkiewicz *et al.*, 2019; Hays *et al.*, 2005; Taylor *et al.*, 2002). With rapid life cycles, population growth rates and almost exclusive abiotic control (Hays *et al.*, 2005; Racault *et al.*, 2017; Taylor

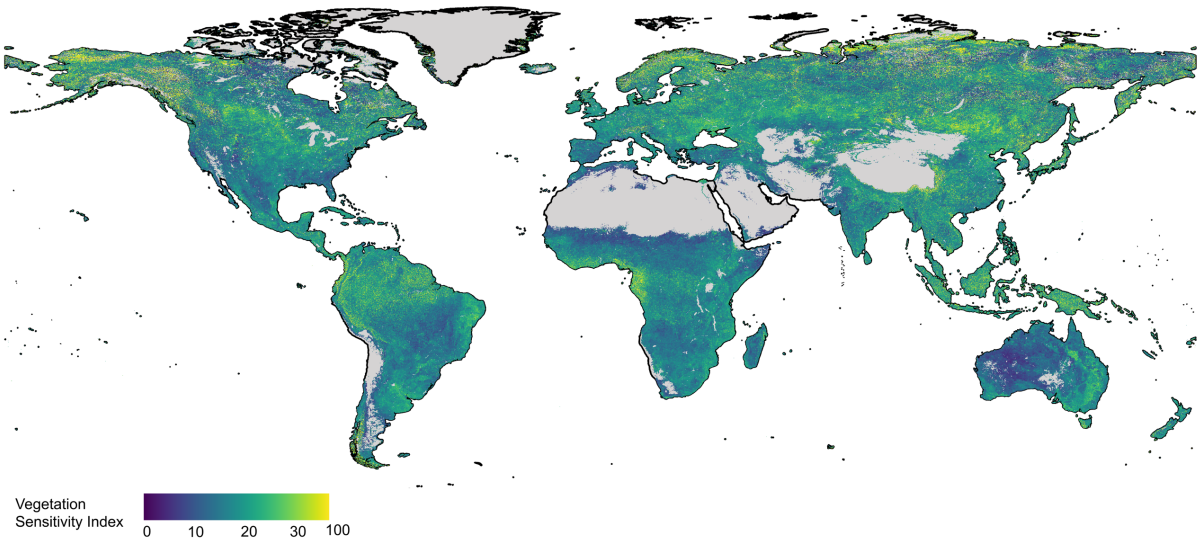

Figure 1.2: Vegetation Sensitivity Index. A global map of terrestrial primary productivity sensitivity relative to variability in temperature, precipitation and cloud cover. The index ranges from 0 (low sensitivity) to 100 (high sensitivity). Due to right skew in the data and the volume of data points, the colour scale has been band shifted by 2.5 standard deviations (the default in ArcGIS) to better reflect the spread of the data. Pixel resolution, 5 km; time period, 2000-2013. Continental outlines were modified from a shapefile using QGIS. Raw data and code to produce the figure were sourced from Seddon *et al.* (2016).

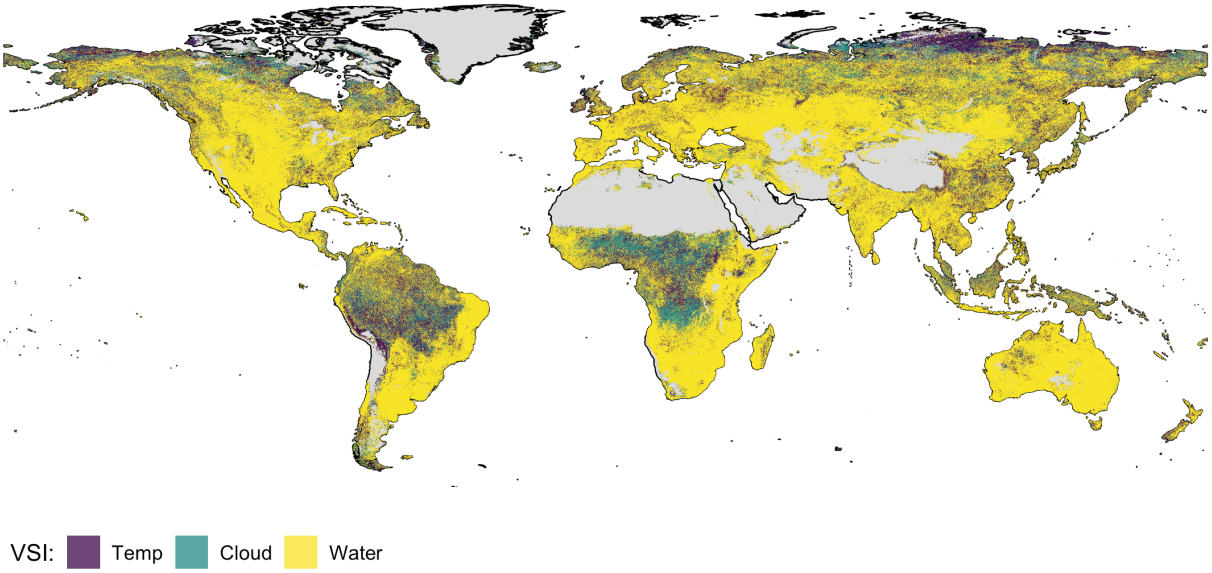

Figure 1.3: Composite map of the Vegetation Sensitivity Index. Composite map of the contribution of climatic driver variability to the VSI, showing which climate variable has the highest influence on sensitivity in a given pixel (temperature (blue), cloud cover (green) and precipitation (yellow)). Pixel resolution, 5 km; time period, 2000-2013. Continental outlines were modified from a shapefile using QGIS. Raw data and code to produce the figure were sourced from Seddon *et al.* (2016).

et al., 2002), both the abundance, phenology and global distribution of phytoplankton can be attributed to variability in environmental parameters and particularly to temperature and wind (Botsford *et al.*, 2006; Drinkwater *et al.*, 2003; Falkowski and Oliver, 2007; González Taboada and Anadón, 2014; Kahru *et al.*, 2010; Raitsos *et al.*, 2006; Righetti *et al.*, 2019; Yokomizo *et al.*, 2010). By acting in synergy to control stratification of the water column, the upwelling of nutrients, and the position and strength of major surface currents in the ocean, these abiotic variables determine the occurrence of suitable oceanic conditions, light and nutrient availability necessary for phytoplankton growth (Hays *et al.*, 2005; Hinder *et al.*, 2012; Kahru *et al.*, 2010). Phytoplankton blooms support the vast majority of marine food webs and due to tight trophic coupling in the marine realm (Steele, 1991b) the effects of variability in phytoplankton biomass can quickly propagate up the food web via trophic amplification (Henson *et al.*, 2009; Kirby and Beaugrand, 2009; Poloczanska *et al.*, 2016; Stock *et al.*, 2014), with potential impacts for ecosystem structure and composition (Beaugrand, 2009; Edwards and Richardson, 2004a; Harley *et al.*, 2006; Richardson and Schoeman, 2004) and higher trophic level recruitment (Beaugrand *et al.*, 2003; Cushing, 1990; Hjort, 1914; Platt *et al.*, 2003). In extreme cases producers are predicted to be the first to go extinct in response to changes in environmental variability: phytoplankton are particularly susceptible to temperature variability (Burgmer and Hillebrand, 2011), which has the potential to trigger bottom-up extinction cascades within food-webs (Kaneryd *et al.*, 2012). Species rich ecosystems are particularly at risk where high inter-specific competition results in lower mean phytoplankton population densities (Borrvall and Ebenman, 2008a; Kaneryd *et al.*, 2012). The effects of environmental variability throughout marine systems will therefore largely be mediated via phytoplankton responses (Hays *et al.*, 2005).

Despite the importance of environmental variability as a driver of marine primary productivity and the ecological implications of it altering with climate change, a corresponding global index to the VSI of marine primary productivity sensitivity to environmental variability has yet to be derived. Obtaining a spatially resolved, global picture of phytoplankton responses to climate variability is particularly important to understand the full scope of marine responses to climate change at broad scales, as phytoplankton responses to changes in average climatic conditions are known to vary considerably across ecosystems, preventing extrapolation across regions (Häder *et al.*, 2014). Global declines in marine primary productivity levels have also been recorded in recent decades (Capuzzo *et al.*, 2018; Edwards *et al.*, 2020; Gregg and Rousseaux, 2014, 2019; Roxy *et al.*, 2016) and global gradients of marine primary producer diversity and richness can be modified by environmental variability (Righetti *et al.*, 2019). A Phytoplankton Sensitivity Index (PSI) would provide a base layer from which the resilience of marine ecosystems to current environmental variability at the primary production level could

be determined, along with the specific climate elements responsible. This in turn could be used to predict future responses to global change, providing a clear path from climate variability to primary productivity and on to higher trophic level species responses, whilst also bridging the marine-terrestrial divide by enabling general cross-realm patterns to be identified by combining a PSI with the existing VSI. Thanks to advances in remote sensing, reliable ocean colour estimates are now also available for global phytoplankton biomass (Section 1.3.2.1). Whilst these datasets do not capture the entirety of marine primary production (e.g. subsurface phytoplankton (Blondeau-Patissier *et al.*, 2014; Cullen, 1982, 2015; Huisman *et al.*, 2006), they provide sufficient estimates for assessing change at large spatial and temporal scales. Using these remotely sensed recordings of greenness as a measure of total primary productivity across realms could also overcome the differences in temporal scale of individual marine and terrestrial primary producers.

1.4.3 Linking a sensitivity index to higher trophic levels

Environmental variability also affects species dynamics and processes at higher trophic levels (Section 1.2.1; Dawson and Hamner, 2008; Ma *et al.*, 2015; Suryan *et al.*, 2009), influencing population dynamics (Ruokolainen *et al.*, 2009), growth rates (Lawson *et al.*, 2015), extinction risk (Ruokolainen and Fowler, 2008) and the turnover and abundance of species within communities (Ives *et al.*, 1999). Alongside general environmental variability, extreme environmental events are increasing in frequency (Section 1.2.2; Easterling *et al.*, 2000; Ma *et al.*, 2015) with extreme temperature events in particular causing a significant threat to higher trophic level community dynamics (Ma *et al.*, 2015; Vasseur *et al.*, 2014). Species responses to environmental variability can vary markedly (Morris *et al.*, 2008; Stenseth *et al.*, 2002; Vasseur *et al.*, 2014) and evidence suggests that compositional change (Blowes *et al.*, 2019) and species turnover (Pinsky *et al.*, 2019) in populations is currently occurring at different rates across realms (Section 1.2.2). With increasing levels of change occurring in natural systems, reliable measures for effective detection of change across trophic levels are needed.

Combining global estimates of climatic variability and primary productivity sensitivity with macroecological diversity indices describing the abundance distribution of diverse marine and terrestrial assemblages could be an effective way of achieving this. Due to primary producers forming the base of the food web and the tight coupling between production and consumption in trophic interactions (Cushing, 1990; Durant *et al.*, 2007), the availability and predictability of primary producers are integrally linked to the abundance and distribution of higher trophic level populations (Cushing, 1990; Durant *et al.*, 2005). As a result, regions that are sensitive to current variability at a primary producer level might already be exhibiting detectable signals of

related change at higher trophic levels. Species abundance distributions (SADs) identify patterns of commonness and rarity in communities, and can provide an early warning signal of community change or disturbance (Matthews and Whittaker, 2014; Sæther *et al.*, 2013b) as their descriptive parameters vary systematically with external influences, including environmental variance (Sæther *et al.*, 2013b). Furthermore, a principal feature of SADs is that species identities are not included in the distributions (McGill *et al.*, 2007), lending them to comparisons of contrasting communities with few or no shared species (e.g. Whittaker, 1975) and cross-realm communities (e.g. Gray *et al.*, 2006). SADs can also be used to compare community structure along environmental gradients (Cotgreave and Harvey, 1994; Hubbell, 1979; Hurlbert, 2004; Whittaker, 1960), to identify changes in core and transient species through time (Magurran and Henderson, 2003), and to detect directional long-term community changes (Thibault *et al.*, 2004).

In correlating the VSI and PSI with parameters describing well-known macroecological patterns of higher trophic level diversity such as SADs, an indirect link would be provided to determine environmental variability impacts on the stability of dependent higher trophic level populations. Patterns in higher trophic level responses could also be examined both along gradients of primary productivity sensitivity and across realms to identify similarities and differences in population responses. By incorporating a level of environmental explanation into exhibited trends, having predictive capacity across both trophic levels and realms, and being able to feed into existing macroecological patterns of species diversity, a fully global index of primary productivity sensitivity to environmental variability could both bridge the marine-terrestrial divide and make a valuable contribution to a more mechanistic and process-driven macroecology.

1.5 Thesis structure

In this thesis I aim to determine whether an explicit consideration of patterns of environmental variation and species responses to these, can help to move beyond binary marine-terrestrial distinctions towards a more generalised formulation of ecological responses to environmental change, that hold across marine and terrestrial systems and across trophic levels. The remainder of this thesis is structured as follows:

Chapter 2 The Phytoplankton Sensitivity Index: Determining the sensitivity of marine primary productivity to environmental variability

In Chapter 2 I adapt the methods of Seddon *et al.* (2016) to produce a Phytoplankton Sensitivity Index (PSI) for the marine realm, determining global marine primary productivity sensitivity

relative to current levels of variability in three governing drivers of phytoplankton growth: temperature, wind speed and light availability. I produce a series of global maps to visualise different aspects of the PSI, including the global distribution of phytoplankton sensitivity to climate variability and geographic variation in the influence of specific climate driver variability on phytoplankton sensitivity. I identify marine regions exhibiting amplified responses in primary productivity that are less likely to be resilient to future changes in environmental variability. I discuss possible causes of the spatial distribution of high and low sensitivity areas and the subsequent implications of the index for the marine realm under a changing climate.

Chapter 3 A global picture of sensitivity: Comparing the sensitivity of marine and terrestrial primary productivity to environmental variability

In Chapter 3 I combine the PSI developed in Chapter 2 with Seddon *et al's* (2016) Vegetation Sensitivity Index (VSI) for the terrestrial realm. I investigate the potential of this Combined Sensitivity Index (CSI) to bridge the marine-terrestrial divide, in terms of its ability to aide in the identification of global cross-realm patterns and potential to direct future research into higher trophic level responses. I investigate if differences in the spatial and temporal scales of marine and terrestrial environments can be overcome by examining patterns in sensitivity at a range of spatial scales, including global degrees of latitude, hemispheres and biogeographic regions. To be effective as a mechanistic and dynamic macroecological pattern, the CSI needs to provide both explanatory power in terms of its environmental drivers and facilitate analyses of its temporal dynamics (Fisher *et al.*, 2008). I therefore also examine patterns in climate driver influence on sensitivity at both global and regional spatial scales across realms and explore links between the temporal scales of environmental and primary productivity variability along gradients of sensitivity.

Chapter 4 Temporal trends in Species Abundance Distributions: Comparing marine and terrestrial community structure along gradients of environmental variability

In Chapter 4 I use global community assemblage data from the BioTIME database (Dornelas *et al.*, 2018) and sensitivity data from the PSI (Chapter 2) and VSI (Seddon *et al.*, 2016) for the marine and terrestrial realms respectively, to investigate the structure of species abundance distributions (SADs) for cross-realm communities along gradients of primary productivity sensitivity. I investigate whether there are differences in the evenness of communities existing in high versus low primary productivity sensitivity environments, and whether there are similarities in this across realms. By combining temporally explicit SADs with environmental variability derived ecosystem sensitivity, I aim to identify trends in marine and

terrestrial community structure attributable to environmental pressure. In doing so I aim to show that the effects of environmental variability via the PSI and VSI are detectable in higher trophic level systems dependent on primary productivity stability, providing a contiguous link through macroecological patterns from the abiotic to the biotic from which underlying processes can be better determined. Given the dominance of temperature as a driver of higher trophic level community change and climate sensitivity (Ma *et al.*, 2015; Pinsky *et al.*, 2019), I also examine the relationship between SAD structure and temperature variability.

Chapter 5 General Discussion

In Chapter 5 I synthesise the results of Chapters 2-4, discussing the main findings and the contributions they make to advancing a process-driven macroecology. I also discuss avenues of future research which could further build on the work presented here.

2 The Phytoplankton Sensitivity Index: Determining the sensitivity of marine primary productivity to environmental variability

2.1 Abstract

Identifying how sensitive or resilient ecosystems are to changes in current, short term environmental variability gives important insight into a region's likely responses to future environmental change. With growth and biomass predominantly under abiotic control, variability in primary productivity within an ecosystem can be used to determine sensitivity to climate variability. In 2016 Seddon *et al*. published a new metric, the Vegetation Sensitivity Index (VSI), which maps global terrestrial vegetation sensitivity to variability in three climate parameters (temperature, precipitation and cloudiness). Here, I use remote sensing data to produce a corresponding Phytoplankton Sensitivity Index (PSI) for the marine realm, identifying global phytoplankton sensitivity to current environmental variability within a 14-year time series (2000-2013). Adapted from Seddon *et al's* (2016) VSI, the PSI enables the identification of marine regions exhibiting amplified responses in primary productivity relative to current levels of variability in three governing drivers of phytoplankton growth: temperature, wind speed and light availability. A series of global maps are produced to visualise different aspects of the PSI, including the global distribution of phytoplankton sensitivity to climate variability and geographic variation in the influence of specific climate driver variability on phytoplankton sensitivity. High sensitivity marine regions are concentrated in species rich tropical and polar regions, whilst low sensitivity regions are concentrated in oligotrophic gyres at temperate latitudes. Temperature variability drives sensitivity in consistent latitudinal bands, whilst light and wind influence is more interspersed. By highlighting regions with lower resilience to current environmental variability at the primary producer level, the PSI provides crucial guidance on where wider ecosystem impacts are likely to occur as a result of changes in resource availability and predictability and a changing environmental variability regime, thus focussing future research efforts.

2.2 Introduction

The environmental conditions ecosystems are exposed to vary in both time and space. In marine ecosystems this ranges from large-scale, semi-predictable climate cycles such as the El Niño Southern Oscillation (ENSO; Philander, 1990) in the Pacific Ocean, to localised extreme weather events such as tropical storms (Stenseth *et al.*, 2003). This variability influences numerous aspects of ecosystem structure and function including species richness (Righetti *et al.*, 2019), population dynamics (Pöysä *et al.*, 2016), life history traits (Suryan *et al.*, 2009) and subsequent extinction risk (Kaneryd *et al.*, 2012; Mustin *et al.*, 2013). The ability to withstand such variability is a key component of an ecosystem's stability (Harrison, 1979b) and with predictions of continued change in both the mean and variability of environmental conditions (IPCC, 2019; Jentsch *et al.*, 2007), it is of vital importance to understand how marine ecosystems respond to both existing variability and unexpected fluctuations in their governing environmental conditions (Easterling *et al.*, 2000; Harrison, 1979b).

The inherent level of environmental variability within a region, in part, determines an ecosystem's ability to withstand climate fluctuations. The Climatic Variability Hypothesis (Stevens, 1989) has demonstrated that populations living in more variable environments, such as high latitudes and shallower waters, have wider environmental tolerance and are therefore more able to absorb fluctuating environmental conditions. High variability regions also promote generalist species with 'fast' life history traits (Winemiller and Rose, 1992), which combined with a wider environmental tolerance, increases their resistance to environmental fluctuations (Holling, 1973). Less variable environments on the other hand are more likely to favour specialist species (Righetti *et al.*, 2019) with persistence or 'slow' life history traits such as late maturity, suited to long runs of predictable conditions (Kindsvater *et al.*, 2016). As a result, these populations are typically less well adapted to fluctuating environmental conditions and are less able to absorb climate anomalies (Holling, 1973; Pintor *et al.*, 2015). Considerable concern therefore exists about the ecosystem impacts of inherent levels of environmental variability altering with climate change (García-Carreras and Reuman, 2011; Wigley *et al.*, 1998). Evidence already suggests that El Niño years are increasing in frequency (Power *et al.*, 2013) whilst Northern Hemisphere weather systems are experiencing longer 'stalled periods' of the same weather pattern, increasing the likelihood of persistent heat and associated extreme weather events (Mann *et al.*, 2017).

An ecosystem's ability to persist in its current state in the face of external pressure is a marker of both its resilience and resistance to stress events (Harrison, 1979b; Holling, 1973; Webster *et al.*, 1975). Resistance is typically defined in terms of a population or ecosystem's immediate

response to a stress event, with a resistant population showing smaller fluctuations in size and avoiding displacement (Webster *et al.*, 1975). Resilience on the other hand is a population or ecosystem's ability to return to its pre-impact state after the stress period has passed (Webster *et al.*, 1975). 'Sensitivity' encapsulates this combination of resistance and resilience and provides a measure of ecosystem health and stability relative to the magnitude of a stress event (Seddon *et al.*, 2016). Healthy ecosystems with high resistance and/or high resilience and therefore low sensitivity are able to persist for long periods of time in the face of environmental variability, expected or otherwise, by either exhibiting minimal perturbation and absorbing the impact in the first instance (resistance) or by quickly returning to normal post-event (resilience; Holling, 1973). However, many of the world's marine ecosystems are currently degraded from decades of anthropogenic exploitation and pollution (Halpern *et al.*, 2008) and are now facing a barrage of new pressures from a changing climate. Increasing pressure on already degraded ecosystems progressively reduces their resilience so that when an unexpected event such as a climate anomaly occurs, their resiliency limits are passed resulting in a rapid change to a new ecosystem state (Beaugrand *et al.*, 2008; Holling, 1973). Amplified responses in populations to unexpected climate events are indicative of an ecosystem having low resistance and being highly sensitive to environmental variability (Scheffer *et al.*, 2009; Smith, 2011a). Reduced recovery rates (low resilience) in a population can be indicated by high memory effects, whereby population anomalies are strongly determined by anomalous values at previous time points (De Keersmaecker *et al.*, 2015). Identifying ecosystems exhibiting amplified responses and high memory effects could therefore help to assess which regions are most at risk from a changing environmental variability regime.

Marine phytoplankton are likely to be the first indicators of a marine ecosystem's changing sensitivity to environmental variability (Hays *et al.*, 2005). With rapid life cycles, population growth rates and almost exclusive abiotic control (Hays *et al.*, 2005; Racault *et al.*, 2017; Taylor *et al.*, 2002), both the abundance, phenology and global distribution of phytoplankton can be attributed to variability in environmental parameters and particularly to temperature and wind (Drinkwater *et al.*, 2003; Falkowski and Oliver, 2007; González Taboada and Anadón, 2014; Raitsos *et al.*, 2006; Yokomizo *et al.*, 2010). The dominance of phytoplankton as the sole producer across much of the oceans also means that phytoplankton blooms support the vast majority of marine food webs, and due to tight trophic coupling in the marine realm the effects of variability in phytoplankton biomass can quickly propagate up the food web via trophic amplification (Henson *et al.*, 2009; Kirby and Beaugrand, 2009; Poloczanska *et al.*, 2016; Stock *et al.*, 2014), with potential impacts for ecosystem structure and composition (Beaugrand, 2009; Edwards and Richardson, 2004a; Harley *et al.*, 2006; Richardson and Schoeman, 2004)

and higher trophic level recruitment (Beaugrand *et al.*, 2003; Cushing, 1990; Hjort, 1914; Platt *et al.*, 2003). This is particularly the case in species rich ecosystems where high inter-specific competition results in lower mean phytoplankton population densities (Kaneryd *et al.*, 2012). Taken together, this means that despite not being a poster child of marine climate change impacts (e.g. coral bleaching, kelp die-off), the effects of environmental variability throughout marine systems will be largely mediated through phytoplankton responses (Hays *et al.*, 2005).

Here, I adapt an existing Vegetation Sensitivity Index (VSI) for the terrestrial realm (Seddon *et al.*, 2016) to create a Phytoplankton Sensitivity Index (PSI) for the marine realm, identifying global phytoplankton sensitivity to current environmental variability within a 14-year time series (2000-2013; as used in the VSI to enable future cross-realm comparability (Chapter 3)). Obtaining a spatially-resolved global picture of phytoplankton responses to climate variability is particularly important as their responses to changes in average climatic conditions are known to vary considerably across ecosystems, preventing extrapolation to other regions (Häder *et al.*, 2014). The PSI enables the identification of marine regions exhibiting amplified responses in primary productivity relative to current levels of variability in three governing drivers of phytoplankton growth: temperature, wind speed and light availability. I produce a series of maps to investigate global marine primary productivity sensitivity, each visualising a different aspect of the PSI. These include the global distribution of phytoplankton resistance (amplified responses) and resilience (memory effects) to climate variability and global geographic variation in the influence of specific climate driver variability on phytoplankton sensitivity.

2.3 Materials and Methods

2.3.1 Satellite data

14 year (2000–2013) monthly time series were retrieved for all variables on a geographic projection. Using monthly composites as opposed to daily data reduces the impact of missing data on estimated values (Morel *et al.*, 2007; Racault *et al.*, 2014). Where possible, datasets were chosen that contained data merged from multiple satellites, which has been shown to improve spatial and temporal coverage compared to individual satellite sensors (Kahru *et al.*, 2010; Morel *et al.*, 2007; Racault *et al.*, 2015). Table 2.1 provides a summary of all variable datasets used.

Ocean colour derived Chlorophyll a (Chl-a; mg m^{-3}), a commonly used proxy for phytoplankton biomass (Blondeau-Patissier *et al.*, 2014; Cullen, 1982; Hirata *et al.*, 2012; McClain, 2009;

Sathyendranath and Platt, 1997) and Essential Climate Variable (ECV; Bojinski *et al.*, 2014), was used to estimate marine primary productivity. Remotely sensed level 3 Chl-a at 9 km resolution was retrieved from Version 3.1 of the European Space Agency (ESA) Ocean Colour Climate Change Initiative (OC-CCI) project (Hollmann *et al.*, 2013; Lavender *et al.*, 2015; Sathyendranath *et al.*, 2018); http://www.esa-oceancolour-cci.org/). The OC-CCI dataset features an updated algorithm selection to improve coverage in Case 2 (coastal) waters (Brewin *et al.*, 2015; Lavender *et al.*, 2015; Müller *et al.*, 2015), and merges ocean colour data from the Medium Resolution Imaging Spectrometer (MERIS), Moderate Resolution Imaging Spectroradiometer (MODIS)-Aqua and Visible Infrared Imaging Radiometer Suite (VIIRS) satellites, which are band-shifted and bias-corrected to the Sea-viewing Wide Field-of-view Sensor (SeaWiFs) satellite. Data was logarithmically transformed (base10) and bias corrected (OC-CCI PUG; Grant *et al.*, 2017) prior to analysis due to the log-normal distribution of global Chl-a.

Blended sea surface winds (SSW; m s^{-1}) at 0.25° spatial resolution were obtained from the National Climatic Data Centre (NCDC) and the National Ocean and Atmospheric Administration (NOAA; Zhang *et al.*, 2006; http://www.ncdc.noaa.gov/data-access/marineocean-data/blended-global/blended-sea-winds). This dataset is a blend of six satellites: Advanced Microwave Scanning Radiometer on the Earth Observing System (AMSR-E), Special Sensor Microwave Imager (SSMI) F15, F14 and F13, Quick Scatterometer (QuikSCAT) and the Tropical Rainfall Measuring Mission (TRMM) Microwave Imager (TMI), with daily means calculated from four 6-hourly global snapshots per day, at 10 m above sea level. Vector wind speeds were calculated according to the formula:

$$w = \sqrt{u^2 + v^2} \quad (1)$$

where u is the sea surface wind *x*-component and v is the sea surface wind *y*-component. Bilinear interpolation was used to transform the data to 9 km resolution. April and May 2008 were found to have anomalous maximum values (6.5 x 10^8 m s^{-1}) which were removed prior to calculating wind speed. Wind speed was used as opposed to wind stress as the corresponding wind stress product to the blended sea winds dataset ended in 2011.

Photosynthetically available radiation (PAR; Einstein m^{-2} d^{-1}) gives a measure of the amount of sunlight reaching the ocean surface, calculated by subtracting the amount of light reflected by the surface (satellite recorded) from a constant value for light availability above the cloud layer, and performs as a proxy for cloudiness. No merged, multi-satellite datasets were available for this variable, so data was obtained for the SeaWiFs, MODIS Terra and Aqua satellites separately and averaged. These datasets have previously been corrected for spatial

and temporal biases with respect to each other (Frouin *et al.*, 2003, 2012). All data were level 3 Standard Mapped Images (SMI) at 9 km resolution and were sourced from NASA's ocean colour website (http://oceancolor.gsfc.nasa.gov/cms/). Negative minimum values present in the MODIS Terra data for months 01, 02 and 11 across all years were removed prior to averaging.

Sea surface temperature (SST; °C), also an ECV (Bojinski *et al.*, 2014), at 0.25° spatial resolution was obtained from the NOAA Optimum Interpolation Sea Surface Temperature (OISST) V.2 datasets (Reynolds, 2009; Reynolds *et al.*, 2007; http://www.ncdc.noaa.gov/oisst). The OISST comprises two datasets: an integrated dataset using Advanced Very High Resolution Radiometer (AVHRR) infrared satellite data, bias adjusted to in situ ship and buoy data (available for 2000-2013), and AVHRR data merged with AMSR-E data (available for 2002-2011). The addition of AMSR-E improves spatial coverage over the open ocean due to the lower susceptibility of microwave scanners to cloud cover (Reynolds *et al.*, 2007). A correction procedure akin to that done for PAR by Frouin *et al.* (2012) was conducted to correct the AVHRR dataset for the years AMSR-E was not active. Briefly, 8-year monthly means were calculated for the overlap time period of both datasets (2003-2010). The AVHRR combined means were then subtracted from the AVHRR + AMSR-E means for each month to obtain a correction factor, which was then added to AVHRR months outside of AVHRR + AMSR-E activity. Plots showed better alignment between the datasets after addition of the correction factor (Appendix A Figure A-1). Bilinear interpolation was used to transform the data to 9 km resolution.

A land mask was created to exclude land areas from the analysis using the MODIS version 6 digital elevation model (DEM) land-water layer (ftp://landsc1.nascom.nasa.gov/outgoing/c6_dem/geo/). The DEM is provided as a set of tiles at nominal 500 m and 1 km resolution, which were extracted and mosaicked onto a 1 km global grid. This was transformed to 9 km resolution in QGIS. Of the 8 categories in the land-water layer specifying inland water, ocean and land areas, data points containing shallow ocean, deep ocean and moderate or continental ocean were retained, all other values were masked as land.

Table 2.1: Summary of input variables used and source information.

Variable	Description	Source
Chl-a (mg m^{-3})	9 km resolution, monthly Merge of: SeaWiFs, MERIS, MODIS-Aqua & VIIRS	ESA OC-CCI; http://catalogue.ceda.ac.uk/uuid/9c334fbe6d424a708cf3c4cf0c6a53f5 (Sathyendranath *et al.*, 2018)
Sea surface temperature (°C)	0.25° resolution, daily AVHRR & AMSR-E	NOAA OISST; http://www.ncdc.noaa.gov/oisst (Reynolds, 2009; Reynolds *et al.*, 2007)
Sea surface winds (m s^{-1})	0.25° resolution, daily Merge of: SSM/I, AMSR-E, TMI, QuikSCAT,	NCDC; http://www.ncdc.noaa.gov/data-access/marineocean-data/blended-global/blended-sea-winds (Zhang *et al.*, 2006)
Photosynthetically available radiation (Einstein m^{-2} d^{-1})	9 km resolution, daily Merge of: SeaWiFs, MERIS, MODIS-Aqua & MODIS-Terra	NASA; http://oceancolor.gsfc.nasa.gov/cms/ (Frouin *et al.*, 2012)

2.3.2 Phytoplankton Sensitivity Index

To ensure the global index of primary productivity sensitivity was comparable across realms for future analyses (Chapter 3), the PSI was calculated following Seddon *et al's* (2016) methodology for the VSI wherever possible. A summary schematic of the calculation procedure for the PSI is presented in Figure 2.1.

2.3.2.1 Determining drivers of productivity

In addition to the 3 climate variables already described, a one-month-lagged (*t*-1) Chl-a anomaly variable was created from the Chl-a time series (months in the time series shifted forward by one month, i.e. Jan 01 becomes Feb 01) to investigate the role of memory effects in determining sensitivity (i.e. do anomalies of Chl-a in the previous month determine Chl-a anomalies in subsequent months, indicating lack of recovery and low resilience). As evidence already exists to show that phytoplankton are capable of responding to climate perturbations within a month (Schaum and Collins, 2014) it wasn't deemed necessary to try alternative

lengths of time lag for the PSI. Months across all variable time series with a mean SST below -2 °C were then masked to remove ice covered areas from the analysis.

As I was specifically interested in the effects of variability, each variable time series was transformed and standardised to *z*-score anomalies (Equation 2), giving the number of standard deviations a value is away from the population mean.

$$Z_{p,m} = \frac{x_{p,m,v} - \mu_{p,\vec{m},v}}{\sigma_{p,\vec{m},v}} \quad (2)$$

Where x is a variable's (v) value for a specific month (m) and pixel (p), μ is the per pixel mean for a month over the 14-year time series ($\vec{m}$) and σ is the per pixel standard deviation for a month over the time series.

To account for collinearity between the climate variables, principal components regression (PCR) was used to estimate the relative importance of each climate variable in driving Chl-a variability per pixel. First, principal components analysis (PCA) was performed on the 4 explanatory variables (3 climate and *t*-1) per pixel, per month across the *z*-score anomaly time series. The PCA was only performed for months which had more than 4 years of complete cases within the time series (i.e. the same month in more than 4 years where all variables had available data after temperature masking and removal of missing data). The linearly uncorrelated principal components produced were then regressed against the monthly Chl-a *z*-score anomalies using ordinary least squares regression to give estimated regression coefficients (Equation 3).

$$lm\left(Chla_{Z,p,\vec{m}} \sim PC1_{p,\vec{m}} + PC2_{p,\vec{m}} + PC3_{p,\vec{m}} + PC4_{p,\vec{m}}\right) \quad (3)$$

Where lm denotes a linear model, Z indicates the *z*-score anomaly time series and PCx are the principal components for each pixel and month over the time series.

Following Seddon *et al.* (2016), the estimated regression coefficients for principal components found to have a significant relationship (setting $P < 0.1$ as in Seddon *et al.* (2016) to increase sample size) with Chl-a were multiplied by the loading scores of their respective principal component axis to transform them back to the scale of the original *z*-score anomalies. These were then summed across the principal components for each variable (Equation 4).

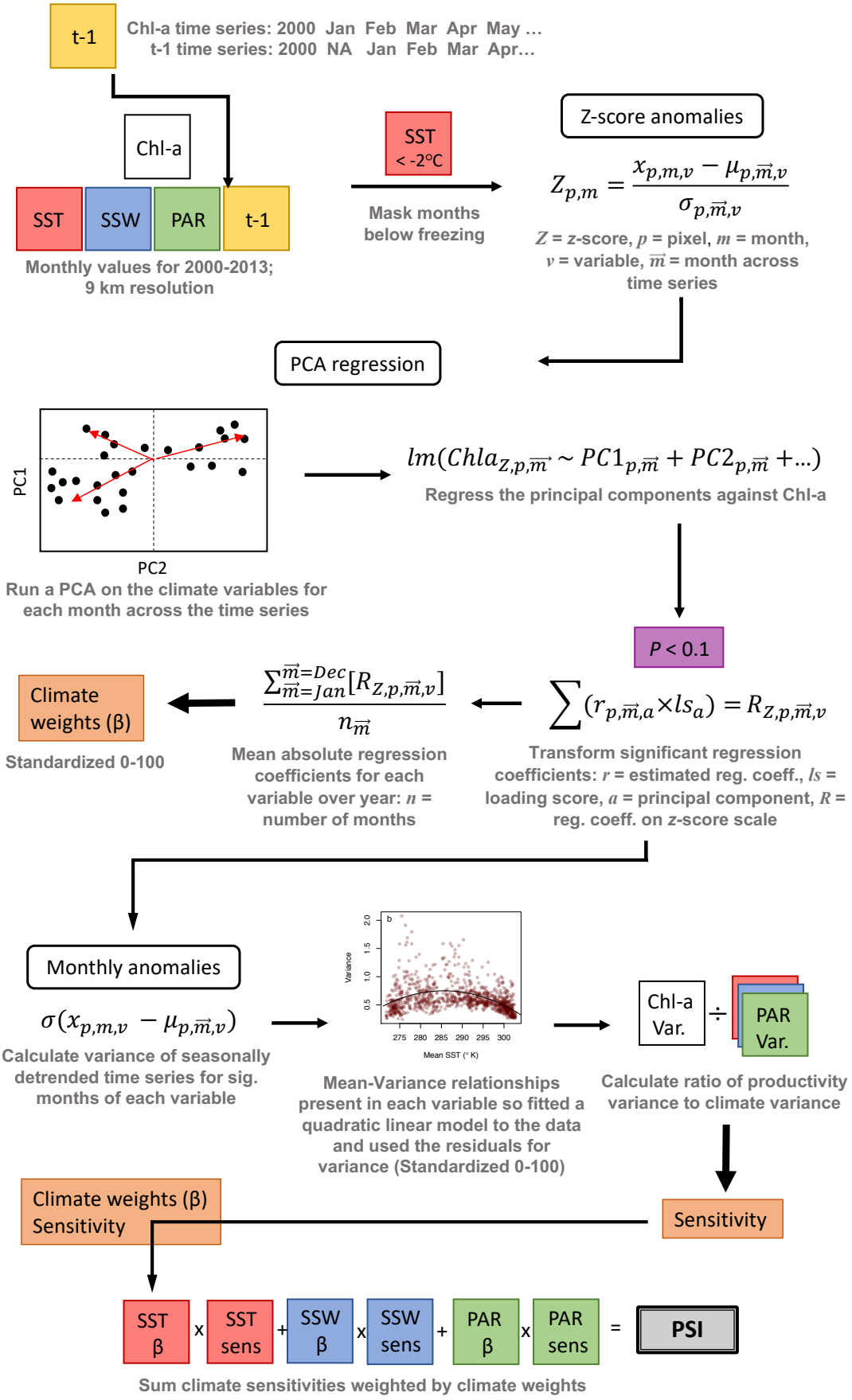

Figure 2.1: Summary schematic of the Phytoplankton Sensitivity Index (PSI) calculation methods. Flow chart summarising the methods used to calculate the PSI.

$$\sum\left(r_{p,\vec{m},a} \times ls_a\right) = R_{Z,p,\vec{m},v} \quad (4)$$

Where r is the estimated regression coefficient for a pixel and month over the time series for each principal component axis (a), ls is the loading scores for the principal component axis and R is the regression coefficient transformed back to the scale of the *z*-score anomalies for each variable. The absolute values of the final regression coefficients were then summed across months for each variable and divided by the number of months with significant regression coefficients to give the relative strength of global Chl-a - climate variability relationships (Equation 5), hereafter referred to as climate weights.

$$CW_{p,v} = \frac{\sum_{\vec{m}=Jan}^{\vec{m}=Dec}\left[R_{Z,p,\vec{m},v}\right]}{n_{\vec{m},p,v}} \quad (5)$$

The climate weights were then scaled between 0 and 100 with respect to each other, using the minimum and maximum regression coefficient values across all four variables for use in the final PSI calculation (Section 2.3.2.2, Equation 7).

2.3.2.2 Determining sensitivity of productivity

To calculate the final sensitivity metric, months found to have a significant Chl-a – climate relationship in the PCR were extracted for each variable from the raw (pre *z*-score transformed) times series. These time series were then seasonally de-trended by subtracting the 14-year monthly mean from each per pixel monthly value for each variable, and the standard deviation was calculated (Equation 6).

$$\sigma\left(x_{p,m,v} - \mu_{p,\vec{m},v}\right) \quad (6)$$

Plotting the mean against the standard deviation for each variable's time series revealed the presence of non-linear mean-variance relationships in the data (Appendix A Figure A-2). Non-linear (quadratic) least squares regression models were therefore fitted to the mean-variance relationship for each variable, the residuals of which were standardised between 0-100 and used for the final estimated variance anomaly values. Using the estimated variances for each variable, the per-pixel ratio of Chl-a - climate anomalies was calculated, $\log_{10}$ transformed and standardised to bring all variables onto a common scale and provide a non-weighted measure of sensitivity. The final sensitivity value per pixel was then calculated as the sum of the non-weighted sensitivity for each variable multiplied by its respective climate weight (Equation 7).

$$PSI_p = \sum \log_{10}\left((Chla_{p,anom} + 1)/(v_{p,anom} + 1)\right) * CW_{p,v} \quad (7)$$

2.3.2.3 Uncertainty layers

Uncertainties for the specific satellite datasets used can be found in their source materials; for our purposes here, uncertainties refer solely to their use within the index. To examine the global accuracy of the Chl-a satellite data, the standard error of the mean for each pixel was mapped using the standard deviation of satellite error per pixel divided by the square root of the number of satellite observations per pixel, averaged over the times series. The standard deviation of the error of the pixels is a centred, bias corrected measure of the likelihood of satellite measurements differing from in situ measurements based on the root-mean-square difference of satellite and in situ values (Equation 8; Grant *et al.*, 2017). Both the root-mean-square difference and number of observations per pixel are available as variables in the OC-CCI Chl-a product.

$$\sigma_p = \sqrt{\left| rmsd_p^2 - \delta_p^2 \right|} \tag{8}$$

Where σ is the standard deviation, $rmsd$ is the root-mean-square difference and δ is the satellite bias correction factor. Standard errors for Chl-a are low in all the major ocean basins, moderately high along equatorial currents and highly productive coastal areas (see Appendix A Figure A-3 for global Chl-a distribution) and highest in sub-polar regions (Appendix A Figure A-4). In highly productive, turbid waters characteristic of coastal seas the depth range of satellites can be substantially reduced (Grant *et al.*, 2017), resulting in a lower Chl-a recording than may be obtained from an in situ measurement. Differences between satellite and in situ measurements can also be a result of the large differences in the spatial scales of measurements being compared and/or the quantity of in situ measurements available in a region for comparison. Having said this, 97% of pixels in the PSI have at least 15 observations per recording and 99% of pixels have standard deviations lower than 0.3, and the absolute values of the standard errors are not high enough to compromise the integrity of the results.

2.3.3 Visualising the Phytoplankton Sensitivity Index

Several maps were produced to visualise different aspects of the PSI. Firstly, the PSI sensitivity values were mapped to visualise the global distribution of marine primary productivity sensitivity to climate variability. Due to right skew in the index a stretch was applied to the mapped colour scale in QGIS, saturating values either side of the top and bottom 2.5 standard deviations of the index (the default in ArcGIS and used by Seddon *et al.* (2016) for mapping the VSI). This maximised the clarity of geographical variability within the central 95% of the indices whilst saturating fewer than 5% of pixels.

To identify geographic variation in the influence of climate variability on sensitivity, composite maps were produced for the PSI. These maps allocate each climate variable to a separate colour band and plot the highest valued (i.e. most important) variable per pixel. To determine the contribution of an individual climate variable's variability on final sensitivity, the coefficient-weighted sensitivities for each variable were extracted and plotted before being combined to give the final index (Section 2.3.2.2, Equation 7). To visualise regional differences in correlation strength between primary productivity and climate anomalies, a composite map was also produced for the climate weights of each variable (Section 2.3.2.1, Equation 5).

To investigate the global distribution of memory effects and their role in determining primary productivity sensitivity, a map of the regression coefficients for the Chl-a one-month time lag (*t*-1) variable was produced. Data was also recorded and mapped for the PSI on how many months during the year a significant relationship ($P < 0.1$) between Chl-a and climate anomalies occurred per pixel, to determine if regional differences are present in the continuity of climate correlation with primary productivity.

Data was downloaded via FTP using the FileZilla Client 3.21.0, or via Wget for HTTP. Satellite data modification was conducted in the Unix shell using a combination of Climate Data Operators (CDO, version 1.8.2) and NetCDF Operators (NCO; Zender, 2008). Data analyses were conducted in MATLAB and the R project for statistical computing (R Core Team 2015, version 3.3.2) using the `cowplot` (Wilke, 2018), `data.table` (Dowle and Srinivasan, 2018), `dev.tools` (Wickham *et al*., 2018), `dplyr` (Wickham *et al*., 2018), `ggplot2` (Wickham, 2016), `grateful` (Rodriguez-Sanchez, 2017), `maptools` (Bivand and Lewin-Koh, 2018), `nlme` (Pinheiro *et al.,* 2018), `raster` (Hijmans, 2017), `readr` (Wickham *et al*., 2017), `rgdal` (Bivand *et al*., 2018), `rgeos` (Bivand and Rundel, 2018), `sp` (Pebesma and Bivand, 2005), `tidyr` (Wickham and Henry, 2018), `tidyverse` (Wickham, 2017), `viridis` (Garnier, 2018a) and `viridisLite` (Garnier, 2018b) packages. Image processing was carried out in QGIS and R version 3.3.2.

2.4 Results

The PSI provides a global picture of marine primary productivity sensitivity to environmental variability, from which areas with amplified responses in primary productivity relative to environmental variability can be identified (Figure 2.2). Sensitivity in the PSI ranges from 0 (low sensitivity) to 100 (high sensitivity). As ocean-colour derived Chl-a is a proxy for phytoplankton biomass, high sensitivity indicates a large response in phytoplankton biomass relative to environmental variability, whilst low sensitivity indicates a small or equivalent

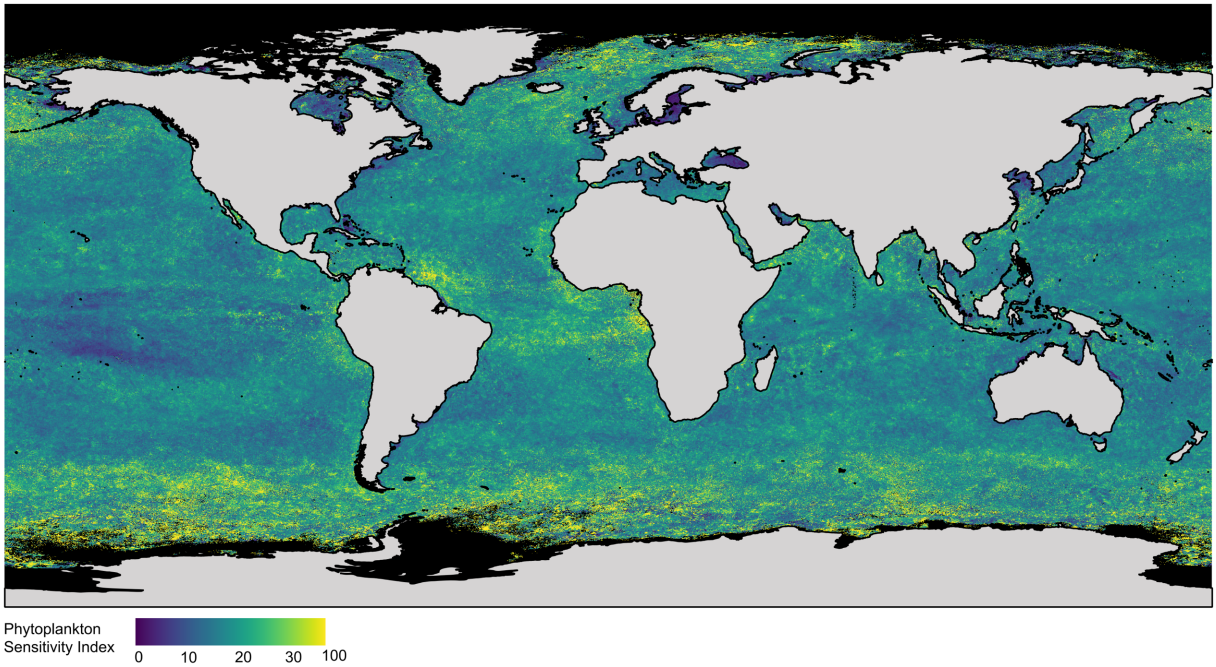

Figure 2.2: Phytoplankton Sensitivity Index. A global map of marine primary productivity (based on satellite derived measurements of ocean colour – Chl-a) sensitivity relative to variability in sea surface temperature, sea surface winds and photosynthetically available radiation. The index ranges from 0 (low sensitivity) to 100 (high sensitivity). Due to right skew in the data and the volume of data points, the colour scale has been band shifted by 2.5 standard deviations (the default in ArcGIS) to better reflect the spread of the data. Pixel resolution, 9 km; time period, 2000-2013. Areas in black indicate no data availability. Continental outlines were modified from a shapefile using QGIS.

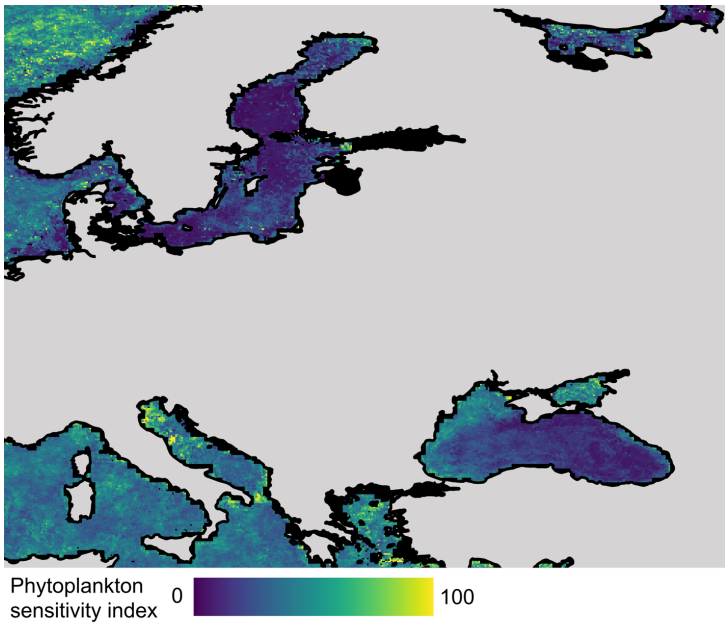

Figure 2.3: Low sensitivity regions of the Phytoplankton Sensitivity Index (PSI). A zoomed in map of the PSI showing the Baltic (top left) and Black Seas (bottom right), which exhibit low marine primary productivity sensitivity relative to variability in sea surface temperature, sea surface winds and photosynthetically available radiation. In other words, phytoplankton biomass is less variable than the environment in these regions. The index ranges from 0 (low sensitivity) to 100 (high sensitivity). Due to right skew in the data and the volume of data points, the colour scale has been band shifted by 2.5 standard deviations (the default in ArcGIS) to better reflect the spread of the data. Pixel resolution, 9 km; time period, 2000-2013. Areas in black indicate no data availability. Continental outlines were modified from a shapefile using QGIS.

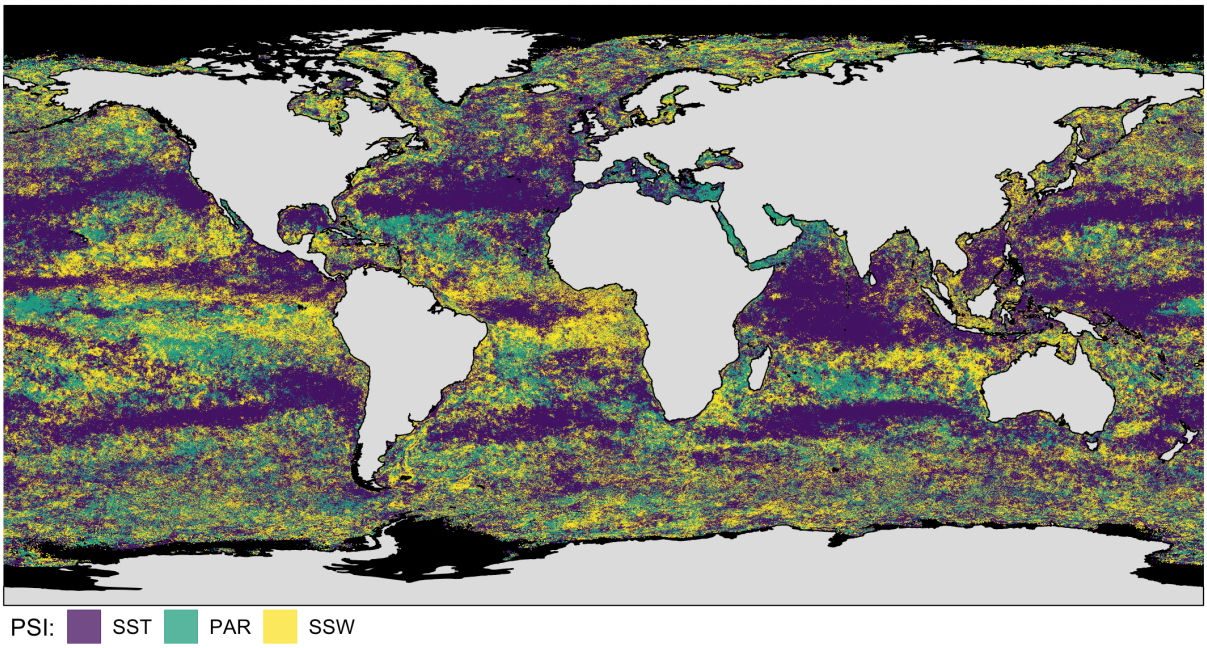

Figure 2.4: Composite map of the Phytoplankton Sensitivity Index. Composite map of the contribution of climatic driver variability to the PSI, showing which driver has the highest influence on sensitivity in a given pixel (sea surface temperature (SST; blue), photosynthetically available radiation (PAR; green) and sea surface wind (SSW; yellow)). Pixel resolution, 9 km; time period, 2000-2013. Areas in black indicate no data availability. Continental outlines were modified from a shapefile using QGIS.

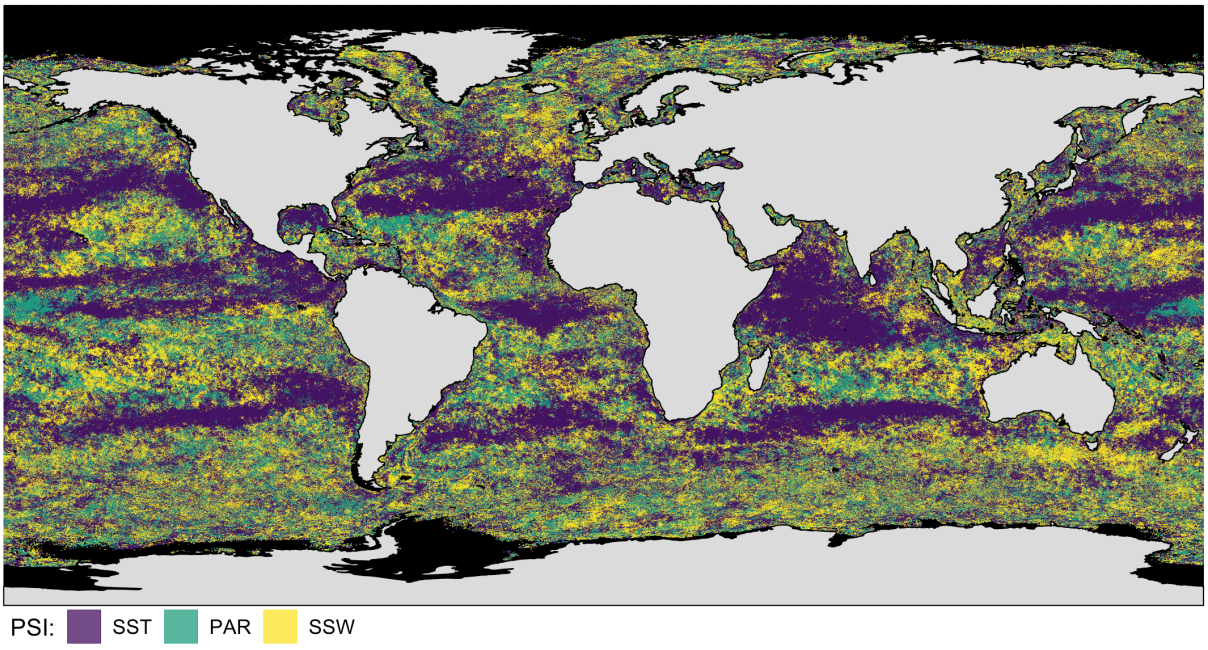

Figure 2.5: Composite map of marine climate weights. Composite map of the mean climate coefficient weights for the PSI from multiple linear regressions between primary productivity and three climate drivers, showing which climate driver has the strongest correlation with primary productivity in a given pixel (sea surface temperature (SST; blue), photosynthetically available radiation (PAR; green) and sea surface wind (SSW; yellow)). Pixel resolution, 9 km; time period, 2000-2013. Areas in black indicate no data availability. Continental outlines were modified from a shapefile using QGIS.

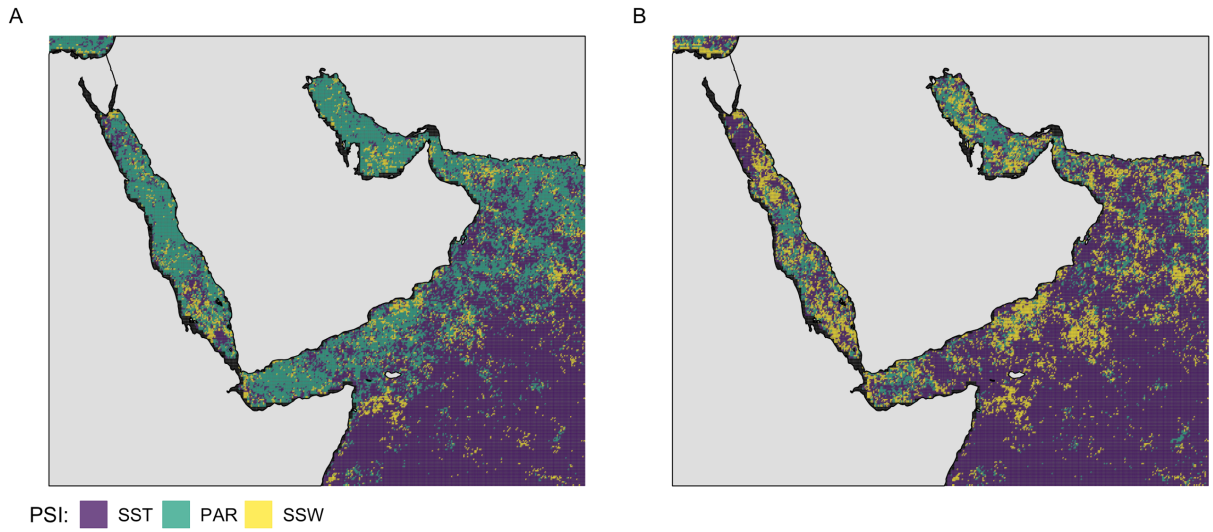

Figure 2.6: Differences in climate influence in the Arabian and Red Sea. Composite maps of the Arabian and Red Sea showing climatic driver variability influence on the PSI (A) and mean climate coefficient weights for the PSI (B) from multiple linear regressions between primary productivity, sea surface temperature (SST; blue), photosynthetically available radiation (PAR; green) and sea surface wind (SSW; yellow). PAR has the highest influence on primary productivity sensitivity in the Arabian and Red Sea region (A) despite SSW being more strongly correlated with primary productivity (B). Pixel resolution, 9 km; time period, 2000-2013. Areas in black indicate no data availability. Continental outlines were modified from a shapefile using QGIS.

response in phytoplankton biomass relative to environmental variability. High primary productivity sensitivity is largely concentrated in sub-polar and equatorial regions (Figure 2.2), and particularly in the Guinea and Canary Current, North Brazil Shelf, Antarctic, Barents and Greenland Sea large marine ecosystems (LME; Appendix A Figure A-5). The major ocean basins are dominated by mid-low sensitivities with particularly low sensitivity areas present in the Baltic Sea, the Black Sea (Figure 2.3) and the South Pacific Ocean basin (Figure 2.2). The PSI is heavily right skewed with a mean sensitivity of 16.98 ± 6.72 sd and only 0.65% of pixels exhibiting sensitivity greater than or equal to 50, equating to an area of 304,137 km^2 of the total ocean index area of 46,706,040 km^2.

Distinct regions of climate variability influence on primary productivity sensitivity are present in the PSI (Figure 2.4). Across the major ocean basins SST influence dominates in relatively consistent latitudinal bands, interspersed with overlapping bands of PAR and SSW influence (Figure 2.4). Areas of PAR and SST influence are predominantly focussed in upwelling regions and along South Equatorial Currents (see Appendix A Figure A-6 for a global map of ocean currents). The polar regions of the PSI appear a lot more mixed, with no particular climate variable having a consistently dominant influence on sensitivity. Geographic patterns in the climate weights broadly correspond to those seen in climate variability influence on sensitivity, with SST variability maintaining distinctive bands across the major ocean basins (Figure 2.5). However, there are some instances where dominant climate variability influence on sensitivity

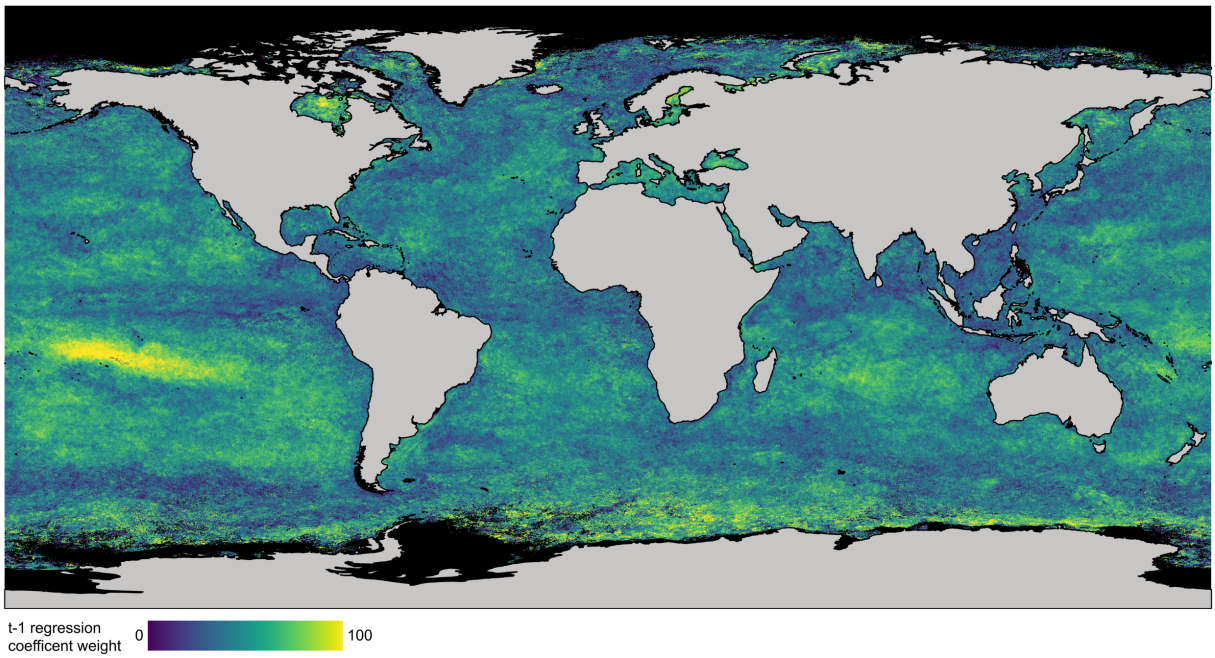

Figure 2.7: Global map of the memory effects coefficient. A global map of the coefficient weights for the one-month primary productivity (Chl-a) time lag (*t*-1) variable from monthly linear regressions between Chl-a and Chl-a at *t*-1. This shows areas where Chl-a anomalies in previous months are a strong predictor of Chl-a anomalies in subsequent months. High values indicate strong memory effects and reduced recovery rates within the system, suggesting decreased resilience. The coefficient weights are scaled between 0 (low memory effects) and 100 (high memory effects). Pixel resolution, 9 km; time period, 2000-2013. Areas in black indicate no data availability. Continental outlines were modified from a shapefile using QGIS.

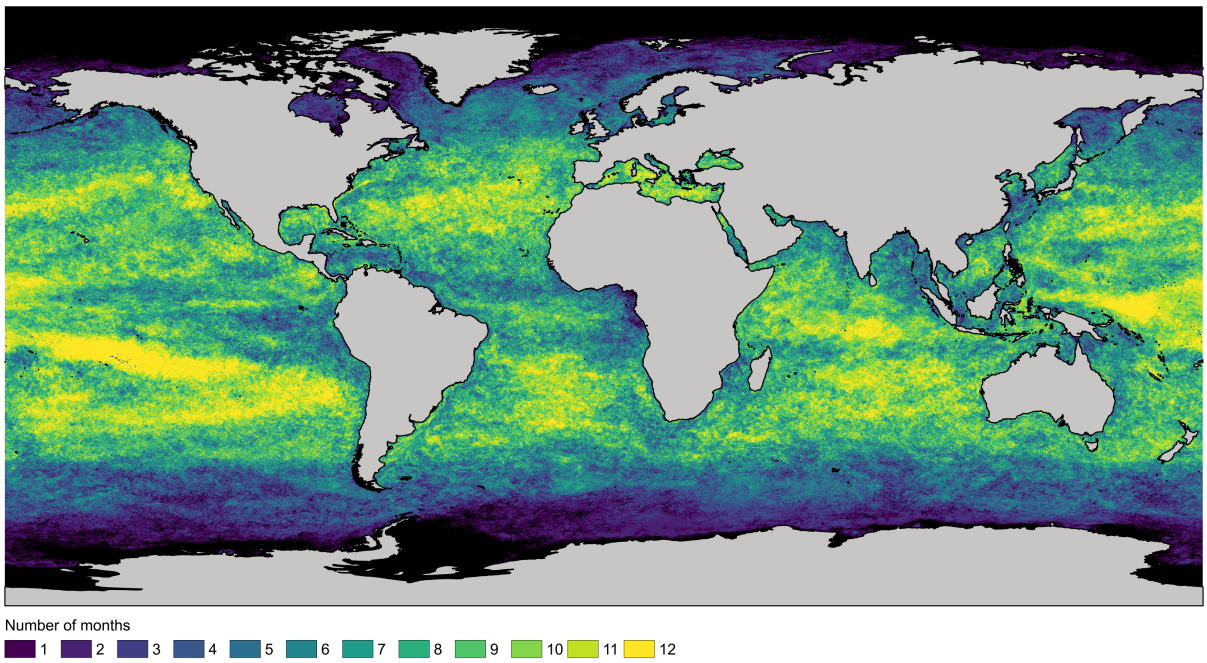

Figure 2.8: Number of months with a significant ($P < 0.1$) coefficient in the principal components regression. Number of months per pixel with a significant ($P < 0.1$) relationship between primary productivity (Chl-a), climate variation (sea surface temperature, sea surface wind and photosynthetically available radiation) and a one-month Chl-a time lag (t-1) variable in the principal components regression, highlighting areas with consistent, year-round Chl-a climate relationships. Pixel resolution, 9 km; time period, 2000-2013. Areas in black indicate no data availability. Continental outlines were modified from a shapefile using QGIS.

does not correspond to the variable with the strongest correlation with Chl-a anomalies, for example in coastal areas of the Arabian and Red Seas (Figure 2.6).

There is a strong correlation between sensitivity, memory effects and year-round continuity of significant ($P < 0.1$) Chl-a–climate variability relationships. Low sensitivity areas such as the South Pacific basin correspond to areas which exhibit high memory effects (Figure 2.7) and year-round significant ($P < 0.1$) relationships between primary productivity variability and climate variability (Figure 2.8). Conversely, high sensitivity areas such as the Guinea Current LME and sub-polar regions correspond to areas with low memory effects (Figure 2.7) and fewer months in a year with a significant relationship between primary productivity variability and climate variability (Figure 2.8).

2.5 Discussion

Satellite derived measures of phytoplankton biomass (Chl-a) were used to produce a global index of georeferenced marine primary productivity sensitivity to variability in three governing variables of the marine environment: temperature, wind and radiation. The global PSI identifies regions with amplified primary productivity responses, and hence higher sensitivity, to environmental variability. The PSI also identifies regions which remain stable in spite of high variability, suggesting that they may be more resistant to future increases in climate variability. Together, this provides a base layer from which the sensitivity of marine ecosystems to current environmental variability at a primary production level can be determined, along with the specific climate elements responsible; this in turn can be used to predict future responses to global change.

2.5.1 Global patterns of sensitivity

2.5.1.1 Low sensitivity

Low sensitivity is achieved in the PSI when primary productivity variability is similar to, or lower than climate variability (Appendix A Figure A-7) and when correlation between primary productivity and climate anomalies is weak (Appendix A Figure A-8), but consistent throughout the year (Figure 2.8). The year-round correlation between Chl-a and climate anomalies indicates that low sensitivity regions have high predictability throughout the year, whilst the low strength of the correlations suggests that primary productivity is minimally responsive to climate variability in these regions. This low responsiveness to climate variability is further

reflected in the high memory effects observed in these regions (Figure 2.7), indicating that previous primary productivity anomalies are a bigger driver of sensitivity than climate.

The regions exhibiting the lowest phytoplankton sensitivity in the PSI were in the temperate mid-latitudes where environmental variability is higher and generalist species with wide tolerance limits are preferentially selected (Pintor *et al.*, 2015; Righetti *et al.*, 2019; Stevens, 1989). The mid-latitudes are also characterised by low phytoplankton species richness (Righetti *et al.*, 2019), which increases mean population densities so that unexpected population fluctuations driven by climate anomalies are less likely to cross extinction thresholds (Kaneryd *et al.*, 2012). In combination this enables an extreme climate event to occur without triggering an amplified ecological response, reflecting the increased resistance and resilience of certain ecosystems to anomalous environmental conditions (Smith, 2011b). The Hudson Bay region of North-East Canada for example, exhibits low primary productivity sensitivity (Figure 2.2) despite experiencing anomalous climate conditions (Appendix A Figure A-7).

The lowest sensitivities in the PSI predominantly occur in the large oligotrophic gyres of the Pacific, Atlantic and Indian ocean basins, which are often considered ‘ocean deserts’ (Signorini *et al.*, 2015) due to their low productivity and biomass. Oligotrophic gyres are governed by large-scale patterns of atmospheric circulation which drive large, circulating oceanic currents (Appendix A Figure A-6). The sides of these circulatory currents are broad and slow moving, with westward flow of the equatorial currents deepening the mixed layer depth on the western edge preventing the upwelling of nutrient rich water for phytoplankton growth (Mann and Lazier, 2006). The narrow, fast eastward flow concentrates productivity along the Eastern boundaries of the gyres where a shallower pycnocline enables the upwelling of nutrient-rich water to the euphotic zone (Mann and Lazier, 2006), creating an Eastern Boundary Upwelling System (EBUS). The central regions of the gyres remain permanently stratified, causing the vertical profile of Chl-a and nutrients to be more or less constant year-round (Mann and Lazier, 2006). Whilst these regions are not as unproductive as commonly thought (locally occurring eddies can stimulate random bursts of growth; Mann and Lazier, 2006), production is still considerably lower in the central gyres than in shelf, coastal and upwelling areas. As a result, there is little phytoplankton biomass to amplify regardless of climate variability, and small bursts of productivity that do occur might not be reflected in the final index if they occur infrequently during the 14-year time series. The Pacific gyres are most likely to see phytoplankton variability through the aeolian transport of iron, as iron limitation is more likely to prevent growth in these regions than nitrate limitation (Behrenfeld and Kolber, 1999; Kolber *et al.*, 1994; Martin *et al.*, 1994).

The oligotrophic gyres cover ~60% of the ocean surface (Marañón *et al.*, 2003), and climate change is causing them both to increase in size (McClain *et al.*, 2004; Polovina *et al.*, 2008; Signorini *et al.*, 2015) and become more oligotrophic (Signorini *et al.*, 2015). Whilst the expansion of low sensitivity areas of the oceans could be considered a beneficial result of climate change, the reality may not be desirable. Dominant phytoplankton types are known to be regionally variable (Alvain *et al.*, 2008; Cabré *et al.*, 2016; Uitz *et al.*, 2010), with low biomass regions typically characterised by smaller phytoplankton types (e.g. picophytoplankton; Marañón *et al.*, 2001) than high biomass regions (e.g. nano- and microphytoplankton; Cabré *et al.*, 2016). Expansion of low productivity areas (Behrenfeld *et al.*, 2006) could therefore lead to regional changes in dominant phytoplankton size class and functional type, with increases in picophytoplankton likely (Agawin *et al.*, 2000) at the expense of microphytoplankton. This has the potential to cause regime shifts and/or considerable restructuring of ecosystems as changes in phytoplankton community composition could lead to changes in zooplankton composition through consumer specificity, which could then be propagated up the food web. Indeed, global declines in marine primary productivity have already been recorded in recent decades (Capuzzo *et al.*, 2018; Gregg and Rousseaux, 2014, 2019; Rousseaux and Gregg, 2015; Roxy *et al.*, 2016) with wider ecosystem effects already apparent (Capuzzo *et al.*, 2018). It is worth noting that reported declines in marine primary productivity are not universal. Marrari *et al.* (2017) identified increasing trends in LMEs surrounding South America over the last ~20 years, however this could be the result of climate induced geographic shifts in plankton distribution which could also have negative consequences for marine ecosystems (Section 2.5.1.2).

2.5.1.2 High sensitivity

High sensitivity occurs in the PSI when primary productivity variability is amplified relative to environmental variability, for example in the Southern Ocean surrounding Antarctica (Appendix A Figure A-7), and when correlation between primary productivity and climate anomalies is infrequent (Figure 2.8) but strong (Appendix A Figure A-8). The infrequent correlation between Chl-a and climate anomalies indicates that these environments have low predictability from month to month, whilst the strength of correlations when they do occur suggests that primary productivity can be very responsive and hence has low resistance to climate in these regions. The low memory effects observed in these regions (Figure 2.7) suggest that whilst not being resistant to variability these regions could be resilient, with producers exhibiting an increased ability to recover from perturbations, however they also suggest that climate is the strongest driver of primary productivity anomalies thus resulting in high sensitivity.

High phytoplankton sensitivity in the PSI is largely concentrated in tropical and polar LMEs (Appendix A Figure A-5) typified by high productivity (Appendix A Figure A-3) and is likely caused by a combination of factors. First, organisms living at latitudinal extremes are more likely to be living closer to their environmental tolerance limits and adapted to a narrow abiotic niche (Sunday *et al.*, 2011, 2012), making them more vulnerable and less resistant to anomalous environmental conditions (Brierley and Kingsford, 2009; Poloczanska *et al.*, 2013). Combined with this the pace of climate change is most rapid in the tropics and polar regions (IPCC, 2018). The latitudinal gradient in high sensitivity observed in the PSI (Figure 2.2) could therefore be reflective of where the biggest changes in both the mean and variability of climate are currently occurring. As a result, even if climate anomalies are relatively low, mean conditions could have already increased to a point where species have been forced to the edge of their tolerance limits. Additionally, high anthropogenic exploitation in tropical and polar LMEs will have degraded these ecosystems and progressively lowered their resilience (Halpern *et al.*, 2008).

As well as being highly productive, high sensitivity tropical LMEs are also species rich (De Monte *et al.*, 2013; Righetti *et al.*, 2019; Soccodato *et al.*, 2016), supporting existing theoretical work showing a positive correlation between species richness and vulnerability to climate variability (Borrvall and Ebenman, 2008a; Burgmer and Hillebrand, 2011; Kaneryd *et al.*, 2012). Species rich environments are more vulnerable to variability due to increased interspecific competition reducing population sizes closer to extinction thresholds (Kaneryd *et al.*, 2012). Low correlation between species responses to environmental variability can further increase vulnerability as differential population fluctuations are further amplified by anomalous climate events (Borrvall and Ebenman, 2008a; Kaneryd *et al.*, 2012). Combined with lower mean population densities from high species richness, the increased climatic stability of tropical environments will promote specialist species with persistence traits adapted to a narrow abiotic niche, further reducing their ability to absorb climate fluctuations (Righetti *et al.*, 2019).

High productivity in tropical regions is typically driven by the upwelling of nutrient rich waters in EBUS (Section 2.5.1.1), or by the addition of nutrients from riverine run off in coastal areas (Reid *et al.*, 2003). These regions are also usually shelf areas which exhibit seasonal stratification and shallower mixed layer depths, both of which promote phytoplankton growth and are predominantly governed by temperature and wind (Mann and Lazier, 2006). Temperature and wind anomalies can therefore considerably alter biomass levels by causing a stronger stratification barrier to mixing if the temperature gradient increases above average, or by driving phytoplankton and nutrients out of the euphotic zone with increased wind-driven turbulence and upwelling (Bakun, 1990; Bakun *et al.*, 2015; Kahru *et al.*, 2010; Thomas and

Brickley, 2006). The Chile-Peruvian EBUS and Pacific equatorial currents are also heavily influenced by the El Niño Southern Oscillation (ENSO) index (Bakun *et al.*, 2015), which has been shown to affect the inter-annual variability of phytoplankton (Behrenfeld *et al.*, 2006) and oscillated between strong El Niño and La Niña years 6 times during the 2000-2013 time series. Whilst it might be expected that wind would be the biggest driver of sensitivity in EBUS governed by ENSO, as it is changes in atmospheric circulation that trigger a change from El Niño to La Niña, in the ocean the switch is reflected in temperature anomalies (Philander, 1990; Stenseth *et al.*, 2003). As such, temperature and radiation anomalies are the strongest drivers of sensitivity along the length of eastern boundary currents such as the Peru and Benguela currents (Figure 2.4) and have the strongest relationship with Chl-a in upwelling regions (Figure 2.5). Wind influence on sensitivity becomes more important as these currents diverge at the equator and are forced West along the South Equatorial currents due to the Coriolis force, with the displaced water being replaced by nutrient-rich upwelling from the Equatorial Counter Current. It is in these areas, such as the Gulf of Guinea, that high sensitivity occurs.

Not all high sensitivity areas in the PSI are EBUS. The waters off Costa Rica and Angola are also high sensitivity, high biodiversity hotspots due to the presence of thermal domes (Mazeika, 1967; Wyrtki, 1964). Thermal domes are caused by the interaction of wind and circulating currents allowing a central core of nutrient-rich cold water to upwell to the euphotic zone, whilst maintaining a deeper pycnocline in the waters surrounding the dome (Wyrtki, 1964). The domes can be seasonal (e.g. Angola dome; Mazeika, 1967) or persist year-round (e.g. Costa Rica; Wyrtki, 1964). The centre and size of the domes, and hence productivity levels, fluctuate from year to year in response to variability in currents driven by climate variability (Fiedler, 2002). The sub-polar regions of Antarctica are also dominated by a continuous band of high sensitivity. This region is highly productive due to upwelling caused by divergence between the Antarctic Circumpolar and Antarctic Subpolar currents, driven by opposing East and West wind drifts circling Antarctica (Mann and Lazier, 2006), however no single climate variable appears to dominate as a driver of sensitivity here (Figure 2.4).

Whilst the majority of the oceans were found to exhibit mid-low sensitivities and are likely resilient to environmental variability, high sensitivities being concentrated in regions of high phytoplankton biomass is concerning. These high primary productivity regions support some of the most highly productive, diverse and commercially valuable higher trophic level ecosystems (Bakun *et al.*, 2015). If current climate variability is already leading to amplified responses in primary productivity, the increased variability which is predicted to occur in these locations (Henson *et al.*, 2017) could cause more variable and less predictable patterns of

primary production, affecting resource availability and predictability throughout the food web. Furthermore, whilst the breadth of an organism's tolerance to environmental variability in terms of abiotic requirements is applicable at all trophic levels, higher trophic levels will also be affected by the breadth of food sources available to them. The wider ecosystem impacts of high phytoplankton sensitivity could therefore be far greater in tropical and polar ecosystems where specialist consumers are restricted by both their environmental niche and food availability, increasing the likelihood of extinction cascades (Kaneryd *et al.*, 2012). The expansion of Hadley cells, which govern sub-tropical atmospheric circulation and winds, could also see poleward shifts in both upwelling location and intensity in EBUS (Bakun *et al.*, 2015; Kang and Lu, 2012; Lu *et al.*, 2007; Rykaczewski *et al.*, 2015), leading to poleward transfers in productivity (Thomas *et al.*, 2012) and perhaps extending areas of high sensitivity along their extent.

2.5.2 Limitations and future research

A caveat of all satellite measures of primary productivity is that they can only record what is observable at the surface (Blondeau-Patissier *et al.*, 2014); production occurring either deeper within the water column or consumed by grazers is not recorded (Cullen, 1982; Huisman *et al.*, 2006). In many marine environments, especially during summer periods, the Chl-a and production maxima (which may be separate) can occur subsurface (Mann and Lazier, 2006), Cullen 2015). For example, if the pycnocline is within the euphotic zone and there is enough turbulence to cause some mixing across it but not enough to carry nutrients all the way to the surface, the highest nutrient availability for phytoplankton growth will be just above the pycnocline causing the production maxima to occur there (Mann and Lazier, 2006). The production maxima might also not be reflected by the Chl-a maxima due to zooplankton grazing decreasing phytoplankton biomass as it is produced. It is possible that increased mixing and a transport of productivity from the surface to near nutrient upwelling at the pycnocline could be interpreted as a considerable drop in phytoplankton biomass due to a wind anomaly, thus classifying an area as more sensitive than it actually is. However, high productivity within the water column occurs in those areas already identified by the PSI as the most productive and sensitive and so its exclusion should not have a major qualitative effect on the index or its interpretation.

Nutrient availability is a key governing factor of phytoplankton growth and whilst the climate variables chosen as phytoplankton drivers in the PSI act as proxies for nutrient availability, the explicit inclusion of nutrient availability as a driving variable would undoubtedly improve the index. Nutrient availability was not included in the PSI due to poor data availability; there are

currently no datasets with appropriate spatial and temporal coverage for oceanic nutrient levels. This is starting to improve however, with the development of datasets such as Yasunaka *et al's* (2014) nutrient dataset for the North Pacific basin. Whilst it is not currently possible to include nutrients as a driving variable in the global PSI, for areas where high resolution nutrient data is available the PSI could be recalculated at a regional level to include this. This could be particularly useful for accurately assessing the contribution of environmental variability to sensitivity in coastal areas receiving high riverine nutrient input (Reid *et al.*, 2003) such as Amazonia and the South China Sea (Weber *et al.*, 2019), as this will not be captured by wind-driven mixing and will be further affected in the future by variability in terrestrial precipitation (Harley *et al.*, 2006).

The global PSI provides a baseline against which responses to environmental variability across marine ecosystems can be further investigated. By highlighting regions with lower resilience to current environmental variability at the primary producer level, the index provides crucial guidance on where wider ecosystem impacts are likely to occur as a result of changes in resource availability and predictability and a changing environmental variability regime, thus focussing future research efforts. However, as found in the global distribution of phytoplankton responses to changing mean conditions (Häder *et al.*, 2014), phytoplankton responses to environmental variability are not consistent across ecosystems. Whilst there may be some consistency within ecosystems of a similar type such as EBUS, my results suggest that extrapolation across latitudes or functionally different ecosystems would be inappropriate. Even within similar systems, care would have to be taken to ensure regional differences in dominant climate driver influence on sensitivity were accounted for in any predictions of future change.

Given these caveats, the PSI is not intended to be viewed as a final, definitive picture of marine primary productivity responses to climate variability. However, it does provide an important – and global reference layer of primary productivity responses to current climate variability that can be used in its current form to guide future research, and as a data product it can be expanded and further developed. The broad correspondence between the climate weights (Figure 2.5) and climate variability influence on sensitivity (Figure 2.4), can help to guide monitoring programmes aimed at predicting outcomes of future variability as those variables most closely correlated with primary productivity also determine climate influence on primary productivity. More generally, by applying the same basic methodology as used for the terrestrial VSI (Seddon *et al.*, 2016), there is also potential to link the two indices to create a truly global picture of the sensitivity of primary productivity to environmental variability (Chapter 3). This is of interest because, despite differences in the typical spatial and temporal scales of

climatic variability in the two realms (Steele, 1991b), they can be affected by similar climatic processes (e.g. ENSO (Philander, 1990) and the North Atlantic Oscillation (Ottersen *et al.*, 2001)), and there is some evidence that human activity is causing marine and terrestrial variability regimes to become more similar (Steele, 1989, 1991b). Equally important, the PSI provides an additional environmental layer which can be used to better understand the environmental drivers of spatial and temporal patterns in the distributions of species at higher trophic levels, including those from which humanity most benefits.

3 A global picture of sensitivity: Comparing the sensitivity of marine and terrestrial primary productivity to environmental variability

3.1 Abstract

Marine and terrestrial ecology have traditionally been viewed as separate disciplines due to the existence of 'fundamental differences' between the realms (Steele, 1985), however the need to determine how both realms will respond to a changing climate has resulted in an increased focus on cross-realm approaches to ecology. Primary productivity provides an ideal foundation for a cross-realm, macroecological approach, as it can be directly associated with both environmental data (e.g. Hays *et al.* 2005) and higher trophic level responses (e.g. Visser and Holleman, 2001). Furthermore, similarities in cross-realm primary productivity responses to environmental change have already been demonstrated (e.g. Chambers *et al.*, 2013). Here, I combine the Phytoplankton Sensitivity Index (PSI) developed in Chapter 2 with Seddon *et al's* (2016) Vegetation Sensitivity Index (VSI) for the terrestrial realm. I investigate the potential of this Combined Sensitivity Index (CSI) to bridge the marine-terrestrial divide in terms of its ability to aide in the identification of global cross-realm patterns of sensitivity at a range of spatial scales (global degrees of latitude, hemispheres and biogeographic regions), to provide explanatory power in terms of its environmental drivers and to facilitate analyses of its temporal dynamics. A global, cross-realm latitudinal gradient of increased primary productivity sensitivity relative to environmental variability in the tropics and towards the poles is identified at both degree of latitude and hemispheric scales in the CSI and within each individual index; regional scales are less effective for reliably demonstrating the gradient. The influence of climate drivers on sensitivity shows strong realm dependence, with marginal differences between the influence of driving climate variables present in the marine realm compared to strongly varied influence in the terrestrial realm. In combining these indices, a truly global macroecological view of environmental variability influence on primary productivity is provided, that can be used as a basis on which to examine the responses of communities at higher trophic levels.

3.2 Introduction

In 1985 John Steele published the first of a series of papers advocating the need for increased integration of marine and terrestrial ecology. Despite the commonly held view of the time that 'fundamental differences' between the two realms prevented such research, Steele (1985, 1991a, 1991b) argued that at appropriate spatial and temporal scales cross-realm comparisons were both possible and more importantly, valid, with the potential to provide rigorous testing of ecological hypotheses and reveal generalised patterns that held across realms. Over the last three decades the idea of fundamental differences between marine and terrestrial realms has persisted (Dawson and Hamner, 2008) and continued to manifest in the ways we teach, publish and develop marine and terrestrial disciplines (Chase, 2000; Menge *et al.*, 2009; Rafaelli *et al.*, 2005; Stergiou and Browman, 2005). The global scope of the threat of climate change has made this separation increasingly disadvantageous, and the need to determine how both realms will respond to the growing pressures of a changing climate has resulted in an increasing number of studies now beginning to examine the benefits of a cross-realm approach to ecology (Blowes *et al.*, 2019; Pinsky *et al.*, 2019; Wiens, 2016). However, differences in the spatial and temporal scales of biological and physical processes in marine and terrestrial environments (Figure 1.1; Steele, 1991a) can prove problematic for comparative studies when comparisons are attempted at the same scale in each realm (Steele, 1991a).

The unifying potential of macroecology for marine and terrestrial research was identified by Steele (1991b), who proposed that looking at a macroecological scale could overcome the challenges posed by the different temporal and spatial scales encountered in marine and terrestrial systems. Macroecology can be used both to discern generalised patterns and reveal key differences in the abiotic and biotic features of marine and terrestrial data (Dawson and Hamner, 2008; Lawton, 1999; Rafaelli *et al.*, 2005; Webb, 2012) due to the relative simplicity of phenomena which are emergent at large scales, compared to the complexity when looking at a community ecology level (Lawton, 1999). This simplifying approach is not without problems, however. Whilst macroecological patterns such as the species abundance distribution and latitudinal diversity gradient provide valuable insights on global demography, their explanatory power in isolation is limited (Fisher *et al.*, 2008, 2010; McGill, 2003). To further improve the utility of macroecological patterns, a more dynamic, mechanistic macroecology with temporal and spatial data implicitly included in analyses is developing to aide in the interpretation of the underlying processes behind observed patterns (Beck *et al.*, 2012; Fisher *et al.*, 2010; McGill, 2010a; McGill *et al.*, 2007; Tyler *et al.*, 2012; Webb, 2012). The prevalence of cross-realm climatic linkages (discussed below) makes it reasonable to

assume that variability in macro-scale patterns of climate will affect marine and terrestrial realms in tandem, however whether there are corresponding similarities in the sensitivity of their responses across realms, and hence in their resilience to environmental variability, is currently unknown.

Marine and terrestrial systems are known to both be affected by large scale patterns of climate variability, due to tight coupling between ocean and atmospheric processes (Steele, 1991b; Steele and Henderson, 1994). For example, the El Niño Southern Oscillation (ENSO; Philander, 1990) and the North Atlantic Oscillation (NAO) drive the micro-scale weather conditions which determine the physical and biological processes controlling primary productivity in freshwater, terrestrial and marine systems (Blenckner and Hillebrand, 2002; Mysterud *et al.*, 2003; Ottersen *et al.*, 2001). Despite the presence of such cross-realm linkages, the different physical mediums of marine and terrestrial environments (water versus air based) result in contrasting levels of inherent environmental variability manifesting in each realm (Steele, 1985). This level of inherent environmental variability can be better described in terms of its autocorrelation structure and position on the colour spectrum (Halley, 1996; Keshner, 1982). Marine ecosystems, which have low inherent environmental variability, are characterised by a 'red noise' variability structure (Steele, 1985) due to the buffering effects of the ocean causing positive temporal autocorrelation within environmental time series (Rohani, 2004). Terrestrial environments on the other hand are typified by 'white noise' (Steele, 1985), with environmental time series that are temporally uncorrelated and highly variable at both short and long temporal scales (Halley, 1996; Rohani, 2004). Whilst predominantly a characteristic of abiotic variables (Weber and Talkner, 2001), variability structure can also interact with demographic processes to influence life history traits (Dawson and Hamner, 2008). For example, specialist species are favoured in predictable, reddened environments, whereas generalists are favoured in white environments with greater stochasticity (Righetti *et al.*, 2019; Suryan *et al.*, 2009; Weimerskirch, 2007). Coupled with large differences in the temporal scales of functionally equivalent marine and terrestrial organisms (e.g. marine phytoplankton live for a matter of days, compared to centuries for trees; Steele, 1991b), anomalous environmental conditions could be expected to elicit different responses in marine and terrestrial ecosystems.

Primary productivity provides an ideal foundation for a cross-realm macroecological pattern as it can be directly associated with both environmental data (e.g. Hays *et al.* 2005) and higher trophic level responses (e.g. Visser and Holleman, 2001), due to the dependence of primary producers on abiotic forcing and their essential role at the base of marine and terrestrial food webs. Cross-realm similarities in primary productivity responses to environmental change have

already been demonstrated for phenology (Chambers *et al.*, 2013; Parmesan and Yohe, 2003; Root *et al.*, 2003; Thackeray *et al.*, 2010), with warming temperatures causing earlier leaf emergence, flower blooming and lengthened growing seasons in terrestrial systems (Mysterud *et al.*, 2003; Post and Stenseth, 1999), comparable to earlier bloom times observed in marine phytoplankton (Edwards and Richardson, 2004b). Furthermore, whilst terrestrial primary producers are typically not as closely coupled to scales of environmental variability as marine producers (Steele, 1991b), their responses to environmental variation are similarly variable across space (von Holle *et al.*, 2010) and trophic level (Durant *et al.*, 2007; Thackeray *et al.*, 2010, 2016) as in marine systems, with trophic mismatch and wider ecosystem consequences an inevitable result (Durant *et al.*, 2005; Stenseth and Mysterud, 2002; Toszogyova and Storch, 2019; Visser and Holleman, 2001). Environmental variability is also known to modify global gradients of primary producer diversity and richness (Righetti 2019) and can differentially effect higher trophic level patterns of richness depending on the mean productivity of an area, with high variability and high mean productivity associated with reductions in richness (Toszogyova and Storch, 2019). As a result, primary resource availability and predictability can act as both an explanatory and predictive mechanism for population responses to environmental change.

The Phytoplankton Sensitivity Index (PSI) developed in Chapter 2 successfully identified marine regions in which primary productivity is especially sensitive to different elements of climate variation, thus indicating where environmental variability is influencing marine primary productivity resilience at a global scale. Here, I combine the PSI with Seddon *et al's* (2016) corresponding Vegetation Sensitivity Index (VSI) for the terrestrial realm, which determines the sensitivity of global terrestrial primary productivity to variation in temperature, water availability and cloud cover, over a 14-year time series (2000-2013). I investigate the potential of this Combined Sensitivity Index (CSI) for primary productivity sensitivity relative to environmental variability to bridge the marine-terrestrial divide, in terms of its ability to aide in the identification of global cross-realm patterns and potential to direct future research into higher trophic level responses. I investigate if differences in the spatial and temporal scales of marine and terrestrial environments can be overcome by examining patterns in sensitivity at a range of spatial scales, including global degrees of latitude, hemispheres and biogeographic regions. Exploring patterns in sensitivity across global degrees of latitude, I test whether the latitudinal gradient in sensitivity qualitatively identified in the PSI (Chapter 2), holds quantitatively in both realms. A hemispheric scale will show if there are any key differences in primary productivity responses in Northern and Southern hemispheres, shedding light on the potential disadvantages of the current northern, temperate bias in climate change research. By incorporating analyses at a regional scale I examine at what spatial scale patterns are best

captured in each realm. I also compare and contrast patterns of sensitivity within each realm to ascertain at what level primary productivity responses to climate variability are realm dependent. To be effective as a mechanistic and dynamic macroecological pattern, the CSI needs to provide both explanatory power in terms of its environmental drivers and facilitate analyses of its temporal dynamics (Fisher *et al.*, 2008, 2010). I therefore also examine patterns in climate driver influence on sensitivity at both global and regional spatial scales across realms and explore links between the temporal scales of environmental and primary productivity variability along gradients of sensitivity.

3.3 Materials and Methods

3.3.1 The Vegetation Sensitivity Index (VSI)

Full details of the methods used to calculate the VSI can be found in Seddon *et al.* (2016). A summary of the input variables used and any differences in methodology between the calculation of the PSI (Chapter 2, 2.3.2) and VSI are given below. All code and raw data for calculating the VSI was downloaded from the Oxford University Research Archive repository (available at: https://ora.ox.ac.uk/objects/uuid:896bf37f-a56b-4bc0-9595-8c9201161973).

As with the PSI, a 14 year (2000–2013) monthly time series was used for all variables for the VSI. The Moderate Resolution Imaging Spectroradiometer (MODIS) MOD13C2 Enhanced Vegetation Index (EVI; Solano *et al.*, 2010) was used as a measure of terrestrial primary productivity. The EVI measures vegetation canopy greenness and employs a feedback system to minimise canopy-soil variations and provide higher sensitivity in high biomass regions than earlier products, such as the Normalized Difference Vegetation Index (NDVI) (Justice *et al.*, 1998; Solano *et al.*, 2010). The EVI also saturates less easily in high density areas than the NDVI (Solano *et al.*, 2010). Whilst other satellite products are available that more closely correlate with total terrestrial producer biomass, by measuring just ‘greenness’ the EVI only records the photosynthetic component of terrestrial producers (i.e. leaves versus tree trunks) and therefore more closely correlates with the ocean colour measurements used to calculate the PSI. Precipitation, cloudiness and temperature were used as driving climate variables of productivity, which were also obtained from MODIS derived products. The MOD07_L2 Atmospheric Profile product was used for air temperature. An insolation proxy was developed for cloud cover based on the MOD35_L2 Cloud Mask product, which gives a ratio of the proportion of cloudy to clear sky days per pixel. For precipitation, a ratio of actual evapotranspiration to potential evapotranspiration was used, derived from the MOD16 Global Evapotranspiration product. All variables were available at, or transformed to, 5 km spatial

resolution on a geographic projection. To calculate the VSI, minimum thresholds were used for EVI and temperature; pixels with EVIs < 0.1 were excluded due to being predominantly barren, and months with mean temperatures < 0 °C were excluded. All other methods are as described for the PSI in Chapter 2, Section 2.3.2.

Whilst the Chlorophyll-a (Chl-a) and Photosynthetically Available Radiation (PAR) variables used to calculate the PSI were available at high spatial resolutions (4 km), the coarser resolution (0.25°) of Sea Surface Temperature and Wind (SST/W) satellite data available for the marine environment prevented the PSI from also being calculated at 5 km resolution. It was instead calculated at 9 km resolution as described in Chapter 2. This difference in spatial resolution between the VSI and the PSI prevented a single global index from being produced, however the two indices were combined into a single data frame post-calculation to enable global analyses of sensitivity.

3.3.2 Selecting biogeographic regions for spatial analyses

Several methods exist for partitioning the world's oceans into defined regions (reviewed in Krug *et al.* (2017)). Most notably, Longhurst (1995, 2007) and Sathyendranath *et al.* (1995) categorised the global oceans into 4 primary biomes (Coastal, Westerlies, Trades and Polar) and 54 biogeochemical provinces based on the physical parameters expected to drive phytoplankton production. Here, I use Longhurst's biogeographic provinces as a foundation for further analysis within the PSI. As the PSI is a global snapshot of the combined time series with seasonality removed, the fixed boundary approach of Longhurst's biomes is considered appropriate. Satellite data retrieval in polar regions can be inefficient through large parts of the year due to limited light availability, leading some studies to exclude the Polar biomes from analyses (e.g. Roy, 2018). I retained all of the biomes for initial analyses however, to establish if anomalous results required their removal. For the terrestrial realm, the Ecoregions2017 (Dinerstein *et al.*, 2017) classification system was used. Ecoregions2017 is an updated version of the Terrestrial Ecoregions of the World (TEOW; Olson *et al.*, 2001) regionalisation and categorises the world into 8 biogeographic realms, each containing 14 possible biomes further split into a total of 846 distinct ecoregions. 846 was deemed too many regions for our purposes and so regions were grouped solely by biogeographic realm and biome, giving a total of 63 distinct regions. Full details and mapped representations of the regionalisations can be found in Appendix B (Figure B-1-Figure B-3). For consistency with the Longhurst scheme, hereafter I refer to the eight Ecoregions2017 biogeographic realms as 'biomes' and the fourteen biomes as 'provinces'. I use 'realm' to distinguish between the marine and terrestrial environment.

3.3.3 Scales of sensitivity

The PSI and VSI were first mapped together to produce a Combined Sensitivity Index (CSI) and visualise the global distribution of the sensitivity of primary productivity relative to climate variability. Due to right skew in the indices a stretch was applied to the mapped colour scale in QGIS, saturating values either side of the top and bottom 2.5 standard deviations of the indices (the default in ArcGIS, and as used in Seddon *et al.* (2016)). This maximised the clarity of geographical variability within the central 95% of the indices, whilst saturating fewer than 5% of pixels. A Pearson's correlation test was performed to determine if there was a simple relationship between the median sensitivity of both the CSI and each individual index with absolute degrees of latitude. To test whether the observed range of sensitivity varied with latitude at a global scale, the correlation between the 2.5%-97.5% (95%) range in sensitivity and absolute degrees of latitude was also calculated for the three indices. To account for potentially more complex relationships, Generalized Additive Models (GAMs) were fitted to each index individually and to the combined index. GAMs were modelled using the `mgcv` package (Wood, 2011) in R version 3.3.2 (R Core Team, 2018), with absolute latitude fitted as a smooth term (grouped by hemisphere) using the default thin plate regression splines, a Gaussian distribution and identity link function. Each model was weighted by the number of pixels present in each degree of latitude. To investigate similarities in within realm hemispheric trends of sensitivity, the difference between median sensitivities and the 95% range of sensitivities at corresponding Northern and Southern latitudes were calculated for each index. To investigate similarities in between realm hemispheric trends of sensitivity, quadratic linear models were fitted to the median and 95% range of sensitivities per degree of latitude for each hemisphere, with realm fitted as an interaction. Due to the disparity in land and ocean extent between the hemispheres, models were fitted up to -60° Latitude in the Southern hemisphere and up to 80° Latitude in the Northern hemisphere.

To establish if latitudinal differences in sensitivity were detectable at smaller spatial scales, the above analyses were repeated at the province level (as defined in Section 3.3.2) for both the PSI and VSI, with province centroid latitude used as the measure of absolute latitude. Relationships within and between biomes and sensitivity for each index were further investigated using a linear mixed effects model with random intercepts (`lme4`; Bates *et al.*, 2012). Sensitivity was modelled as a function of biome as a fixed effect in the model, with province nested within biomes fitted as random effects to account for non-independence within the data due to geographic structuring (Harrison *et al.*, 2018b). Finally, linear models were fitted to the $\log_{10}$-transformed mean sensitivity of each province against $\log_{10}$-transformed variance, to test for mean-variance relationships in each index.

3.3.4 Temporal dynamics of sensitivity

I predicted that similar realm-independent characteristics in primary productivity and climate variability would be found along gradients of sensitivity. To investigate this, the temporal dynamics of the raw time series of the input variables were examined. For initial exploratory analyses, marine and terrestrial coordinates were selected from the global sensitivity index map that were coastally adjacent and/or latitudinally equivalent and of comparable sensitivity. Time series were extracted for 1° grid squares around the selected coordinates for the VSI and 2° grid squares for the PSI to ensure a similar number of pixels were analysed for each index (400 and 493 for the VSI and PSI respectively). Mean monthly values were then calculated for Chl-a and EVI for each grid square across the time series, and monthly *z*-score anomalies were calculated for Chl-a, EVI and the climate variables. The *z*-score anomalies provide a standardised measure of variability across variables by transforming monthly values to the number of standard deviations the value is away from the 14-year monthly mean (See Chapter 2, Equation 2 for full calculation details).

After initial inspection of the mean and anomaly time series plots, spectral analysis was performed on a wider range of coordinates to investigate trends in the temporal autocorrelation of environmental and primary productivity variability within the time series, across gradients of sensitivity. Spectral analysis quantifies the temporal autocorrelation within a time series, which can then be used to produce colour coefficients, classifying variability as white (no autocorrelation) or reddened (positive autocorrelation). For the spectral analysis, 50 pixels were randomly selected from each index with low (0-20), medium (40-60) and high (80-100) sensitivities, using a seed of 27 (150 pixels selected in total per index). As with the initial exploratory plots, the raw time series for all variables were extracted from pixels within a 1° and 2° grid square from the randomly selected pixel for the VSI and PSI respectively, and *z*-score anomalies were calculated. Spectral densities and frequencies were then calculated for each time series using the `spec.pgram` function in R, using the default settings for zero-padding and tapering. Spectral density can only be calculated on complete time series so pixels with missing data were excluded from the analyses. The final number of locations included in the analysis for each variable and sensitivity index are summarised in Appendix B, Table B-1. The spectral component (ß) or 'noise', was estimated following Vasseur and Yodzis (2004) as the negative slope of a linear regression between $\log_{10}$ spectral density and $\log_{10}$ frequency. Each time series was then categorised as white ($0 \leq ß \leq 0.5$), pink ($0.5 < ß \leq 1.5$) or red ($1.5 < ß \leq 2$). The mean sensitivity of pixels within each grid square was also calculated to rank ß by sensitivity level. A linear regression model was fitted to each variable's ß values to test for effects of mean sensitivity and realm on noise frequency.

3.3.5 Climate influence on sensitivity

To identify geographic variation in the influence of climate variability on sensitivity, composite maps were produced for the global index. These maps allocate each climate variable to a separate colour band and plot the highest valued (i.e. most important) variable per pixel. To determine the contribution of an individual climate variable's variability on final sensitivity, the coefficient-weighted sensitivities for each variable were extracted and plotted before being combined to give the final index (see Chapter 2, Section 2.3.2.2 for full details). To visualise regional differences in correlation strength between primary productivity and climate variability, a composite map was also produced for the climate weights of each index (see Chapter 2, Section 2.3.2.1 for climate weight details). Whilst these maps show which climate variable has the highest influence per pixel, no information is given on the interactions between climate variables across regions.

To quantify the relative importance of each climate variable's anomalies (climate variability normalised by mean and variance) on the final sensitivity metric and to identify interactions between them at regional scales, a boosted regression tree (BRT) analysis was performed using R's `gbm` package (Ridgeway, 2017), with primary productivity sensitivity modelled against the three climate drivers' anomalies for each index. BRT models combine regression trees and boosting to model complex data and improve predictive performance (Elith *et al.*, 2008). Regression trees use recursive binary splits to partition data into smaller, simpler segments which models can be fitted to. With boosting, trees are added sequentially and adaptively to the residuals of prior trees without altering the trees already fitted, with the final model being a linear combination of thousands of trees (Elith *et al.*, 2008). BRT models offer several advantages over other modelling techniques as they can inherently model variables of different classes (e.g. continuous, binomial, categorical), can fit complex non-linear relationships with interactions between variables, require no data transformations and are able to handle missing data and outliers (Elith *et al.*, 2008).

The two main parameters which must be set for a BRT are tree complexity (*tc*) and learning rate (*lr*). *tc*, the number of nodes or splits a tree can have, is used to model interactions between the predictor variables (Elith *et al.*, 2008). A *tc* of 1 means that no interactions are modelled. *lr* determines the amount of influence each new tree has on the model, a smaller *lr* increases the number of trees required (Elith *et al.*, 2008). Cross-validation (CV) error is used to select the values of *tc* and *lr* which produce the best fitting model. With each iteration (addition of a tree), CV tests a model fitted to a training fraction of the dataset against the remaining portion of the dataset and produces an error value (Elith *et al.*, 2008). Data is selected randomly from the training fraction without replacement using a bag fraction

parameter to introduce stochasticity, i.e. a bag fraction of 0.5 will randomly select 50% of the training dataset at each iteration to fit the model (Elith *et al.*, 2008). This process determines the optimum number of trees, *tc* and *lr* required for lowest error, which is then applied to the full dataset for the final model.

To account for spatial variation in sensitivity and climate driver influence, the BRT models were derived at the province level with the best fitting model selected from learning rates of 0.01, 0.005, 0.001 and 0.0005 and tree complexities of 4, 6, 10 and 20. As recommended by Elith *et al.* (2008), a bag fraction of 0.5 and training fraction of 0.8 were also used in the initial parameter set up, with a Gaussian distribution and a maximum number of 10,000 trees fitted. Each dataset was shuffled before use to ensure the training fraction wasn't geographically ordered and the same random seed (27) was set for each model run. Best fitting models were those with the lowest CV error and a minimum of 1000 trees. As I was interested in the interplay between the three climate variables on sensitivity in each province, further tests were not conducted to see if variables could be dropped to further improve model fit. Three VSI biomes (AF08, AU11 and IN10) could not be included in the BRT analysis as they contained too few pixels for a model to be fitted. The final input parameters for the best BRT model fit for each province can be found in Appendix B Table B-2 and Table B-3 for the PSI and VSI respectively.

From the final model output, the relative importance of each variable's anomalies to sensitivity prediction were extracted and plotted for each province to conduct regional comparisons of the relative influence of each climate variable on sensitivity. These values are scaled between 0-100 to enable comparison between variables, with low values indicating that the variable is not relevant for sensitivity prediction. To compare the BRT model output for climate variable influence with the climate interactions observed within the indices, the climate composite maps were also reproduced as normalised bar plots with values for sensitivity influence and climate weights averaged over each province.

Data analyses were conducted in the R project for statistical computing (R Core Team 2018, version 3.3.2) using the `caret` (Jed Wing *et al*., 2018), `cowplot` (Wilke, 2018), `data.table` (Dowle and Srinivasan 2018), `dev.tools` (Wickham *et al*., 2018), `dplyr` (Wickham *et al*., 2018), `ggplot2` (Wickham, 2016), `grateful` (Rodriguez-Sanchez, 2017), `lattice` (Sarkar, 2008), `Matrix` (Bates and Maechler, 2018), `raster` (Hijmans, 2017), `readr` (Wickham *et al*., 2017), `reshape2` (Wickham, 2007), `rgdal` (Bivand *et al*., 2018), `rgeos` (Bivand and Rundel, 2018), `sp` (Pebesma and Bivand, 2005), `viridis` (Garnier, 2018a), `viridisLite` (Garnier, 2018b) and `zoo` (Zeileis and Grothendieck, 2005) packages. Image processing was carried out in QGIS and R.

3.4 Results

3.4.1 Scales of sensitivity

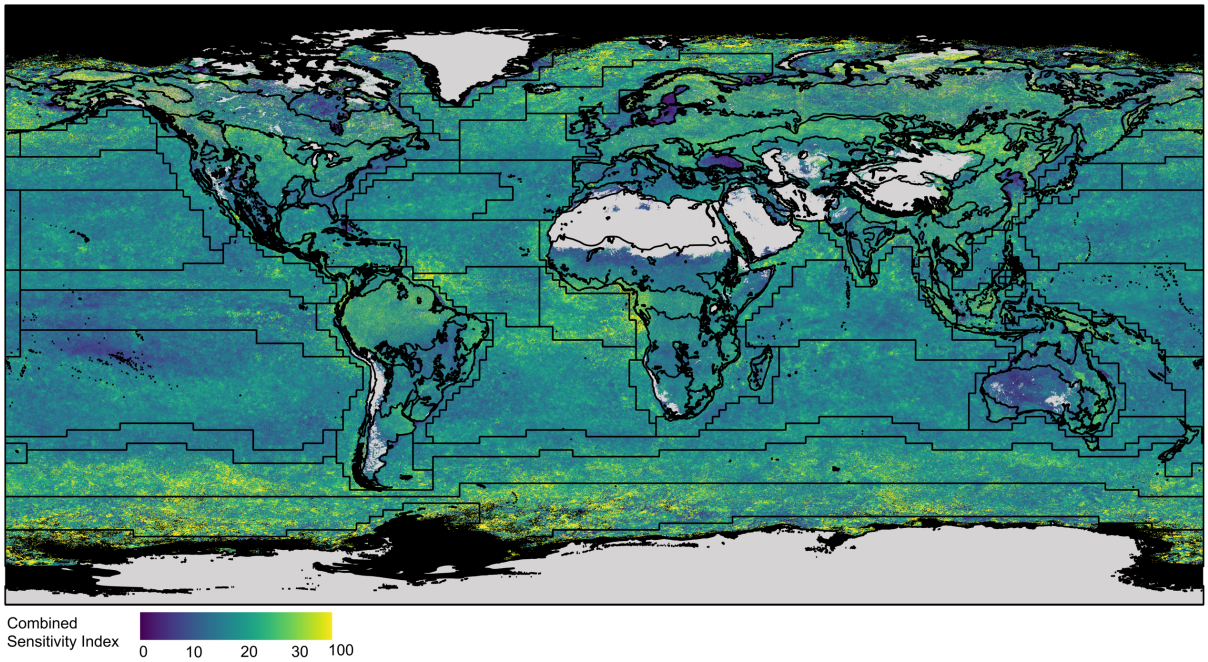

Figure 3.1: Combined Phytoplankton and Vegetation Sensitivity Indices (P/VSI) with regionalisation. A global map of primary productivity sensitivity relative to variability in three climate variables (PSI: sea surface temperature, sea surface winds, photosynthetically available radiation; VSI: temperature, precipitation, cloudiness). The index ranges from 0 (low sensitivity) to 100 (high sensitivity). The sensitivity index is overlaid with Longhurst's Marine Biogeographic Regions (PSI) and Ecoregions2017 (VSI) boundaries (black lines), which are used for all spatial analyses. Full details of biomes and provinces used can be found in Appendix B (Figure B-1-Figure B-3). Due to right skew in the data and the volume of data points, the colour scale has been band shifted by 2.5 standard deviations (the default in ArcGIS) to better reflect the spread of the data. Pixel resolution, 9 km (PSI), 5 km (VSI); time period, 2000-2013. Areas in black indicate no data availability. Terrestrial areas in grey are predominantly barren areas, created using a minimum vegetation threshold. Continental outlines were modified from a shapefile using QGIS.

Combining the VSI with the PSI produces a global, cross-realm picture of primary productivity sensitivity to climate variability, from which patterns in amplified primary productivity responses relative to climate variability can be discerned at a range of scales. In both indices, sensitivity ranges from 0 (low sensitivity) to 100 (high sensitivity). My results show that latitudinal gradients in global primary productivity sensitivity are realm-independent, with high sensitivity marine areas carrying over terrestrial landmasses in sub-polar and equatorial regions (Figure 3.1). Likewise, the mid-low sensitivities of the major ocean basins carry across landmasses at their respective latitudes (Figure 3.1). Both median sensitivity ($r = 0.56$, $P < 0.001$) and the 95% range of sensitivities ($r = 0.78$, $P < 0.001$) are significantly, positively correlated with absolute degree of latitude at a global scale. GAM analysis further confirmed that significant positive correlations exist between median sensitivity ($P < 0.001$, deviance explained = 92.6%), the 95% range of sensitivities ($P < 0.001$, deviance explained = 98.8%) and absolute degrees

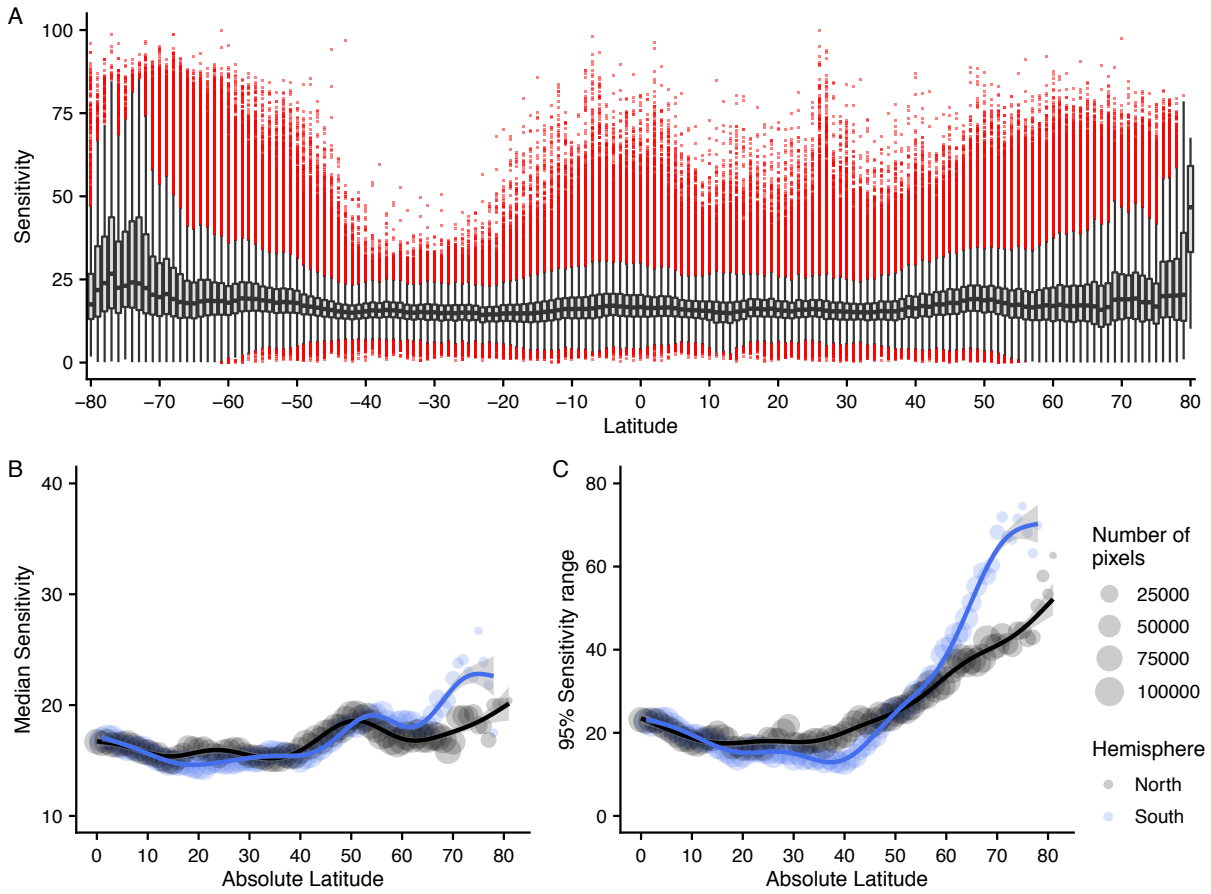

Figure 3.2: Latitudinal gradients of sensitivity for the combined index. Boxplot showing the spread of sensitivity for each degree of latitude for the combined sensitivities of the marine PSI and terrestrial VSI (A), and the results of generalized additive models (GAM) fitted to the median (B) and 95% range (97.5% quantile–2.5% quantile) (C) of sensitivities for each degree of latitude, by hemisphere. GAMs are weighted by the number of pixels in each latitudinal band.

of latitude in each hemisphere, with similar non-linear trends present in each (Figure 3.2). In the Northern hemisphere median sensitivity peaks at 24.7°N and 50.6°N and troughs at 15.0°N, 34.9°N and 60.3°N, compared to peaks at 32.9°S, 54.0°S and 75.5°S and troughs at 20.9°S, 38.7°S and 61.3°S in the Southern hemisphere (Figure 3.2B). The 95% range of sensitivities peaks at 25.0°N, 25.8°S and 74.9°S, and troughs at 16.4°N, 31.4°N, 20.7°S and 37.0°S. For both the median and 95% range of sensitivities, the highest values occur in the Southern hemisphere (Figure 3.2).

Within the individual indexes average sensitivity is similar (Mean sensitivity: VSI, 18.02 ± 7.12 sd; PSI, 16.98 ± 6.72 sd), with each index also exhibiting a similar proportion of sensitive to non-sensitive regions (number of pixels with sensitivity > 50: number of pixels with sensitivity ≤ 50; PSI, 0.006; VSI, 0.004 equating to areas of 304,137 km^2 and 85,905 km^2 out of a total of 46,706,040 km^2 and 23,732,010 km^2 for the PSI and VSI respectively). Median sensitivity is significantly positively correlated with degree of absolute latitude in both the PSI ($r = 0.54$, $P < 0.001$) and VSI ($r = 0.41$, $P < 0.001$) in a non-linear relationship (Figure 3.3A-B; Figure 3.4A-

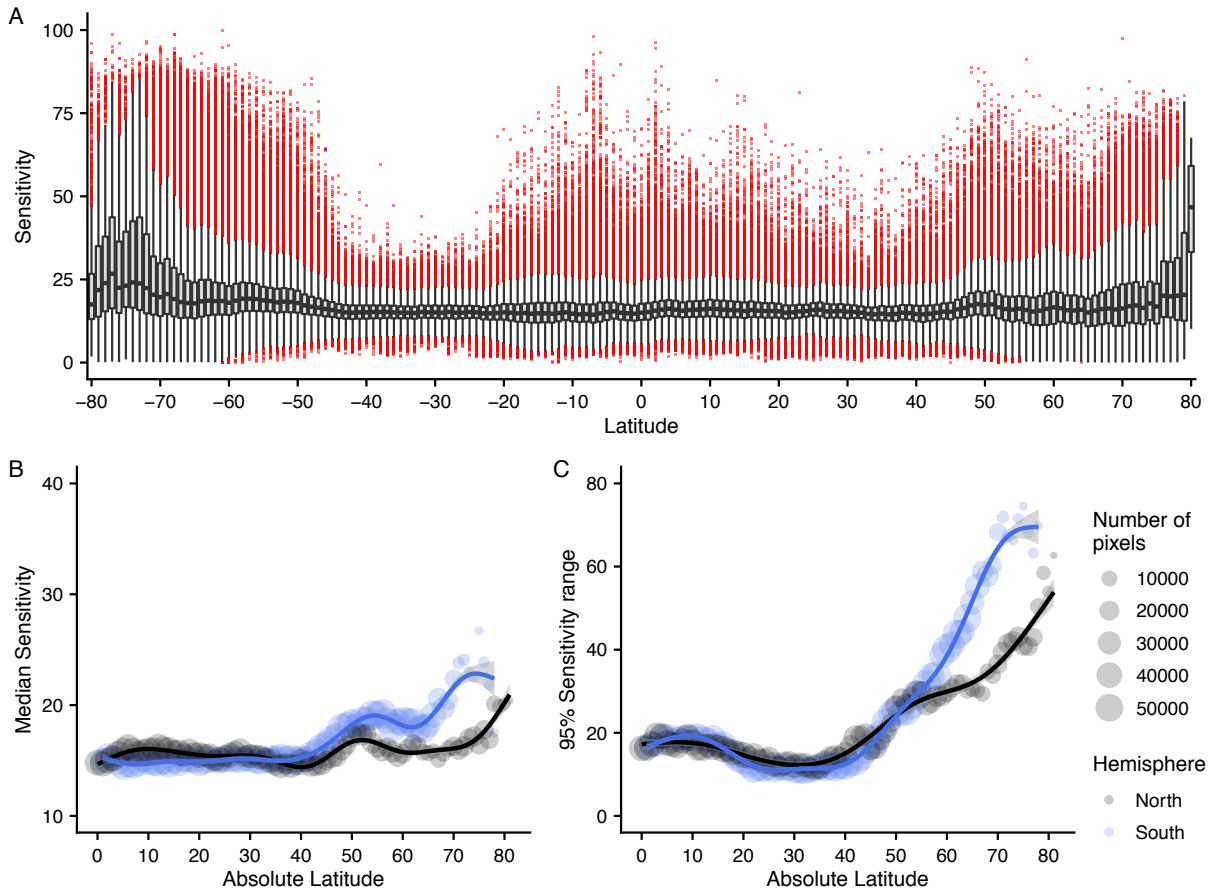

Figure 3.3: Latitudinal gradients of sensitivity in the marine PSI. Boxplot showing the spread of sensitivity for each degree of latitude in the PSI (A), and the results of generalized additive models (GAM) fitted to the median (B) and 95% range (97.5% quantile–2.5% quantile; C) of sensitivities for each degree of latitude, by hemisphere. GAMs are weighted by the number of pixels in each latitudinal band.

B), present in both Northern and Southern hemispheres (GAM: PSI, $P < 0.001$, deviance explained = 95.1%; VSI, $P < 0.001$, deviance explained = 86.8%). The variability of this relationship does however differ between the two realms. In the PSI, median sensitivity in both hemispheres shows marginal changes between 0-40° Latitude, before increasing towards polar latitudes (Figure 3.3B). The VSI on the other hand shows considerably more variation in median sensitivity in both hemispheres, even at low latitudes (Figure 3.4B). In the Northern hemisphere median sensitivity peaks at 9.7°N, 25.7°N and 53.7°N in the PSI (Figure 3.3B) and at 24.7°N and 48.4°N in the VSI (Figure 3.4B). Troughs occur at 20.9°N, 38.8°N and 65.5°N in the PSI versus 13.5°N, 34.3°N and 65.0°N in the VSI. In the Southern hemisphere median sensitivity peaks at 17.7°S, 53.8°S and 74.9°S in the PSI (Figure 3.3B) and 38.0°S in the VSI (Figure 3.4B). Troughs occur at 8.1°S, 37.9°S and 61.3°S in the PSI and at 20.9°S and 47.8°S in the VSI. Whilst the number and respective latitudes of peaks and troughs are similar in each realm, the magnitude of change is much larger in the VSI. Despite this difference, both marine and terrestrial indexes exhibit similar median sensitivities across hemispheres at equivalent latitudes (Figure 3.5).

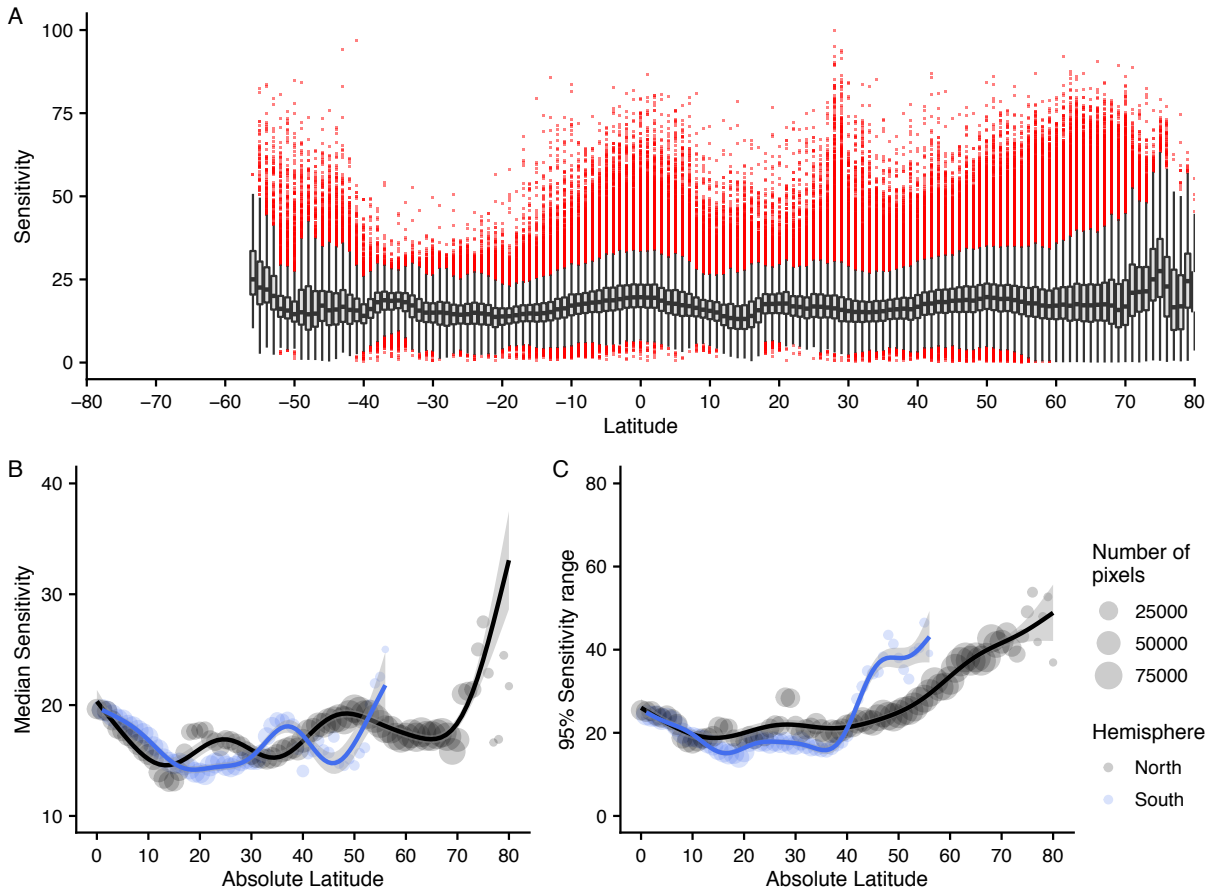

Figure 3.4: Latitudinal gradients of sensitivity in the terrestrial VSI. Boxplot showing the spread of sensitivity for each degree of latitude in the VSI (A), and the results of generalized additive models (GAM) fitted to the median (B) and 95% range (97.5% quantile–2.5% quantile; C) of sensitivities for each degree of latitude, by hemisphere. GAMs are weighted by the number of pixels in each latitudinal band

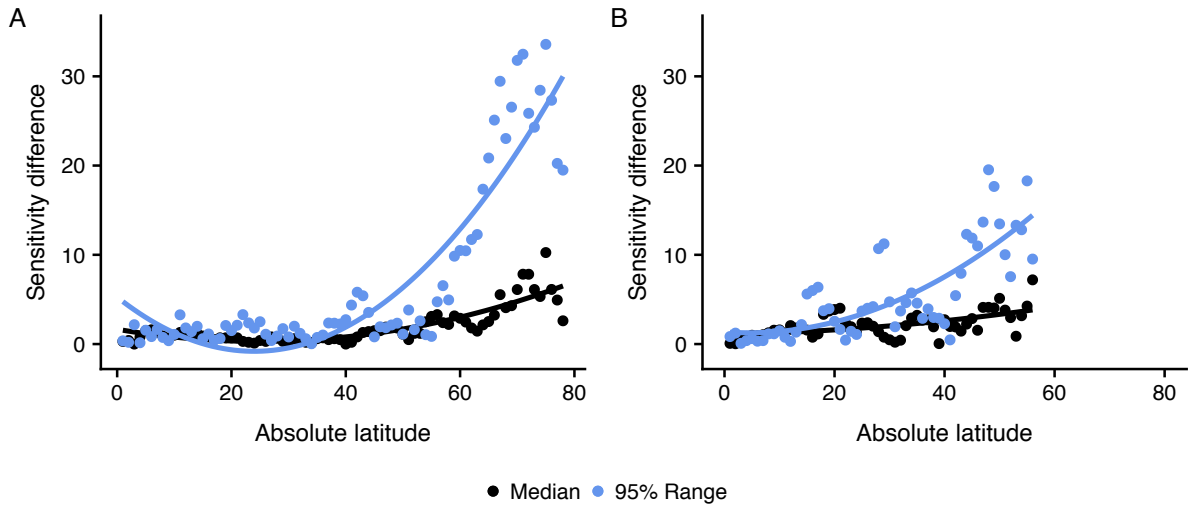

Figure 3.5: Hemispheric differences in sensitivity in the PSI and VSI. The difference between median sensitivity and the 95% range of sensitivities in the Northern and Southern hemispheres at single, absolute degrees of latitude, with quadratic linear models fitted to each variable, in the PSI (A) and VSI (B).

The 95% range of sensitivity values are more strongly correlated with degree of absolute latitude than median sensitivities in both the PSI (r = 0.77, $P < 0.001$) and VSI (r = 0.77, $P < 0.001$), with an exponential increase in ranges occurring above ~40 °Latitude (Figure 3.3C; Figure 3.4C). As with median sensitivity this significant, positive relationship is non-linear (Figure 3.3C; Figure 3.4C) and present in both Northern and Southern hemispheres (GAM: PSI, $P < 0.001$, deviance explained = 99%; VSI, $P < 0.001$, deviance explained = 97.1%). In the Northern hemisphere the 95% range of sensitivities peak at 6.9 °N in the PSI (Figure 3.3C) and at 27.4°N in the VSI (Figure 3.4C), and trough at 30.9°N for the PSI and at 14.3°N and 36.5°N for the VSI. In the Southern hemisphere the 95% range of sensitivities peaks at 8.7°S and 74.4°S in the PSI and at 26.7°S and 49.2°S in the VSI, and troughs at 28.0°S in the PSI and at 17.3°S, 34.6°S and 52.0°S in the VSI. The 95% range of sensitivities are not as consistent across hemispheres as median sensitivities in either index, particularly above ~40° Latitude (Figure 3.5), where the Southern hemisphere exhibits higher values. Within hemispheres a significant interaction of realm was found for the 95% range of sensitivities against latitude in both the Northern ($F_{5,158} = 426.1$, $R^2 = 0.929$, $P < 0.001$) and Southern ($F_{5,106} = 147.4$, $R^2 = 0.868$, $P < 0.01$) hemispheres, and for median sensitivity in the Southern hemisphere ($F_{5, 106} = 31.1$, $R^2 = 0.576$, $P < 0.001$). No interaction between realm and latitude was found for median sensitivity in the Northern hemisphere ($F_{5,158} = 15.7$, $R^2 = 0.311$, $P = 0.390$), though this is likely due to poor model fit (Appendix B Figure B-4A).

Latitudinal gradients in sensitivity are less easily detected at regional scales in both the PSI and the VSI, with median sensitivity broadly similar across biomes and provinces (Figure 3.6). Median province sensitivity was uncorrelated with latitude for both indices (PSI, r = -0.002, $P = 0.988$; VSI, r = 0.095, $P = 0.455$) and GAM model fit was poor (Appendix B Figure B-5A & C). Within and between biome variance (95% range) in province sensitivity is however significantly correlated with latitude in both indices (PSI, r = 0.445, $P < 0.001$; VSI, r = 0.546, $P < 0.001$), with an increase in variance towards the poles particularly visible for the PSI (Figure 3.6A). The 95% range of province sensitivities significantly increase with latitude in both hemispheres for the PSI (GAM: $P < 0.001$, deviance explained = 93.3%) with troughs at 22.8°N and 31.0°S (Appendix B Figure B-5B). The VSI also exhibits a significant relationship in both hemispheres between latitude and the 95% range of province sensitivities (GAM: $P < 0.01$, deviance explained = 88.2%). The Northern hemisphere exhibits a smooth increase with small changes in gradient occurring at 20.1°N and 27.9°N in the northern hemisphere. The Southern hemisphere relationship is more variable with peaks at 5.0°S, 21.0°S, and 36.3°S and troughs at 13.6°S, 28.5°S and 39.1°S (Appendix B Figure B-5D). Further supporting this latitudinal gradient, the polar biome in the PSI has higher sensitivity (3.003 ± 0.924 se, t = 3.250) than the trades, westerlies and coastal biomes which showed minimal differences. This pattern is

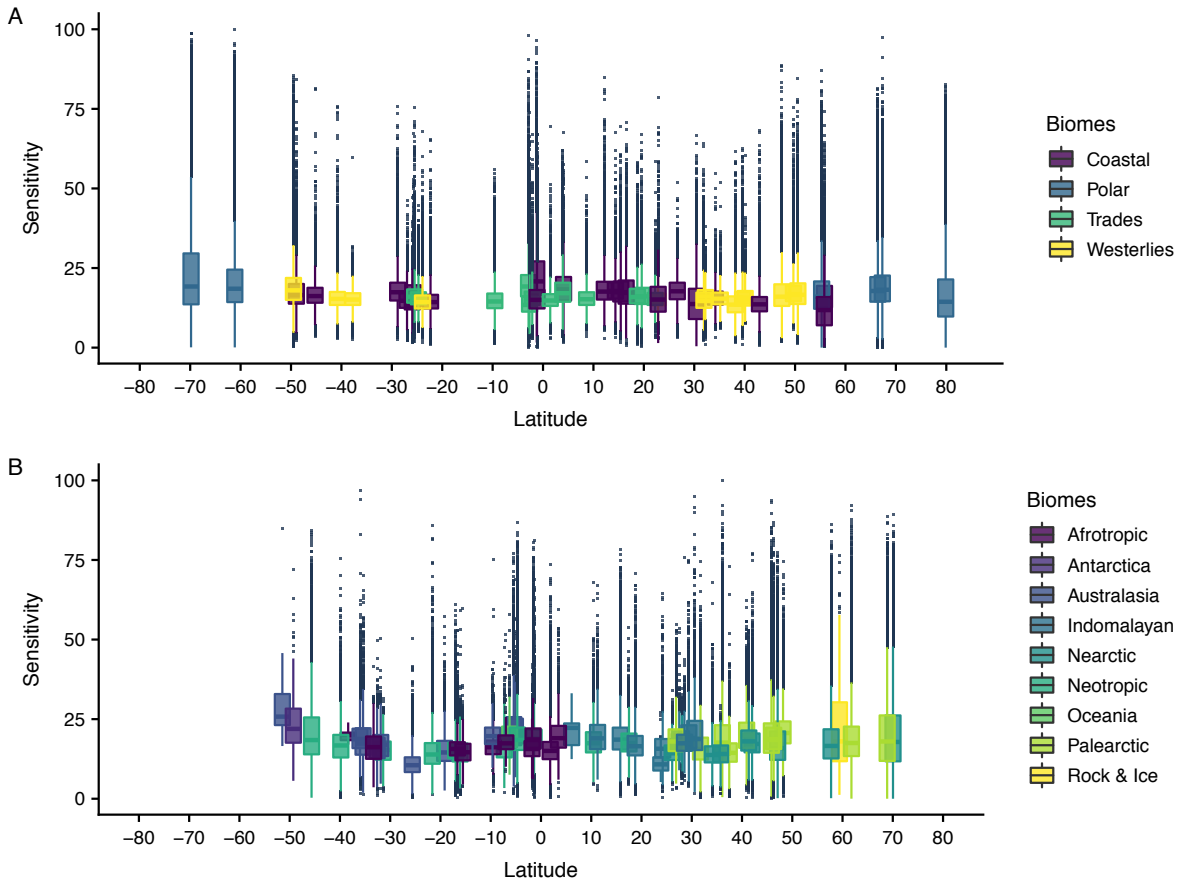

Figure 3.6: Latitudinal gradients of marine and terrestrial province sensitivity. Boxplots showing the spread of sensitivity for each province, grouped by biome for the marine PSI (A) and terrestrial VSI (B). The boxplots are ordered by the latitude of the centroid of each province. Biomes and provinces are based on Longhurst's Marine Biogeographic Regions for the PSI and Ecoregions2017 for the VSI. Full details of biomes and provinces can be found in Appendix B (Figure B-1-Figure B-3).

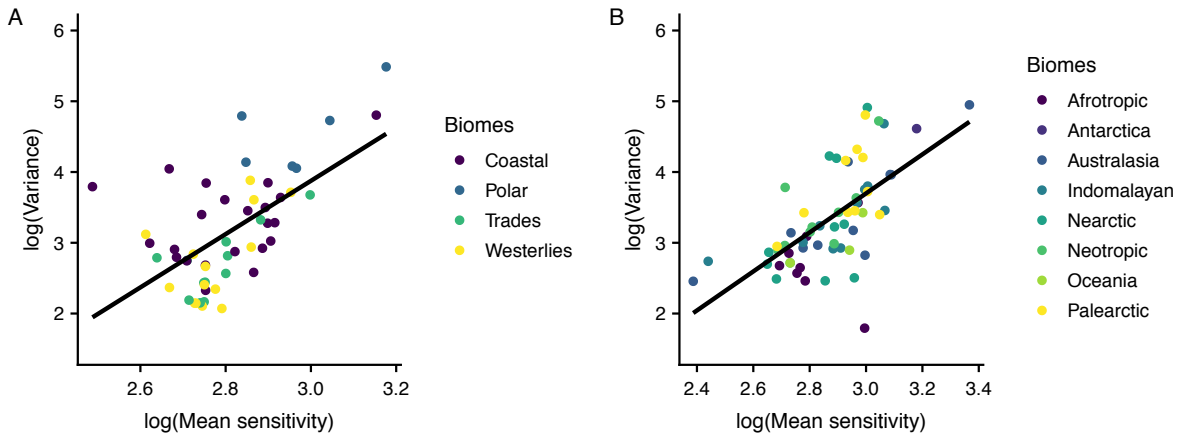

Figure 3.7: Mean-Variance relationships in marine and terrestrial province sensitivities. The relationship between the mean and variance of sensitivity in each province, grouped by biome, for the marine PSI (A) and terrestrial VSI (B). The solid line represents a linear model fitted to the $\log_{10}$-transformed mean and variance of each province. Longhurst's Marine Biogeographic Regions biomes are used for the PSI and Ecoregions2017 biomes are used for the VSI. Full details of biomes and provinces can be found in Appendix B (Figure B-1-Figure B-3).

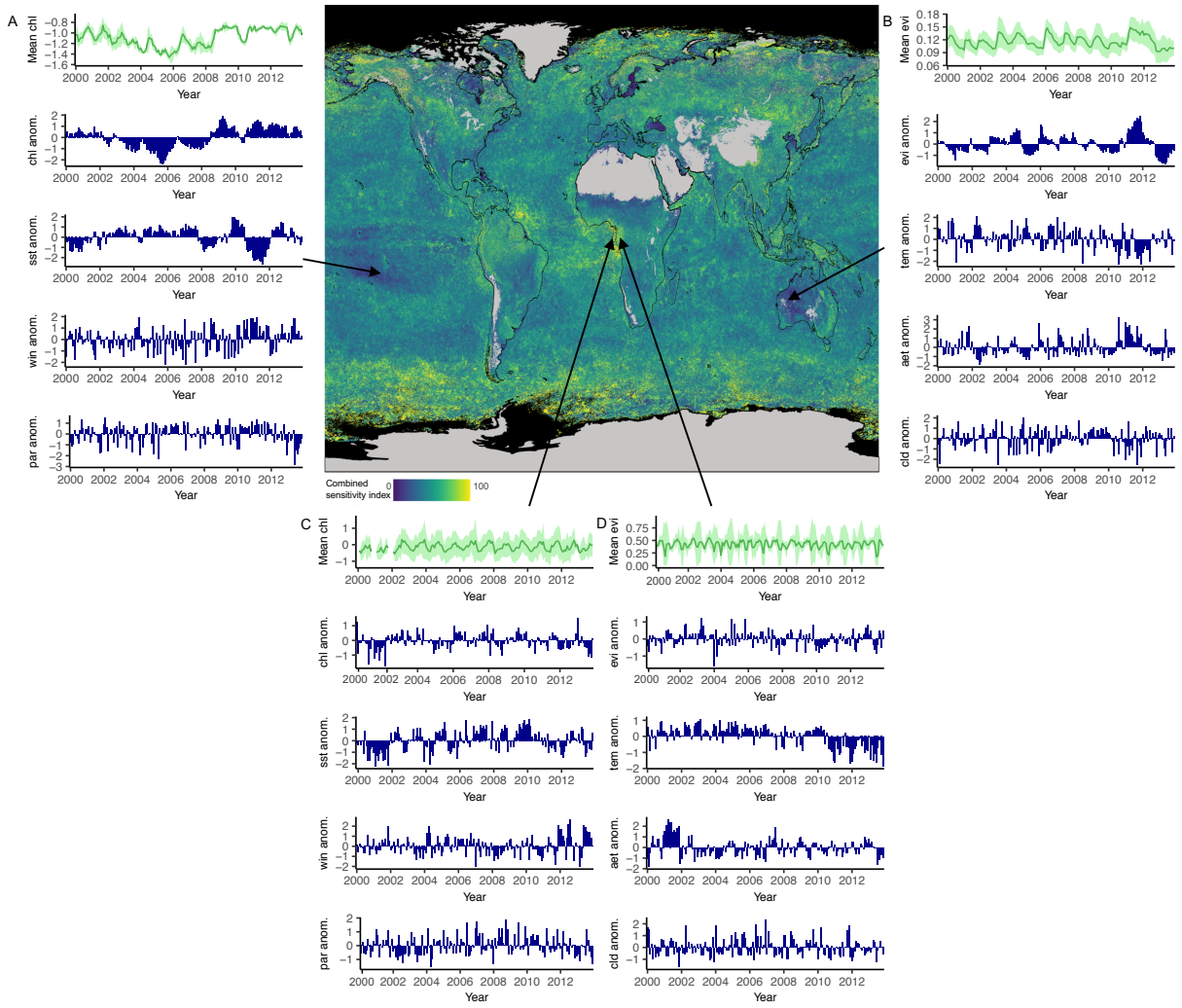

Figure 3.8: Time series plots of marine and terrestrial high and low sensitivity areas. Mean primary productivity (green) and primary productivity and climate z-score anomalies (blue) for corresponding marine and terrestrial regions of low (A, B) and high (C, D) sensitivity. Mean monthly values were calculated for 1° (400 pixels) grid squares for the terrestrial VSI and 2° (493 pixels) grid squares for the marine PSI. The green shaded area in the mean primary productivity plots shows the mean ± standard deviation. Anomalies show the difference in standard deviations between the mean monthly value and the 14-year (2000-2013) monthly mean. (A) South Pacific Gyre (SPSG; 151 W, 14 S); (B) Australian shrubland (AU13; 126 E, 28.7 S); (C) Gulf of Guinea (GUIN; 8.3 E, 2.2 N); (D) African tropical forest (AF01; 11.4 E, 2.2 N). The central map panel shows the combined Phytoplankton and Vegetation Sensitivity Index.

repeated in the VSI with polar biomes having higher sensitivity (Antarctica: 7.105 ± 2.961 se, t = 2.400; Palearctic: 1.894 ± 1.292, t= 1.466; Rock and Ice: 2.092 ± 2.946, t= 1.728) than temperate and equatorial biomes. The only terrestrial biome that differed from this pattern was Australasia, which is also more sensitive than surrounding biomes (1.946 ± 1.297, t=1.501). Provinces with higher mean sensitivities were also found to be significantly more variable in both the PSI (Figure 3.7A; $F_{1,52} = 30.43$, $R^2 = 0.357$, $P < 0.001$) and VSI (Figure 3.7B; $F_{1,61} = 44.15$, $R^2 = 0.410$, $P < 0.001$).

Examination of the input variable time series for locations within the PSI and VSI of comparable sensitivity and latitude, revealed distinct and realm-independent characteristics in primary

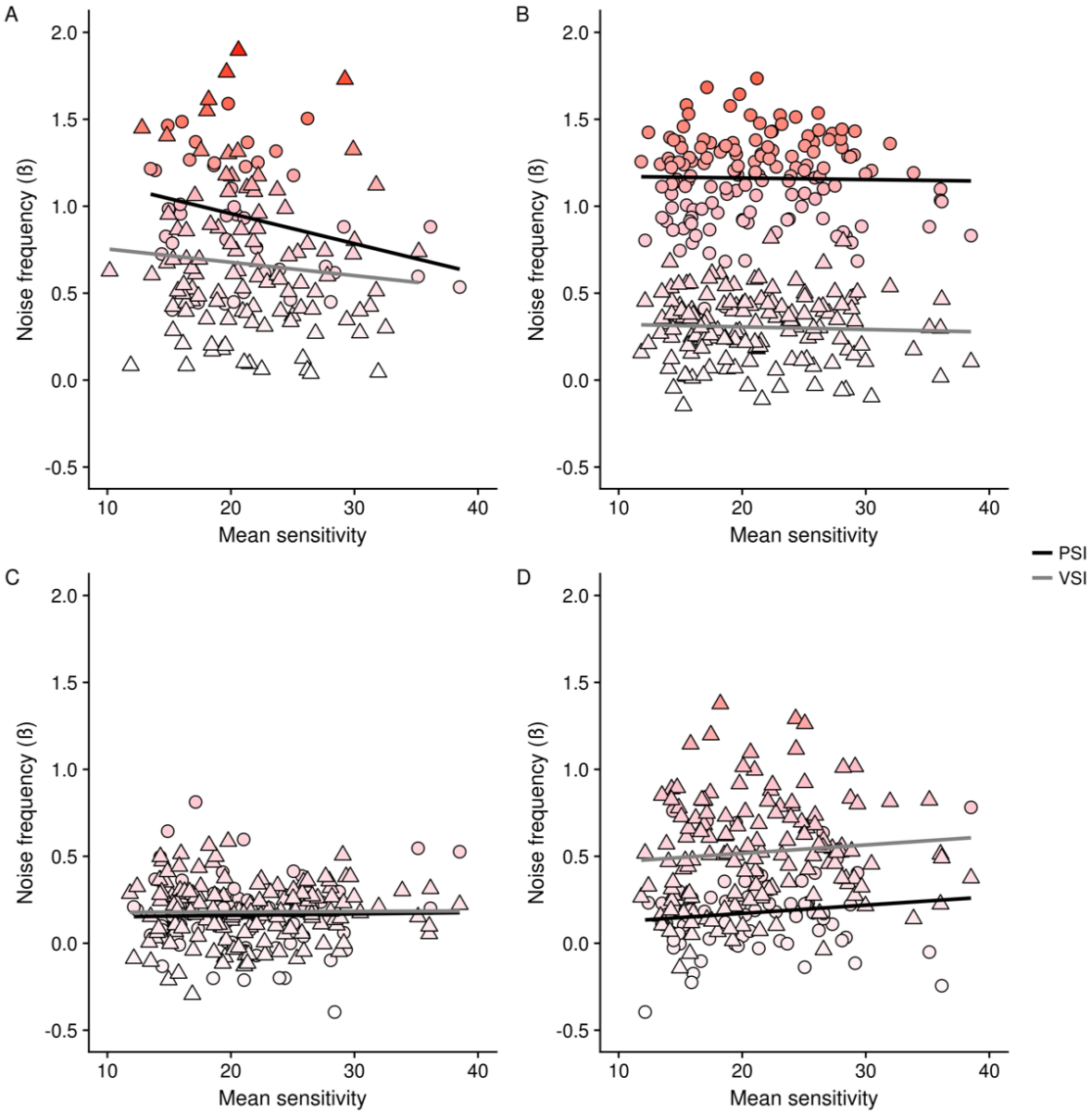

Figure 3.9: Spectral frequency plots for PSI and VSI variables. Plots showing the spectral component (ß) and 'colour' of variance in primary productivity (A), temperature (B), radiation (C) and wind and precipitation (D) z-score anomaly time series for the PSI (○) and VSI (△). The colour of time-series noise is categorised as white ($0 \leq ß \leq 0.5$), pink ($0.5 < ß \leq 1.5$) or red ($1.5 < ß \leq 2$), with reddened spectra indicating positivite temporal autocorrelation in the anomalies. The spectral component was estimated as the negative slope of a $\log_{10}$ linear regression between the spectral density and frequency of each time series. Lines show linear regressions fitted to noise frequency against mean sensitivity for the PSI (black) and VSI (grey).

productivity (Figure 3.8). Areas characterised by low sensitivity in both realms exhibit long periods with consistently positive or negative primary productivity anomalies and have a lower frequency of yearly changes in mean primary productivity (Figure 3.8A-B). By contrast, high sensitivity areas show constant switching between positive and negative primary productivity anomalies throughout the time series, with a higher frequency repeating pattern in mean primary productivity (Figure 3.8C-D). The time series also suggest closer coupling between climate and primary productivity anomalies throughout the time series in low sensitivity regions.

In the South Pacific oligotrophic gyre (Figure 3.8A) positive SST anomalies align with negative Chl-a anomalies and vice versa, whilst in Western Australia (Figure 3.8B) positive precipitation and negative temperature anomalies coincide with positive EVI anomalies. In high sensitivity areas, consistent correlations between primary productivity and climate anomalies are less apparent due to the high frequency of positive to negative switches in the primary productivity anomalies.

Despite these apparent trends, spectral analysis did not find evidence of realm-independent patterns in the temporal autocorrelation of primary productivity anomalies across gradients of sensitivity (Figure 3.9A). Mean sensitivity and noise frequency were also unrelated for all climate variables in the PSI and VSI. Temporal autocorrelation did however significantly differ between marine and terrestrial realms for three of the four variables. Primary productivity (Figure 3.9A; $F_{2,145} = 8.99$, $R^2 = 0.098$, $P < 0.001$) and temperature (Figure 3.9B; $F_{2,285} = 543$, $R^2 = 0.791$, $P < 0.001$) were both significantly reddened in the marine realm compared to the terrestrial realm. The reverse was seen for wind and precipitation with the terrestrial variable (precipitation) being significantly pinker than the marine variable (Figure 3.9D; $F_{2,216} = 39.6$, $R^2 = 0.261$, $P < 0.001$). Both radiation variables (PAR and cloudiness) were characterised by white noise frequencies, with no difference observed between the marine and terrestrial realms (Figure 3.9C).

3.4.2 Climate influence on sensitivity

Distinct regions of climate variable influence on primary productivity sensitivity are present in both indices (Figure 3.10). In the VSI, precipitation and cloudiness variability are the dominant drivers of primary productivity sensitivity (Figure 3.10) and have the strongest relationships with EVI (Appendix B Figure B-7). Eastern continental margins are particularly driven by precipitation, whilst cloudiness drives sensitivity in large tropical forested areas. In the PSI, SST influence dominates across the major ocean basins in relatively consistent latitudinal bands, interspersed with overlapping bands of PAR and SSW influence (Figure 3.10). This pattern is also broadly reflected in the strength of Chl-a relationships with climate (Appendix B Figure B-7), with both dominating in relatively consistent latitudinal bands, particularly in the sub-tropics. The polar regions of the PSI appear a lot more mixed, with no particular climate variable having a consistently dominant influence on sensitivity. Interactions between climate variables and their influence on sensitivity differ markedly between the PSI and VSI at regional scales (Figure 3.11). Within and between biomes in the PSI, differences between the three climate variables in terms of importance to sensitivity prediction are marginal (Figure 3.11A). SST has slightly higher overall importance for sensitivity in 20 of the 54 provinces, whilst SSW

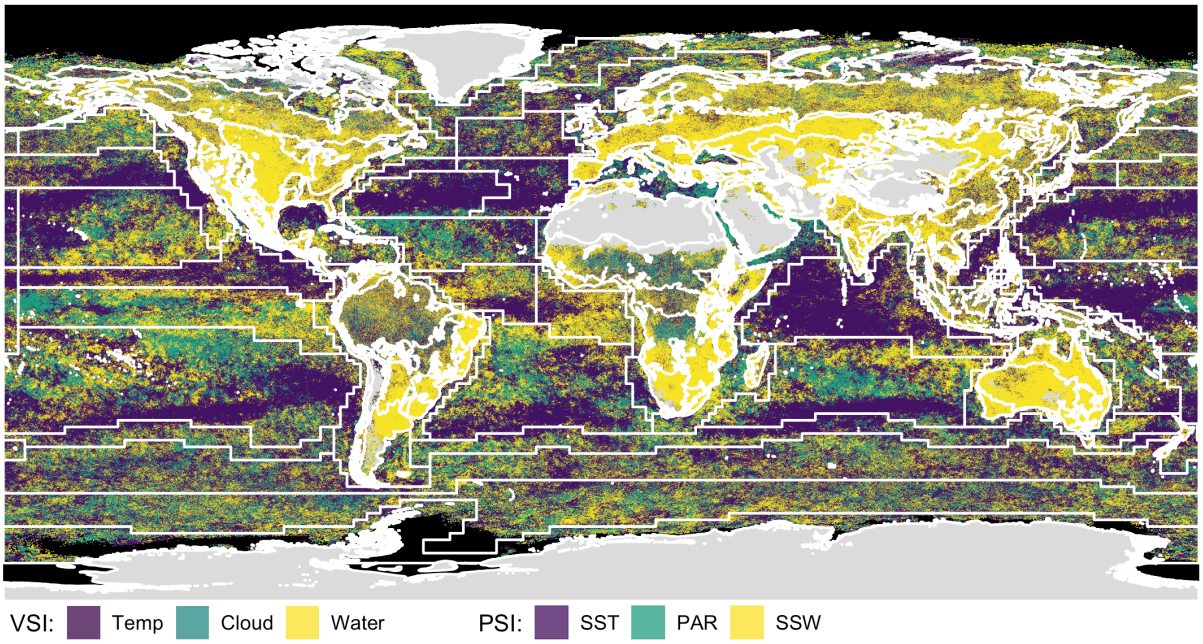

Figure 3.10: Composite map of the global sensitivity index. Composite map of the contribution of climatic driver variability in the terrestrial VSI (temperature (blue), cloudiness (green), precipitation (yellow)) and marine PSI (sea surface temperature (SST; blue), photosynthetically available radiation (PAR; green) and sea surface wind (SSW; yellow)), showing which driver has the highest influence on sensitivity in a given pixel. The sensitivity index is overlaid with Longhurst's Marine Biogeographic Regions (PSI) and Ecoregions2017 (VSI) boundaries (white lines), which are used for all spatial analyses**.** Full details of biomes and provinces used can be found in Appendix B (Figure B-1-Figure B-3). Pixel resolution, 9 km (PSI), 5 km (VSI); time period, 2000-2013. Areas in black indicate no data availability. Terrestrial areas in grey are predominantly barren areas, created using a minimum vegetation threshold. Continental outlines were modified from a shapefile using QGIS.

and PAR both have the highest influence in 17 provinces. There are some exceptions where a province has one particularly dominant or insignificant variable, including the Sub Antarctic Province (SANT) where PAR anomalies have particularly little influence and the Australia-Indonesia Coastal Province (AUSW) where SST anomalies have lower influence (Figure 3.11A). This uniformity in climate variable importance in the PSI was also observed in both the overall influence of climate within the sensitivity index (Appendix B Figure B-10A) and in the strength of climate – Chl-a relationships (Figure B-7 & Figure B-10B). BRT models performed best in the Trades and Westerlies biomes and poorest in the Polar biome. In the Coastal biome model fit was generally good except for in the Guinea Current Coastal Province (GUIN).

In contrast to the PSI, considerable differences were found in within- and between-biome climate influence in the VSI (Figure 3.11B). Precipitation has the highest relative importance to sensitivity prediction in 34 of the 60 provinces, with cloudiness and temperature having the highest importance in 11 and 15 provinces respectively. Single variable dominance in prediction importance is visible for several provinces, for example in Afrotropic Mediterranean forests, woodland and scrub (AF12) and Indomalayan deserts and xeric shrublands (IN13) upwards of 60% of climate influence was contributed by a single variable (Figure 3.11B). When

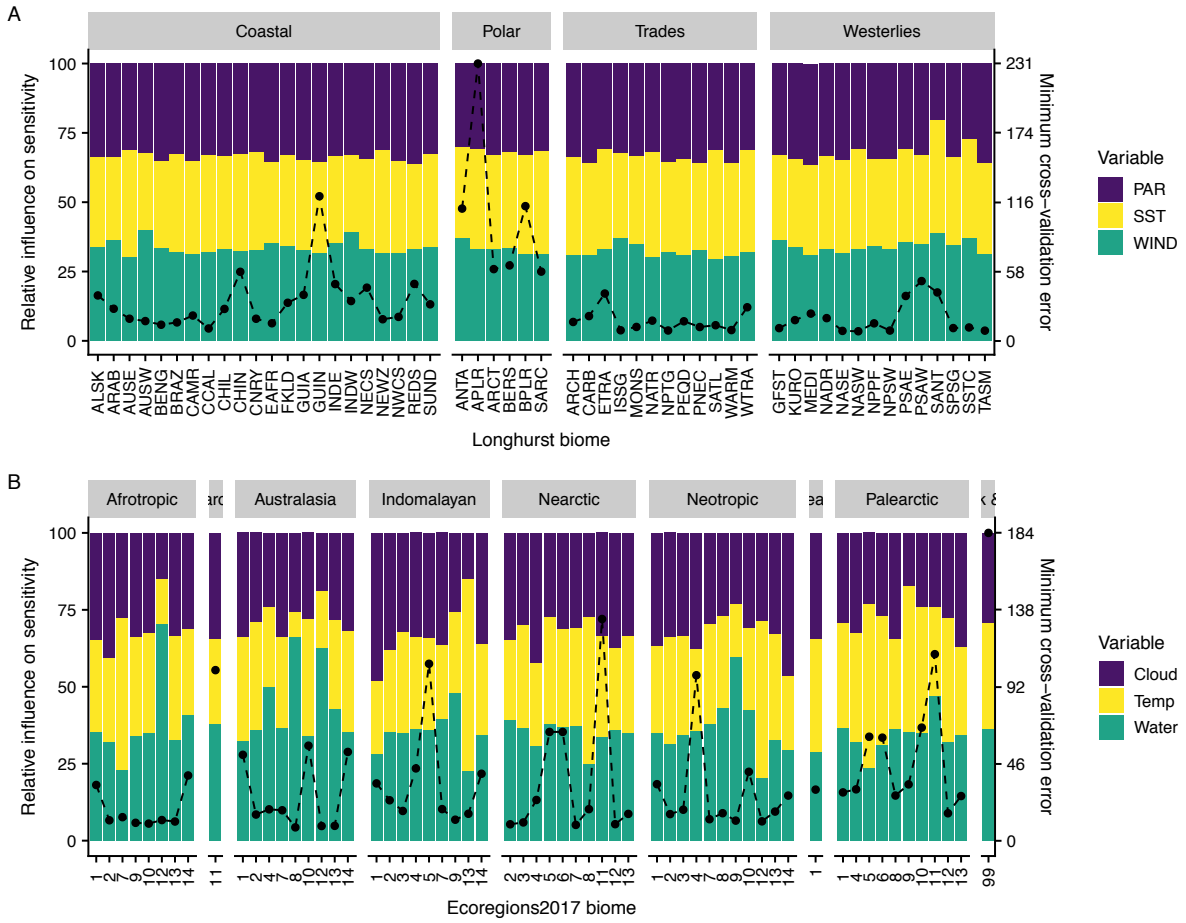

Figure 3.11: Regional influence of climate on the PSI and VSI. The relative importance of each climate variable's anomalies on final sensitivity prediction for the PSI (A) and VSI (B) from the results of a boosted regression tree analysis fitted to each province. The dashed line shows the minimum cross-validation error for each province's model fit. A lower value indicates a better model fit. Biomes in the VSI with only one province are from left to right, Antarctica, Oceania and Rock and Ice.

looking at climate interactions within the VSI composites (Appendix B Figure B-11) precipitation dominance is even higher, having the highest overall influence on sensitivity in 52 of the 63 provinces and contributing 50% or more of the sensitivity in 26 of those (Appendix B Figure B-11A). Precipitation also displays the strongest correlation with EVI in the majority of provinces (Appendix B Figure B-11B). Not all provinces show such extremes of climate influence however, tundra (**11) provinces in particular show evenness between the climate variables across all biomes comparable to that seen in the PSI. BRT model fit for the VSI performed best in the Afrotropic, Australasia and Oceania biomes. Model fit is good on the whole in the remaining biomes, with each having a single poorly performing province.

3.5 Discussion

The Phytoplankton Sensitivity Index (PSI; Chapter 2) for the marine realm was combined with the Vegetation Sensitivity Index (VSI; Seddon *et al.*, 2016) for the terrestrial realm to produce

a Combined Sensitivity Index (CSI) of global primary productivity sensitivity relative to environmental variability. I investigated the potential of the CSI to identify generalised, global patterns in cross-realm sensitivity, to provide explanatory power in terms of its environmental drivers and to facilitate analyses of its temporal dynamics. In doing so, I have shown the existence of a global, cross-realm macroecological pattern in primary productivity sensitivity relative to environmental variability, which holds across a range of spatial scales. A latitudinal gradient of increasing sensitivity towards the poles is visible at both degree of latitude and hemispheric scales in the CSI and within each individual index; regional scales are less effective for reliably demonstrating the gradient. I have also identified evidence of realm-independent trends in the temporal dynamics of primary productivity and climate anomalies along gradients of sensitivity. By combining the two indexes, I have produced a truly global macroecological view of environmental variability that can be used as a basis on which to examine the responses of communities at higher trophic levels.

3.5.1 Scales of sensitivity

3.5.1.1 Global latitudinal gradient

Latitudinal gradients form the basis of numerous macroecological patterns known to occur in both marine and terrestrial realms for a range of attributes (e.g. species diversity (Fisher *et al.*, 2008), range size (Stevens, 1989)). Qualitative analysis of the PSI and VSI indicated that this might also be the case for primary productivity sensitivity (Figure 3.1). Quantitative analyses confirmed the existence of a significant positive correlation in both the median and 95% range of sensitivities with degree of latitude, indicating the presence of a global gradient of increasing sensitivity towards the poles in both the CSI (Figure 3.2), PSI (Figure 3.3) and VSI (Figure 3.4). In all three indexes the latitudinal gradient is strongest in the 95% range of sensitivities, reflecting the heavy right skew present in the PSI and VSI. This also suggests that whilst the highest sensitivities are concentrated in sub-polar and tropical latitudes, these latitudes also contain the widest, and in many cases full, range of sensitivities. As a result, high latitude alone cannot be directly predictive of high sensitivity but does increase its likelihood. This is in contrast to low sensitivity temperate regions (~20-40° Latitude) particularly in the Southern hemisphere, where the range of sensitivities is much narrower (Figure 3.2A) giving latitude higher predictive power. Incorporating longitudinal bins into the analyses could help to further delineate trends in sensitivity at latitudes with high sensitivity ranges.

Whilst the latitudinal gradient observed in the CSI is present in both the PSI and VSI, inter-realm differences in the sensitivity gradient do occur that are either masked in the CSI or driven specifically by one index. Firstly, an increase in tropical sensitivity is present in both the median

and 95% range of sensitivities in the VSI (Figure 3.4B-C), which is subsequently reflected in the CSI (Figure 3.2). In the PSI an equatorial peak is only apparent in the 95% range of sensitivities (Figure 3.3C), with median sensitivity remaining consistently low throughout the tropics (Figure 3.3A-B). Secondly, high sensitivity in high Southern latitudes in the CSI is driven exclusively by the PSI due to the VSI not extending beyond 60°S, however the trajectory of sensitivities in the VSI for the Southern hemisphere (Figure 3.4B-C) suggests that if the VSI also continued beyond 60°S, it would support the pattern observed in the PSI and CSI. The increased variability of the median and 95% range of sensitivities in the Southern hemisphere for the VSI is also diluted in the CSI when combined with the less variable PSI. These differences suggest that whilst the latitudinal gradient holds true at a global, integrated level, examining the individual indexes could provide a greater level of explanatory power in terms of realm specific detail and should be considered in future comparative studies.

3.5.1.2 Hemispheric scale

Significant, positive relationships between latitude and sensitivity were identified via GAM analysis in both Northern and Southern hemispheres for the CSI (Figure 3.2B-C), PSI (Figure 3.3B-C) and VSI (Figure 3.4B-C). Within each index, these hemispheric trends in sensitivity exhibit a high degree of similarity at corresponding degrees of latitude (Figure 3.5). Median sensitivity in particular shows minimal differences between hemispheres along the full range of latitudes in each index (Figure 3.5). The 95% range of sensitivities also share a high degree of similarity across hemispheres between ~0-40° Latitude, after which the range of sensitivity in the Southern hemisphere surpasses that in the Northern hemisphere in both indexes (Figure 3.5). These results indicate that within 40°N – 40°S, primary productivity vulnerability to climate variability is equivalent across hemispheres within each index and could perhaps allow for extrapolation across hemispheres. Beyond this range the hemispheres should be considered separately as a northern, temperate focus could result in Southern hemisphere vulnerability being underestimated. Within hemispheres a significant interaction of realm was identified for both the median and 95% range of sensitivities in the Southern hemisphere, and for the 95% range of sensitivities in the Northern hemisphere, indicating that whilst the overall latitudinal gradient is similar in each realm, marine and terrestrial hemispheric trends are distinguishable from one another. This is due to the terrestrial realm exhibiting slightly higher 95% range values than the marine realm in both the Northern (Appendix B Figure B-4B) and Southern (Appendix B Figure B-4D) hemispheres. Differences in curvature of the trend, though significant, are marginal (Appendix B Table B-4-Table B-7). For median sensitivity an interaction with realm was only identified in the Southern hemisphere, with the VSI exhibiting more curvature than the marine PSI (Appendix B Figure B-4C). The lack of a significant interaction of realm for

median sensitivity in the Northern hemisphere could suggest that the trends are realm independent, however it is more likely a result of poor model fit (R^2 = 0.311) owing to the increased variability of the terrestrial gradient (Appendix B Figure B-4A). These results reaffirm that the latitudinal gradient in increasing sensitivity towards the poles is a general pattern that holds true in both realms and hemispheres but requires realm dependent consideration for maximum inference. Full statistical output can be found in Appendix B Table B-4-Table B-7.

3.5.1.3 Regional scale

A latitudinal gradient in sensitivity could not be demonstrated at a regional spatial scale for either the marine or terrestrial realm. Median province sensitivities were uncorrelated with province centroid latitude in both indexes and correlation between the 95% range of sensitivities and province centroid latitude, whilst significant, was weaker than for sensitivity per degree of latitude. Regional levels of geographical organisation are therefore of limited use for inferring sensitivity, due to the overlapping spread of sensitivities between provinces and the lack of differentiation between biomes in both indexes (Figure 3.6). The large ranges in pixel sensitivity observed within the majority of marine provinces (Figure 3.6A) suggests that sensitivity within individual provinces isn't cohesive, however it could also indicate that the Longhurst regionalisation isn't fine scale enough to accurately capture patterns within the index (discussed further in Section 3.5.3). Whilst the terrestrial provinces also display high variance within province sensitivities (Figure 3.6B), the Ecoregions2017 includes a finer scale regionalisation than the level employed here (see Section 3.3.2) which might reduce this variance. Despite the lack of cohesiveness within provinces, there is weak evidence of cohesiveness at a biome level. In keeping with higher sensitivities being found at higher latitudes, the mixed effects model results identified the polar biomes as having significantly higher sensitivities than temperate and tropical biomes in both realms, and also as having higher province variances (Figure 3.7). Due to the previously discussed uncertainties with polar satellite data (Section 3.3.2) these results should be treated with caution, however as they are neither anomalous nor unexpected, it was not thought necessary to exclude the data. Additionally, whilst the polar biomes could be distinguished from other biomes, the regionalisation is still of limited use as any inference could just as easily be obtained from latitude, given the high latitude positioning of polar biomes.

3.5.2 Temporal dynamics

A key component of advancing macroecological theory is the ability to incorporate and infer temporal dynamics related to the pattern, in order to better determine underlying processes (Fisher *et al.*, 2008, 2010). In examining cross-realm primary productivity mean and anomaly

times series alongside climate anomaly time series for regions of equivalent sensitivity and latitude, I found evidence of similar trends in the temporal dynamics of primary productivity occurring within regions of similar sensitivity, irrespective of realm (Figure 3.8). Low sensitivity areas in both realms showed greater stability and higher temporal autocorrelation across years indicative of 'red noise', compared to low temporal autocorrelation and instability (white noise) across years in high sensitivity regions. Similarities in cross-realm variability structures such as in these time series are not without precedent; white-red gradients in variability from terrestrial-marine environments are known to occur, particularly in coastal environments (Vasseur and Yodzis, 2004). The consistent correlation between climate and primary productivity anomalies visible in the low sensitivity yearly time series, particularly with respect to temperature and precipitation for the marine and terrestrial realms respectively (Figure 3.8A-B), is further reflected in the year-round significant climate-primary productivity anomaly relationships identified in the P/VSI (Appendix B Figure B-6). High sensitivity regions on the other hand exhibit fewer months in a year with significant climate-primary productivity anomaly relationships (Appendix B Figure B-6), consistent with there being minimal discernible patterns between the primary productivity and climate anomaly time series (Figure 3.8C-D). These results suggest that similar processes determine sensitivity in both marine and terrestrial realms, and that despite differences in the temporal and spatial scales of producer life histories (Steele, 1991a), their responses to environmental variability are comparable.

Further examination of these trends via spectral analysis did not find further support for them, however. In light of the apparent trends in the anomaly time series, I expected to find trends of increasing sensitivity with decreasing temporal autocorrelation (i.e. a correlation between high sensitivity and white noise). Conversely, spectral analysis results found all variable spectral densities to be uncorrelated with gradients of sensitivity, and primary productivity, temperature, wind and precipitation anomaly time series to be significantly realm-dependent (Figure 3.9). Radiation was the only climate variable to exhibit a white frequency structure in both the PSI and VSI, with no discernible difference in spectral frequencies between the two realms. Inter-realm differences in the autocorrelation structure of climate variable anomalies are not surprising. The buffering effects of the ocean promote reddened environmental spectra (Rohani, 2004; Steele, 1985), whilst terrestrial abiotic variables exhibit white or weakly reddened variance structures (Gilljam *et al.*, 2019). Within primary productivity anomalies there is weak evidence of the expected negative trend between sensitivity and temporal variability structure, with higher mean sensitivities exhibiting lower spectral frequencies of variation (Figure 3.9A), however it is not significant. The lack of significance between temporal autocorrelation and mean sensitivity could be a result of the right skew present in the PSI and VSI towards lower sensitivities. Whilst initial pixels were selected based on their sensitivity

level from low-high, the pixels selected within each 1° or 2° square surrounding the initial pixel would not necessarily have been of a similar sensitivity level due to the predominance of low sensitivities in the indices, resulting in there being no mean sensitivity values above 40 in the analyses. Another possible cause is missing data. Spectral frequency analysis requires complete time series to run, however missing data disproportionately affects Chl-a in high sensitivity pixels in the marine index (Appendix B Figure B-8), further reducing the chances of high sensitivity pixels being included in the analyses. Whilst as a proportion of high sensitivity pixels the amount of missing data appears large, in terms of the total number of pixels it is a very small amount and largely due to data being unavailable in the Southern Ocean during Southern hemisphere winter months (Dr Tom Jackson, ESA OC-CCI developer, *pers comm.*), where there are high concentrations of high sensitivity pixels. All other variables in both the PSI and VSI had complete data series. Whilst EVI in the terrestrial index had complete time series (Appendix B Figure B-9), the small number of high sensitivity pixels could have prevented a trend from being detected.

To date, estimating colour for environmental variables explicitly linked to biotic data has only been done once and only for variables correlated with terrestrial animal populations (Gilljam *et al.*, 2019). Our work suggests that at the current time, spectral frequency cannot be used as an indicator of primary productivity sensitivity in the marine or terrestrial realm and further analyses at longer temporal scales or with more complete time series would be required to clarify the contrast in results between the time series trends and spectral analysis. Having said this, whilst the time series of the examined variables displayed realm-dependent spectral frequencies, the relationship (or lack thereof) with sensitivity exhibited by each variable was realm-independent. It is therefore possible that further analyses with improved data coverage could identify common trends between time-series variance and sensitivity across realms.

3.5.3 Climate influence on sensitivity

Despite the latitudinal similarities in sensitivity across realms, there are considerable differences in climate influence on sensitivity between the two realms. Water limitation is the dominant driver of primary productivity sensitivity across much of the terrestrial realm, whereas in the marine realm dominant influence is much more evenly spread across the three climate drivers (Figure 3.10). When looking at interactions between climate variables and the level of climate driver dominance, inter-realm differences are even more pronounced (Figure 3.11). In the marine realm BRT analysis identified temperature, wind and radiation anomalies as all being equally important to sensitivity prediction, with marginal differences present between variables within provinces and no visible distinctions between biomes (Figure 3.11A). The

terrestrial realm by contrast exhibits highly varied and dominant climate influences both within and between provinces, and also shows some biome continuity (Figure 3.11B). Precipitation anomalies are the best predictor of primary productivity sensitivity in tropical terrestrial biomes which are most likely to suffer water limitation, with the exception of tropical forest provinces which favour cloudiness. Given the canopy density in these regions and the micro-climates that exist in tropical forests this is not surprising. The Arctic biomes are more even in their climate interactions; temperature is generally the most important driver of sensitivity in the Palearctic biome over Europe and Russia, whilst cloudiness and precipitation tend to dominate in the North American Nearctic biome. Interestingly, provinces which appear in multiple biomes exhibit vastly different results. For example, for the Mediterranean Forests, Woodlands and Scrub province (**12) precipitation accounts for over 60% of sensitivity in the Afrotropic and Australasia biomes with temperature having minimal influence, however in the Neotropic biome temperature is the dominant variable accounting for ~55% of predictive power. This suggests that generalising climate influence across recurring provinces would be inappropriate, requiring them to be considered either individually or in conjunction with their corresponding biome.

The lack of variation in climate variable influence observed in the BRT results for the PSI could be due to the greater inertia of the marine realm, and the longer timescales required for climate anomalies to induce change in the physical composition of large bodies of water. It is also possible that variables not included in the index, such as nutrient availability, could be more directly influential on marine primary productivity sensitivity than climate anomalies. A third possibility is the size of the provinces used in the analysis. When patterns of climate influence in the marine realm are compared against the Longhurst provinces (Figure 3.10) multiple areas of influence within the same province are apparent in certain regions, such as the Indian S. Subtropical Gyre (ISSG) province. With each BRT model being fitted to an entire province it is likely that within province differentiation is masked and averaged in the final output, thus not accurately reflecting the patterns observed within the data. This could also be contributing to provinces which have best fitting models with tree complexities of 20 (Appendix B Table B-2-Table B-3), indicating a high level of interaction occurring within the data.

The Ecoregions2017 provinces used for the VSI are considerably smaller than the Longhurst provinces so may better capture variation present in the terrestrial data, resulting in the considerable between biome variation observed in the VSI model output. Nieto and Mélin's (2017) BRT analysis of the Gulf of Guinea lends support to this. Nieto and Mélin (2017) found considerable variation in climate driver influence on chlorophyll variation when employing a BRT analysis with a much finer scale regionalisation than used here for the marine realm,

dividing the GUIN Longhurst province into 56 cells. This could also explain the poor model fit found here when operating at the scale of the entire GUIN province. As BRT analysis puts breaks in the data until best fit is achieved, it had originally been intended to run the BRT with increasing levels of geographic structuring complexity (i.e. run on the PSI with no structuring, run with biomes included and then run with provinces included) to determine if the model would agree with the structuring suggested by the biogeographic classification system used. Unfortunately, the computing power and time required to run the BRT for one marine biome alone made it unfeasible to apply the method to biomes or the full dataset.

My results suggest that the Longhurst classification structure could be prohibitively large for capturing regional patterns in marine responses to environmental variability. Particularly in dynamic regions, phytoplankton habitats can be considerably smaller than Longhurst's delineations (Weber *et al.*, 2019). Alternative classification systems for the marine realm have been proposed more recently such as Marine Ecoregions of the World (MEOW; Spalding *et al.*, 2007), an in-depth delineation of coastal and shelf waters into 232 distinct ecoregions, and the Pelagic Provinces of the World (PPOW; Spalding *et al.*, 2012), which uses oceanographic and taxonomic biogeographic features to classify the pelagic realm into 37 provinces and 7 biomes. The PPOW could be a more appropriate alternative to the Longhurst biomes for these analyses given it is more recent and places a larger emphasis on biological patterns in setting its boundaries, however the lack of coverage in coastal areas would have proved problematic (Appendix B Figure B-12). The PPOW is intended for use in conjunction with the MEOW to provide global coverage, however many of the 232 MEOW coastal ecoregions would have been too small to adequately fit models to for both the GAM and BRT analyses. For more temporally or spatially explicit analyses than performed here, a dynamic boundary approach to account for seasonal variation as seen in Reygondeau *et al.* (2013) for pelagic areas, or a more fine scale regionalisation such as the MEOW for coastal areas would be beneficial.

Whilst a regional spatial scale proved ineffective for identifying patterns in climate drivers, this does not reduce the efficacy of the sensitivity indices to act as mechanistic macroecological patterns, given that climate influence can be examined on a pixel by pixel basis. It does however mean that averaging over regions, particularly in the PSI, would be unwise. The lack of cross-realm trends in climate influence on sensitivity suggests that whilst the outcomes of the indices in terms of primary productivity responses and ecosystem resilience are comparable across realms, the influence of climate must be considered separately. The BRT analysis also shows that simply identifying the dominant driving climate variable of sensitivity, without accounting for interactions between climate variables or their level of dominance may lead to inaccurate conclusions about their importance on the observed primary productivity

response. Incorporating climate interactions therefore provides valuable additional information on vulnerable areas identified in the sensitivity indices and for the terrestrial realm in particular, establishes key climate variables for monitoring and/or predicting future vulnerability to environmental variability in different regions.

3.5.4 Implications and future research

In combining the PSI with the VSI I have shown the existence of a global, cross-realm macroecological pattern in the latitudinal gradient of primary productivity sensitivity relative to environmental variability. Visible at both global and hemispheric scales, the gradient shows both where extrapolation across hemispheres could be possible and where the hemispheres must be considered separately, with subsequent implications for the northern, temperate focus of much climate research. Whilst inter-realm differences in sensitivity are minor, they suggest that examining the individual indexes could provide a greater level of explanatory power in terms of realm specific detail and should be considered in future comparative studies. Differences in the influence of dominant climate variables on sensitivity between the realms, and particularly their interactions with other climate drivers, must also be taken into account when making cross-realm comparisons in sensitivity, and particularly when predicting or inferring causal mechanisms. Overall, the CSI reveals interesting structure in the global distribution of primary productivity sensitivity. Whilst some of this structure can be predicted by latitude, not all of it can. The lack of clear marine – terrestrial distinction in primary productivity sensitivity, with both realms exhibiting similar levels of high and low sensitivity, lends the CSI to further use as a base layer for cross-realm comparative studies. If we accept that environmental variability – and responses to it – are key in driving community composition and life history evolution, then properly accounting for it is important. By incorporating the CSI into future comparative studies on responses to climate change and the global distribution of species, more nuanced analyses and interpretations will be possible than with a simple marine versus terrestrial model. It will also enable predictions for marine and terrestrial communities that are likely to share certain features, for example in terms of macroecological summaries of diversity such as species abundance distributions (SADs; Chapter 4) or species composition in terms of life history.

4 Temporal trends in Species Abundance Distributions: Comparing marine and terrestrial community structure along gradients of environmental variability

4.1 Abstract

Species responses to environmental variability can vary markedly (Morris *et al.*, 2008; Stenseth *et al.*, 2002; Vasseur *et al.*, 2014) and are not guaranteed to be consistent across realms. With increasing levels of change occurring in natural systems, reliable measures for effective detection of change across trophic levels are needed. Species abundance distributions (SADs) identify patterns of commonness and rarity in communities, and can provide an early warning signal of community change or disturbance (Matthews and Whittaker, 2014; Sæther *et al.*, 2013b). Here, I use global community assemblage data from the BioTIME database (Dornelas *et al.*, 2018) with sensitivity data from the Phytoplankton Sensitivity Index (PSI; Chapter 2) and Vegetation Sensitivity Index (VSI; Seddon *et al.*, 2016) for the marine and terrestrial realms respectively, to investigate the structure of SADs for cross-realm communities along gradients of primary productivity sensitivity to environmental variability through time. A significant trend of decreasing community evenness with increasing primary productivity sensitivity was identified in the terrestrial realm, however no significant evidence was found of a corresponding correlation between marine community structure and gradients of primary productivity sensitivity. There was also no evidence of changes in community mean through time in either realm. Overall, marine communities exhibited lower evenness than terrestrial communities. By combining temporally explicit SADs with environmental variability derived ecosystem sensitivity, I have identified trends in marine and terrestrial community composition attributable to environmental pressure, providing a contiguous link through macroecological patterns from the abiotic to the biotic from which underlying processes can be better determined.

4.2 Introduction

Environmental variability affects species dynamics and processes (Dawson and Hamner, 2008; Ma *et al.*, 2015; Suryan *et al.*, 2009) influencing population dynamics (Ruokolainen *et al.*, 2009), growth rates (Lawson *et al.*, 2015), extinction risk (Ruokolainen and Fowler, 2008) and the turnover and abundance of species within communities (Ives *et al.*, 1999). Alongside general environmental variability, extreme environmental events are increasing in frequency (Easterling *et al.*, 2000; Ma *et al.*, 2015) with extreme temperature events in particular causing a significant threat to higher trophic level community dynamics (Ma *et al.*, 2015; Vasseur *et al.*, 2014). Species responses to environmental variability can vary markedly (Morris *et al.*, 2008; Stenseth *et al.*, 2002; Vasseur *et al.*, 2014) and population responses to global change are not guaranteed to be consistent across realms. Evidence already suggests that compositional change (Blowes *et al.*, 2019) and species turnover (Pinsky *et al.*, 2019) in populations is currently occurring faster in the marine than terrestrial realm. With increasing levels of change occurring in natural systems, increased understanding of the drivers of population and community dynamics is needed to enable effective detection of change across trophic levels.

Whilst higher trophic level species can be directly impacted by abiotic conditions, for example through temperature effects on metabolic rates, a major route of environmental variability impacts on higher trophic level populations is via indirect effects on resource availability and predictability (Durant *et al.*, 2007). Primary producers respond directly to direct environmental control, and form a link between production and consumption in trophic interactions, such that the availability and predictability of primary producers is integrally linked to both the abundance and distribution of higher trophic level communities (Cushing, 1990; Toszogyova and Storch, 2019) and abiotic conditions. Combining estimates of primary productivity sensitivity to climatic variability with metrics describing the distribution and structure of diverse marine and terrestrial population assemblages could therefore provide a way of identifying the drivers behind higher trophic level population change. Regions that are sensitive to current variability at a primary producer level might already be exhibiting detectable signals of related change at higher trophic levels. To test this, a measure of higher trophic level community dynamics is required that can be correlated to environmental drivers and resource availability; the species abundance distribution (SAD; Preston, 1948) is one such measure.

SADs are one of the most universal descriptors of community structure in ecology, identifying and quantifying patterns of commonness and rarity in communities by considering how abundance (total number of individuals) is distributed between species within a community. Across all ecosystems examined to date, both marine and terrestrial, a classic hollow- or J-

curve is produced on the arithmetic scale, indicative of many rare species and few common ones (McGill *et al.*, 2007). A principal feature of SADs is that they are unlabelled: species identities are not included in the distributions (McGill *et al.*, 2007). This makes the SAD well-suited to comparisons of contrasting communities with few or no shared species (e.g. Whittaker, 1975), including cross-realm communities (e.g. Gray *et al.*, 2006). Comparisons of contrasting cross-realm communities have identified differences in the structure of marine and terrestrial SADs (Gray *et al.*, 2005), however very similar structures can be observed when examining communities within the same functional groups (Gray *et al.*, 2006). As well as comparing different communities, SADs have also been used to compare community structure along environmental gradients of productivity (Latitudinal: Hubbell, 1979; Elevational: Whittaker, 1960) and habitat complexity (Cotgreave and Harvey, 1994; Hurlbert, 2004), with all showing greater evenness in distributions at higher levels of productivity and complexity.

Although spatial SAD studies have revealed important trends, it has been argued that temporal scale must also be accounted for when calculating SADs (Magurran, 2007), as it will undoubtedly affect the shape of the distribution and could lead to better inference of the underlying ecological processes behind observed distributions. For example, changes in SAD structure through time can identify both changes in core and transient species within a population (Magurran and Henderson, 2003) and directional long-term community changes due to resource allocation (Thibault *et al.*, 2004), succession (Wilson *et al.*, 1996) and anthropogenic pressure (Bhat and Magurran, 2006). Placing SADs into the context of the abiotic environment has also been advocated to aid the identification of processes and mechanisms responsible for patterns observed in SADs (McGill *et al.*, 2007). It has since been shown that environmental stochasticity can influence the shape of the final SAD distribution with the parameters describing SADs varying systematically with environmental variance (Sæther *et al.*, 2013b), meaning that SADs can provide an early warning signal of community change or disturbance due to environmental variability (Dornelas, 2010; Matthews and Whittaker, 2015; Sæther *et al.*, 2013b).

Several models exist for fitting SADs to abundance data (reviewed in Baldridge *et al.,* 2016 and McGill *et al.,* 2007), however the Poisson lognormal distribution (Bulmer, 1974) has several benefits if the aim is to determine change in assemblages resulting from environmental forcing. Firstly, it employs a discrete parametric approach with well-defined sampling assumptions, complementary to both the normal distribution typical of logarithmic population abundances (Sæther *et al.*, 2013b) and the discrete nature of count abundance data (Bulmer, 1974). Secondly, the lognormal distribution provides an equivalently good fit to empirical SADs as the log-series and negative binomial distributions (Baldridge *et al.*, 2016) and performs

particularly well in marine communities (Connolly *et al.*, 2014). Whilst some studies have found contrasting results to this (e.g. Ulrich *et al.*, 2010), these have typically looked at the goodness of fit of SAD distributions on rank abundance data as opposed to count abundance data (Baldridge *et al.*, 2016). Perhaps most importantly however, is the ease of interpretation of its two key parameters describing community structure: *mu* and *sigma*. *mu* provides a measure of the mean abundance of a community whilst *sigma* provides a measure of the evenness, or spread, of abundances within a community (Sæther *et al.*, 2013b). A community with high evenness indicates that the majority of species have similar abundances, resulting in the spread of abundances (*sigma*) being low. A community with low evenness on the other hand contains species with a wide range of abundances (high *sigma*) and can be an indication of high species turnover. It is through variation in the *sigma* parameter that changes in assemblage structure can be identified (Sæther *et al.*, 2013b).

By correlating the Vegetation Sensitivity Index (VSI; Seddon *et al.*, 2016) and Phytoplankton Sensitivity Index (PSI; Chapter 2) with parameters describing SADs that emerge at the community level, an indirect link would be provided to determine environmental variability impacts on community stability across trophic levels, including dependent higher trophic level populations. Incorporating measures of environmental variability would also allow for more nuanced comparisons to be made than in previous comparative analyses of community structure that have relied on simple marine-terrestrial divisions. Here, I compare the structure of Poisson lognormal SADs through time fitted to 43 marine and 49 terrestrial communities extracted from the BioTIME community assemblage database (Dornelas *et al.*, 2018) along gradients of primary productivity sensitivity. By combining temporally explicit SADs with ecosystem sensitivity derived from environmental variability, I aim to identify trends in marine and terrestrial community structure attributable to environmental pressure, which could lead to their use as environmental indicators of change (McGill *et al.*, 2007). To do this, I also test for differences in the evenness (*sigma*) of communities existing in high versus low primary productivity sensitivity environments within and across realms. I predict that areas characterised by high sensitivity and high environmental variability will show lower evenness in SADs, and hence higher *sigma* values, though time. Given the dominance of temperature as a driver of higher trophic level community change and climate sensitivity (Ma *et al.*, 2015; Pinsky *et al.*, 2019), I also investigate trends in community structure against the temporal autocorrelation structure of temperature variability. In this chapter I aim to show that the effects of environmental variability via the PSI and VSI are detectable in higher trophic level communities dependent on primary productivity stability, providing a contiguous link through macroecological patterns from the abiotic to the biotic from which underlying processes can be better determined.

4.3 Materials and Methods

4.3.1 Biodiversity data

All abundance data was obtained from the BioTIME database (Dornelas *et al.*, 2018). BioTIME is an open-source database of compiled assemblage time series, comprising 12,623,386 species abundance records for marine, freshwater and terrestrial taxa covering all the major continents and marine biomes (Dornelas *et al.*, 2018). To be included in BioTIME, datasets are required to have a minimum of 2 years of recordings, a consistent sampling methodology through time, a majority of individuals identified to species level, and to have sampled assemblages with all observed individuals identified and counted (Dornelas *et al.*, 2018). From the initial BioTIME database (downloaded on 20/08/2018) datasets were selected which covered the 2000-2013 time series of the PSI and VSI, contained recordings for month as well as year, and used count abundance as oppose to density or biomass to ensure that the SADs were not influenced by methodological differences in the abundance measurements (Connolly *et al.*, 2005). After filtering for these conditions and SAD calculation compatibility (Section 4.3.3), 56 marine and 56 terrestrial datasets remained for analysis. Abundance observations within datasets were temporally aggregated on a monthly basis and then within months were spatially aggregated to 0.1° (~121 km^2) Latitude and Longitude. Within monthly 0.1° aggregations separate sampling events were not differentiated, thereby assuming that repeated species observations were repeated observations of the same individuals. The maximum observed count was therefore used for the final abundance of any repeated observations within monthly aggregations. As previously stated, this method assumes that repeated observations across sampling events are recording the same individuals. This could lead to species abundances being underestimated if sampling events are recording different individuals, which are then being aggregated. An alternative approach would be to maintain sample integrity within 0.1° monthly aggregations, whereby repeated observations of species would be classed as distinct observations. In this case the species would have increased abundance in the SAD, however this could also lead to overestimations of abundance. A third option would be to calculate SADs at the sample level rather than the study/dataset level. From this point forward individual BioTIME datasets will be referred to as ‘communities’.

4.3.2 Sensitivity and climate data

To calculate the average primary productivity sensitivity associated with individual BioTIME communities, the coordinates of abundance observations for each selected BioTIME community were used to extract corresponding sensitivity values from a raster grid of the PSI

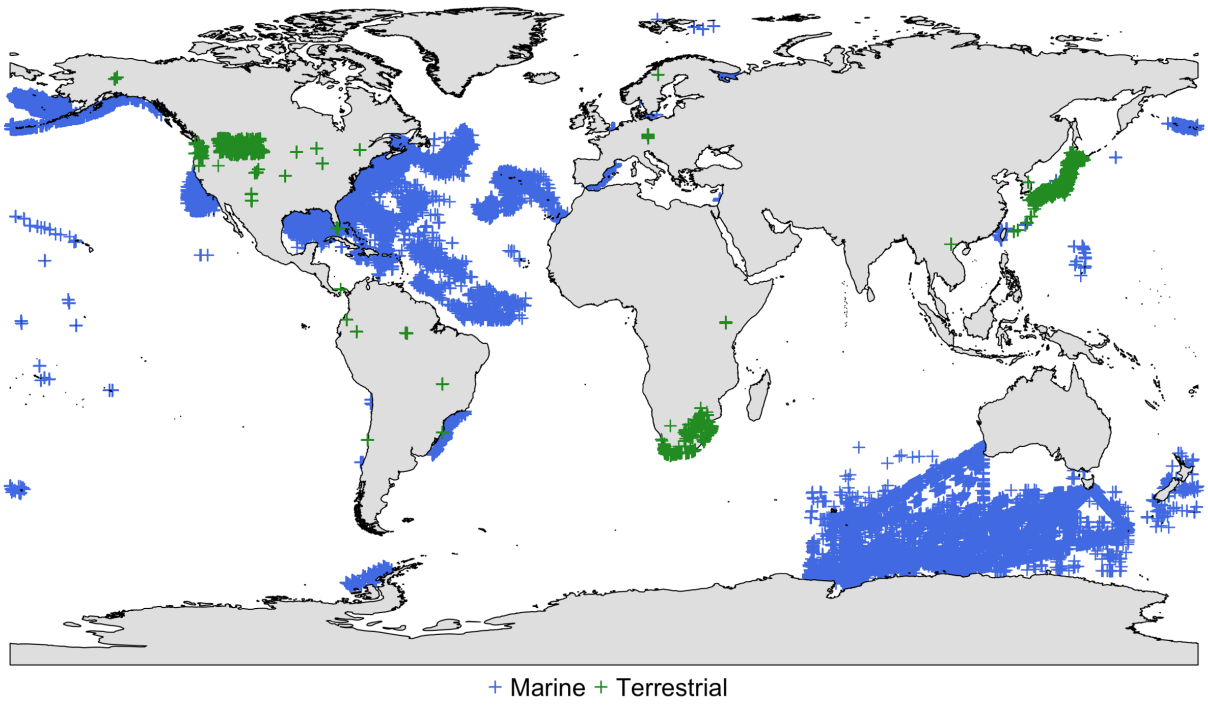

Figure 4.1: BioTIME abundance data distribution. Distribution of BioTIME abundance sampling data used to calculate Species Abundance Distributions for the marine (blue) and terrestrial (green) realms. 43 datasets were selected for the marine realm and 49 for the terrestrial realm. All datasets either partially, or fully cover the 2000-2013 time period used to calculate the Phytoplankton Sensitivity Index (Chapter 2) and Vegetation Sensitivity Index (Seddon *et al.,* 2016).

Table 4.1: Summary details of BioTIME datasets included in analyses.

Realm	Datasets	Observations	Biomes	Taxa
Marine	43	551,892	Polar ecoregions; Temperate shelf and sea ecoregions; Tropical seas; Tropical coral;	Benthos; Plants; Birds; Fish; Invertebrates; Mammals
Terrestrial	49	123,670	Boreal forests/Taiga Tundra; Deserts and xeric shrublands; Mediterranean forests, woodlands and scrubs; Temperate broadleaf and mixed forests; Temperate coniferous forest; Temperate grasslands, savannas and shrublands; Tropical and subtropical grasslands, savannas and shrublands; Tropical and subtropical moist broadleaf forests;	Plants; Birds; Reptiles; Invertebrates; Mammals;

(9 km, 81 km^2 resolution) and VSI (5 km, 25 km^2 resolution) using the `raster` package (Hijmans, 2020) in R (R Core Team 2018, Version 3.5.1). These community specific sensitivity values were then averaged to provide a mean value of sensitivity per community, from which community SAD parameters could be ranked. As the results of Chapter 3 suggested that trends could be better captured by variation in PSI and VSI sensitivities rather than the mean, the standard deviation of sensitivities corresponding to abundance observations within each BioTIME community were also calculated. Abundance values with no corresponding sensitivity value (i.e. no matching coordinates between the dataset and the P/VSI) were removed, reducing the final number of BioTIME communities to 43 for the marine realm and 49 for the terrestrial realm (See Figure 4.1 for final BioTIME coverage, Table 4.1 for summary details of the included communities and Appendix C Table C-1 for full details). Sea surface and air temperature data was extracted from the raw time series used to calculate the PSI and VSI for the coordinates of each abundance observation within the selected BioTIME communities. To compare SADs along gradients of temperature variability, spectral analysis was performed on the temperature *z*-score anomalies following the methods detailed in Chapter 3, Section 3.3.4. Spectral analysis quantifies the level of temporal autocorrelation within a time series, which can then be used to produce colour coefficients, classifying variability as white (no autocorrelation) or reddened (positive autocorrelation; Vasseur and Yodzis, 2004).

4.3.3 Species Abundance Distributions

The `poilog` package (Grøtan and Engen, 2008) was used in R (R Core Team 2018, Version 3.5.1) to fit the Poisson lognormal distribution to the BioTIME abundance data and estimate the mean (*mu*) and standard deviation (*sigma*) parameters for each distribution using maximum likelihood estimation (MLE; Matthews and Whittaker, 2014). Following Baldridge *et al.*, (2016), the start values for the *mu* and *sigma* parameters were set as the mean and standard deviation of $\log_{10}$ abundance for each distribution. Due to this, months with a single observation, months where each observation had an abundance count of 1 and individual abundance counts of zero had to be removed as the standard deviation could not be calculated on single data points or zeros ($\log_{10}1$), and zero values could not be logged. SAD models were fitted to each BioTIME study ID (signifying an independent dataset/community) and date (mm-yyyy) combination to produce temporal SAD parameters of community structure, resulting in 1,171 SADs for the marine realm and 877 for the terrestrial realm. The mean and standard deviation of community *mu* and *sigma* values were then calculated to obtain average SAD parameter values for each community for further analysis (Section 4.3.4). Parametric bootstrapping was used to determine the goodness-of-fit of the models, as recommended by (Matthews and Whittaker, 2014). Parametric bootstrapping simulates new sets of observations

using the estimated species abundance model parameters, from which the deviance between the model and the simulated data and the model and the empirical data can be compared to determine model fit (Connolly *et al.*, 2009). An aggregate goodness-of-fit statistic is produced from the bootstraps whereby values of < 0.5 and > 0.95 indicate lack of fit. Here, 1,000 bootstraps were performed for each SAD model. The Poisson lognormal distribution provided a good fit for all models (Appendix D Figure D-1).

4.3.4 Community trends across realms

To investigate the relationship between the mean and evenness of community SADs along gradients of sensitivity, linear mixed effects models with random intercepts (`lme4`; Bates *et al*., 2015) were fitted to the average *mu* and *sigma* parameters of each community's SADs, against the mean and standard deviation of community sensitivities fitted as fixed effects. To account for variation between the focal species of SADs the broad taxonomic group of each community, as defined by BioTIME (Table 4.1), was fitted as a random effect. Significance was determined using a likelihood ratio test with Kenward Roger approximation (`pbkrtest`; Halekoh and Højsgaard, 2014) as recommended by Luke (2017). To determine if there was a relationship between community structure through time and sensitivity level, linear regression models were fitted to each community's *mu* and *sigma* parameters against the date (mm-yyyy) of the distributions. Communities were required to have a minimum of 8 time series points to be included in the analyses. The slopes of these linear regressions were then plotted against mean community sensitivity. To determine if community composition is influenced by temperature variability, the averaged *mu* and *sigma* parameters for each community over the whole time series were plotted against the spectral frequency of sea surface temperature and air temperature within each marine and terrestrial community area respectively. To test for realm dependence in the structure of community SAD distributions, Student's *t*-Tests were performed on the average *mu* and *sigma* parameters for each community, by realm.

Data analyses were conducted in the R project for statistical computing (R Core Team 2018, version 3.5.1) using the `car` (Fox and Weisberg, 2019), `carData` (Fox et al., 2019), `cowplot` (Wilke, 2019), `dev.tools` (Wickham *et al*., 2018), `dplyr` (Wickham *et al.,* 2020), `ggplot2` (Wickham, 2016), `grateful` (Rodriguez-Sanchez, 2018), `lme4` (Bates et al., 2015), `Matrix` (Bates and Maechler, 2019), `mgcv` (Wood, 2011), `nlme` (Pinheiro *et al.,* 2019), `pbkrtest` (Halekoh and Højsgaard, 2014), `poilog` (Grøtan and Engen, 2008), `purrr` (Henry and Wickham, 2019), `raster` (Hijmans, 2020), `readr` (Wickham *et al.,* 2018), `rgdal` (Bivand et al., 2019), `sp` (Pebesma and Bivand, 2005), `stringr` (Wickham, 2019b), `tibble` (Müller and

Wickham, 2019), `tidyr` (Wickham and Henry, 2020), `tidyverse` (Wickham *et al.,* 2019), `viridis` (Garnier, 2018a) and `viridisLite` (Garnier, 2018b) packages.

4.4 Results

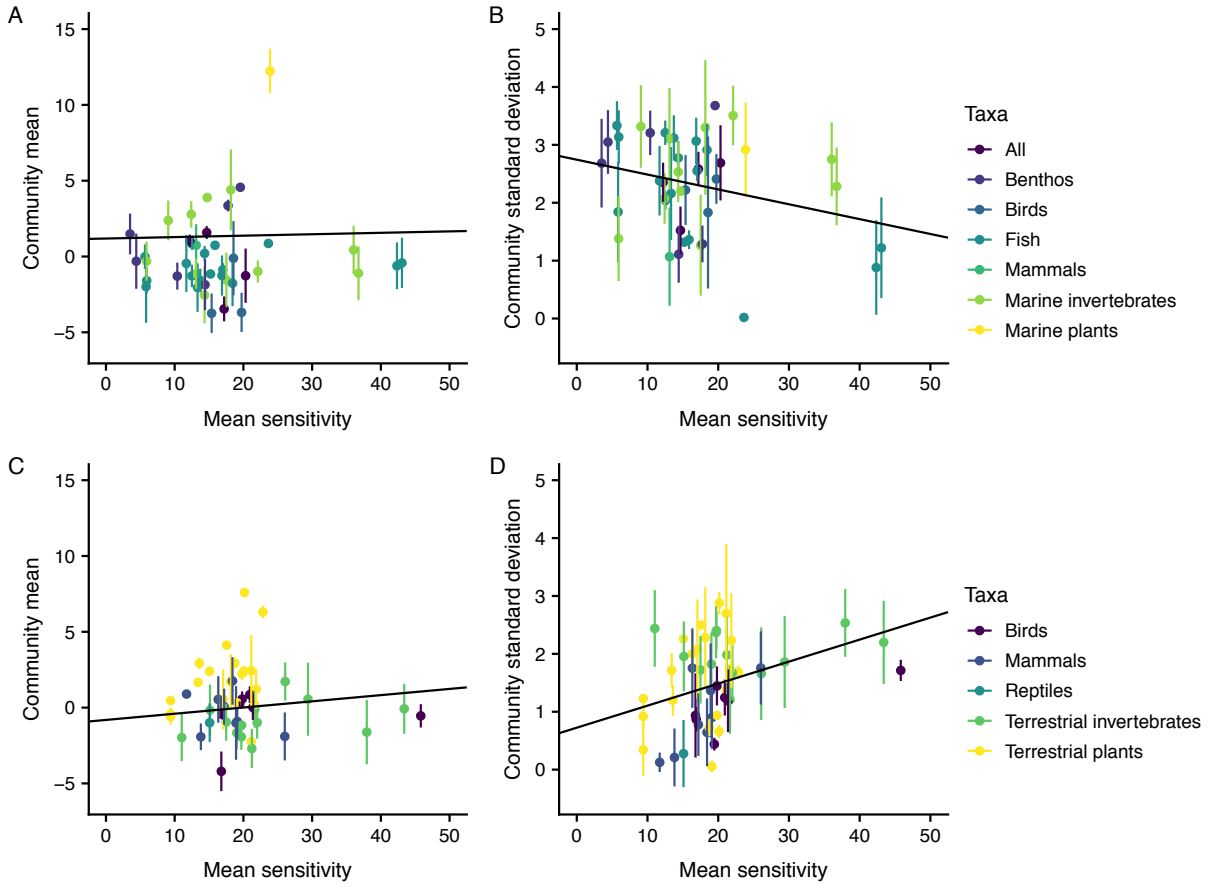

Figure 4.2: Species Abundance Distributions along gradients of PSI and VSI mean sensitivity. The average mean (mu parameter; A, C) and evenness (sigma parameter; B, D) with associated error (sd) of species abundances for each community, plotted against the mean PSI or VSI sensitivity of each community for the marine (A, B) and terrestrial (C, D) realm. SADs were calculated for each month-year combination of a community's time series within 2000-2013. Sensitivity values were extracted from the PSI and VSI for the corresponding coordinates of community abundance measurements. Trendlines are based on the results of linear mixed effects models fitted to average community mu and sigma values against mean community sensitivity from the PSI or VSI, with taxa included as a random effect. Communities are grouped by their BioTIME associated taxa.

The mean sensitivity of communities was uncorrelated with the means (*mu*) of community SAD distributions in both the marine (0.009 ± 0.347 se, t = 0.272; Figure 4.2A) and terrestrial realm (0.041 ± 0.039 se, t = 1.048; Figure 4.2C). Mean community standard deviation or evenness (*sigma*) on the other hand displayed a significant positive trend with mean community sensitivity in the terrestrial realm (0.030 ± 0.013 se, t = 2.267; $F_{1,45.7} = 4.952$, $P < 0.05$; Figure 4.2D). A weak, negative trend was visible in the marine realm (Figure 4.2B), however this was not significant (-0.026 ± 0.014 se, t = -1.801; $F_{1,40.1} = 3.121$, $P = 0.085$). The means of

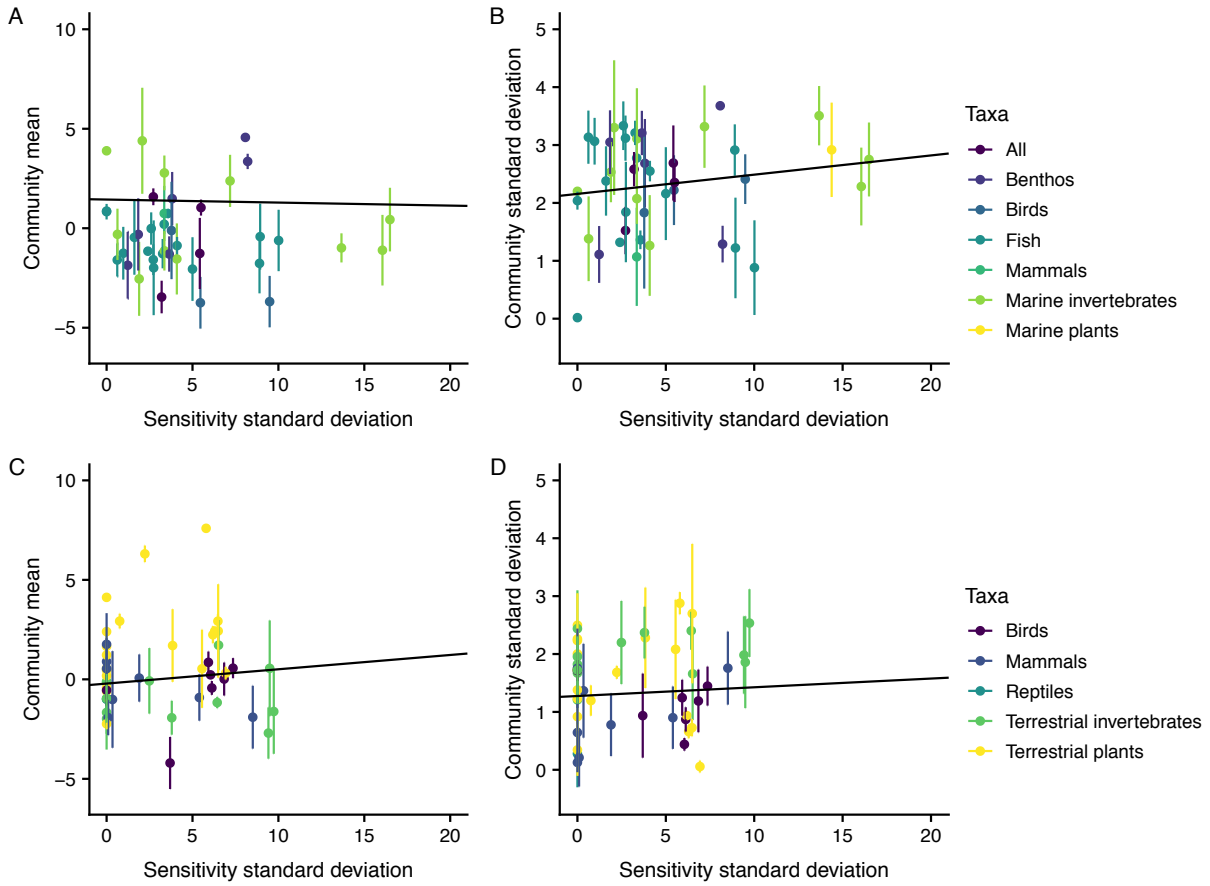

Figure 4.3: Species Abundance Distributions along gradients of PSI and VSI sensitivity standard deviation. The average mean (mu parameter; A, C) and evenness (sigma parameter; B, D) with associated error (sd) of species abundances for each community, plotted against the standard deviation of PSI or VSI sensitivity for each community for the marine (A, B) and terrestrial (C, D) realm. SADs were calculated for each month-year combination of a community's time series within 2000-2013. Sensitivity values were extracted from the PSI and VSI for the corresponding coordinates of community abundance measurements. Trendlines are based on the results of linear mixed effects models fitted to average community mu and sigma values against the standard deviation of community sensitivity from the PSI or VSI, with taxa included as a random effect. Communities are grouped by their BioTIME associated taxa.

community SAD distributions were also uncorrelated with the standard deviation of community sensitivity in both the marine (-0.015 ± 1.442 se, t = -0.195; Figure 4.3A) and terrestrial realm (0.072 ± -0.212 se, t = 0.881; Figure 4.3C), as were community standard deviations (Marine: 0.033 ± 2.156 se, t = 1.078; Terrestrial: 0.015 ± 1.275 se, t = 0.519). No evidence was found of a relationship between community composition through time and sensitivity level: the slopes of linear regressions for *mu* and *sigma* through time were uncorrelated with community sensitivity, with the majority of communities exhibiting a slope of zero across all sensitivity levels (Figure 4.4). No relationship was found between the structure of SAD distributions and temperature variability in either realm (Figure 4.5; Marine: *mu*, 1.260 ± 0.091 se, t = 0.064, *sigma*, 1.377 ± 0.965 se, t = 1.631; Terrestrial: *mu*, 0.573 ± -1.484 se, t = -0.794, *sigma*, 1.357 ± -0.7754 se, t = -0.111). Community SAD distributions are realm dependent with respect to evenness but not to mean, with average community *sigma* parameters being significantly

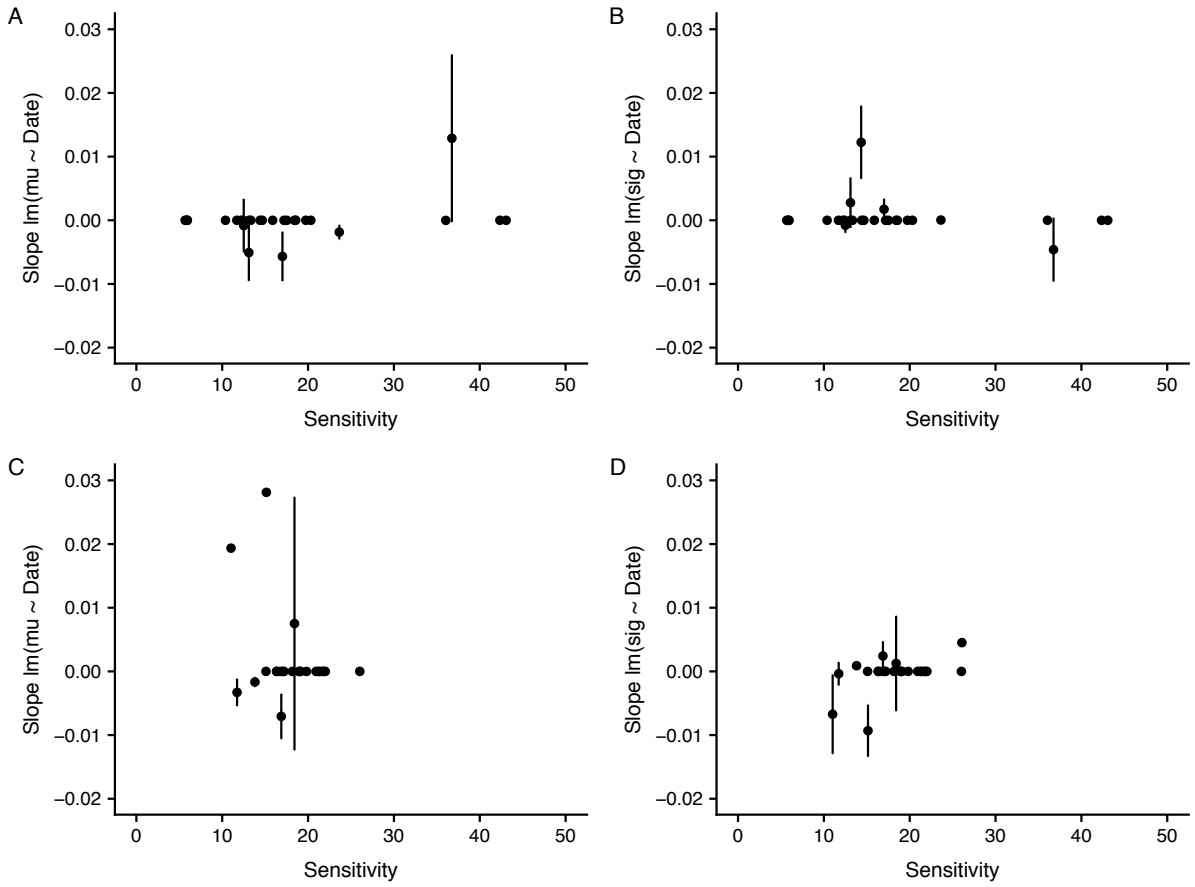

Figure 4.4: Community composition through time against mean community sensitivity for the marine (A,B) and terrestrial (C,D) realm. The slope of linear regressions between the mean (mu; A, C) and evenness (sigma; B, D) of species abundance distributions through time for each community, against the mean sensitivity of each community. Communities were required to have a minimum of 8 time points to be included in the analyses.

higher in the marine than terrestrial realm (Marine: 2.318; Terrestrial: 1.490; t = 4.964, df = 83.845, $P < 0.01$). No significant difference was found between average community *mu* parameters for the marine and terrestrial realms (Marine: 0.073; Terrestrial: 0.381; t = -0.591, df = 78.99, $P = 0.556$). Removal of outliers with unusually high mean values in both realms (Appendix D Figure D-2) did not change the result and the outliers were not obviously anomalous to warrant their removal. Within each realm the *mu* and *sigma* parameters were uncorrelated (Appendix D Figure D-3).

4.5 Discussion

Environmental stochasticity is known to affect species dynamics and processes (Dawson and Hamner, 2008; Ma *et al.*, 2015; Suryan *et al.*, 2009), influencing the turnover and abundance of species within communities (Ives *et al.*, 1999). This influence can be detected in changes in the structure of species abundance distributions (SADs), with communities expected to become less even (have a greater spread of species abundances) with increasing

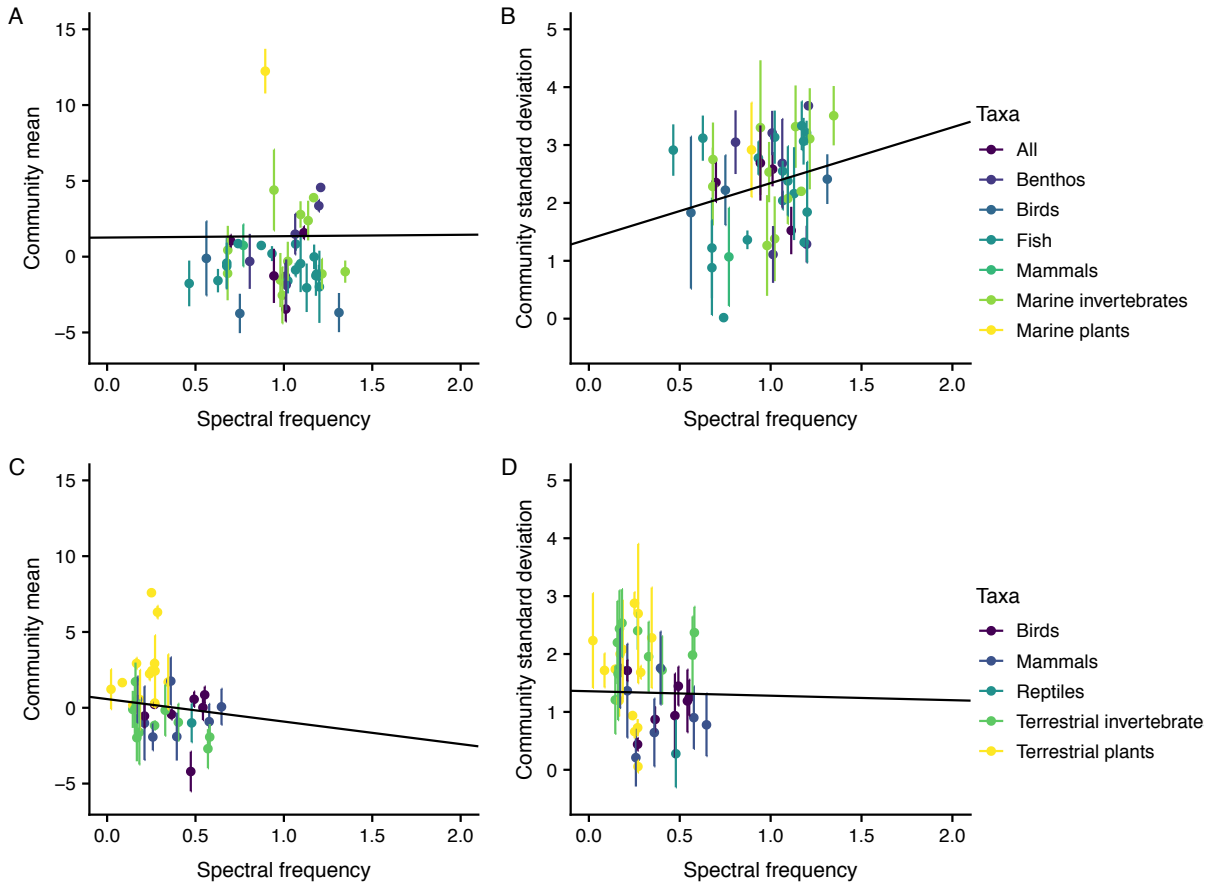

Figure 4.5: Species Abundance Distributions along gradients of temperature temporal autocorrelation. The average mean (mu parameter; A, C) and evenness (sigma parameter; B, D) with associated error (sd) of species abundances for each community, plotted against the spectral frequency of temperature for each community in the marine (A, B) and terrestrial (C, D) realm. SADs were calculated for each month-year combination of a community's time series within 2000-2013. Spectral frequencies were calculated for sea surface temperature and air temperature for the 2000-2013 time series for the corresponding coordinates of each community's abundance measurements. Trendlines are based on the results of linear mixed effects models fitted to average community mu and sigma values against the spectral frequency of community temperature through the time series, with taxa included as a random effect. Communities are grouped by their BioTIME associated taxa.

environmental variability (Sæther *et al.*, 2013b). One way these effects can manifest in higher trophic levels is through population responses to variability in primary productivity. Here, marine and terrestrial assemblage data from the BioTIME database (Dornelas *et al.*, 2018) was combined with sensitivity data from the Phytoplankton Sensitivity Index (PSI; Chapter 2) and Vegetation Sensitivity Index (VSI; Seddon *et al.*, 2016) to investigate if trends were detectable in the structure of cross-realm community SADs along gradients of primary productivity sensitivity relative to environmental variability. A significant trend of decreasing community evenness with increasing primary productivity sensitivity was identified in the terrestrial realm. However, trends were inconsistent across realms with no significant evidence being found of marine community structure being correlated with gradients of primary productivity sensitivity. In placing SADs into the context of the abiotic environment I have shown that it is possible to detect trends in macroecological patterns of higher trophic level

species diversity that are directly related to global indices of primary productivity sensitivity, and hence indirectly to environmental variability.

The *sigma* parameter of an SAD represents the standard deviation or evenness of abundances within a community, with a high *sigma* value indicating high standard deviation and low evenness and vice versa. The positive relationship identified between the *sigma* parameter for BioTIME community SADs and increasing primary productivity sensitivity in the terrestrial realm supports my prediction that communities would exhibit lower evenness, and hence a larger spread of species abundances, with increasing primary productivity sensitivity and environmental variability. Increased primary productivity sensitivity reflects lower resilience in producers to anomalous environmental variability, with an associated increased extinction risk (Burgmer and Hillebrand, 2011; Kaneryd *et al.*, 2012). Increased environmental variability can also cause increased species turnover in populations, which can be indicated by low evenness (Sæther *et al.*, 2013b). As a result, this trend suggests that certain terrestrial populations have low resilience to current increased fluctuations in primary resource availability and could be at increased risk of structural change with future increases in environmental variability. The positive trend demonstrated here also confirms that increased variability at the primary producer level can have a detectable influence on macroecological parameters describing higher trophic level community structure in the terrestrial realm.

Past research examining SADs along productivity gradients found that greater evenness (lower *sigma*) occurs in regions with higher productivity (Hubbell, 1979; Hurlbert, 2004; Whittaker, 1960). Whilst I have not explicitly examined productivity levels here, I showed in Chapter 3 that increased sensitivity is associated with highly productive and species rich environments. Taken together, these results suggest the presence of inverse relationships between productivity and sensitivity with evenness. However, it is worth noting that an ecosystem can have high productivity without also having high sensitivity, diversity or richness (Whittaker, 1960), particularly at temperate latitudes where the majority of our community data is concentrated (Figure 4.1). Temperate regions typically have fewer species and have had less time to evolve niche differentiation, making it harder for rare species to take hold (Whittaker, 1965). Their SADs are therefore rather even, with more species of intermediate abundance and hence lower *sigma* (Whittaker, 1965). Tropical ecosystems on the other hand have more established niche differentiation and can maintain high species diversity resulting in more rare species, a greater spread of abundances and a less even population (Whittaker, 1965). It would be interesting to see if existing trends in evenness with productivity gradients are supported with more recent data for tropical regions, or if this trend is counteracted by the increased sensitivity in these regions.

No significant evidence was found of community SAD structures varying with primary productivity sensitivity in the marine realm. However, whilst marine community structure is not significantly correlated with gradients of primary productivity sensitivity, a strong negative trend is present between community standard deviation and sensitivity suggesting that marine populations show increasing evenness with increasing sensitivity. The lack of significant trend could be due to weaker trophic coupling between primary productivity and higher trophic level taxa in the marine realm compared to in the terrestrial realm. Food chains in the marine realm are typically linear with zooplankton being the dominant consumer of phytoplankton. As a result, most marine taxa included in these analyses would be indirectly affected by phytoplankton sensitivity (surface phytoplankton fluctuations) through effects on their prey, e.g. marine mammals. The terrestrial realm by contrast contains herbivores within every included taxon, which are directly dependent upon primary producer stability. The trend not being significant and being the opposite direction to the trend found for the terrestrial realm could also suggest that community evenness in the marine realm is driven by factors other than primary productivity sensitivity.

As well as cross-realm differences in trends between community SAD structural parameters and primary productivity sensitivity, cross-realm differences were also found in the SAD structural parameters themselves, with marine communities exhibiting significantly lower evenness (higher *sigma*) than terrestrial communities overall. This is perhaps surprising given the supposed homogeneity of the marine realm, as it could be expected that the increased stability of the marine realm would enable more similar species abundances to occur within communities. However, this result does support previous findings of higher species turnover in the marine realm (Blowes *et al.*, 2019; Pinsky *et al.*, 2019), which low evenness can be reflective of. The lack of relationship between *mu* and *sigma* within each realm despite this significant difference in cross-realm *sigma* is surprising and could have several causes. Increased dominance in the marine realm (i.e. common species being more common) would lead to an increased community standard deviation, as would a higher proportion of rare species, which could be reflective of poorer sampling in the marine realm. However, it is also possible that it is simply the result of a measurement effect whereby communities are censused differently in the two realms (Rafaelli *et al.*, 2005). No compelling evidence was found of trends between taxonomic class and sensitivity in either realm, likely due to the small sample sizes of communities available for each taxon. I also found no evidence of differences in assemblage structure across taxa both within and between realms, again likely due to the small sample sizes.

The prevalence of slopes at, or close to zero in linear models of SAD parameters against time suggests that the communities have not undergone substantial change during the time series examined, at least at this aggregate scale. This is in contrast to the results of Blowes *et al.* (2019) who identified a faster rate of compositional change in marine versus terrestrial communities. This contrast between SAD and compositional metrics is likely due to the unlabelled nature of SADs, whereby species identities are not included in analyses. If immigration, emigration and/or extinction of species occur with a similar frequency and affect similar abundances within a time series, the overall evenness and richness of a community can remain the same, resulting in no detectable trend in SAD structure despite potentially high turnover of species (Brown *et al.*, 2001; Dornelas *et al.*, 2014; Hillebrand *et al.*, 2018). However, whether masking of species turnover has occurred or not the lack of directional change in slopes is unsurprising given the short length of the time series examined. Despite the short time series, it is encouraging to note that communities in both low and mid-sensitivity environments across realms show no sign of significant change, suggesting that the communities are resilient to current levels of environmental variability effects on primary productivity. Whilst there was no evidence of directional change through time in community SAD structures, the error bars for each community in Figure 4.2 -Figure 4.3 suggest that there is some temporal variance within the individual communities during the time series.

Despite temperature being a major driver of community change (Easterling *et al.*, 2000; Ma *et al.*, 2015; Pinsky *et al.*, 2019; Poloczanska *et al.*, 2013; Vasseur *et al.*, 2014), no significant trends between community SAD structure and temperature autocorrelation were found in either realm. Whilst there is some suggestion of a positive trend between spectral frequency and community spread for the marine realm (Figure 4.5B), which would be consistent with marine communities experiencing more reddened temperature variability having lower evenness of abundances, this was not significant. My results do, however, further reflect the whiter nature of temperature temporal autocorrelation in terrestrial systems demonstrated in Chapter 3 (Figure 3.9), with terrestrial communities exhibiting spectral frequencies almost exclusively between $0 \leq ß \leq 0.5$ compared to $0.5 \leq ß \leq 1.5$ for marine communities (Figure 4.5). The lack of trends found here is perhaps surprising given the recent wealth of research showing the considerable ecosystem effects of temperature anomalies over changes in mean conditions (Blowes *et al.*, 2019; Easterling *et al.*, 2000; Ma *et al.*, 2015; Pinsky *et al.*, 2019). This could indicate that individual extreme events are more important drivers of change than the general structure of variability experienced by an ecosystem, or that a longer time series would be required to detect trends due to general variability over single anomalous events. I also considered whether precipitation would be a more appropriate variable to use for the terrestrial realm, given that large parts of the terrestrial realm are water limited (Pearce-Higgins

et al., 2015; Seddon *et al.*, 2016) and precipitation had been identified as the biggest driver of sensitivity in several regions (Chapter 3, Figure 3.11). However, preliminary investigations showed this not to be the case (Appendix D Figure D-4).

Whilst within the PSI and VSI trends in sensitivity were strongest when looking at the range of sensitivities (Chapter 3), here trends in SAD structure were less visible when compared against the standard deviation of community PSI and VSI sensitivity rather than mean sensitivity. This could be due to the different focus of the analyses performed here. Trends in the spread of sensitivities within the PSI and VSI identified in Chapter 3 were most visible in spatial analyses of latitudinal gradients. The SAD analyses conducted here were focussed on temporal trends, with SADs fitted to BioTIME community-month (mm-yyyy) combinations regardless of the spatial extent of observations within each month. As a result, some BioTIME community-month combinations SADs were fitted to contained observations covering a large spatial extent (Appendix D Figure D-5A & C). Whilst I considered that the purely temporal focus of the analyses conducted here made it reasonable to spatially collate the abundance observations (the majority of SADs fitted cover less than 1° Latitude and Longitude (Appendix D Figure D-5B & D, Table D-1), spatial analysis such as conducted by Blowes *et al.* (2019) might be more likely to reveal gradients similar to those observed in the PSI and VSI. Data limitations however prevented a more thorough spatial analysis from being conducted. Despite the breadth of the BioTIME database, after filtering for abundance measure (i.e. count versus density) and time series the spatial extent of terrestrial community data was almost exclusively limited to a narrow range of latitudes and longitudes in North America, South Africa and East Asia, whilst marine data was heavily biased towards the West Atlantic and Southern Ocean surrounding Australia (Figure 4.1). The limited spatial coverage restricted the possibilities of doing spatial analyses along latitudinal gradients, similar to that of Blowes *et al.* (2019), which could further reveal where the effects of environmental variability on primary productivity resilience are already being felt in the community structure and stability of dependent higher trophic level populations.

The limited spatial coverage also resulted in there being no communities with mean primary productivity sensitivities from the PSI and VSI above 50 included in the analyses, limiting the ability to draw conclusions regarding the effects of high sensitivity on community structure. Given visual indications of a negative trend between community evenness (*sigma*) and sensitivity in the marine realm (Figure 4.2B), it is possible that with an extended sensitivity axis this would have become significant and presented the opposite trend to that found in the terrestrial realm. It would also have enabled geographic separation of the existing terrestrial trend to investigate if evenness is correlated with the latitude and/or species richness of a

community as well as producer sensitivity, providing an extra layer of explanatory value. Theoretical studies suggest that species rich ecosystems are more vulnerable to the effects of increased climatic variability and face higher risks of extinction, particularly if species responses are uncorrelated within a community (Borrvall and Ebenman, 2008b; Kaneryd *et al.*, 2012). With increased data availability the visual trends detected in spectral frequency might also become significant and inter-taxon patterns might be revealed.

4.6 Conclusions

In this study I have placed SADs into the context of the abiotic environment via global indexes of primary productivity sensitivity relative to environmental variability. In doing so, I have shown that it is possible to detect trends in the structure of higher trophic level communities directly related to primary productivity sensitivity and hence indirectly to environmental variability, providing a possible method of detecting future variability induced ecosystem change. I have shown that responses across realms are not consistent, with the lack of significant trends in the marine realm suggesting that (accepting the caveats discussed above) community stability is more resilient to increasing primary productivity sensitivity in marine than terrestrial communities. Having shown that the structure of SADs can be correlated with environmental variability and primary productivity sensitivity, a logical next step would be to introduce labelled SADs to increase understanding of individual species patterns within communities (McGill *et al.*, 2007) and to further look into the roles of species turnover and core and transient species in community responses to environmental variability and primary resource sensitivity. Species turnover in labelled SADs would provide more detailed information on immigrations and extinctions, and is both more sensitive to (Dornelas *et al.*, 2014) and more easily related to (Hillebrand *et al.*, 2018) environmental change. Focal species identified during this process could then be further investigated in terms of their life history traits to determine which traits promote or impede longevity or community stability along gradients of climate sensitivity.

5 General Discussion

The main aim of this thesis was to determine whether an explicit consideration of patterns of environmental variation, and species responses to these, could help to move beyond binary marine-terrestrial distinctions towards a more generalised formulation of ecological responses to environmental change, that hold across marine and terrestrial systems. To achieve this, I have created a new index of marine primary productivity sensitivity relative to environmental variability (Chapter 2) and explored its potential to bridge the marine-terrestrial divide (Chapter 3), to explain environmental drivers of sensitivity (Chapter 3), and to understand variability in macroecological patterns of species abundance diversity (Chapter 4). Here, I summarise the key findings of this research (Section 5.1) and the contributions they make towards the advancement of cross-realm macroecology (Section 5.2). I also provide an overview of the main limitations of the work (Section 5.3) and detail future avenues of research that could further build on the work presented here (Section 5.4).

5.1 Key findings

I. The Phytoplankton Sensitivity Index (PSI) provides a global baseline of marine primary productivity sensitivity relative to environmental variability. Marine primary productivity is most sensitive to fluctuating environmental conditions in tropical and polar regions, coinciding with highly diverse and species rich ecosystems, indicating that these regions will be less resilient to future increases in environmental variability. The majority of the oceans exhibit low-mid sensitivities and are likely resistant to environmental variability at a primary producer level, however predicted expansion of low sensitivity areas could have considerable consequences for global phytoplankton composition. In adapting the methods of Seddon *et al's* (2016) existing Vegetation Sensitivity Index (VSI) for the terrestrial realm to create the PSI, the two indices are comparable and can be combined to create a truly global picture of primary productivity sensitivity and enable the identification of generalised cross-realm trends (Chapter 3).

II. Primary productivity sensitivity successfully reveals general trends that hold across both marine and terrestrial realms and a range of spatial scales. Supporting the visual trends identified in Chapter 2, a cross-realm latitudinal gradient is present in primary productivity sensitivity at global and hemispheric scales, showing increasing sensitivity in the tropics and towards the poles. The gradient is more pronounced in the range of sensitivities than the mean across all spatial scales, suggesting that more widely used

average measures of change might miss key information. The Southern hemisphere is more sensitive than the Northern hemisphere at high latitudes (>40° Latitude) in both realms, indicating that the Northern bias in research effort may lead to underestimations of the predicted impacts of climate change in the Southern hemisphere. Regional scales are less effective for reliably demonstrating both the latitudinal gradient in sensitivity and for capturing patterns in climate driver influence, particularly in the marine realm, however this could be a reflection of the suitability of the regionalisation used. Whilst trends in sensitivity are realm-independent, there are considerable differences in the influence of - and interactions between - environmental drivers on sensitivity between the marine and terrestrial realms. In the marine realm, differences between the climate variables in their influence on sensitivity are marginal, whereas the terrestrial realm exhibits dominant climate influences which vary considerably in space and may have predictive value both within and between biomes. These differences in climate influence across realms must therefore be accounted for when interpreting the causes of sensitivity. I provide evidence of similar patterns of temporal structure in primary productivity anomalies across realms with similar abiotic correlations, however this warrants further investigation due to the lack of quantitative support in spectral analyses. This global, macroecological view of sensitivity to environmental variability can be used to examine the responses of higher trophic level communities along gradients of sensitivity (Chapter 4).

III. Trends are detectable in the parameters of species abundance distributions (SADs) along gradients of primary productivity sensitivity. In accordance with predictions from theory, the community structure of terrestrial populations exhibits decreasing evenness with increasing sensitivity. Thus, trends can be detected in macroecological patterns of higher trophic level species diversity, directly related to indices of primary productivity sensitivity relative to environmental variability. Whilst marine community structure is not significantly correlated with gradients of primary productivity sensitivity, a strong negative trend is present between community standard deviation and sensitivity, suggesting that marine populations show increasing evenness with increasing sensitivity. Community structure shows further realm-dependence with marine populations having significantly lower evenness than terrestrial populations, supporting findings that species turnover is occurring faster in the marine than terrestrial realm (Blowes *et al.*, 2019; Pinsky *et al.*, 2019).

5.2 Contributions to cross-realm macroecology

The work presented in this thesis provides several unique contributions to the development of cross-realm macroecology with integrated environmental explanatory power. By adapting the methods of Seddon *et al.* (2016) to create the PSI (Chapter 2) I have shown that examining the literature outside of your main realm of study can have fruitful results, and that methods developed for a feature of one realm (i.e. primary productivity; De Keersmaecker *et al.*, 2015; Seddon *et al.*, 2016) can successfully be applied to an equivalent feature in a different realm. This is important as journalistic separations between marine and 'general' ecology can reduce the examination of cross-realm literature and the subsequent extent of cross-realm fertilisation of ideas, impeding the rate of development and integration of ecological methods and theories across disciplines (Dawson, 2009; Menge *et al.*, 2009; Rafaelli *et al.*, 2005; Webb, 2012). I have also shown that by considering a common feature of all primary producers that can be measured in real time at a global scale (i.e. chlorophyll-a (Chl-a)), the differences in temporal and spatial scales of marine and terrestrial producer life histories can be overcome and generalised trends can successfully be identified across realms and at a range of spatial scales (Chapter 3). This work lends support to the approaches of Webb, (2012), who proposed that looking at a macroecological scale would likely be both revealing and unifying for marine-terrestrial comparative studies, and Dawson and Hamner (2008), who argued that quantifying a feature in common units across realms would be a more effective way to approach comparative studies than simply stating 'marine v terrestrial' divisions. Dawson and Hamner (2008) used the example of Reynolds number for quantifying interactions between organisms and their fluid environment, here I have shown primary productivity sensitivity to be equally effective.

The PSI is the first global measure to show phytoplankton sensitivity to variability in three governing variables of the marine environment, shedding light on the global distribution of marine resilience to short term environmental variability. From this I have identified a new latitudinal gradient in phytoplankton sensitivity concurrent with latitudinal gradients of phytoplankton species richness (Menegotto and Rangel, 2018; Righetti *et al.*, 2019), with low sensitivity and low species richness coinciding in the midlatitudes and high sensitivity and high species richness occurring in the tropics. The PSI also shows that phytoplankton responses to environmental variability are not consistent across ecosystems, comparable to the global distribution of phytoplankton responses to changing mean conditions (Häder *et al.*, 2014). In combining the PSI with the VSI (Chapter 3) the sensitivity status of marine and terrestrial realms to current levels of variability was found to be very similar, with both realms being dominated by low sensitivities. This is perhaps cause for some optimism given its implications

for global resiliency, however my results also reaffirm the results of other global studies (e.g. Beaumont *et al.*, 2011; Diffenbaugh and Giorgi, 2012) that the impacts of climate change will be most strongly felt in the tropics and high latitudes, as they are already exhibiting signs of increased sensitivity and low resilience to current climate conditions. The P/VSI indices are also specific to primary productivity responses to environmental variability, however there are a multitude of other pressures currently facing both realms including ocean acidification, pollution, overexploitation and habitat change. As such, ecosystems must respond to the cumulative impact of all of these stressors and anthropogenic climate change at once and at a rate that has not previously been experienced. A valuable avenue of future research would be to combine the PSI and VSI with metrics of ecosystem responses to other stressors, which could shed light on cumulative ecosystem sensitivity to multiple stressors.

To effectively bridge the marine-terrestrial divide, the PSI and VSI needed to exhibit general trends that held across realms at a range of spatial scales. The latitudinal gradient identified in primary productivity sensitivity achieved this at both global and hemispheric scales. The gradient also demonstrated where biases and/or conventions in current research practices could result in inaccurate or missed predictions. For example, the latitudinal sensitivity gradient shows that primary productivity responses between 40°N and 40°S are very similar and would perhaps allow for extrapolation across hemispheres, however above these ranges sensitivity in the Southern hemisphere outstrips that in the Northern hemisphere, particularly in the marine realm. This further confirms the disadvantages of the Northern, temperate bias in ecological research (Beck *et al.*, 2012; Chambers *et al.*, 2013; Pearce-Higgins *et al.*, 2015), as it could result in predicted impacts in the Southern hemisphere being considerably underestimated. My findings at the regional scale also suggest that the widely used Longhurst classification structure (Longhurst, 1995a, 2007) could be prohibitively large for capturing regional patterns in marine responses to environmental variability and that within region variance needs to be considered when interpreting results. Finally, the gradient being considerably stronger in the range of sensitivities than the mean, suggests that the traditional focus on mean changes within regions or populations could result in missing important elements of variation or trends in population responses to change.

The boosted regression tree analysis (BRT; Elith *et al.*, 2008) performed in Chapter 3 to model interactions between climate drivers in the PSI and VSI was inspired by Nieto and Mélin (2017), who performed a similar BRT analysis for the Gulf of Guinea to determine the variability of ocean colour derived Chl-a in relation to a suite of 8 physical variables, including temperature and wind. The main difference between the BRT analysis conducted by Nieto and Mélin (2017) and the one conducted here was the spatial scale. Nieto and Mélin (2017) conducted their

analysis on 56, 200 x ~67 km cells, whereas my analysis was scaled up to global biogeographic regions. As far as I am aware, this is the first time BRT analysis has been attempted both at such a large spatial scale and to compare cross-realm environmental drivers of biotic change. Whilst the analysis conducted here revealed valuable insights on the relative dominance of drivers of primary productivity sensitivity, the increased scale did present some limitations. Due to computing power and time requirements it was not possible to run the analysis at either full index or biome scales as had originally been planned. The smaller spatial scale employed by Nieto and Mélin (2017) also enabled them to incorporate a greater range of driving variables than would be possible at larger spatial scales due to reduced data availability. Nonetheless, the BRT analysis provided valuable additional information with respect to climate influence on primary productivity sensitivity and established the upper spatial limits that BRT analyses can effectively be applied to for future studies.

The analyses conducted in Chapter 4 build on the work of Sæther *et al.* (2013b), who promoted parametric methods of SAD analysis as a means to identify the influence of environmental stochasticity on community dynamics. Through the use of lognormal SAD distributions, I have shown that the statistical parameters of macroecological distributions of species diversity can be analysed in conjunction with gradients of primary productivity sensitivity, identifying differences in community structure across realms indirectly attributable to environmental variability, due to direct influences on primary resource stability. My results support existing work showing that increased environmental stochasticity causes lower evenness in lognormal population abundance models (Sæther *et al.*, 2013b) in the terrestrial realm. The negative (non-significant) trend identified in the marine realm of increasing community evenness with increasing stochasticity presents an interesting juxtaposition to this theory and requires additional work to determine if the expected influences of external variability on community structure are realm dependent. That being said, I have shown that gradients of primary productivity sensitivity can provide an effective link for correlating environmental stochasticity with community structure both across realms and trophic levels, thus demonstrating that primary productivity is an effective currency on which to build cross-realm macroecology.

5.3 Limitations

The main limitations of the PSI are the uncertainties associated with using satellite data, given that it is entirely created from remotely sensed variables and can only represent sea surface production. Ocean colour measurements in particular are known to be less accurate in coastal waters due to increased suspended sediments and dissolved organic matter in surface run off, however the European Space Agency (ESA) Ocean Colour Climate Change Initiative (OC-

CCI; Plummer 2017) Chlorophyll-a (Version 3.1) product I used featured an updated algorithm to improve coverage in such waters (Brewin *et al.*, 2015; Lavender *et al.*, 2015; Müller *et al.*, 2015) and was the best available dataset at the time. A new version of the OC-CCI product (Version 4.0) was released in March 2019 (followed by Version 4.2 in December 2019 as the Chl-a variable in Version 4.0 was faulty) using NASA's most recent reprocessing of the satellites, however the algorithms used to calculate the final Chl-a product were the same as in Version 3.1 so differences will be minimal and unlikely to have an effect on the PSI output. No marine wind datasets are considered to be without limitations (Kent *et al.*, 2013) and the dataset used to create the PSI exhibits higher variability than in situ buoy data (Peng *et al.*, 2013), however it was chosen as it was the highest spatial resolution global dataset available for the time period of the study. Any biases present in the data could be accounted for in regional studies as regional quantifications of over or under-estimates of wind speed are available (Kent *et al.*, 2013; Peng *et al.*, 2013).

In all cases I chose datasets that combined data from multiple satellite datasets bias-corrected with respect to one another, to both maximise spatial and temporal coverage and to reduce uncertainties and missing data. Even with combined products missing data can still occur as was found for Chl-a pixels during Southern hemisphere winter months, however this affected fewer than 14% of pixels and so would have been unlikely to affect the results of the final index. Even with the caveats discussed, these datasets are the best we currently have. They make it possible to determine the amount of primary productivity across the globe at any given time, removing the need to rely on spatially and temporally limited in situ datasets and vastly increasing the scope of macroecological studies. Furthermore, the Essential Climate Variable initiative (Bojinski *et al.*, 2014; GCOS, 2010) ensures that they are produced to the high standard necessary for climate modelling.

Whilst the PSI was created following the methods of Seddon *et al.* (2016), the PSI could actually be a more accurate reflection of primary producer sensitivity than the VSI. Due to the small size of phytoplankton, ocean colour measurements of Chl-a correspond almost directly to primary producer biomass. Combined with no anthropogenic exploitation, phytoplankton responses can be attributed entirely to abiotic drivers and zooplankton grazing. The relationship between terrestrial producer Chl-a measurements and biomass is more dynamic given the differences in mass between terrestrial producers and their photosynthetic components i.e. grass versus trees. On top of this, deforestation and agricultural practices could have large impacts on terrestrial primary productivity unrelated to climate which are not accounted for in the VSI. Whilst terrestrial Chl-a measurements may not directly correspond to producer biomass, by simply measuring 'greenness' the Enhanced Vegetation Index (EVI)

used in the VSI only records the photosynthetic component of terrestrial producers and therefore still closely correlates with the ocean colour measurements used in the PSI.

Both the PSI and VSI are strongly right skewed towards low sensitivities. Whilst this is an encouraging result in terms of resilience implications for primary productivity in each realm, it restricted the possibilities for determining sensitivity-specific attributes of primary producers and their driving climate variables, as there are too few high sensitivity pixels to create an adequate gradient that spans the full spectrum of sensitivities. This limited both the spectral analysis investigating sensitivity specific traits in the temporal structures of primary productivity and climate driver variability (Chapter 3) and the identification of trends in higher trophic level community structure with sensitivity (Chapter 4), as there were insufficient mid-high sensitivity pixels to create a sensitivity gradient that went much above 40. Given that this is due to the current status of primary productivity sensitivity it is not something that necessarily requires correction or improvement per se, however there are theoretical and hypothetical future means of obtaining a full gradient for better identification of trends. For example, as satellite data continues to be collected in the future and the indices are updated, these analyses could be rerun at 10 yearly intervals to determine if trends in sensitivity have changed, potentially resulting in a full sensitivity gradient for trend analyses. Alternatively, the frequency of variation of the input variables to the indices could be modulated in line with climate predictions to predict where will become sensitive in the future, with analyses repeated on the sensitivity gradients produced.

The spatial distribution of data availability in Chapter 4 limited the trend analyses that could be conducted. Despite the BioTIME database (Dornelas *et al.*, 2018) containing an extensive amalgamation of species observation records, after filtering to meet the analysis requirements observations were almost exclusively limited to a narrow range of locations in North America, South Africa and East Asia on land, whilst marine data was heavily biased towards the North West Atlantic and Southern Ocean surrounding Australia (Figure 4.1). Even without filtering, gaps in global sampling intensity and coverage are evident within BioTIME and other similar large data compilations (e.g. the Ocean Biogeographic Information System (OBIS; https://www.obis.org) and the Global Biodiversity Information Facility (GBIF; https://www.gbif.org) due to the northern, temperate (and largely coastal) bias in global data collection (Chambers *et al.*, 2013; Marco *et al.*, 2017; Menegotto and Rangel, 2018; Titley *et al.*, 2017; Trimble and van Aarde, 2012). Increased data coverage of Southern hemisphere oceanic systems and continental Africa, Asia and South America could both strengthen the trends identified here between community structure and environmental variability sensitivity

and enable the identification of new trends, particularly if biases in global taxa coverage improved in line with geographic coverage.

5.4 Future directions

Several avenues of further research are available which would make a valuable continuation of the work presented here, extending our understanding of both the causes of sensitivity and ecological responses to environmental variability, thus providing further explanations of the underlying processes behind observed trends in macroecological patterns in response to environmental variability. Here, I detail what I consider to be the most promising and/or urgent avenues of further investigation including: investigating the cause of sensitivity at a primary producer level (Section 5.4.1); extending SAD analyses to enable the identification of exemplar species and/or assemblages exhibiting persistence or change along gradients of environmental variability sensitivity (Section 5.4.2); and examining the life history traits of identified assemblages along gradients of sensitivity (Section 5.4.3).

5.4.1 The causes of phytoplankton sensitivity

In producing the PSI, I identified the spatial distribution of phytoplankton sensitivity to environmental variability (Chapter 2). Whilst I have discussed the possible causes of sensitivity in terms of abiotic conditions (Chapter 2, 2.5), examining the community composition and associated life history traits of phytoplankton along gradients of sensitivity would provide valuable explanatory information on why certain regions exhibit high or low sensitivity from a biotic perspective. Despite the relatively ‘open’ nature of the marine realm, phytoplankton composition is regionally variable (Alvain *et al.*, 2008; Cabré *et al.*, 2016; Uitz *et al.*, 2010) with low biomass regions typically characterised by smaller phytoplankton types (e.g. picophytoplankton; Marañón *et al.*, 2001) than high biomass regions (e.g. nano- and microphytoplankton; Cabré *et al.*, 2016). The community composition of phytoplankton populations can also determine how likely productivity is to vary with environmental variability (Aiken *et al.*, 2008; Cabré *et al.*, 2016; Edwards and Richardson, 2004a; Hinder *et al.*, 2012; Rousseaux and Gregg, 2012, 2015) and with a strong influence on oceanic optical properties, can be one of the fastest and most easily detected signals of climate driven change (Dutkiewicz *et al.*, 2019). Furthermore, considerable shifts in both the distribution, composition and abundance of phytoplankton communities have been projected under climate change (Barton *et al.*, 2016), on top of the global declines already occurring (Capuzzo *et al.*, 2018; Rousseaux and Gregg, 2015).

The ocean colour measurements used to calculate the PSI do not provide the species identities associated with phytoplankton biomass recordings; however, remote sensing data is now available that can identify the size structure (Brewin *et al.*, 2010; Kostadinov *et al.*, 2010), class (e.g. diatoms, cyanobacteria, dinoflagellates; Brewin *et al.*, 2017; Raitsos *et al.*, 2008) and hence functional type (e.g. nitrogen fixers, calcifiers; IOCCG, 2014) of phytoplankton. This data could be used to identify trends in both the biological attributes of phytoplankton and rates of change in phytoplankton community composition along gradients of sensitivity (e.g. via labelled SADs, Section 5.4.2). The life history traits of identified phytoplankton classes such as cell size, nutrient requirements and stoichiometry (Litchman and Klausmeier, 2008; Moreno and Martiny, 2018) could then also be investigated to see if similar responses in phytoplankton to environmental variability can be explained by the traits of the producers in those environments (Litchman and Klausmeier, 2008). This methodology could be extended across the terrestrial realm to identify if there are cross-realm similarities in traits that promote persistence and resilience in producers in response to environmental variability. Whilst differences in the temporal and spatial scales at which marine and terrestrial producers live could make direct comparisons more problematic than simply comparing 'greenness', highlighting differences across the realms can still prove beneficial (Dawson and Hamner, 2008).

5.4.2 Extending the SAD

Having shown that the structure of SADs can be correlated with environmental variability and primary productivity sensitivity (Chapter 4), a natural extension would be to introduce labelled SADs, which have been proposed as a method of increasing the understanding of individual species patterns within communities that might otherwise be masked (Dornelas *et al.*, 2006; McGill *et al.*, 2007; Webb *et al.*, 2002). For example, I found no evidence of trends in community evenness through time (Chapter 4), however this does not mean that community composition remained constant during the examined time series. If immigration, emigration and/or extinction events occur with a similar frequency and affect similar abundances the overall evenness of a population will remain the same, resulting in no detectable trend in SAD structure (Dornelas *et al.*, 2014; Hillebrand *et al.*, 2018). By labelling species these events would be identifiable and the role of species turnover via changes to core and transient species in community responses to environmental variability could be further investigated (e.g. Magurran and Henderson, 2003). This approach would combine trends in SAD community structure focussing on alpha diversity with temporal and spatial trends in species turnover focussed on beta diversity, whereby similarity indices such as Sørensen's index (e.g. Santini *et al.*, 2017) or Jaccard's dissimilarity index (e.g. Baselga, (2010), Blowes *et al.* (2019) and Dornelas *et al.* (2014)) can be used to determine change in single communities through time

or multiple communities across space, thus allowing for the comparison of both within realm and cross-realm assemblages along gradients of sensitivity (McGill *et al.*, 2015). Furthermore, species turnover is both more sensitive to (Dornelas *et al.*, 2014) and more easily related to (Hillebrand *et al.*, 2018) environmental change. As well as providing greater mechanistic inference of underlying processes in SADs, assemblages of interest identified during this process due to either their persistence or high rates of change could be further investigated in terms of their life history traits (Section 5.4.3), to determine which traits promote or impede longevity and community stability along gradients of climate sensitivity.

5.4.3 Life history traits along gradients of sensitivity

Life history traits (e.g. body size, age at maturity) can be examined either individually or in combination to assign organisms to particular life history strategies (LHS; Kindsvater *et al.*, 2016; Pecuchet *et al.*, 2017). These strategies are adapted to the environmental variability regime an organism inhabits and are typically expressed along a slow-fast continuum (Kindsvater *et al.*, 2016; Pecuchet *et al.*, 2017), whereby slow LHS are characterised by species with low adult mortality, low abundance, large body size and few, large offspring (e.g. whales), and fast LHS reflect high adult mortality, high abundance, small body size and many, small offspring (e.g. sardines). Numerous LHS frameworks have been developed for different organisms, including the Competition – Stress – Ruderal (CSR) model for plants (Grime, 1988) and the Equilibrium – Periodic – Opportunistic (EPO) model for fish (Winemiller and Rose, 1992). More recently, Kindsvater *et al.* (2016) extended the EPO and standard slow-fast continuum to include juvenile mortality, resulting in the Precocial – Opportunistic – Survivor – Episodic (POSE) framework. In the POSE framework adults and juveniles can have opposing strategies, for example a species with the Episodic LHS might have many small offspring but a large adult body size and life span to increase recruitment and survival in variable but predictable environments (Juan-Jordá *et al.*, 2013; Kindsvater *et al.*, 2016). The LHS expressed by an organism is adapted to environmental conditions through the influence of environmental variability structure (Dawson and Hamner, 2008) and resource availability and predictability (Durant *et al.*, 2005; Weimerskirch, 2007) on demographic processes. Whether an organism finds variability in environmental conditions to be advantageous or detrimental is therefore dependent on its specific life history traits (Morris *et al.*, 2008; Weimerskirch, 2007). Consequently, determining the traits and/or strategies that promote susceptibility versus resistance to primary productivity sensitivity is a logical next step in connecting the PSI and VSI with higher trophic level responses to environmental variability.

The spatial distribution of trait responses along environmental gradients can differ among organisms, preventing generalisations across groups (Pecuchet *et al.*, 2018; Sunday *et al.*, 2012). As a result, a need has been expressed for increased "*cross-habitat multi-trait analyses to foresee how environmental change will affect community structure and biodiversity at large"* (Pecuchet *et al.*, 2018). Examining cross-realm assemblages identified in labelled SAD analyses (Section 5.4.2) to determine cross-realm life history traits and corresponding strategies, both spatially and across trophic levels, associated with gradients of environmental variability sensitivity could make a valuable contribution towards this. Various methods are available for comparing trait distributions and/or life history strategies over environmental gradients, including biological traits analysis (e.g. Hewitt *et al.*, 2019), community-weighted mean redundancy analysis (e.g. Pecuchet *et al.*, 2018; see Kleyer *et al.*, 2012 for a review of further multivariate methods) and demographic matrix population models (e.g. Capdevila *et al.*, 2019). By using traits applicable to all organisms such as adult body size, offspring size, fecundity (number of offspring) and feeding type, trait responses can be compared across unrelated species and assemblages (Van der Plas *et al.*, 2012). These traits also cover a range of biological processes (i.e. growth, reproduction and trophic interactions) and are likely to be influenced by environmental gradients (Beauchard *et al.*, 2017; Pecuchet *et al.*, 2018). The results of trait-based analyses could then be applied to a LHS framework such as POSE framework (Kindsvater *et al.*, 2016) to investigate trends in the LHS of cross-realm assemblages. Whilst POSE was developed for the marine realm as a tool to detect the influence of fishing pressure on LHS, it could easily be applied to the terrestrial realm to enable cross-realm influences of environmental variability to be determined.

Despite promising advances in methodologies for investigating the responses of life history traits to environmental forcing (Hewitt *et al.*, 2019; Kindsvater *et al.*, 2016; Pecuchet *et al.*, 2018; Sæther *et al.*, 2013a; Suryan *et al.*, 2009) and new initiatives such as the Open Traits Network (OTN; https://opentraits.org/), for many taxa data is too limited at present to make a global comparative study viable, particularly in the marine realm (Tyler *et al.*, 2012). As a result, an initial within realm pilot study would likely have to be conducted on a taxon with known life history data availability such as zooplankton (Marine Species Traits; Marine Species Traits editorial board, 2020) or fish (FishBase; Froese and Pauly, 2019). If this were successful it would then present the opportunity to continue with a cross-realm comparison of equivalent functional types i.e. comparing zooplankton and terrestrial herbivores. In doing this I would be able to start the process of determining whether the influence of environmental variability can be detected in life history traits at a macroecological level.

5.5 Concluding remarks

In 1991 Steele posited the question of whether satellite data for primary production would one day be the unifying tool macroecology needed, to bridge the gap between marine and terrestrial ecology and overcome the differences in scales of physical and biological processes:

"To what extent do the physical and biological scales coincide: can these production rates (from satellite data) be related to the comparable physical data from remote sensing? And are the relationships similar in the oceans and on the land?" (Steele, 1991b)

In this thesis I have shown that satellite derived measures of marine and terrestrial primary productivity can be successfully combined with remotely sensed measures of their physical drivers. Using an approach that provides a clear path from climate variability to primary productivity and on to higher trophic level species, I have identified generalised cross-realm patterns in primary productivity sensitivity relative to environmental variability that overcome the different scales of the marine and terrestrial realm, and integrated these with macroecological patterns of higher trophic level species diversity. This work provides a foundation for future cross-real comparative macroecological studies aimed at understanding the role that environmental variability has played in shaping the distribution of life on Earth, and how this is likely to change with our changing climate.

References

Agawin, N. S. R., Duarte, C. M., and Agustí, S. 2000. Nutrient and temperature control of the contribution of picoplankton to phytoplankton biomass and production. Limnology and Oceanography, 45: 591–600.

Aiken, J., Hardman-Mountford, N. J., Barlow, R., Fishwick, J., Hirata, T., and Smyth, T. 2008, November 16. Functional links between bioenergetics and bio-optical traits of phytoplankton taxonomic groups: An overarching hypothesis with applications for ocean colour remote sensing. Oxford Academic.

Alheit, J., and Niquen, M. 2004. Regime shifts in the Humboldt Current ecosystem. Progress in Oceanography, 60: 201–222.

Alvain, S., Moulin, C., Dandonneau, Y., and Loisel, H. 2008. Seasonal distribution and succession of dominant phytoplankton groups in the global ocean: A satellite view. Global Biogeochemical Cycles, 22: 1–15.

Ariño, A., and Pimm, S. L. 1995. On the nature of population extremes. Evolutionary Ecology, 9: 429–443.

Bakun, A. 1990. Global climate change and intensification of coastal ocean upwelling. Science, 247: 198–201.

Bakun, A., Black, B. A., Bograd, S. J., García-Reyes, M., Miller, A. J., Rykaczewski, R. R., and Sydeman, W. J. 2015. Anticipated Effects of Climate Change on Coastal Upwelling Ecosystems. Current Climate Change Reports, 1: 85–93.

Baldridge, E., Harris, D. J., Xiao, X., and White, E. P. 2016. An extensive comparison of species-abundance distribution models. PeerJ, 4: e2823. PeerJ Inc.

Barton, A. D., Irwin, A. J., Finkel, Z. V., and Stock, C. A. 2016. Anthropogenic climate change drives shift and shuffle in North Atlantic phytoplankton communities. Proceedings of the National Academy of Sciences of the United States of America, 113: 2964–2969. National Academy of Sciences.

Baselga, A. 2010. Partitioning the turnover and nestedness components of beta diversity. Global Ecology and Biogeography, 19: 134–143. John Wiley & Sons, Ltd.

Bates, A. E., Helmuth, B., Burrows, M. T., Duncan, M. I., Garrabou, J., Guy-Haim, T., Lima, F., *et al.* 2018, August 1. Biologists ignore ocean weather at their peril. Nature Publishing Group.

Bates, D., Mächler, M., Bolker, B., and Walker, S. 2015. “Fitting Linear Mixed-Effects Models Using lme4.” Journal of Statistical Software 67 (1): 1–48. doi:10.18637/jss.v067.i01.

Bates, D., and Maechler, M. 2018 & 2019. Matrix: Sparse and Dense Matrix Classes and Methods. https://CRAN.R-project.org/package=Matrix.

Beauchard, O., Veríssimo, H., Queirós, A. M., and Herman, P. M. J. 2017, May 1. The use of multiple biological traits in marine community ecology and its potential in ecological indicator development. Elsevier B.V.

Beaugrand, G. 2009. Decadal changes in climate and ecosystems in the North Atlantic Ocean and adjacent seas. Deep-Sea Research Part II: Topical Studies in Oceanography, 56: 656–673.

Beaugrand, G., Brander, K. M., Alistair Lindley, J., Souissi, S., and Reid, P. C. 2003. Plankton effect on cod recruitment in the North Sea. Nature, 426: 661–664. Nature Publishing Group.

Beaugrand, G., Edwards, M., Brander, K., Luczak, C., and Ibanez, F. 2008. Causes and projections of abrupt climate-driven ecosystem shifts in the North Atlantic. Ecology Letters, 11: 1157–1168. Blackwell Publishing Ltd.

Beaulieu, C., Henson, S. A., Sarmiento, J. L., Dunne, J. P., Doney, S. C., Rykaczewski, R. R., and Bopp, L. 2013. Factors challenging our ability to detect long-term trends in ocean chlorophyll. Biogeosciences, 10: 2711–2724. Copernicus GmbH.

Beaumont, L. J., Pitman, A., Perkins, S., Zimmermann, N. E., Yoccoz, N. G., and Thuiller, W. 2011. Impacts of climate change on the world’s most exceptional ecoregions. Proceedings of the National Academy of Sciences of the United States of America, 108: 2306–2311. National Academy of Sciences.

Beck, J., Ballesteros-Mejia, L., Buchmann, C. M., Dengler, J., Fritz, S. A., Gruber, B., Hof, C., *et al.* 2012. What’s on the horizon for macroecology? Ecography, 35: 673–683.

Behrenfeld, M. J., and Kolber, Z. S. 1999. Widespread Iron Limitation of Phytoplankton in the South Pacific Ocean. Science, 283: 840–843.

Behrenfeld, M. J., O'Malley, R. T., Siegel, D. A., McClain, C. R., Sarmiento, J. L., Feldman, G. C., Milligan, A. J., *et al.* 2006. Climate-driven trends in contemporary ocean productivity. Nature, 444: 752–755. Nature Publishing Group.

Bhat, A., and Magurran, A. E. 2006. Taxonomic distinctness in a linear system: A test using a tropical freshwater fish assemblage. Ecography, 29: 104–110.

Bivand, R., and Lewin-Koh, N. 2018. Maptools: Tools for Reading and Handling Spatial Objects. https://CRAN.R-project.org/package=maptools.

Bivand, R., and Rundel, C. 2018. Rgeos: Interface to Geometry Engine - Open Source ('Geos'). https://CRAN.R-project.org/package=rgeos.

Bivand, R., Keitt, T., and Rowlingson, B. 2018 & 2019. Rgdal: Bindings for the 'Geospatial' Data Abstraction Library. https://CRAN.R-project.org/package=rgdal.

Blenckner, T., and Hillebrand, H. 2002. North Atlantic Oscillation signatures in aquatic and terrestrial ecosystems-a meta-analysis. Global Change Biology, 8: 203–212.

Blondeau-Patissier, D., Gower, J. F. R., Dekker, A. G., Phinn, S. R., and Brando, V. E. 2014. A review of ocean color remote sensing methods and statistical techniques for the detection, mapping and analysis of phytoplankton blooms in coastal and open oceans. Progress in Oceanography, 123: 123–144.

Blowes, S. A., Supp, S. R., Antão, L. H., Bates, A., Bruelheide, H., Chase, J. M., Moyes, F., *et al.* 2019. The geography of biodiversity change in marine and terrestrial assemblages. Science, 366: 339–345.

Bojinski, S., Verstraete, M., Peterson, T. C., Richter, C., Simmons, A., Zemp, M., Bojinski, S., *et al.* 2014. The Concept of Essential Climate Variables in Support of Climate Research, Applications, and Policy. Bulletin of the American Meteorological Society, 95: 1431–1443. American Meteorological Society .

Borrvall, C., and Ebenman, B. 2008a. Biodiversity and persistence of ecological communities in variable environments. Ecological Complexity, 5: 99–105.

Borrvall, C., and Ebenman, B. 2008b. Biodiversity and persistence of ecological communities in variable environments. Ecological Complexity, 5: 99–105.

Botsford, L. W., Lawrence, C. A., Dever, E. P., Hastings, A., and Largier, J. 2006. Effects of variable winds on biological productivity on continental shelves in coastal upwelling

systems. Deep-Sea Research Part II: Topical Studies in Oceanography, 53: 3116–3140.

Brewin, R. J. W., Ciavatta, S., Sathyendranath, S., Jackson, T., Tilstone, G., Curran, K., Airs, R. L., *et al.* 2017. Uncertainty in ocean-color estimates of chlorophyll for phytoplankton groups. Frontiers in Marine Science, 4: 104. Frontiers Media S. A.

Brewin, R. J. W., Lavender, S. J., and Hardmanmountford, N. J. 2010. Mapping size-specific phytoplankton primary production on a global scale. Journal of Maps, 6: 12–25. Taylor & Francis Group.

Brewin, R. J. W., Sathyendranath, S., Müller, D., Brockmann, C., Deschamps, P.-Y., Devred, E., Doerffer, R., *et al.* 2015. The Ocean Colour Climate Change Initiative: III. A round-robin comparison on in-water bio-optical algorithms. Remote Sensing of Environment, 162: 271–294.

Brierley, A. S., and Kingsford, M. J. 2009. Impacts of Climate Change on Marine Organisms and Ecosystems.

Brown, J. H., and Maurer, B. A. 1989. Macroecology: The division of food and space among species on continents. Science, 243: 1145–1150.

Brown, J. H., Morgan Ernest, S. K., Parody, J. M., and Haskell, J. P. 2001. Regulation of diversity: Maintenance of species richness in changing environments. Oecologia, 126: 321–332. Springer.

Bulmer, M. G. 1974. On Fitting the Poisson Lognormal Distribution to Species-Abundance Data. Biometrics, 30: 101.

Burgmer, T., and Hillebrand, H. 2011. Temperature mean and variance alter phytoplankton biomass and biodiversity in a long-term microcosm experiment. Oikos, 120: 922–933.

Burrows, M. T., Schoeman, D. S., Buckley, L. B., Moore, P., Poloczanska, E. S., Brander, K. M., Brown, C., *et al.* 2011. The pace of shifting climate in marine and terrestrial ecosystems. Science, 334: 652–655.

Burrows, M. T., Schoeman, D. S., Richardson, A. J., Molinos, J. G., Hoffmann, A., Buckley, L. B., Moore, P. J., *et al.* 2014. Geographical limits to species-range shifts are suggested by climate velocity. Nature, 507: 492–5. Nature Publishing Group, a division of Macmillan Publishers Limited. All Rights Reserved.

Cabré, A., Shields, D., Marinov, I., and Kostadinov, T. S. 2016. Phenology of Size-Partitioned

Phytoplankton Carbon-Biomass from Ocean Color Remote Sensing and CMIP5 Models. Frontiers in Marine Science, 3: 39. Frontiers.

Cane, M. A., Eshel, G., and Buckland, R. W. 1994. Forecasting Zimbabwean maize yield using eastern equatorial Pacific sea surface temperature. Nature, 370: 204–205.

Capdevila, P., Beger, M., Blomberg, S. P., and Hereu, B. 2019. Aquatic and terrestrial organisms display contrasting life history strategies as a result of environmental adaptations. bioRxiv. Cold Spring Harbor Laboratory.

Capuzzo, E., Lynam, C. P., Barry, J., Stephens, D., Forster, R. M., Greenwood, N., McQuatters-Gollop, A., *et al.* 2018. A decline in primary production in the North Sea over 25 years, associated with reductions in zooplankton abundance and fish stock recruitment. Global Change Biology, 24: e352–e364. Blackwell Publishing Ltd.

Carr, M. H., Neigel, J. E., Estes, J. A., Andelman, S., Warner, R. R., and Largier, J. L. 2003. Comparing marine and terrestrial ecosystems: implications for the design of coastal marine reserves. Ecological Applications, 13: 90–107.

Cebrian, J. 2015. Energy flows in ecosystems. Science, 349: 1053–1054.

Chambers, L. E., Altwegg, R., Barbraud, C., Barnard, P., Beaumont, L. J., Crawford, R. J. M., Durant, J. M., *et al.* 2013. Phenological Changes in the Southern Hemisphere. PLoS ONE, 8: e75514. Public Library of Science.

Chase, J. M. 2000. Are there real differences among aquatic and terrestrial food webs? Trends in Ecology & Evolution, 15: 408–412.

Connolly, S. R., Dornelas, M., Bellwood, D. R., and Hughes, T. P. 2009. Testing species abundance models: A new bootstrap approach applied to Indo-Pacific coral reefs. Ecology, 90: 3138–3149.

Connolly, S. R., Hughes, T. P., Bellwood, D. R., and Karlson, R. H. 2005. Community structure of corals and reef fishes at multiple scales. Science (New York, N.Y.), 309: 1363–5. American Association for the Advancement of Science.

Connolly, S. R., Keith, S. A., Colwell, R. K., and Rahbek, C. 2017, November 1. Process, Mechanism, and Modeling in Macroecology. Elsevier Ltd.

Connolly, S. R., MacNeil, M. A., Caley, M. J., Knowlton, N., Cripps, E., Hisano, M., Thibaut, L. M., *et al.* 2014. Commonness and rarity in the marine biosphere. Proceedings of the

National Academy of Sciences of the United States of America, 111: 8524–9.

Cotgreave, P., and Harvey, P. H. 1994. Evenness of Abundance in Bird Communities. The Journal of Animal Ecology, 63: 365.

Cullen, J. J. 1982. The Deep Chlorophyll Maximum: Comparing Vertical Profiles of Chlorophyll *a*. Canadian Journal of Fisheries and Aquatic Sciences, 39: 791–803. NRC Research Press Ottawa, Canada .

Cullen, J. J. 2015. Subsurface Chlorophyll Maximum Layers: Enduring Enigma or Mystery Solved? Annual Review of Marine Science, 7: 207–239.

Cushing, D. H. 1990. Plankton Production and Year-class Strength in Fish Populations: an Update of the Match/Mismatch Hypothesis. Advances in Marine Biology, 26: 249–293.

Cyr, H., and Cyr, I. 2003. Temporal scaling of temperature variability from land to oceans. Evolutionary Ecology Research, 5: 1183–1197. Evolutionary Ecology, Ltd.

Dawson, M. N. 2009. Trans-realm biogeography: an immergent interface. Frontiers of Biogeography, 1: 62–70.

Dawson, M. N., and Hamner, W. M. 2008. A biophysical perspective on dispersal and the geography of evolution in marine and terrestrial systems. Journal of the Royal Society, Interface / the Royal Society, 5: 135–50.

De Keersmaecker, W., Lhermitte, S., Tits, L., Honnay, O., Somers, B., and Coppin, P. 2015. A model quantifying global vegetation resistance and resilience to short-term climate anomalies and their relationship with vegetation cover. Global Ecology and Biogeography, 24: 539–548. Blackwell Publishing Ltd.

De Monte, S., Soccodato, A., Alvain, S., and d'Ovidio, F. 2013. Can we detect oceanic biodiversity hotspots from space? The ISME journal, 7: 2054–6. Nature Publishing Group.

Diffenbaugh, N. S., and Giorgi, F. 2012. Climate change hotspots in the CMIP5 global climate model ensemble. Climatic Change, 114: 813–822. Springer Netherlands.

Dinerstein, E., Olson, D., Joshi, A., Vynne, C., Burgess, N. D., Wikramanayake, E., Hahn, N., *et al.* 2017, June 1. An Ecoregion-Based Approach to Protecting Half the Terrestrial Realm. Island Press,.

Dornelas, M. 2010. Disturbance and change in biodiversity. Philosophical Transactions of the

Royal Society B: Biological Sciences, 365: 3719–3727.

Dornelas, M., Antão, L. H., Moyes, F., Bates, A. E., Magurran, A. E., Adam, D., Akhmetzhanova, A. A., *et al.* 2018. BioTIME: A database of biodiversity time series for the Anthropocene. Global Ecology and Biogeography, 27: 760–786. Wiley/Blackwell (10.1111).

Dornelas, M., Connolly, S. R., and Hughes, T. P. 2006. Coral reef diversity refutes the neutral theory of biodiversity. Nature, 440: 80–82. Nature Publishing Group.

Dornelas, M., Gotelli, N. J., McGill, B., Shimadzu, H., Moyes, F., Sievers, C., and Magurran, A. E. 2014. Assemblage Time Series Reveal Biodiversity Change but Not Systematic Loss. Science, 344: 296–9.

Dowle, M., and Srinivasan, A. 2018. Data.table: Extension of 'Data.frame'. https://CRAN.R-project.org/package=data.table.

Drakare, S., Lennon, J. J., and Hillebrand, H. 2006. The imprint of the geographical, evolutionary and ecological context on species-area relationships. Ecology letters, 9: 215–27.

Drinkwater, K. F., Belgrano, A., Borja, A., Conversi, A., Edwards, M., Greene, C. H., Ottersen, G., *et al.* 2003. The Response of Marine Ecosystems to Climate Variability Associated With the North Atlantic Oscillation. *In* The North Atlantic Oscillation: Climatic Significance and Environmental Impact, pp. 211–234. American Geophysical Union.

Durant, J. M., Hjermann, D. O., Anker-Nilssen, T., Beaugrand, G., Mysterud, A., Pettorelli, N., and Stenseth, N. C. 2005. Timing and abundance as key mechanisms affecting trophic interactions in variable environments. Ecology Letters, 8: 952–958.

Durant, J. M., Hjermann, D., Ottersen, G., and Stenseth, N. C. 2007, April 20. Climate and the match or mismatch between predator requirements and resource availability.

Dutkiewicz, S., Hickman, A. E., Jahn, O., Henson, S., Beaulieu, C., and Monier, E. 2019. Ocean colour signature of climate change. Nature Communications, 10.

Easterling, D. R., Meehl, G. A., Parmesan, C., Changnon, S. A., Karl, T. R., and Mearns, L. O. 2000, September 22. Climate extremes: Observations, modeling, and impacts. American Association for the Advancement of Science.

Edgar, G. J., Bates, A. E., Bird, T. J., Jones, A. H., Kininmonth, S., Stuart-Smith, R. D., and

Webb, T. J. 2016. New Approaches to Marine Conservation Through Scaling Up of Ecological Data. Annual review of marine science, 8: 435–461.

Edwards, M., Atkinson, A., Bresnan, E., Hélaouët, P., McQuatters-Gollop, A., Ostle, C., Pitois, S., *et al.* 2020. Plankton, jellyfish and climate in the North-East Atlantic. MCCIP Science Review 2020: 322–353.

Edwards, M., and Richardson, A. J. 2004a. Impact of climate change on marine pelagic phenology and trophic mismatch. Nature, 430: 881–4.

Edwards, M., and Richardson, A. J. 2004b. Impact of climate change on marine pelagic phenology and trophic mismatch. Nature, 430: 881–4. Nature Publishing Group.

Elith, J., Leathwick, J. R., and Hastie, T. 2008. A working guide to boosted regression trees. Journal of Animal Ecology, 77: 802–813. Blackwell Publishing Ltd.

Enfield, D. B., Mestas-Nuñez, A. M., and Trimble, P. J. 2001. The Atlantic multidecadal oscillation and its relation to rainfall and river flows in the continental U.S. Geophysical Research Letters, 28: 2077–2080.

Falkowski, P. G., and Oliver, M. J. 2007. Mix and match: how climate selects phytoplankton. Nature Reviews Microbiology, 5: 813–819. Nature Publishing Group.

Fiedler, P. C. 2002. The annual cycle and biological effects of the Costa Rica Dome. Deep-Sea Research I, 49: 321–338.

Fisher, J. A. D., Frank, K. T., and Leggett, W. C. 2010. Dynamic macroecology on ecological time-scales. Global Ecology and Biogeography, 19: 1–15.

Fisher, J. A. D., Frank, K. T., Petrie, B., Leggett, W. C., and Shackell, N. L. 2008. Temporal dynamics within a contemporary latitudinal diversity gradient. Ecology letters, 11: 883–97.

Fox, J., and Weisberg, S. 2019. An R Companion to Applied Regression. Third. Thousand Oaks CA: Sage. https://socialsciences.mcmaster.ca/jfox/Books/Companion/.

Fox, J., Weisberg, S., and Price, B. 2019. CarData: Companion to Applied Regression Data Sets. https://CRAN.R-project.org/package=carData.

Friedland, K. D., Mouw, C. B., Asch, R. G., Ferreira, A. S. A., Henson, S., Hyde, K. J. W., Morse, R. E., *et al.* 2018. Phenology and time series trends of the dominant seasonal

phytoplankton bloom across global scales. Global Ecology and Biogeography, 27: 551–569.

Froese, R., and Pauly, D. 2019. FishBase. www.fishbase.org (Accessed 12 February 2019).

Frouin, R., Franz, B. A., and Werdell, P. J. 2003. The SeaWiFS PAR product. *In* Algorithm updates for the fourth SeaWiFS data reprocessing, pp. 46–50. Ed. by S. B. Hooker and E. R. Firestone. NASA/TM-2003-206892.

Frouin, R., McPherson, J., Ueyoshi, K., and Franz, B. A. 2012. A time series of photosynthetically available radiation at the ocean surface from SeaWiFS and MODIS data. Proceedings of SPIE, Remote Sensing of the Marine Environment II, 8525: 1–12. International Society for Optics and Photonics.

García-Carreras, B., and Reuman, D. C. 2011. An empirical link between the spectral colour of climate and the spectral colour of field populations in the context of climate change. The Journal of animal ecology, 80: 1042–8.

Garnier, Simon. 2018a. Viridis: Default Color Maps from 'Matplotlib'. https://CRAN.R-project.org/package=viridis.

Garnier, Simon. 2018b. ViridisLite: Default Color Maps from 'Matplotlib' (Lite Version). https://CRAN.R-project.org/package=viridisLite.

Gaston, K. J. 2003. The structure and dynamics of geographic ranges. Oxford University Press, Oxford.

GCOS. 2010. Implementation plan for the global observing system for climate in support of the UNFCCC (2010 update), 138: 186.

Gilljam, D., Knape, J., Lindén, A., Mugabo, M., Sait, S. M., and Fowler, M. S. 2019. The colour of environmental fluctuations associated with terrestrial animal population dynamics. Global Ecology and Biogeography, 28: 118–130. Wiley/Blackwell (10.1111).

Goberville, E., Beaugrand, G., Sautour, B., and Tréguer, P. 2010. Climate-driven changes in coastal marine systems of western Europe. Marine Ecology Progress Series, 408: 129–147.

González Taboada, F., and Anadón, R. 2014. Seasonality of North Atlantic phytoplankton from space: Impact of environmental forcing on a changing phenology (1998-2012). Global Change Biology, 20: 698–712.

Goswami, B. N., Madhusoodanan, M. S., Neema, C. P., and Sengupta, D. 2006. A physical mechanism for North Atlantic SST influence on the Indian summer monsoon. Geophysical Research Letters, 33: L02706.

Grant, M., Jackson, T., Chuprin, A., Sathyendranath, S., Zühlke, M., Dingle, J., Storm, T., *et al.* 2017. Ocean Colour Climate Change Initiative (OC_CCI) Product User Guide 3.1.0. European Space Agency. 1–51 pp.

Gray, J. S., Bjørgesæter, A., and Ugland, K. I. 2005. The impact of rare species on natural assemblages. Journal of Animal Ecology, 74: 1131–1139. Wiley/Blackwell (10.1111).

Gray, J. S., Bjørgesæter, A., Ugland, K. I., and Frank, K. 2006. Are there differences in structure between marine and terrestrial assemblages? Journal of Experimental Marine Biology and Ecology, 330: 19–26.

Gregg, W. W., and Rousseaux, C. S. 2014. Decadal trends in global pelagic ocean chlorophyll: A new assessment integrating multiple satellites, in situ data, and models. Journal of Geophysical Research: Oceans, 119: 5921–5933.

Gregg, W. W., and Rousseaux, C. S. 2019. Global ocean primary production trends in the modern ocean color satellite record (1998–2015). Environmental Research Letters, 14: 124011. IOP Publishing.

Grime, J. P. 1988. The C-S-R model of primary plant strategies — origins, implications and tests. *In* Plant Evolutionary Biology, pp. 371–393. Springer Netherlands.

Grøtan, Vidar., and Engen, S. 2008. Poilog: Poisson Lognormal and Bivariate Poisson Lognormal Distribution.

Häder, D.-P., Villafañe, V. E., and Helbling, E. W. 2014. Productivity of aquatic primary producers under global climate change. Photochem. Photobiol. Sci., 13: 1370–1392. The Royal Society of Chemistry.

Halekoh, U., and Højsgaard, S. 2014. A kenward-Roger approximation and parametric bootstrap methods for tests in linear mixed models-the R package pbkrtest. Journal of Statistical Software, 59: 1–32. American Statistical Association.

Halley, J. M. 1996. Ecology, evolution and 1f-noise. Trends in Ecology & Evolution, 11: 33–37.

Halpern, B. S., Walbridge, S., Selkoe, K. A., Kappel, C. V, Micheli, F., D'Agrosa, C., Bruno, J. F., *et al.* 2008. A global map of human impact on marine ecosystems. Science (New York,

N.Y.), 319: 948–52.

Harley, C. D. G., Hughes, A. R., Hultgren, K. M., Miner, B. G., Sorte, C. J. B., Thornber, C. S., Rodriguez, L. F., *et al.* 2006, February. The impacts of climate change in coastal marine systems. Blackwell Science Ltd.

Harrison, A. L., Costa, D. P., Winship, A. J., Benson, S. R., Bograd, S. J., Antolos, M., Carlisle, A. B., *et al.* 2018a. The political biogeography of migratory marine predators. Nature Ecology and Evolution, 2: 1571–1578. Nature Publishing Group.

Harrison, G. W. 1979a. Stability under Environmental Stress: Resistance, Resilience, Persistence, and Variability. The American Naturalist, 113: 659–669.

Harrison, G. W. 1979b. Stability under Environmental Stress: Resistance, Resilience, Persistence, and Variability. The American Naturalist, 113: 659–669.

Harrison, X. A., Donaldson, L., Correa-Cano, M. E., Evans, J., Fisher, D. N., Goodwin, C. E. D., Robinson, B. S., *et al.* 2018b. A brief introduction to mixed effects modelling and multi-model inference in ecology. PeerJ, 6: e4794.

Hatton, I. A., McCann, K. S., Fryxell, J. M., Davies, T. J., Smerlak, M., Sinclair, A. R. E., and Loreau, M. 2015. The predator-prey power law: Biomass scaling across terrestrial and aquatic biomes. Science, 349: aac6284–aac6284.

Hays, G. C., Carr, M. R., and Taylor, A. H. 1993. The relationship between gulf stream position and copepod abundance derived from the continuous plankton recorder survey: Separating biological signal from sampling noise. Journal of Plankton Research, 15: 1359–1373. Oxford University Press.

Hays, G. C., Richardson, A. J., and Robinson, C. 2005. Climate change and marine plankton. Trends in Ecology & Evolution, 20: 337–344.

Heck, K. L., Carruthers, T. J. B., Duarte, C. M., Hughes, A. R., Kendrick, G., Orth, R. J., and Williams, S. W. 2008. Trophic Transfers from Seagrass Meadows Subsidize Diverse Marine and Terrestrial Consumers. Ecosystems, 11: 1198–1210.

Heino, M., and Sabadell, M. 2003. Influence of coloured noise on the extinction risk in structured population models. Biological Conservation, 110: 315–325.

Henry, L., and Wickham, H. 2019. Purrr: Functional Programming Tools. https://CRAN.R-project.org/package=purrr.

Henson, S. A., Beaulieu, C., Ilyina, T., John, J. G., Long, M., Séférian, R., Tjiputra, J., *et al.* 2017. Rapid emergence of climate change in environmental drivers of marine ecosystems. Nature Communications, 8. Nature Publishing Group.

Henson, S. A., Dunne, J. P., and Sarmiento, J. L. 2009. Decadal variability in North Atlantic phytoplankton blooms. Journal of Geophysical Research: Oceans, 114: C04013.

Henson, S. a., Sarmiento, J. L., Dunne, J. P., Bopp, L., Lima, I., Doney, S. C., John, J., *et al.* 2010. Detection of anthropogenic climate change in satellite records of ocean chlorophyll and productivity. Biogeosciences, 7: 621–640. Copernicus GmbH.

Henson, S., Cole, H., Beaulieu, C., and Yool, A. 2013. The impact of global warming on seasonality of ocean primary production. Biogeosciences, 10: 4357–4369. Copernicus GmbH.

Henson, S., Lampitt, R., and Johns, D. 2012. Variability in phytoplankton community structure in response to the North Atlantic Oscillation and implications for organic carbon flux. Limnology and Oceanography, 57: 1591–1601.

Hewitt, J. E., Lundquist, C. J., and Ellis, J. 2019. Assessing sensitivities of marine areas to stressors based on biological traits. Conservation Biology, 33: 142–151. Wiley/Blackwell (10.1111).

Hijmans, R.J. 2017 & 2020. Raster: Geographic Data Analysis and Modeling. https://CRAN.R-project.org/package=raster.

Hillebrand, H. 2004. On the generality of the latitudinal diversity gradient. The American naturalist, 163: 192–211. The University of Chicago Press.

Hillebrand, H., Blasius, B., Borer, E. T., Chase, J. M., Downing, J. A., Eriksson, B. K., Filstrup, C. T., *et al.* 2018. Biodiversity change is uncoupled from species richness trends: Consequences for conservation and monitoring. Journal of Applied Ecology, 55: 169–184.

Hinder, S. L., Hays, G. C., Edwards, M., Roberts, E. C., Walne, A. W., and Gravenor, M. B. 2012. Changes in marine dinoflagellate and diatom abundance under climate change. Nature Climate Change, 2: 271–275.

Hirata, T., Hardman-Mountford, N., and Brewin, R. J. W. 2012. Comparing satellite-based phytoplankton classification methods. Eos, 93: 59–60.

Hjort, J. 1914. Fluctuations in the great fisheries of Northern Europe. Rapports et Procés-Verbaux, 20: 1–228. Andr. Fred. Høst & Fils, Copenhagen Denmark.

Holling, C. S. 1973. Resilience and Stability of Ecological Systems. Annual Review of Ecology and Systematics, 4: 1–23. Annual Reviews 4139 El Camino Way, P.O. Box 10139, Palo Alto, CA 94303-0139, USA .

Hollmann, R., Merchant, C. J., Saunders, R., Downy, C., Buchwitz, M., Cazenave, A., Chuvieco, E., *et al.* 2013. The ESA Climate Change Initiative: Satellite Data Records for Essential Climate Variables. Bulletin of the American Meteorological Society, 94: 1541–1552. American Meteorological Society .

Holmgren, M., Hirota, M., Van Nes, E. H., and Scheffer, M. 2013. Effects of interannual climate variability on tropical tree cover. Nature Climate Change, 3: 755–758. Nature Publishing Group.

Horne, C. R., Hirst, A. G., and Atkinson, D. 2015. Temperature-size responses match latitudinal-size clines in arthropods, revealing critical differences between aquatic and terrestrial species. Ecology letters, 18: 327–35.

Hubbell, S. P. 1979. Tree Dispersion, Abundance, and Diversity in a Tropical Dry Forest. Science, 203: 1299–1309.

Huisman, J., Pham Thi, N. N., Karl, D. M., and Sommeijer, B. 2006. Reduced mixing generates oscillations and chaos in the oceanic deep chlorophyll maximum. Nature, 439: 322–325. Nature Publishing Group.

Hurlbert, A. H. 2004. Species–energy relationships and habitat complexity in bird communities. Ecology Letters, 7: 714–720. Wiley/Blackwell (10.1111).

Hurrell, J. W., and Deser, C. 2010. North Atlantic climate variability: The role of the North Atlantic Oscillation. Journal of Marine Systems, 79: 231–244.

IOCCG. 2014. Phytoplankton functional types from Space. *In* Reports of the International Ocean-Colour Coordinating Group, No.15, p. 156. Ed. by S. Sathyendranath. IOCCG, Dartmouth, Canada.

IPCC. 2007. Summary for Policy Makers. *In* Climate Change 2007: The Physical Science Basis. Contribution of Working Group I to the Fourth Assessment Report of the Intergovernmental Panel on Climate Change. Ed. by S. Solomon, D. Qin, M. Manning, Z.

Chen, M. Marquis, K. B. Averyt, M. Tignor, et al. Cambridge University Press, Cambridge.

IPCC. 2018. Summary for Policymakers. *In* Global Warming of 1.5°C. An IPCC Special Report on the impacts of global warming of 1.5°C above pre-industrial levels and related global greenhouse gas emission pathways, in the context of strengthening the global response to the threat of climate change,. Ed. by V. Masson-Delmotte, P. Zhai, H. O. Pörtner, D. Roberts, J. Skea, P. R. Shukla, A. Pirani, et al.

IPCC. 2019. Summary for Policymakers. *In* IPCC Special Report on the Ocean and Cryosphere in a Changing Climate, p. 42. Ed. by H. O. Pörtner, D. C. Roberts, V. Masson-Delmotte, P. Zhai, M. Tignor, E. Poloczanska, K. Mintenbeck, et al.

Ives, A. R., Gross, K., and Klug, J. L. 1999. Stability and variability in competitive communities. Science, 286: 542–544.

Jackson, T., Sathyendranath, S., and Mélin, F. 2017. An improved optical classification scheme for the Ocean Colour Essential Climate Variable and its applications. Remote Sensing of Environment, 203: 152–161.

Jentsch, A., Kreyling, J., and Beierkuhnlein, C. 2007, September 1. A new generation of climate-change experiments: Events, not trends. Wiley-Blackwell.

Juan-Jordá, M. J., Mosqueira, I., Freire, J., and Dulvy, N. K. 2013. Life in 3-D: life history strategies in tunas, mackerels and bonitos. Reviews in Fish Biology and Fisheries, 23: 135–155.

Justice, C. O., Vermote, E., Townshend, J. R. G., Defries, R., Roy, D. P., Hall, D. K., Salomonson, V. V., *et al.* 1998. The moderate resolution imaging spectroradiometer (MODIS): Land remote sensing for global change research. IEEE Transactions on Geoscience and Remote Sensing, 36: 1228–1249. Institute of Electrical and Electronics Engineers Inc.

Kahru, M., Gille, S. T., Murtugudde, R., Strutton, P. G., Manzano-Sarabia, M., Wang, H., and Mitchell, B. G. 2010. Global correlations between winds and ocean chlorophyll. Journal of Geophysical Research: Oceans, 115: C12040.

Kaneryd, L., Borrvall, C., Berg, S., Curtsdotter, A., Eklöf, A., Hauzy, C., Jonsson, T., *et al.* 2012. Species-rich ecosystems are vulnerable to cascading extinctions in an increasingly variable world. Ecology and evolution, 2: 858–74.

Kang, S. M., and Lu, J. 2012. Expansion of the Hadley cell under global warming: Winter versus summer. Journal of Climate, 25: 8387–8393.

Keith, S. A., Webb, T. J., Böhning-Gaese, K., Connolly, S. R., Dulvy, N. K., Eigenbrod, F., Jones, K. E., *et al.* 2012. What is Macroecology? *In* Biology Letters, pp. 904–906. Royal Society.

Kent, E. C., Fangohr, S., and Berry, D. I. 2013. A comparative assessment of monthly mean wind speed products over the global ocean. International Journal of Climatology, 33: 2520–2541.

Kerr, J. T., Kharouba, H. M., and Currie, D. J. 2007. The macroecological contribution to global change solutions. Science, 316: 1581–1584.

Keshner, M. S. 1982. 1/f noise. Proceedings of the IEEE, 70: 212–218.

Kindsvater, H. K., Mangel, M., Reynolds, J. D., and Dulvy, N. K. 2016. Ten principles from evolutionary ecology essential for effective marine conservation. Ecology and Evolution, 6: 2125–2138.

Kinlan, B. P., and Gaines, S. D. 2003. Propagule dispersal in marine and terrestrial environments: a community perspective. Ecology, 84: 2007–2020.

Kirby, R. R., and Beaugrand, G. 2009. Trophic amplification of climate warming. Proceedings. Biological sciences / The Royal Society, 276: 4095–103.

Kissling, W. D., Field, R., Korntheuer, H., Heyder, U., and Böhning-Gaese, K. 2010. Woody plants and the prediction of climate-change impacts on bird diversity. Philosophical Transactions of the Royal Society B: Biological Sciences, 365: 2035–2045. Royal Society.

Kleyer, M., Dray, S., Bello, F., Lepš, J., Pakeman, R. J., Strauss, B., Thuiller, W., *et al.* 2012. Assessing species and community functional responses to environmental gradients: which multivariate methods? Journal of Vegetation Science, 23: 805–821. John Wiley & Sons, Ltd.

Kolber, Z. S., Barber, R. T., Coale, K. H., Fitzwateri, S. E., Greene, R. M., Johnson, K. S., Lindley, S., *et al.* 1994. Iron limitation of phytoplankton photosynthesis in the equatorial Pacific Ocean. Nature, 371: 145–149. Nature Publishing Group.

Kostadinov, T. S., Siegel, D. A., and Maritorena, S. 2010. Global variability of phytoplankton functional types from space: assessment via the particle size distribution.

Biogeosciences, 7: 3239–3257.

Krug, L. A., Platt, T., Sathyendranath, S., and Barbosa, A. B. 2017, June 1. Ocean surface partitioning strategies using ocean colour remote Sensing: A review. Pergamon.

Lavender, S., Jackson, T., and Sathyendranath, S. 2015. The Ocean Colour Climate Change Initiative: Merging ocean colour observations seamlessly. Ocean Challenge, 21: 29–31.

Lawson, C. R., Vindenes, Y., Bailey, L., and van de Pol, M. 2015. Environmental variation and population responses to global change. Ecology Letters, 18: 724–736.

Lawton, J. H. 1999. Are there general laws in ecology? Oikos, 84: 177–192.

Litchman, E., and Klausmeier, C. A. 2008. Trait-based community ecology of phytoplankton. Annual Review of Ecology, Evolution, and Systematics, 39: 615–639.

Longhurst, A. 1995a. Seasonal cycles of pelagic production and consumption. Pergamon.

Longhurst, A. 1995b. Seasonal cycles of pelagic production and consumption. Progress in Oceanography, 36: 77–167.

Longhurst, A. R. 2007. Ecological Geography of the Sea. Academic Press. 542 pp.

Lu, J., Vecchi, G. A., and Reichler, T. 2007. Expansion of the Hadley cell under global warming. Geophysical Research Letters, 34: L06805.

Luke, S. G. 2017. Evaluating significance in linear mixed-effects models in R. Behavior Research Methods, 49: 1494–1502. Springer New York LLC.

Ma, G., Rudolf, V. H. W., and Ma, C. sen. 2015. Extreme temperature events alter demographic rates, relative fitness, and community structure. Global Change Biology, 21: 1794–1808.

Magurran, A. E. 2007. Species abundance distributions over time. Ecology letters, 10: 347–54.

Magurran, A. E., and Henderson, P. A. 2003. Explaining the excess of rare species in natural species abundance distributions. Nature, 422: 714–6.

Mann, K. H., and Lazier, J. R. N. 2006. Dynamics of Marine Ecosystems: Biological-Physical Interactions in the Oceans: Blackwell Publishing Ltd., Malden, MA USA. 1–496 pp.

Mann, M. E., Rahmstorf, S., Kornhuber, K., Steinman, B. A., Miller, S. K., and Coumou, D. 2017. Influence of Anthropogenic Climate Change on Planetary Wave Resonance and Extreme Weather Events. Scientific Reports, 7: 45242. Nature Publishing Group.

Marañón, E., Behrenfeld, M. J., González, N., Mouriño, B., and Zubkov, M. V. 2003. High variability of primary production in oligotrophic waters of the Atlantic Ocean uncoupling from phytoplankton biomass and size structure. Inter-Research Science Center.

Marañón, E., Holligan, P. M., Barciela, R., González, N., Mouriño, B., Pazó, M. J., and Varela, M. 2001. Patterns of phytoplankton size structure and productivity in contrasting open-ocean environments. Marine Ecology Progress Series, 216: 43–56.

Marco, M. Di, Chapman, S., Althor, G., Kearney, S., Besancon, C., Butt, N., Maina, J. M., *et al.* 2017. Changing trends and persisting biases in three decades of conservation science. Global Ecology and Conservation, 10: 32–42. Elsevier B.V.

Marine Species Traits editorial board. 2020. Marine Species Traits. http://www.marinespecies.org/traits (Accessed 29 February 2020).

Marrari, M., Piola, A. R., and Valla, D. 2017. Variability and 20-Year Trends in Satellite-Derived Surface Chlorophyll Concentrations in Large Marine Ecosystems around South and Western Central America. Frontiers in Marine Science, 4: 372. Frontiers.

Martin, J. H., Coale, K. H., Johnson, K. S., Fitzwater, S. E., Gordon, R. M., Tanner, S. J., Hunter, C. N., *et al.* 1994. Testing the iron hypothesis in ecosystems of the equatorial Pacific Ocean. Nature, 371: 123–129. Nature Publishing Group.

Matthews, T. J., and Whittaker, R. J. 2014. Fitting and comparing competing models of the species abundance distribution: assessment and prospect. Frontiers of Biogeography, 6: 67–82.

Matthews, T. J., and Whittaker, R. J. 2015, April. On the species abundance distribution in applied ecology and biodiversity management.

Mazeika, P. A. 1967. Thermal domes in the Eastern Tropical Atlantic. Limnology and Oceanography, 12: 537–539. Wiley-Blackwell.

McClain, C. R. 2009. A Decade of Satellite Ocean Color Observations. Annual Review of Marine Science, 1: 19–42. Annual Reviews.

McClain, C. R., Signorini, S. R., and Christian, J. R. 2004. Subtropical gyre variability observed

by ocean-color satellites. Deep Sea Research Part II: Topical Studies in Oceanography, 51: 281–301. Pergamon.

McGill, B. 2003. Strong and weak tests of macroecological theory. Oikos, 102: 679–685.

McGill, B. J. 2010a. Ecology. Matters of scale. Science (New York, N.Y.), 328: 575–6. American Association for the Advancement of Science.

McGill, B. J. 2010b. Towards a unification of unified theories of biodiversity. Ecology letters, 13: 627–42.

McGill, B. J., Dornelas, M., Gotelli, N. J., and Magurran, A. E. 2015. Fifteen forms of biodiversity trend in the anthropocene.

McGill, B. J., Etienne, R. S., Gray, J. S., Alonso, D., Anderson, M. J., Benecha, H. K., Dornelas, M., *et al.* 2007. Species abundance distributions: moving beyond single prediction theories to integration within an ecological framework. Ecology letters, 10: 995–1015.

McGill, B. J., and Potochnik, A. 2018, May 1. Mechanisms Are Causes, Not Components: A Response to Connolly et al. Elsevier Ltd.

Menegotto, A., and Rangel, T. F. 2018. Mapping knowledge gaps in marine diversity reveals a latitudinal gradient of missing species richness. Nature Communications, 9: 1–6. Nature Publishing Group.

Menge, B. A., Chan, F., Dudas, S., Eerkes-Medrano, D., Grorud-Colvert, K., Heiman, K., Hessing-Lewis, M., *et al.* 2009. Terrestrial ecologists ignore aquatic literature: Asymmetry in citation breadth in ecological publications and implications for generality and progress in ecology. Journal of Experimental Marine Biology and Ecology, 377: 93–100.

Morel, A., Huot, Y., Gentili, B., Werdell, P. J., Hooker, S. B., and Franz, B. A. 2007. Examining the consistency of products derived from various ocean color sensors in open ocean (Case 1) waters in the perspective of a multi-sensor approach. Remote Sensing of Environment, 111: 69–88.

Moreno, A. R., and Martiny, A. C. 2018. Ecological Stoichiometry of Ocean Plankton. Annual Review of Marine Science, 10: 43–69. Annual Reviews.

Morris, W. F., Pfister, C. A., Tuljapurkar, S., Haridas, C. V., Boggs, C. L., Boyce, M. S., Bruna, E. M., *et al.* 2008. Longevity can buffer plant and animal populations against changing climatic variability. Ecology, 89: 19–25. Ecological Society of America.

Müller, K. 2018. Bindrcpp: An 'Rcpp' Interface to Active Bindings. https://CRAN.R-project.org/package=bindrcpp.

Müller, D., Krasemann, H., Brewin, R. J. W., Brockmann, C., Deschamps, P.-Y., Doerffer, R., Fomferra, N., *et al.* 2015. The Ocean Colour Climate Change Initiative: I. A methodology for assessing atmospheric correction processors based on in-situ measurements. Remote Sensing of Environment, 162: 242–256.

Müller, K., and Wickham, H. 2019. Tibble: Simple Data Frames. https://CRAN.R-project.org/package=tibble.

Mustin, K., Dytham, C., Benton, T. G., and Travis, J. M. J. 2013. Red noise increases extinction risk during rapid climate change. Diversity and Distributions, 19: 815–824.

Myneni, R. B., Keeling, C. D., Tucker, C. J., Asrar, G., and Nemani, R. R. 1997. Increased plant growth in the northern high latitudes from 1981 to 1991. Nature, 386: 698–702. Nature Publishing Group.

Mysterud, A., Stenseth, N. C., Yoccoz, N. G., Ottersen, G., and Langvatn, R. 2003. The Response of Terrestrial Ecosystems to Climate Variability Associated with the North Atlantic Oscillation. *In* Geophysical Monograph Series, pp. 235–262. American Geophysical Union.

Nemani, R. R., Keeling, C. D., Hashimoto, H., Jolly, W. M., Piper, S. C., Tucker, C. J., Myneni, R. B., *et al.* 2003. Climate-driven increases in global terrestrial net primary production from 1982 to 1999. Science, 300: 1560–1563. American Association for the Advancement of Science.

Nieto, K., and Mélin, F. 2017a. Variability of chlorophyll-a concentration in the Gulf of Guinea and its relation to physical oceanographic variables. Progress in Oceanography, 151: 97–115.

Nieto, K., and Mélin, F. 2017b. Variability of chlorophyll-a concentration in the Gulf of Guinea and its relation to physical oceanographic variables. Progress in Oceanography, 151: 97–115.

Olson, D. M., Dinerstein, E., Wikramanayake, E. D., Burgess, N. D., Powell, G. V. N., Underwood, E. C., D'amico, J. A., *et al.* 2001. Terrestrial Ecoregions of the World: A New Map of Life on Earth. BioScience, 51: 933. Oxford University Press.

Ottersen, G., Planque, B., Belgrano, A., Post, E., Reid, P., and Stenseth, N. 2001. Ecological effects of the North Atlantic Oscillation. Oecologia, 128: 1–14.

Paine, R. T. 2005. Cross environment talk in ecology: fact or fantasy? *In* Bridging the gap between aquatic and terrestrial ecology, pp. 280–283. Ed. by K. I. Stergiou and H. I. Browman. Marine Ecology Progress Series.

Parmesan, C., and Yohe, G. 2003. A globally coherent fingerprint of climate change impacts across natural systems. Nature, 421: 37–42.

Pearce-Higgins, J. W., Ockendon, N., Baker, D. J., Carr, J., White, E. C., Almond, R. E. A., Amano, T., *et al.* 2015. Geographical variation in species' population responses to changes in temperature and precipitation. Proceedings. Biological sciences / The Royal Society, 282: 20151561-.

Pebesma, E.J., and Bivand, R.S. 2005. "Classes and Methods for Spatial Data in R." R News 5 (2): 9–13. https://CRAN.R-project.org/doc/Rnews/.

Pecuchet, L., Lindegren, M., Hidalgo, M., Delgado, M., Esteban, A., Fock, H. O., Gil de Sola, L., *et al.* 2017. From traits to life-history strategies: Deconstructing fish community composition across European seas. Global Ecology and Biogeography, 26: 812–822. Blackwell Publishing Ltd.

Pecuchet, L., Reygondeau, G., Cheung, W. W. L., Licandro, P., van Denderen, P. D., Payne, M. R., and Lindegren, M. 2018. Spatial distribution of life-history traits and their response to environmental gradients across multiple marine taxa. Ecosphere, 9: 1–16.

Peng, G., Zhang, H.-M., Frank, H. P., Bidlot, J.-R., Higaki, M., Stevens, S., and Hankins, W. R. 2013. Evaluation of Various Surface Wind Products with OceanSITES Buoy Measurements. Weather and Forecasting, 28: 1281–1303.

Petchey, O. L. 2000. Environmental colour affects aspects of single-species population dynamics. Proceedings. Biological sciences, 267: 747–54. The Royal Society.

Philander, S. G. H. 1990. El Niño, La Niña and the Southern Oscillation. Academic Press, New York. 1–293 pp.

Pimm, S. L., and Redfearn, A. 1988. The variability of population densities. Nature, 334: 613–614.

Pinheiro, J., Bates, D., DebRoy, S., Sarkar, D., and R Core Team. 2018 & 2019. nlme: Linear

and Nonlinear Mixed Effects Models. https://CRAN.R-project.org/package=nlme.

Pinsky, M. L., Eikeset, A. M., McCauley, D. J., Payne, J. L., and Sunday, J. M. 2019. Greater vulnerability to warming of marine versus terrestrial ectotherms. Nature, 569: 108–111. Nature Publishing Group.

Pintor, A. F. V., Schwarzkopf, L., and Krockenberger, A. K. 2015. Rapoport's Rule: Do climatic variability gradients shape range extent? Ecological Monographs, 85: 643–659. Ecological Society of America.

Platt, T., Fuentes-Yaco, C., and Frank, K. T. 2003. Spring algal bloom and larval fish survival. Nature, 423: 398–399. Nature Publishing Group.

Plummer, S., Lecomte, P., and Doherty, M. 2017. The ESA Climate Change Initiative (CCI): A European contribution to the generation of the Global Climate Observing System. Remote Sensing of Environment, 203: 2–8. Elsevier Inc.

Polis, G. A., and Hurd, S. D. 1996. Linking marine and terrestrial food webs: allochthonus input from the ocean supports high secondary productivity on small islands and coastal land communities. The American naturalist, 147: 396–423.

Poloczanska, E. S., Brown, C. J., Sydeman, W. J., Kiessling, W., Schoeman, D. S., Moore, P. J., Brander, K., *et al.* 2013. Global imprint of climate change on marine life. Nature Climate Change, 3: 919–925. Nature Research.

Poloczanska, E. S., Burrows, M. T., Brown, C. J., Garcia, J., Halpern, B. S., Hoegh-guldberg, O., Kappel, C. V., *et al.* 2016. Responses of marine organisms to climate change across oceans. Frontiers in Marine Science, 3: 1–21. Frontiers.

Polovina, J. J., Howell, E. A., and Abecassis, M. 2008. Ocean's least productive waters are expanding. Geophysical Research Letters, 35: L03618. Wiley-Blackwell.

Post, E., and Stenseth, N. C. 1999. Climatic variability, plant phenology, and northern ungulates. Ecology, 80: 1322–1339. Ecological Society of America.

Power, S., Delage, F., Chung, C., Kociuba, G., and Keay, K. 2013. Robust twenty-first-century projections of El Niño and related precipitation variability. Nature, 502: 541–545. Nature Publishing Group.

Pöysä, H., Rintala, J., Johnson, D. H., Kauppinen, J., Lammi, E., Nudds, T. D., and Väänänen, V.-M. 2016. Environmental variability and population dynamics: do European and North

American ducks play by the same rules? Ecology and Evolution, 6: 7004–7014. John Wiley & Sons, Ltd.

Preston, F. W. 1948. The Commonness, And Rarity, of Species. Ecology, 29: 254–283.

R Core Team. 2018 & 2019. R: A Language and Environment for Statistical Computing. Vienna, Austria: R Foundation for Statistical Computing. https://www.R-project.org/.

Racault, M.-F., Raitsos, D. E., Berumen, M. L., Brewin, R. J. W., Platt, T., Sathyendranath, S., and Hoteit, I. 2015. Phytoplankton phenology indices in coral reef ecosystems: Application to ocean-color observations in the Red Sea. Remote Sensing of Environment, 160: 222–234.

Racault, M. F., Le Quéré, C., Buitenhuis, E., Sathyendranath, S., and Platt, T. 2012. Phytoplankton phenology in the global ocean. Ecological Indicators, 14: 152–163.

Racault, M. F., Sathyendranath, S., Menon, N., and Platt, T. 2017, January 9. Phenological Responses to ENSO in the Global Oceans. Springer Netherlands.

Racault, M. F., Sathyendranath, S., and Platt, T. 2014. Impact of missing data on the estimation of ecological indicators from satellite ocean-colour time-series. Remote Sensing of Environment, 152: 15–28.

Rafaelli, D., Solan, M., and Webb, T. J. 2005. Do marine and terrestrial ecologists do it differently? *In* Bridging the gap between aquatic and terrestrial ecology, pp. 283–289. Ed. by K. I. Stergiou and H. I. Browman. Marine Ecology Progress Series.

Raitsos, D. E., Lavender, S. J., Maravelias, C. D., Haralabous, J., Richardson, A. J., and Reid, P. C. 2008. Identifying four phytoplankton functional types from space: An ecological approach. Limnology and Oceanography, 53: 605–613. American Society of Limnology and Oceanography Inc.

Raitsos, D. E., Lavender, S. J., Pradhan, Y., Tyrrell, T., Reid, P. C., and Edwards, M. 2006. Coccolithophore bloom size variation in response to the regional environment of the subarctic North Atlantic. Limnol. Oceanogr., 51: 2122–2130.

Reid, P. C., Edwards, M., Beaugrand, G., Skogen, M., and Stevens, D. 2003. Periodic changes in the zooplankton of the North Sea during the twentieth century linked to oceanic inflow. *In* Fisheries Oceanography, pp. 260–269.

Reid, P. C., Edwards, M., Hunt, H. G., and Warner, A. J. 1998. Phytoplankton change in the

North Atlantic. Nature, 391: 546–546. Nature Publishing Group.

Reygondeau, G., Longhurst, A., Martinez, E., Beaugrand, G., Antoine, D., and Maury, O. 2013. Dynamic biogeochemical provinces in the global ocean. Global Biogeochemical Cycles, 27: 1046–1058.

Reynolds, R. W. 2009. What's new in version 2. http://www.ncdc.noaa.gov/sites/default/files/attachments/Reynolds2009_oisst_daily_v02r00_version2-features.pdf (Accessed 9 October 2016).

Reynolds, R. W., Smith, T. M., Liu, C., Chelton, D. B., Casey, K. S., and Schlax, M. G. 2007. Daily High-Resolution-Blended Analyses for Sea Surface Temperature. Journal of Climate, 20: 5473–5496.

Richardson, A. J., and Schoeman, D. S. 2004. Climate impact on plankton ecosystems in the Northeast Atlantic. Science, 305: 1609–12. American Association for the Advancement of Science.

Ridgeway, Gr., with contributions from others. 2017. Gbm: Generalized Boosted Regression Models. https://CRAN.R-project.org/package=gbm.

Righetti, D., Vogt, M., Gruber, N., Psomas, A., and Zimmermann, N. E. 2019. Global pattern of phytoplankton diversity driven by temperature and environmental variability. Science Advances, 5: 1–10. American Association for the Advancement of Science.

Ripa, J., and Lundberg, P. 1996. Noise Colour and the Risk of Population Extinctions. Proceedings of the Royal Society B: Biological Sciences, 263: 1751–1753.

Rodriguez-Sanchez, F. 2017 & 2018. Grateful: Facilitate Citation of R Packages. https://github.com/Pakillo/grateful.

Rohani, P. 2004. The colour of noise in short ecological time series data. Mathematical Medicine and Biology, 21: 63–72.

Root, T. L., Price, J. T., Hall, K. R., Schneider, S. H., Rosenzweig, C., and Pounds, J. A. 2003. Fingerprints of global warming on wild animals and plants. Nature, 421: 57–60. Nature Publishing Group.

Rousseaux, C. S., and Gregg, W. W. 2012. Climate variability and phytoplankton composition in the Pacific Ocean. Journal of Geophysical Research: Oceans, 117: n/a-n/a.

Rousseaux, C. S., and Gregg, W. W. 2015. Recent decadal trends in global phytoplankton composition. Global Biogeochemical Cycles, 29: 1674–1688.

Roxy, M. K., Modi, A., Murtugudde, R., Valsala, V., Panickal, S., Prasanna Kumar, S., Ravichandran, M., *et al.* 2016. A reduction in marine primary productivity driven by rapid warming over the tropical Indian Ocean. Geophysical Research Letters, 43: 826–833. Blackwell Publishing Ltd.

Roy, S. 2018. Distributions of phytoplankton carbohydrate, protein and lipid in the world oceans from satellite ocean colour. ISME Journal, 12: 1457–1472. Nature Publishing Group.

Ruokolainen, L., and Fowler, M. S. 2008. Community extinction patterns in coloured environments. Proceedings. Biological sciences / The Royal Society, 275: 1775–83.

Ruokolainen, L., Lindén, A., Kaitala, V., and Fowler, M. S. 2009. Ecological and evolutionary dynamics under coloured environmental variation. Trends in ecology & evolution, 24: 555–63.

Rykaczewski, R. R., Dunne, J. P., Sydeman, W. J., García-Reyes, M., Black, B. A., and Bograd, S. J. 2015. Poleward displacement of coastal upwelling-favorable winds in the ocean's eastern boundary currents through the 21st century. Geophysical Research Letters, 42: 6424–6431.

Sæther, B.-E., Coulson, T., Grøtan, V., Engen, S., Altwegg, R., Armitage, K. B., Barbraud, C., *et al.* 2013a. How Life History Influences Population Dynamics in Fluctuating Environments. The American Naturalist, 182: 743–759.

Sæther, B.-E., Engen, S., and Grøtan, V. 2013b. Species diversity and community similarity in fluctuating environments: parametric approaches using species abundance distributions. The Journal of animal ecology, 82: 721–38.

Salguero-Gómez, R., Jones, O. R., Archer, C. R., Bein, C., de Buhr, H., Farack, C., Gottschalk, F., *et al.* 2016. COMADRE: a global data base of animal demography. Journal of Animal Ecology, 85: 371–384. Blackwell Publishing Ltd.

Salguero-Gómez, R., Jones, O. R., Archer, C. R., Buckley, Y. M., Che-Castaldo, J., Caswell, H., Hodgson, D., *et al.* 2015. The compadre Plant Matrix Database: an open online repository for plant demography. Journal of Ecology, 103: 202–218. John Wiley & Sons, Ltd.

Santini, L., Belmaker, J., Costello, M. J., Pereira, H. M., Rossberg, A. G., Schipper, A. M., Ceauşu, S., *et al.* 2017. Assessing the suitability of diversity metrics to detect biodiversity change. Biological Conservation, 213: 341–350. Elsevier Ltd.

Sarkar, D. 2008. Lattice: Multivariate Data Visualization with R. New York: Springer. http://lmdvr.r-forge.r-project.org.

Sathyendranath, S., Grant, M., Brewin, R. J. W., Brockmann, C., Brotas, V., Chuprin, A., Doerffer, R., *et al.* 2018. ESA Ocean Colour Climate Change Initiative (Ocean_Colour_cci): Version 3.1 Data. Centre for Environmental Data Analysis.

Sathyendranath, S., Longhurst, A., Caverhill, C. M., and Platt, T. 1995. Regionally and seasonally differentiated primary production in the North Atlantic. Deep Sea Research Part I: Oceanographic Research Papers, 42: 1773–1802. Pergamon.

Sathyendranath, S., and Platt, T. 1997. Analytic model of ocean color. Applied optics, 36: 2620–2629. Optical Society of America.

Schaum, C. E., and Collins, S. 2014. Plasticity predicts evolution in a marine alga. Proceedings. Biological sciences, 281: 20141486. The Royal Society.

Scheffer, M., Bascompte, J., Brock, W. A., Brovkin, V., Carpenter, S. R., Dakos, V., Held, H., *et al.* 2009, September 3. Early-warning signals for critical transitions. Nature Publishing Group.

Seddon, A. W. R., Macias-Fauria, M., Long, P. R., Benz, D., and Willis, K. J. 2016. Sensitivity of global terrestrial ecosystems to climate variability. Nature, 531: 229–232. Nature Publishing Group.

Signorini, S. R., Franz, B. A., and McClain, C. R. 2015. Chlorophyll variability in the oligotrophic gyres: mechanisms, seasonality and trends. Frontiers in Marine Science, 2: 1–11.

Smith, M. D. 2011a, May 1. An ecological perspective on extreme climatic events: A synthetic definition and framework to guide future research. Wiley/Blackwell (10.1111).

Smith, M. D. 2011b. The ecological role of climate extremes: Current understanding and future prospects. Journal of Ecology, 99: 651–655. Wiley/Blackwell (10.1111).

Soccodato, A., D'Ovidio, F., Lévy, M., Jahn, O., Follows, M. J., and De Monte, S. 2016. Estimating planktonic diversity through spatial dominance patterns in a model ocean. Marine Genomics, 29: 9–17. Elsevier.

Solano, R., Didan, K., Jacobson, A., and Huete, A. 2010. MODIS vegetation index C5 user's guide (MOD13 Series). 1–42 pp.

Spalding, M. D., Agostini, V. N., Rice, J., and Grant, S. M. 2012. Pelagic provinces of the world: A biogeographic classification of the world's surface pelagic waters. Ocean & Coastal Management, 60: 19–30. Elsevier.

Spalding, M. D., Fox, H. E., Allen, G. R., Davidson, N., Ferdaña, Z. A., Finlayson, M., Halpern, B. S., *et al.* 2007. Marine Ecoregions of the World: A Bioregionalization of Coastal and Shelf Areas. BioScience, 57: 573. Oxford University Press.

Steele, J. H. 1985. A comparison of terrestrial and marine ecological systems. Nature, 313: 355–358.

Steele, J. H. 1989. The ocean 'landscape'. Landscape Ecology, 3: 185–192. Kluwer Academic Publishers.

Steele, J. H. 1991a. Marine ecosystem dynamics: Comparison of scales. Ecological Research, 6: 175–183.

Steele, J. H. 1991b. Can ecological theory cross the land-sea boundary? Journal of Theoretical Biology, 153: 425–436.

Steele, J. H., Brink, K. H., and Scott, B. E. 2019. Comparison of marine and terrestrial ecosystems: suggestions of an evolutionary perspective influenced by environmental variation. ICES Journal of Marine Science, 76: 50–59.

Steele, J. H., and Henderson, E. W. 1994. Coupling between Physical and Biological Scales [and Discussion]. Philosophical Transactions of the Royal Society B: Biological Sciences, 343: 5–9.

Stenseth, N. C., and Mysterud, A. 2002. Climate, changing phenology, and other life history traits: nonlinearity and match-mismatch to the environment. Proceedings of the National Academy of Sciences of the United States of America, 99: 13379–13381. National Academy of Sciences.

Stenseth, N. C., Mysterud, A., Ottersen, G., Hurrell, J. W., Chan, K.-S., and Lima, M. 2002. Ecological effects of climate fluctuations. Science, 297: 1292–6.

Stenseth, N. C., Ottersen, G., Hurrell, J. W., Mysterud, A., Lima, M., Chan, K., Yoccoz, N. G., *et al.* 2003. Studying climate effects on ecology through the use of climate indices: the

North Atlantic Oscillation, El Niño Southern Oscillation and beyond. Proceedings. Biological sciences / The Royal Society, 270: 2087–96.

Stergiou, K. I., and Browman, H. I. 2005. Bridging the gap between aquatic and terrestrial ecology. Marine Ecology Progress Series, 304: 271–307.

Stevens, G. C. 1989. The latitudinal gradient in geographical range: how so many species coexist in the tropics. The American naturalist, 133: 240–256.

Stock, C. A., Dunne, J. P., and John, J. G. 2014. Drivers of trophic amplification of ocean productivity trends in a changing climate. Biogeosciences, 11: 7125–7135. Copernicus GmbH.

Sunday, J. M., Bates, A. E., and Dulvy, N. K. 2011. Global analysis of thermal tolerance and latitude in ectotherms. Proceedings. Biological sciences / The Royal Society, 278: 1823–30.

Sunday, J. M., Bates, A. E., and Dulvy, N. K. 2012. Thermal tolerance and the global redistribution of animals. Nature Climate Change, 2: 686–690. Nature Publishing Group.

Suryan, R. M., Saba, V. S., Wallace, B. P., Hatch, S. A., Frederiksen, M., and Wanless, S. 2009. Environmental forcing on life history strategies: Evidence for multi-trophic level responses at ocean basin scales. Progress in Oceanography, 81: 214–222.

Sydeman, W. J., Santora, J. A., Thompson, S. A., Marinovic, B., and Lorenzo, E. Di. 2013. Increasing variance in North Pacific climate relates to unprecedented ecosystem variability off California. Global Change Biology, 19: 1662–1675.

Tamburello, N., Côté, I. M., and Dulvy, N. K. 2015. Energy and the Scaling of Animal Space Use. The American Naturalist, 186: 196–211. University of Chicago PressChicago, IL.

Taylor, A. H., Allen, J. I., and Clark, P. A. 2002. Extraction of a weak climatic signal by an ecosystem. Nature, 416: 629–632. Nature Publishing Group.

Thackeray, S. J., Henrys, P. A., Hemming, D., Bell, J. R., Botham, M. S., Burthe, S., Helaouet, P., *et al.* 2016. Phenological sensitivity to climate across taxa and trophic levels. Nature, 535: 241–245. Nature Research.

Thackeray, S. J., Sparks, T. H., Frederiksen, M., Burthe, S., Bacon, P. J., Bell, J. R., Botham, M. S., *et al.* 2010. Trophic level asynchrony in rates of phenological change for marine, freshwater and terrestrial environments. Global Change Biology, 16: 3304–3313.

Blackwell Publishing Ltd.

Thibault, K. M., White, E. P., and Ernest, S. K. M. 2004. Temporal dynamics in the structure and composition of a desert rodent community. Ecology, 85: 2649–2655.

Thomas, A. C., and Brickley, P. 2006. Satellite measurements of chlorophyll distribution during spring 2005 in the California current. Geophysical Research Letters, 33: L22S05.

Thomas, M. K., Kremer, C. T., Klausmeier, C. A., and Litchman, E. 2012. A global pattern of thermal adaptation in marine phytoplankton. Science, 338: 1085–1088.

Thornton, P. K., Ericksen, P. J., Herrero, M., and Challinor, A. J. 2014, November. Climate variability and vulnerability to climate change: A review.

Titley, M. A., Snaddon, J. L., and Turner, E. C. 2017. Scientific research on animal biodiversity is systematically biased towards vertebrates and temperate regions. PLOS ONE, 12: e0189577. Public Library of Science.

Toszogyova, A., and Storch, D. 2019. Global diversity patterns are modulated by temporal fluctuations in primary productivity. Global Ecology and Biogeography, 00: 1–12.

Trebilco, R., Baum, J. K., Salomon, A. K., and Dulvy, N. K. 2013. Ecosystem ecology: size-based constraints on the pyramids of life. Trends in Ecology & Evolution, 28: 423–431.

Trimble, M. J., and van Aarde, R. J. 2012. Geographical and taxonomic biases in research on biodiversity in human-modified landscapes. Ecosphere, 3: art119. Wiley.

Tyler, E. H. M., Somerfield, P. J., Berghe, E. Vanden, Bremner, J., Jackson, E., Langmead, O., Palomares, M. L. D., *et al.* 2012. Extensive gaps and biases in our knowledge of a well-known fauna: implications for integrating biological traits into macroecology. Global Ecology and Biogeography, 21: 922–934.

Uitz, J., Claustre, H., Gentili, B., and Stramski, D. 2010. Phytoplankton class-specific primary production in the world's oceans: Seasonal and interannual variability from satellite observations. Global Biogeochemical Cycles, 24: n/a-n/a.

Ulrich, W., Ollik, M., and Ugland, K. I. 2010. A meta-analysis of species-abundance distributions. Oikos, 119: 1149–1155.

Van der Plas, F., Anderson, T. M., and Olff, H. 2012. Trait similarity patterns within grass and grasshopper communities: Multitrophic community assembly at work. Ecology, 93: 836–

846.

Vasseur, D. A., DeLong, J. P., Gilbert, B., Greig, H. S., Harley, C. D. G., McCann, K. S., Savage, V., *et al.* 2014. Increased temperature variation poses a greater risk to species than climate warming. Proceedings of the Royal Society B: Biological Sciences, 281. Royal Society.

Vasseur, D. A., and Yodzis, P. 2004. The color of environmental noise. Ecology, 85: 1146–1152.

Visser, M. E., and Holleman, L. J. M. 2001. Warmer springs disrupt the synchrony of oak and winter moth phenology. Proceedings of the Royal Society B: Biological Sciences, 268: 289–294.

von Holle, B., Wei, Y., and Nickerson, D. 2010. Climatic variability leads to later seasonal flowering of floridian plants. PLoS ONE, 5: e11500. Public Library of Science.

Webb, C. O., Ackerly, D. D., McPeek, M. A., and Donoghue, M. J. 2002, November 28. Phylogenies and community ecology. Annual Reviews.

Webb, T. J. 2009. Biodiversity research sets sail: showcasing the diversity of marine life. Biology letters, 5: 145–7.

Webb, T. J. 2012. Marine and terrestrial ecology: unifying concepts, revealing differences. Trends in ecology & evolution, 27: 535–41.

Weber, R. O., and Talkner, P. 2001. Spectra and correlations of climate data from days to decades. Journal of Geophysical Research, 106: 20131.

Weber, S. C., Subramaniam, A., Montoya, J. P., Doan-Nhu, H., Nguyen-Ngoc, L., Dippner, J. W., and Voss, M. 2019. Habitat delineation in highly variable marine environments. Frontiers in Marine Science, 6: 112. Frontiers.

Webster, J. R., Waide, J. B., and Patten, B. C. 1975. Nutrient recycling and the stability of ecosystems. *In* Mineral Cycling in Southeastern Ecosystems, pp. 1–27. Ed. by F. G. Howell, J. B. Gentry, and M. H. Smith.

Weimerskirch, H. 2007. Are seabirds foraging for unpredictable resources? Deep Sea Research Part II: Topical Studies in Oceanography, 54: 211–223.

Whittaker, R. H. 1960. Vegetation of the Siskiyou Mountains, Oregon and California. Ecological

Monographs, 30: 279–338.

Whittaker, R. H. 1965. Dominance and diversity in land plant communities. Science, 147: 250–260.

Whittaker, R. H. 1975. Communities and ecosystems. MacMillan Pubishers, New York.

Wickham, H. 2007. “Reshaping Data with the reshape Package.” Journal of Statistical Software 21 (12): 1–20. http://www.jstatsoft.org/v21/i12/.

Wickham, H. 2016. Ggplot2: Elegant Graphics for Data Analysis. Springer-Verlag New York. http://ggplot2.org.

Wickham, H. 2017, 2019. Tidyverse: Easily Install and Load the ’Tidyverse’. https://CRAN.R-project.org/package=tidyverse.

Wickham, H. 2019a. Forcats: Tools for Working with Categorical Variables (Factors). https://CRAN.R-project.org/package=forcats.

Wickham, H. 2019b. Stringr: Simple, Consistent Wrappers for Common String Operations. https://CRAN.R-project.org/package=stringr.

Wickham, H., and Henry, L. 2018 & 2020. Tidyr: Easily Tidy Data with ’Spread()’ and ’Gather()’ Functions. https://CRAN.R-project.org/package=tidyr.

Wickham, H., François, R., Henry, L., and Müller, K. 2018, 2020. Dplyr: A Grammar of Data Manipulation. https://CRAN.R-project.org/package=dplyr.

Wickham, H., Hester, J., and Chang, W. 2018. Devtools: Tools to Make Developing R Packages Easier. https://CRAN.R-project.org/package=devtools.

Wickham, H., Hester, J., and Francois, R. 2017 & 2018. Readr: Read Rectangular Text Data. https://CRAN.R-project.org/package=readr.

Wiens, J. J. 2016. Climate-Related Local Extinctions Are Already Widespread among Plant and Animal Species. PLoS Biology, 14: e2001104.

Wigley, T. M. L., Smith, R. L., and Santer, B. D. 1998. Anthropogenic influence on the autocorrelation structure of hemispheric-mean temperatures. Science (New York, N.Y.), 282: 1676–9. American Association for the Advancement of Science.

Wilke, C.O. 2018 & 2019. Cowplot: Streamlined Plot Theme and Plot Annotations for ’Ggplot2’.

https://CRAN.R-project.org/package=cowplot.

Wilson, J. B., Wells, T. C. E., Trueman, I. C., Jones, G., Atkinson, M. D., Crawley, M. J., Dodd, M. E., *et al.* 1996. Are there Assembly Rules for Plant Species Abundance? An Investigation in Relation to Soil Resources and Successional Trends. The Journal of Ecology, 84: 527. JSTOR.

Winemiller, K. O., and Rose, K. A. 1992. Patterns of Life-History Diversification in North American Fishes: implications for Population Regulation. Canadian Journal of Fisheries and Aquatic Sciences, 49: 2196–2218. NRC Research Press Ottawa, Canada .

Wing, J., Kuhn, M. Contributions from, Weston, S., Williams, A., Keefer, C., Engelhardt, A., Cooper, T., Mayer, Z., et al. 2018. Caret: Classification and Regression Training. https://CRAN.R-project.org/package=caret.

Wood, S.N. 2011. “Fast Stable Restricted Maximum Likelihood and Marginal Likelihood Estimation of Semiparametric Generalized Linear Models.” Journal of the Royal Statistical Society (B) 73 (1): 3–36.

Wyrtki, K. 1964. Upwelling in the Costa Rica Dome. Fisheries Bulletin, 63: 355–372.

Yasunaka, S., Nojiri, Y., Nakaoka, S. I., Ono, T., Whitney, F. A., and Telszewski, M. 2014. Mapping of sea surface nutrients in the North Pacific: Basin-wide distribution and seasonal to interannual variability. Journal of Geophysical Research: Oceans, 119: 7756–7771.

Yokomizo, H., Botsford, L. W., Holland, M. D., Lawrence, C. A., and Hastings, A. 2010. Optimal wind patterns for biological production in shelf ecosystems driven by coastal upwelling. Theoretical Ecology, 3: 53–63. Springer Netherlands.

Zeileis, A., and Grothendieck, G. 2005. “Zoo: S3 Infrastructure for Regular and Irregular Time Series.” Journal of Statistical Software 14 (6): 1–27. doi:10.18637/jss.v014.i06.

Zender, C. S. 2008. Analysis of self-describing gridded geoscience data with netCDF Operators (NCO). Environmental Modelling and Software, 23: 1338–1342.

Zhang, H.-M., Bates, J. J., and Reynolds, R. W. 2006. Assessment of composite global sampling: Sea surface wind speed. Geophysical Research Letters, 33: L17714.

Appendices

Appendix A Chapter 2 Supplementary Figures

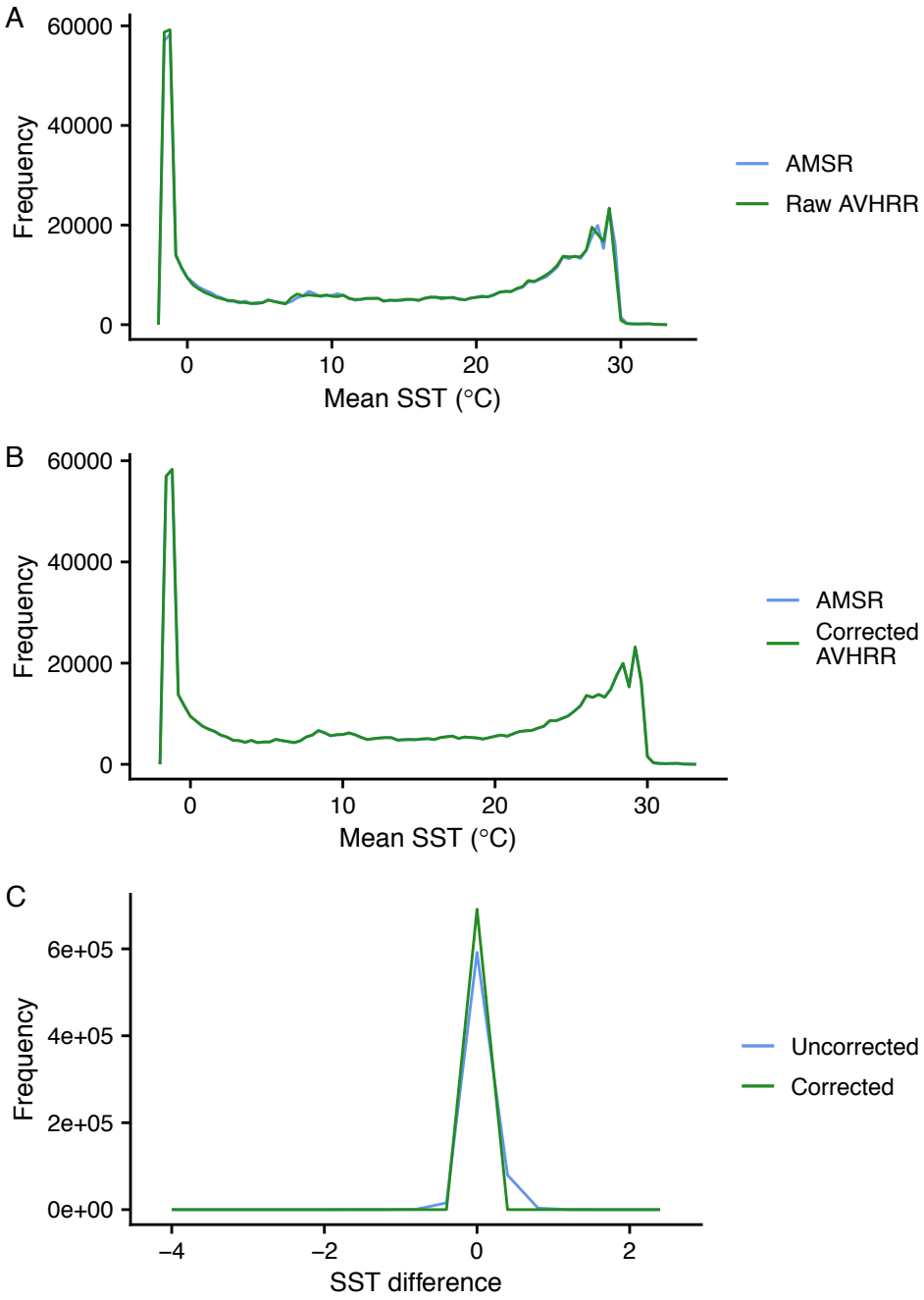

Figure A-1: Correction verification for sea surface temperature (SST) satellite data. Two satellite datasets were used for the SST variable: AVHRR (available 2000-2013) and AVHRR & AMSR-E (available 2002-2011). To correct the AVHRR data outside of the range of AVHRR & AMSR-E, 8-year monthly means were created for the 2003-2010 overlap period for each dataset. The AVHRR monthly means were subtracted from the AVHRR & AMSR-E means to provide a correction factor, which could be added to AVHRR months pre-2002 and post-2011. Plots show frequency polygons of the 8-year monthly means for July for the uncorrected AVHRR and AVHRR & AMSR-E datasets (A), the corrected AVHRR and AVHRR & AMSR-E datasets (B) and the difference between the monthly means of the AVHRR and AVHRR & AMSR-E before and after correction of the AVHRR data (C). Correction procedure methodology based on Frouin *et al.* (2012).

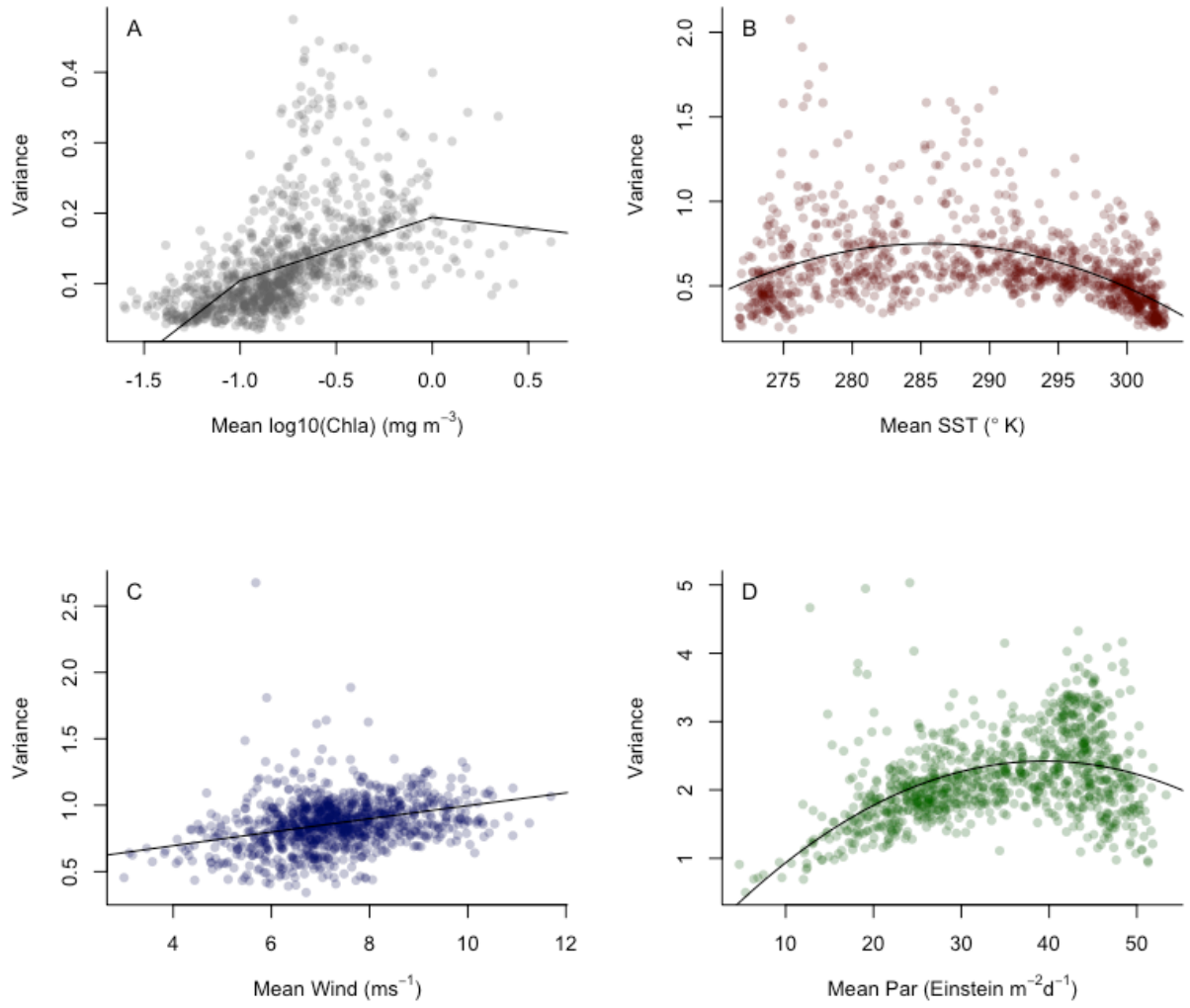

Figure A-2: Mean-variance relationships in the input variables of the Phytoplankton Sensitivity Index (PSI). Plots of the non-linear mean-variance relationships in the input variables for the PSI: log10 Chl-a (A), sea surface temperature (SST; B), sea surface winds (SSW; C) and photosynthetically available radiation (PAR; D). Due to the volume of input pixels (> 9,000,000) a random sample of 1,000 were selected for each variable to create the plots.

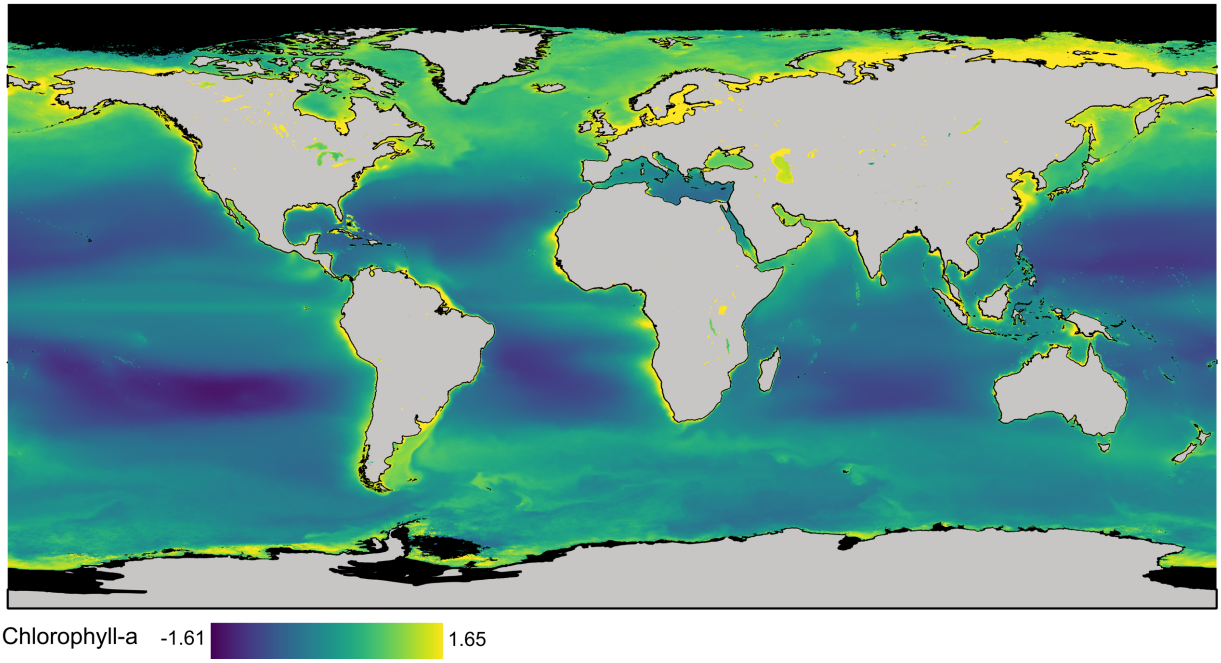

Figure A-3: Annual distribution of global chlorophyll. Global distribution of mean $\log_{10}$ chlorophyll-a (mg m^{-3}) for the 2000-2013 time series.

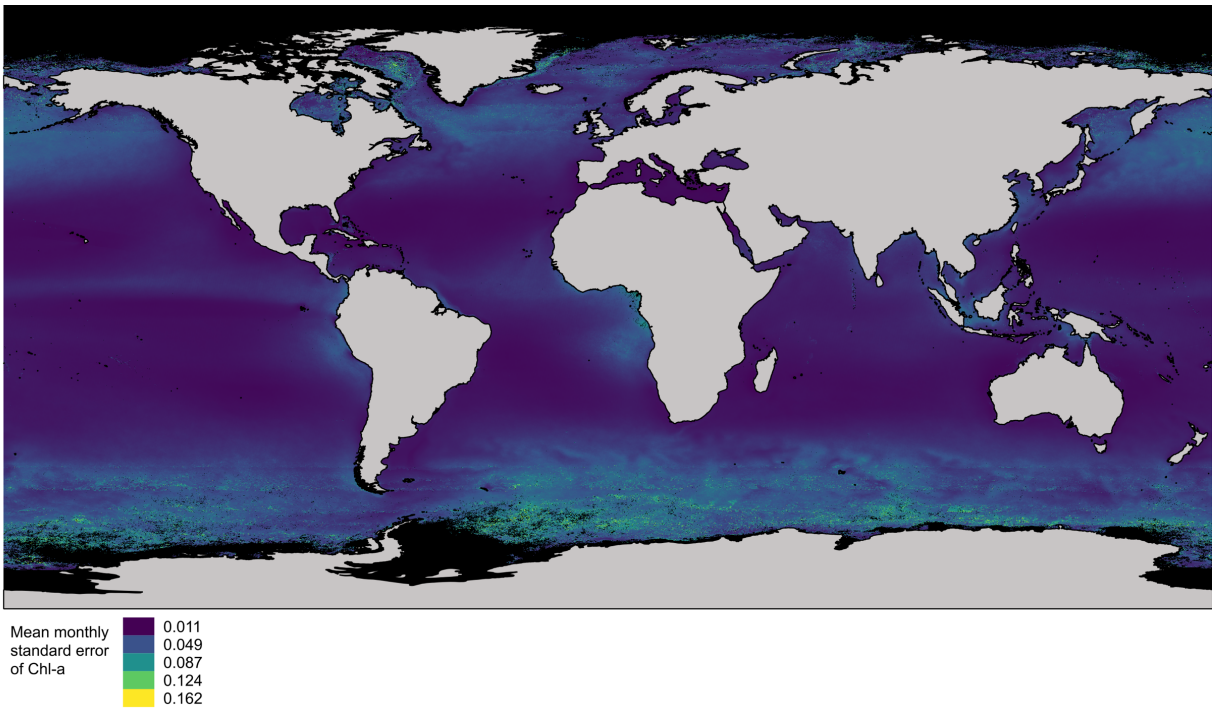

Figure A-4: Mean standard error of the OC-CCI Chl-a observations. Mean standard error of the OC-CCI Chl-a observations, calculated for the period 2000-2013 as the mean monthly standard deviation of all Chl-a observations per 9 km pixel, divided by the square root of the number of observations per pixel. This shows the extent to which satellite observations are likely to differ from in-situ observations. Areas in black indicate no data availability. Continental outlines were modified from a shapefile using QGIS.

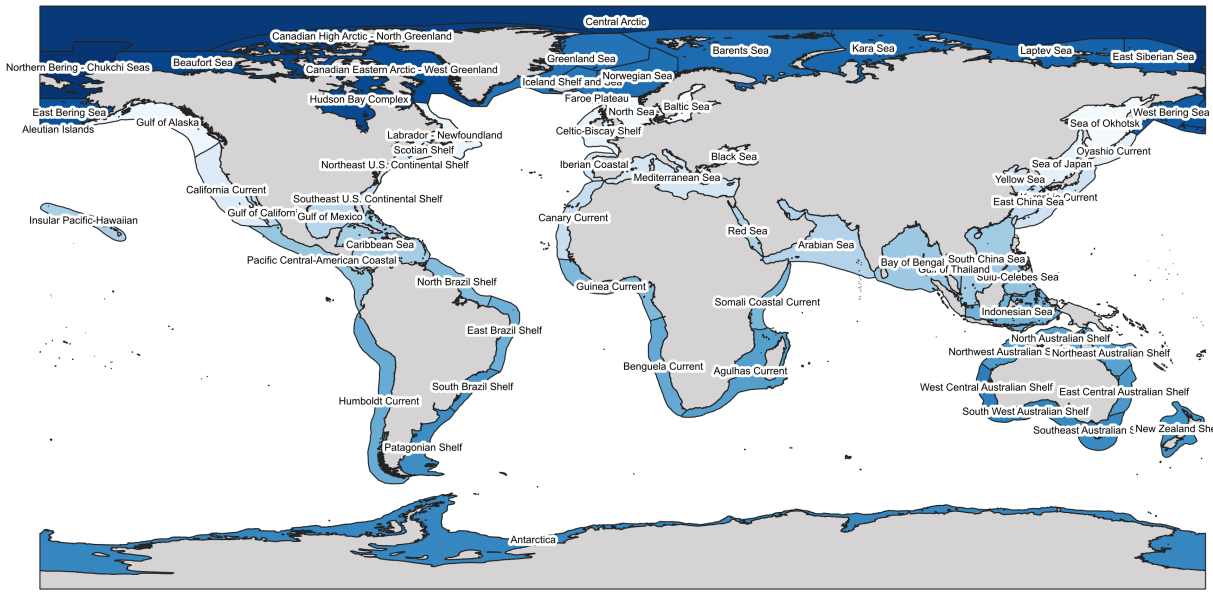

Figure A-5: Map showing large marine ecosystem (LME) designations.

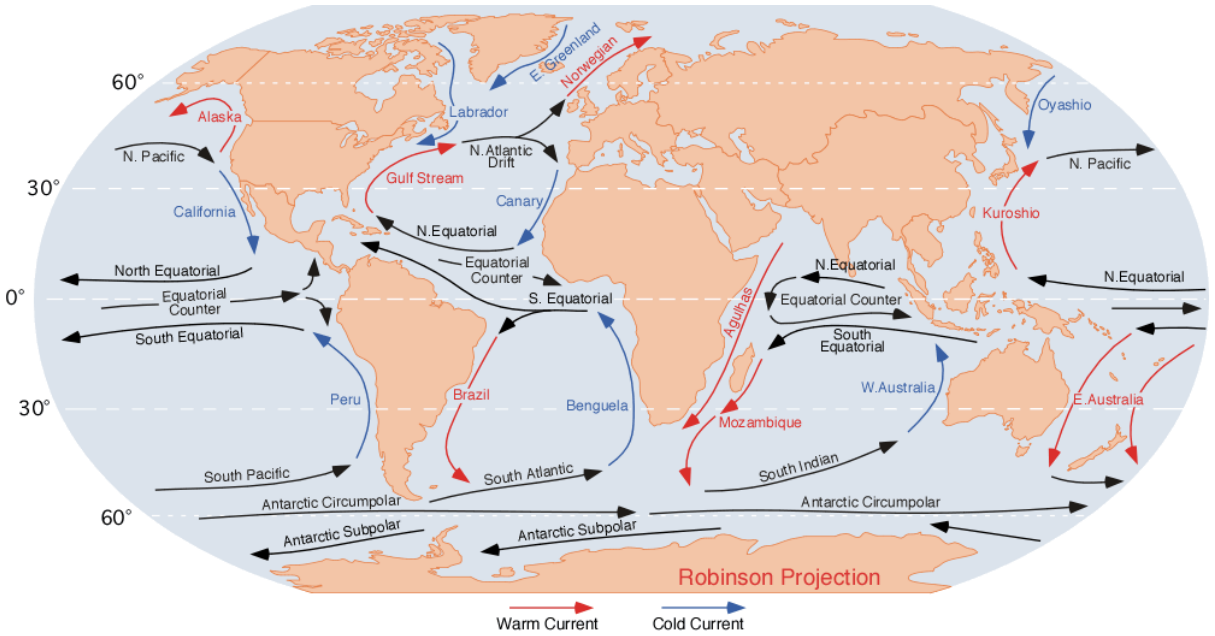

Figure A-6: Global map of the world's major ocean currents. By Dr. Michael Pidwirny (see http://www.physicalgeography.net) - http://blue.utb.edu/paullgj/geog3333/lectures/physgeog.html, [http://skyblue.utb.edu/paullgj/geog3333/lectures/oceancurrents-1.gif original image], Public Domain, https://commons.wikimedia.org/w/index.php?curid=37108971.

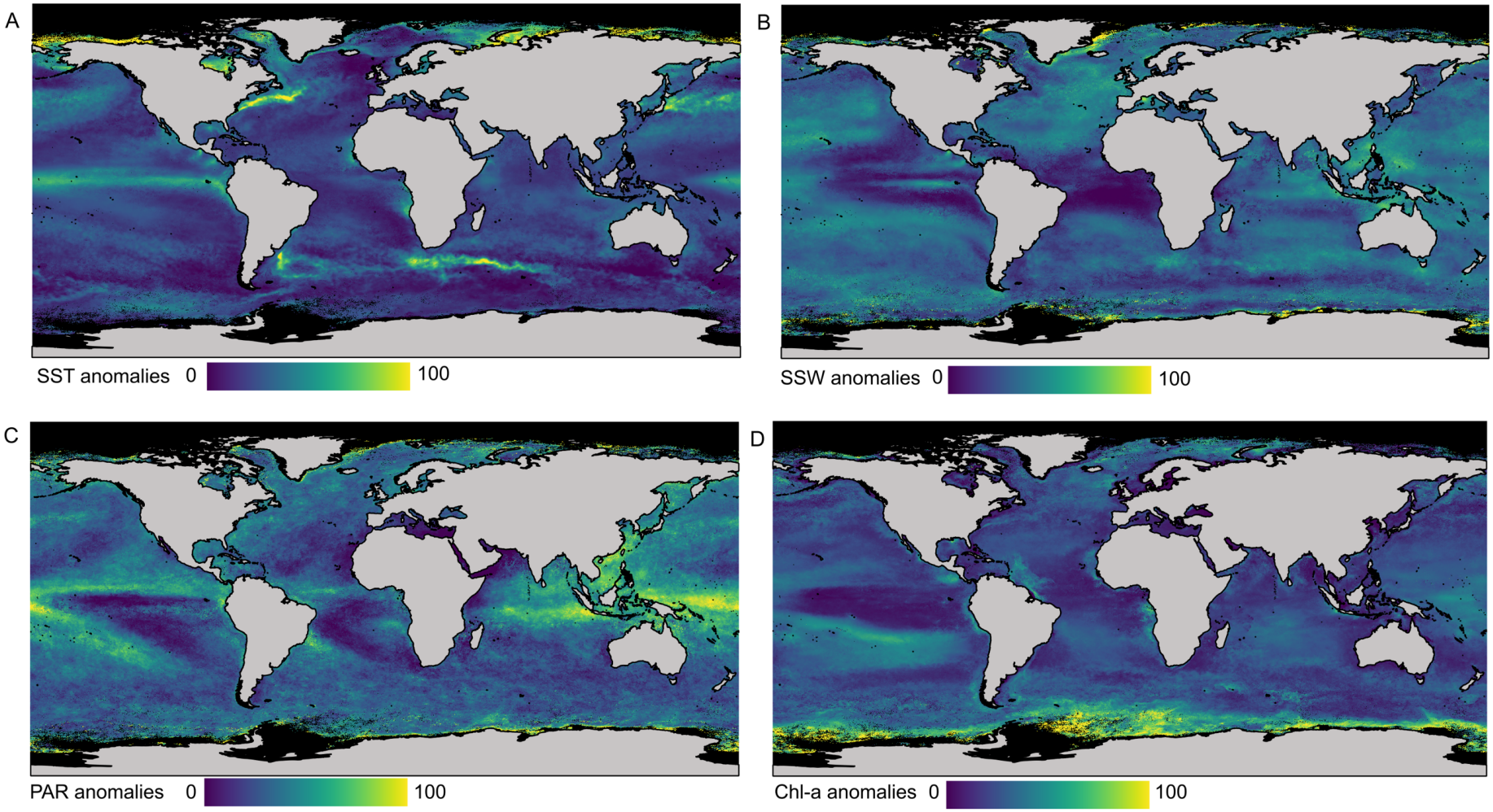

Figure A-7: Global primary productivity and climate anomalies. Maps showing the global anomalies for the 3 climate drivers (sea surface temperature (SST; A), sea surface winds (SSW; B) and photosynthetically available radiation (PAR; C) and chlorophyll-a (Chl-a; D). The anomalies are calculated from seasonally detrended time series for months with a significant ($P < 0.1$) relationship between primary productivity and climate variability in the principal components regression. Anomalies are standardised between 0-100. Areas in black indicate no data availability. Pixel resolution, 9 km; time period, 2000-2013. Continental outlines were modified from a shapefile using QGIS.

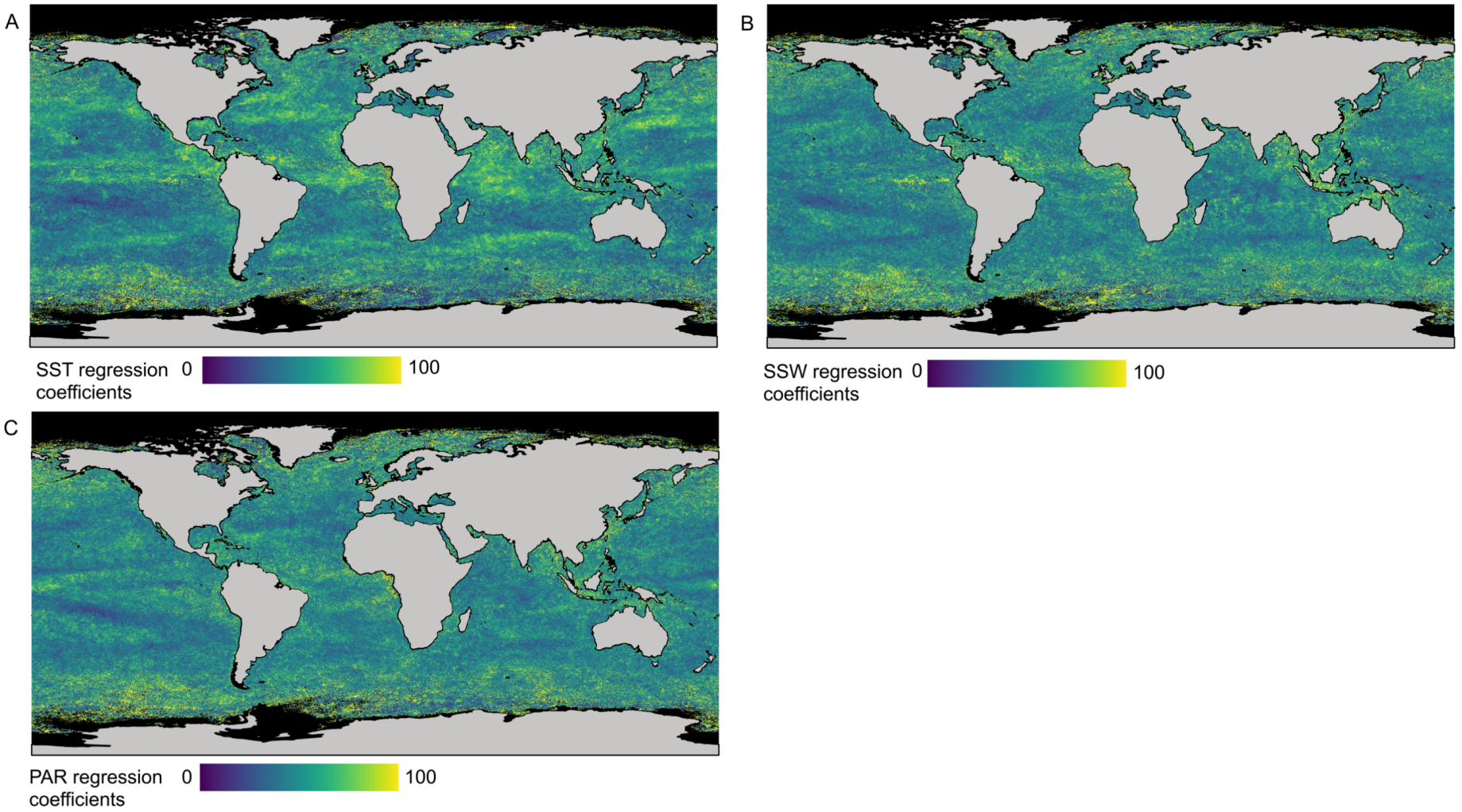

Figure A-8: Global strength of primary productivity-climate variability relationships. Maps of the significant (P < 0.1) regression coefficients from the principal components regression between Chl-a anomalies and sea surface temperature (SST; A), sea surface winds (SSW; B) and photosynthetically available radiation (PAR; C) variability. Coefficients are standardised between 0-100. Areas in black indicate no data availability. Pixel resolution, 9 km; time period, 2000-2013. Continental outlines were modified from a shapefile using QGIS.

Appendix B Chapter 3 Supplementary Figures

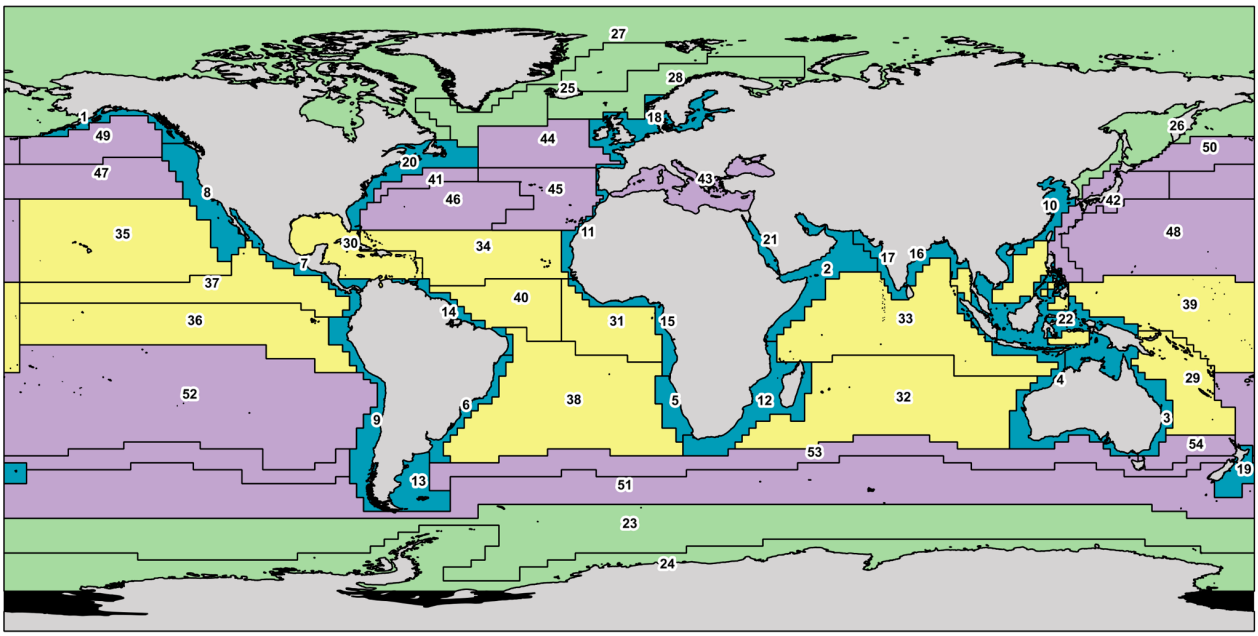

1	ALSK	Coastal - Alaska Downwelling Coastal Province	20	NWCS	Coastal - NW Atlantic Shelves Province	39	WARM	Trades - W. Pacific Warm Pool Province
2	ARAB	Coastal - NW Arabian Upwelling Province	21	REDS	Coastal - Red Sea, Persian Gulf Province	40	WTRA	Trades - Western Tropical Atlantic Province
3	AUSE	Coastal - East Australian Coastal Province	22	SUND	Coastal - Sunda-Arafura Shelves Province	41	GFST	Westerlies - Gulf Stream Province
4	AUSW	Coastal - Australia-Indonesia Coastal Province	23	ANTA	Polar - Antarctic Province	42	KURO	Westerlies - Kuroshio Current Province
5	BENG	Coastal - Benguela Current Coastal Province	24	APLR	Polar - Austral Polar Province	43	MEDI	Westerlies - Mediterranean Sea, Black Sea Province
6	BRAZ	Coastal - Brazil Current Coastal Province	25	ARCT	Polar - Atlantic Arctic Province	44	NADR	Westerlies - N. Atlantic Drift Province (WWDR)
7	CAMR	Coastal - Central American Coastal Province	26	BERS	Polar - N. Pacific Epicontinental Province	45	NASE	Westerlies - N. Atlantic Subtropical Gyral Province (East) (STGE)
8	CCAL	Coastal - California Upwelling Coastal Province	27	BPLR	Polar - Boreal Polar Province (POLR)	46	NASW	Westerlies - N. Atlantic Subtropical Gyral Province (West) (STGW)
9	CHIL	Coastal - Chile-Peru Current Coastal Province	28	SARC	Polar - Atlantic Subarctic Province	47	NPPF	Westerlies - N. Pacific Polar Front Province
10	CHIN	Coastal - China Sea Coastal Province	29	ARCH	Trades - Archipelagic Deep Basins Province	48	NPSW	Westerlies - N. Pacific Subtropical Gyre Province (West)
11	CNRY	Coastal - Canary Coastal Province (EACB)	30	CARB	Trades - Caribbean Province	49	PSAE	Westerlies - Pacific Subarctic Gyres Province (East)
12	EAFR	Coastal - E. Africa Coastal Province	31	ETRA	Trades - Eastern Tropical Atlantic Province	50	PSAW	Westerlies - Pacific Subarctic Gyres Province (West)
13	FKLD	Coastal - SW Atlantic Shelves Province	32	ISSG	Trades - Indian S. Subtropical Gyre Province	51	SANT	Westerlies - Subantarctic Province
14	GUIA	Coastal - Guianas Coastal Province	33	MONS	Trades - Indian Monsoon Gyres Province	52	SPSG	Westerlies - S. Pacific Subtropical Gyre Province
15	GUIN	Coastal - Guinea Current Coastal Province	34	NATR	Trades - N. Atlantic Tropical Gyral Province (TRPG)	53	SSTC	Westerlies - S. Subtropical Convergence Province
16	INDE	Coastal - E. India Coastal Province	35	NPTG	Trades - N. Pacific Tropical Gyre Province	54	TASM	Westerlies - Tasman Sea Province
17	INDW	Coastal - W. India Coastal Province	36	PEQD	Trades - Pacific Equatorial Divergence Province			
18	NECS	Coastal - NE Atlantic Shelves Province	37	PNEC	Trades - N. Pacific Equatorial Countercurrent Province			
19	NEWZ	Coastal - New Zealand Coastal Province	38	SATL	Trades - South Atlantic Gyral Province (SATG)			

Figure B-1: Key of Longhurst's Marine Biogeographic Regions. Map showing the 54 provinces of Longhurst's Marine Biogeographic Regions colour coded by their primary biomes: coastal (blue); polar (green); trades (yellow) and westerlies (purple). The number in each province corresponds to its province code label and name shown in the index below the map.

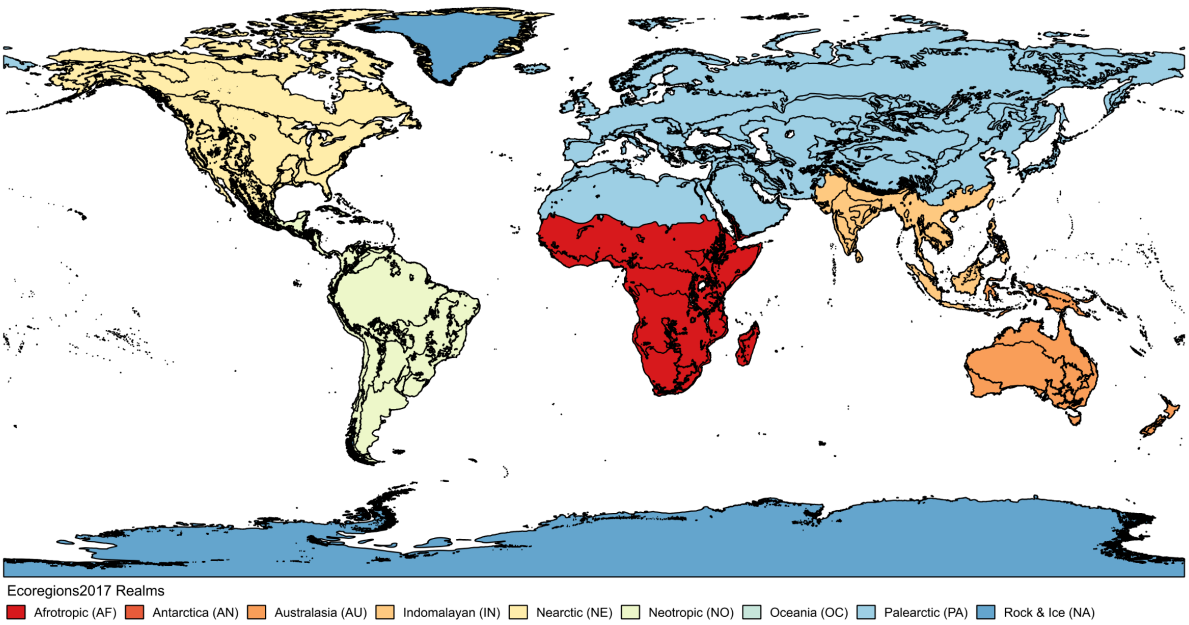

Figure B-2: Key of Ecoregions2017 realms. Map showing the 9 major realms of the Ecoregions2017 classification system. The 2-letter code after each realm name in the legend forms the first half of a region's code, with the second half coming from the biome code (Figure B-3) e.g. Boreal Forests in the Palearctic would be PA06. For consistency with Longhurst's biogeographic regions used to regionalise the PSI, the Ecoregions2017 realms are referred to as biomes within the main text.

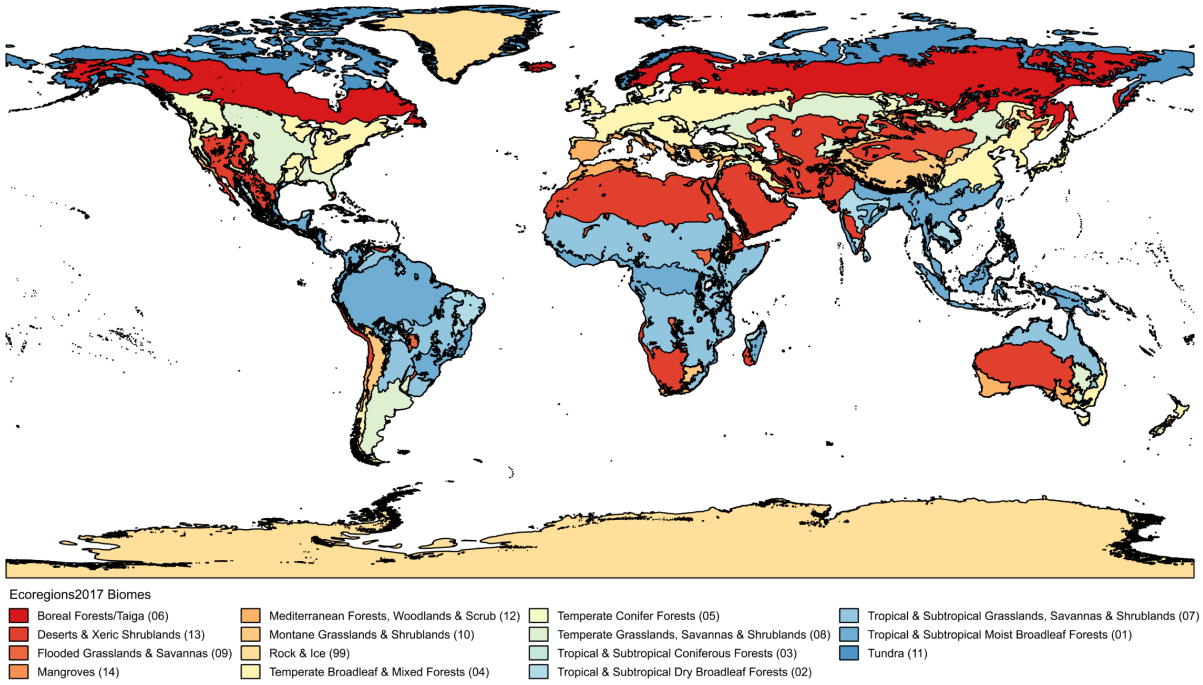

Figure B-3: Key of Ecoregions2017 biomes. Map showing the 14 major biomes of the Ecoregions2017 classification system. The 2-digit number after each biome name in the legend forms the second half of a region's code, with the first half coming from the realm code (Figure B-2) e.g. Boreal Forests in the Palearctic would be PA06. For consistency with Longhurst's biogeographic regions used to regionalise the PSI, the Ecoregions2017 realms are referred to as provinces within the main text.

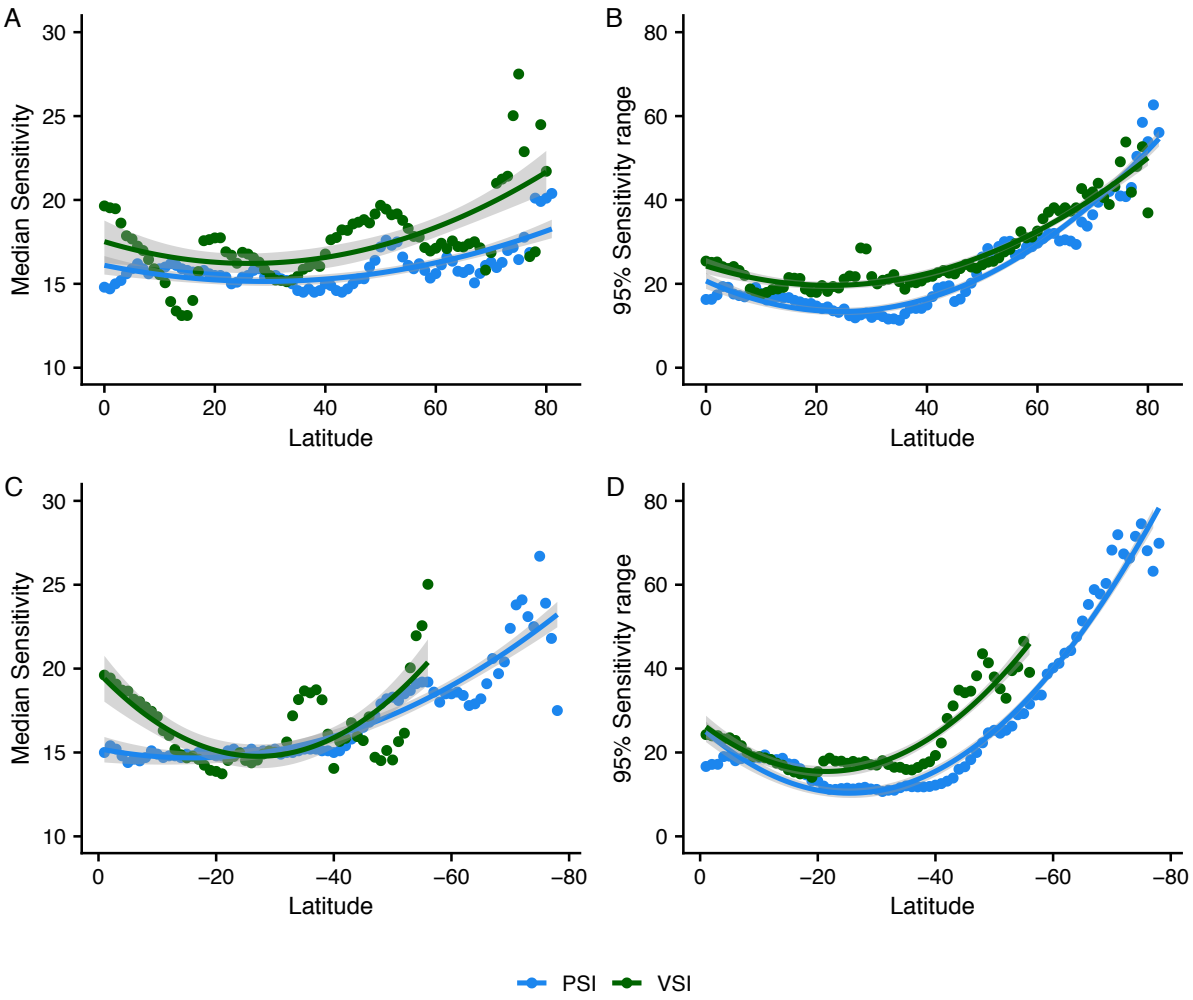

Figure B-4: Hemispheric trends in the median and 95% range of sensitivities for the PSI and VSI. Plots showing the difference in trends between median sensitivity and latitude in the Northern (A) and Southern (C) hemisphere, and between the 95% range of sensitivities and latitude in the Northern (B) and Southern (D) hemisphere for the PSI and VSI. The solid lines represent quadratic linear models fitted to the median and 95% range of sensitivities against degree of latitude. Whilst the plots extend to -80° Latitude in the Southern hemisphere, for statistical analysis the models were only fitted up to -60° Latitude. Shaded areas show the standard error.

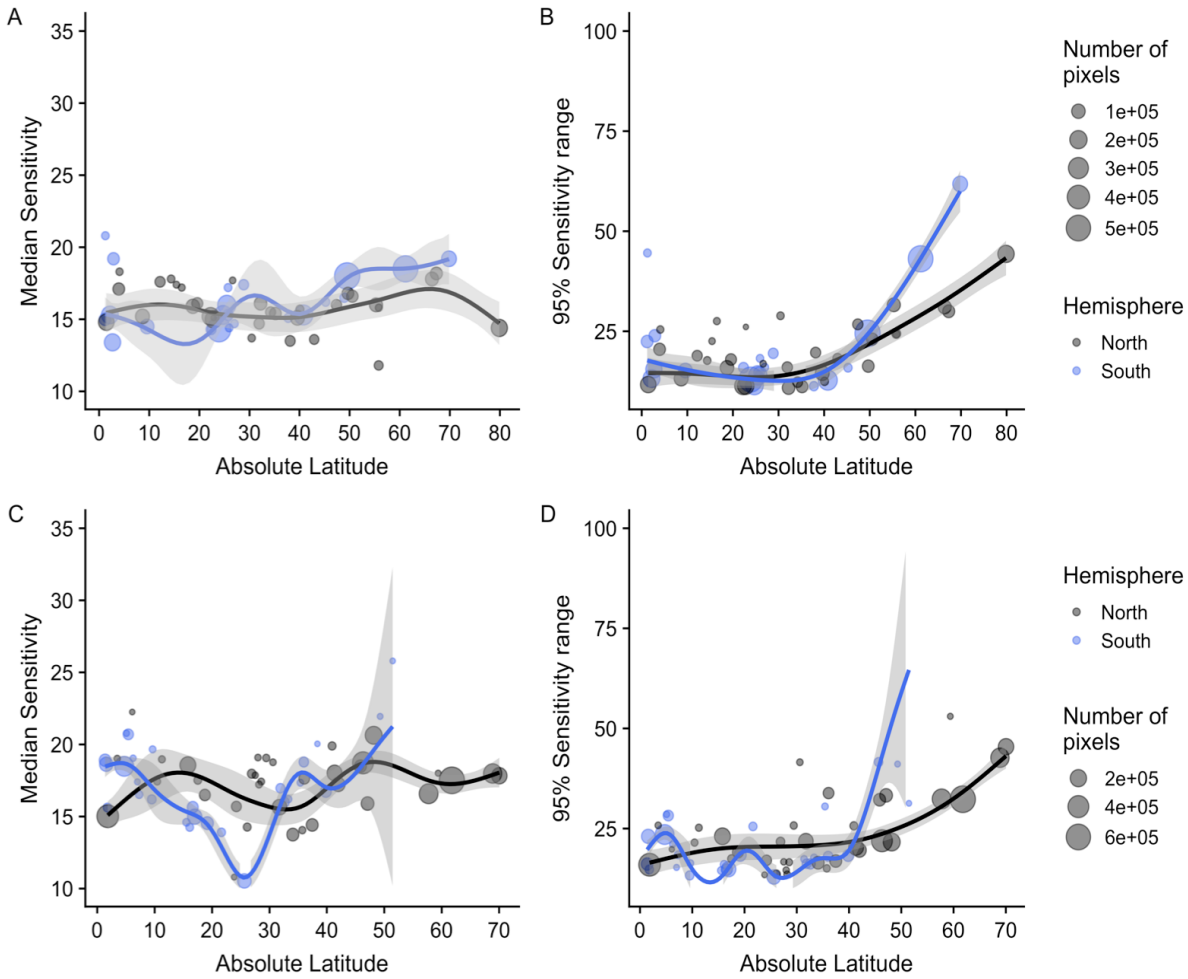

Figure B-5: GAM model fit for the median and 95% range of marine and terrestrial province sensitivities. Results of GAM models fitted to the median (A, C) and 95% range (97.5% quantile – 2.5% quantile) (B, D) of province sensitivities for the marine PSI (A, B) and terrestrial VSI (C, D). GAMs were weighted by the number of pixels in each province.

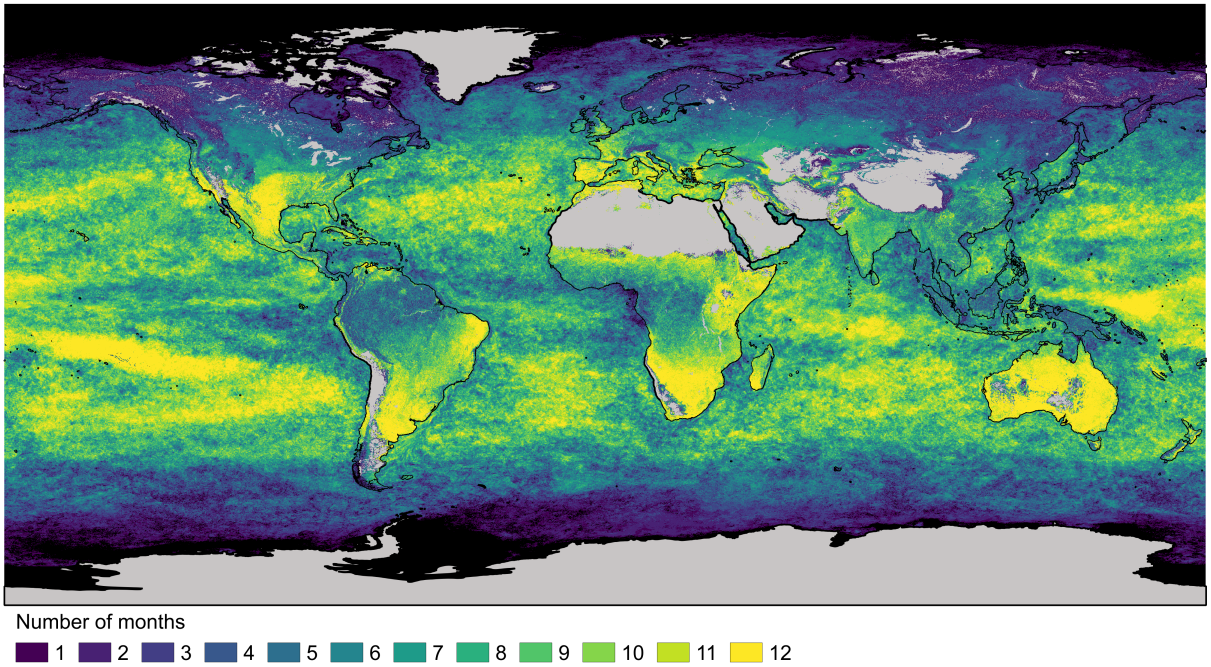

Figure B-6: Number of months with a significant (P < 0.1) coefficient in the principal components regression. Number of months per pixel with a significant (P < 0.1) relationship between primary productivity (PSI: Chl-a; VSI: EVI), climate variation (PSI: sea surface temperature, sea surface wind and photosynthetically available radiation; VSI: temperature, precipitation and cloudiness) and a one-month primary productivity time lag (t-1) variable in the principal components regression, highlighting areas with consistent, year-round Chl-a climate relationships. Pixel resolution, 9 km (PSI), 5 km (VSI); time period, 2000-2013. Areas in black indicate no data availability. Terrestrial areas in grey are predominantly barren areas, created using a minimum vegetation threshold. Continental outlines were modified from a shapefile using QGIS.

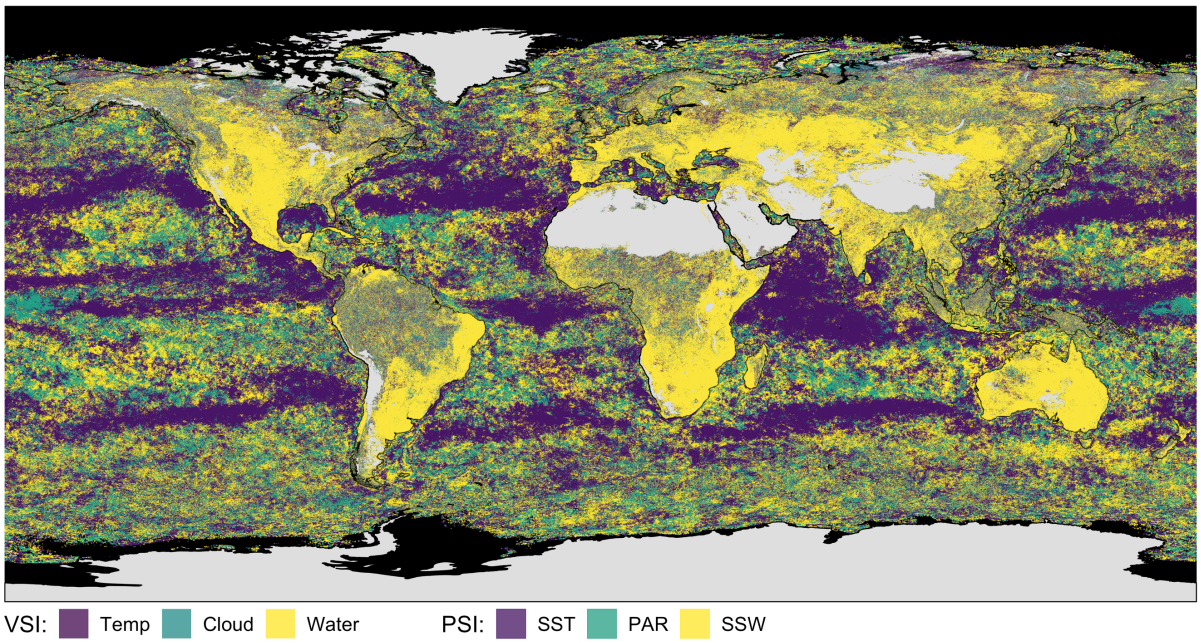

Figure B-7: Composite map of global climate weights. Composite map of the mean climate coefficient weights for the marine PSI and terrestrial VSI from multiple linear regressions between primary productivity and three climatic drivers (PSI: sea surface temperature (blue), photosynthetically available radiation (green) and sea surface wind (yellow); VSI: temperature (blue), cloudiness (green), precipitation (yellow)). Pixel resolution, 9 km (PSI), 5 km (VSI); time period, 2000-2013. Areas in black indicate no data availability. Terrestrial areas in grey are predominantly barren areas, created using a minimum vegetation threshold. Continental outlines were modified from a shapefile using QGIS.

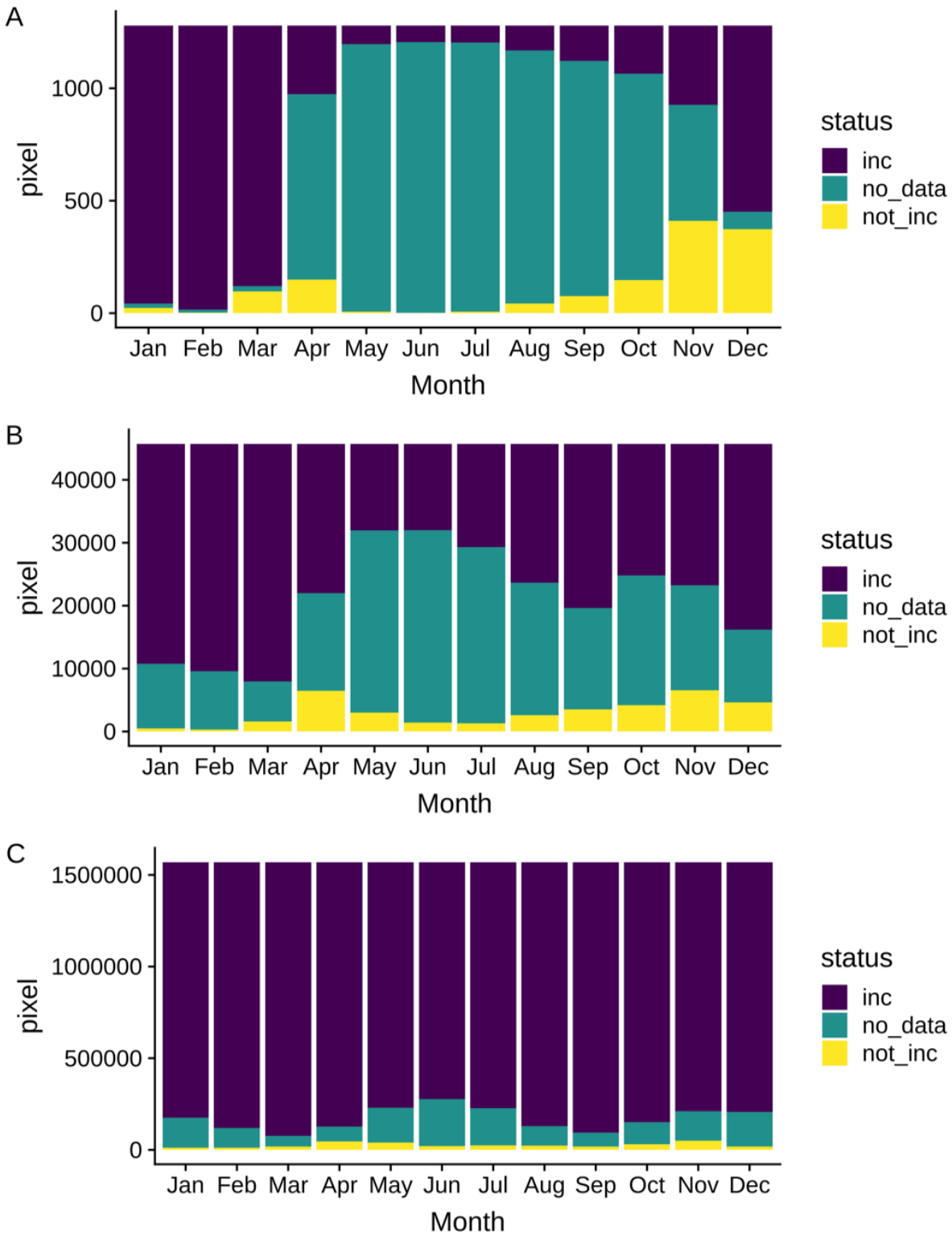

Figure B-8: Data availability of high, medium and low sensitivity Chlorophyll-a pixels. Bar plots showing data availability for high (A; 80-100), medium (B; 40-60) and low (C; 0-20) sensitivity Chl-a pixels. To be included within the sensitivity analyses for a particular month, pixels were required to have a minimum of 4 years of month specific of data across the 2000-2013 time series, i.e. data for July over 4 or more years. Pixels with 4 or more years of data were included in analyses (inc, dark blue), pixels with less than 4 years of data were not included (not_inc, yellow) and some pixels had no data at all (no_data, turquoise). High sensitivity had the highest proportion of pixels with no data availability from Apr-Oct. All pixels within each sensitivity bracket were extracted to determine data availability.

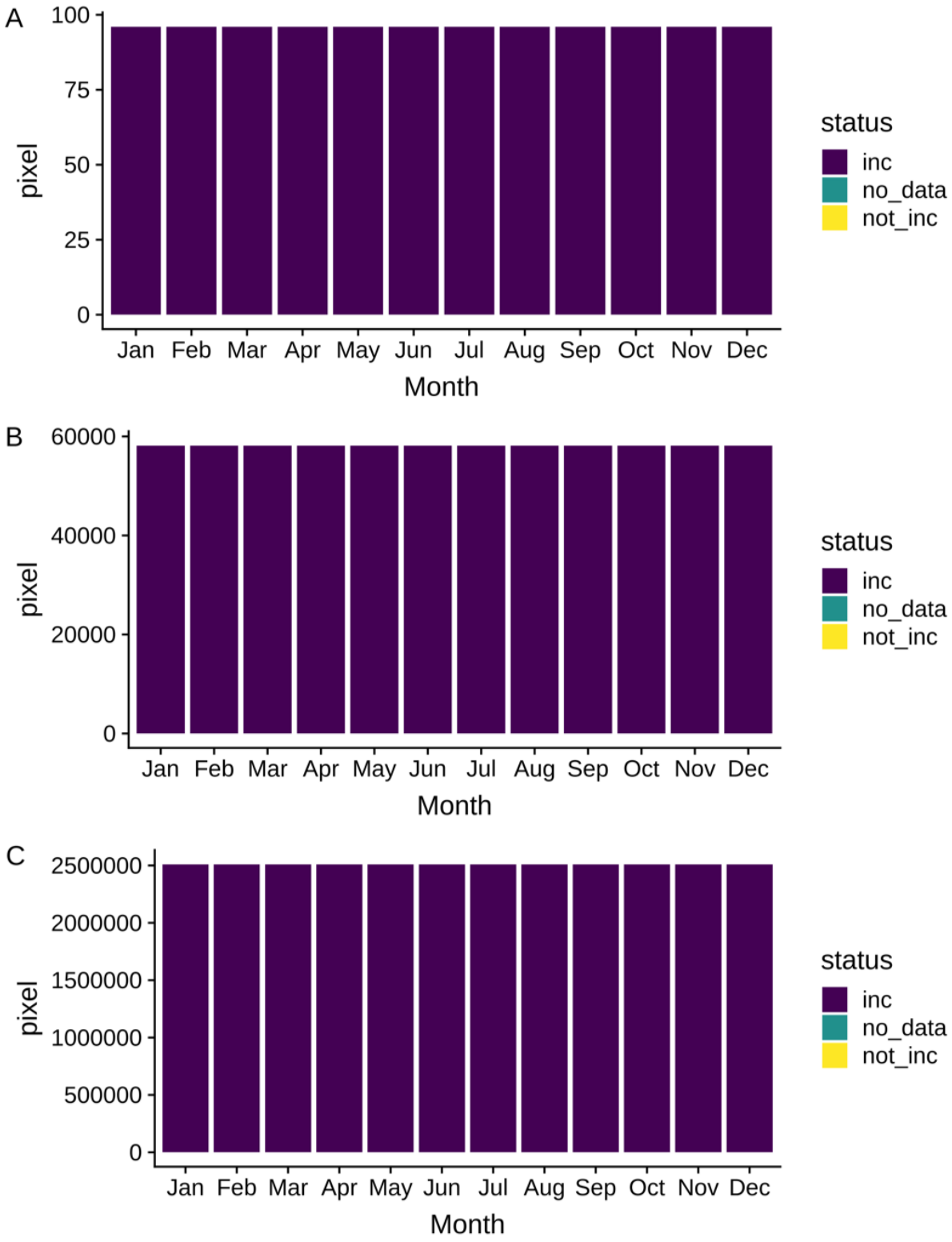

Figure B-9: Data availability of high, medium and low sensitivity Enhanced Vegetation Index pixels. Bar plots showing data availability for high (A; 80-100), medium (B; 40-60) and low (C; 0-20) sensitivity EVI pixels. To be included within the sensitivity analyses for a particular month, pixels were required to have a minimum of 4 years of month specific of data across the 2000-2013 time series, i.e. data for July over 4 or more years. Pixels with 4 or more years of data were included in analyses (inc, dark blue), pixels with less than 4 years of data were not included (not_inc, yellow) and some pixels had no data at all (no_data, turquoise). All pixels had full data availability for EVI. I also found this to be the case for all climate variables used in both the PSI and VSI. All pixels within each sensitivity bracket were extracted to determine data availability.

Table B-1: Number of locations used in spectral analysis for each index. Number of locations from 150 randomly selected pixels with complete time series which could be included in spectral analysis for each variable and index.

Variable	PSI	VSI
Primary productivity	43	105
Temperature	147	141
Radiation	77	141
Wind/Precipitation	78	141

Table B-2: Model fit parameters for each PSI BRT model. Parameters for the best fitting model for each PSI biome in the BRT analysis.

Province	Biome	Learning rate	Tree complexity	Minimum cross-validation error	Number of trees
ALSK	Coastal	0.001	20	37.6	1015
ARAB	Coastal	5e-04	10	26.58	2133
AUSE	Coastal	5e-04	4	18.33	1001
AUSW	Coastal	5e-04	6	16.37	1777
BENG	Coastal	5e-04	20	13.35	1356
BRAZ	Coastal	5e-04	6	15.26	1001
CAMR	Coastal	5e-04	10	20.96	1003
CCAL	Coastal	0.001	20	10.26	2926
CHIL	Coastal	5e-04	10	26.45	1456
CHIN	Coastal	5e-04	20	57.17	1000
CNRY	Coastal	5e-04	10	18.31	1000
EAFR	Coastal	0.001	20	14.56	1028
FKLD	Coastal	5e-04	20	31.52	4488
GUIA	Coastal	5e-04	6	38.09	1095
GUIN	Coastal	5e-04	4	119.71	1955
INDE	Coastal	5e-04	10	47	1646
INDW	Coastal	5e-04	6	32.96	1263
NECS	Coastal	0.001	20	44.04	1144
NEWZ	Coastal	5e-04	20	17.9	1490
NWCS	Coastal	0.001	20	19.83	1018
REDS	Coastal	5e-04	6	47.15	1020
SUND	Coastal	5e-04	4	30.25	1022
ANTA	Polar	0.005	20	109.51	7503
APLR	Polar	0.01	20	229.57	4300
ARCT	Polar	0.001	20	59.4	9917
BERS	Polar	5e-04	20	62.44	9740

BPLR	Polar	0.01	20	111.52	8403
SARC	Polar	5e-04	20	57.33	7656
ARCH	Trades	0.001	10	15.64	2684
CARB	Trades	0.001	20	20.49	1201
ETRA	Trades	5e-04	20	39.18	1833
ISSG	Trades	5e-04	20	8.74	9978
MONS	Trades	0.001	20	11.51	3399
NATR	Trades	0.001	10	16.73	1890
NPTG	Trades	0.005	20	8.59	2179
PEQD	Trades	5e-04	20	16.2	6372
PNEC	Trades	5e-04	20	11.44	4147
SATL	Trades	5e-04	20	12.94	9992
WARM	Trades	0.001	20	8.92	1836
WTRA	Trades	5e-04	20	27.8	1132
GFST	Westerlies	5e-04	6	10.53	1000
KURO	Westerlies	0.001	20	17.17	1031
MEDI	Westerlies	5e-04	20	22.57	4643
NADR	Westerlies	0.005	10	18.82	1011
NASE	Westerlies	5e-04	20	8.25	4902
NASW	Westerlies	5e-04	20	7.94	6149
NPPF	Westerlies	0.005	20	14.49	1180
NPSW	Westerlies	0.005	20	8.53	3147
PSAE	Westerlies	5e-04	10	37.16	3840
PSAW	Westerlies	5e-04	20	49.49	1524
SANT	Westerlies	0.001	20	40.07	9979
SPSG	Westerlies	0.005	20	10.57	4059
SSTC	Westerlies	5e-04	20	11.09	10000
TASM	Westerlies	5e-04	20	8.46	2079

Table B-3: Model fit parameters for each VSI BRT model. Parameters for the best fitting model for each VSI biome in the BRT analysis.

Province	Biome	Learning rate	Tree complexity	Minimum cross-validation error	Number of trees
AF01	Afrotropic	0.005	20	33.28	1108
AF02	Afrotropic	5e-04	20	12.18	7071
AF07	Afrotropic	0.005	20	14.05	8684
AF09	Afrotropic	0.005	20	10.67	1147
AF10	Afrotropic	0.005	20	10.2	1356
AF12	Afrotropic	5e-04	10	12.31	9165
AF13	Afrotropic	0.005	20	11.44	3251
AF14	Afrotropic	0.001	10	38.96	2377
AN11	Antarctica	0.001	6	101.92	1010
AU01	Australasia	0.005	10	51.31	1030
AU02	Australasia	0.001	20	15.61	1692
AU04	Australasia	5e-04	20	18.73	6919
AU07	Australasia	0.005	20	18.17	3889
AU08	Australasia	0.001	20	7.95	9971
AU10	Australasia	0.001	20	56.78	1433
AU12	Australasia	0.005	20	8.74	1696
AU13	Australasia	0.01	20	8.85	4813
AU14	Australasia	0.001	6	53.03	1004
IN01	Indomalayan	5e-04	20	34.22	9865
IN02	Indomalayan	5e-04	20	24.13	9994
IN03	Indomalayan	0.001	20	17.75	1439
IN04	Indomalayan	0.005	6	43.18	1001
IN05	Indomalayan	5e-04	4	105.72	3745
IN07	Indomalayan	0.001	4	18.86	1439
IN09	Indomalayan	5e-04	10	12.52	4785
IN13	Indomalayan	5e-04	20	16.07	10000
IN14	Indomalayan	5e-04	10	40	4316
NA99	Rock & Ice	0.001	4	183.92	1002
NE02	Nearctic	0.001	10	9.79	2774
NE03	Nearctic	0.001	10	10.89	5893
NE04	Nearctic	5e-04	20	24.32	9990
NE05	Nearctic	0.001	20	64.97	2968
NE06	Nearctic	0.005	20	64.99	2062
NE07	Nearctic	0.005	10	9.42	1017
NE08	Nearctic	0.001	20	18.82	9987
NE11	Nearctic	0.001	20	132.46	9997

NE12	Nearctic	5e-04	20	9.85	7806
NE13	Nearctic	0.01	20	16	1161
NO01	Neotropic	0.005	20	33.75	1383
NO02	Neotropic	0.001	20	15.86	9949
NO03	Neotropic	5e-04	20	18.5	6187
NO04	Neotropic	0.001	6	98.86	4891
NO07	Neotropic	0.001	20	12.81	10000
NO08	Neotropic	0.01	20	16.41	1422
NO09	Neotropic	5e-04	20	11.99	6490
NO10	Neotropic	0.001	20	41.16	2526
NO12	Neotropic	5e-04	20	11.54	7011
NO13	Neotropic	5e-04	20	17.39	9980
NO14	Neotropic	0.001	6	26.94	3805
OC01	Oceania	5e-04	10	30.51	1954
PA01	Palearctic	5e-04	20	28.85	6078
PA04	Palearctic	0.005	20	30.67	2312
PA05	Palearctic	5e-04	20	62.11	9235
PA06	Palearctic	0.01	20	61.56	1909
PA08	Palearctic	0.01	20	26.97	1188
PA09	Palearctic	5e-04	10	33.63	9875
PA10	Palearctic	0.001	20	67.57	4709
PA11	Palearctic	0.005	20	111.45	7697
PA12	Palearctic	0.005	20	16.37	1894
PA13	Palearctic	0.01	20	26.66	3413

Table B-4: Quadratic linear model output for median sensitivity against latitude with realm fitted as an interaction for the Northern hemisphere.

	Estimate	**Standard Error**	**t-value**	***P***
(Intercept)	17.034	0.837	20.341	0.000
Latitude_F	-0.16	0.047	-3.385	0.001
RealmTerrestrial	0.48	1.191	0.403	0.687
I(Latitude_F^2)	0.003	0.001	4.643	0.000
Latitude_F:RealmTerrestrial	0.061	0.068	0.896	0.372
RealmTerrestrial:I(Latitude_F^2)	-0.001	0.001	-0.863	0.389

Table B-5: Quadratic linear model output for the 95% range of sensitivities against latitude with realm fitted as an interaction for the Northern hemisphere.

	Estimate	Standard Error	t-value	*P*
(Intercept)	20.681	0.941	21.987	0.000
Latitude_F	-0.6	0.053	-11.325	0.000
RealmTerrestrial	3.566	1.338	2.665	0.008
I(Latitude_F^2)	0.012	0.001	19.771	0.000
Latitude_F:RealmTerrestrial	0.189	0.076	2.473	0.014
RealmTerrestrial:I(Latitude_F^2)	-0.003	0.001	-3.501	0.001

Table B-6: Quadratic linear model output for median sensitivity against latitude with realm fitted as an interaction for the Southern hemisphere.

	Estimate	Standard Error	t-value	*P*
(Intercept)	15.587	0.535	29.136	0.000
Latitude_F	0.117	0.043	2.693	0.008
RealmTerrestrial	4.169	0.757	5.511	0.000
I(Latitude_F^2)	0.003	0.001	4.335	0.000
Latitude_F:RealmTerrestrial	0.25	0.061	4.086	0.000
RealmTerrestrial:I(Latitude_F^2)	0.004	0.001	3.413	0.001

Table B-7: Quadratic linear model output for the 95% range of sensitivities against latitude with realm fitted as an interaction for the Southern hemisphere.

	Estimate	Standard Error	t-value	*P*
(Intercept)	24.212	1.234	19.624	0.000
Latitude_F	0.99	0.1	9.918	0.000
RealmTerrestrial	2.979	1.745	1.708	0.091
I(Latitude_F^2)	0.019	0.002	11.288	0.000
Latitude_F:RealmTerrestrial	0.103	0.141	0.73	0.467
RealmTerrestrial:I(Latitude_F^2)	0.006	0.002	2.645	0.009

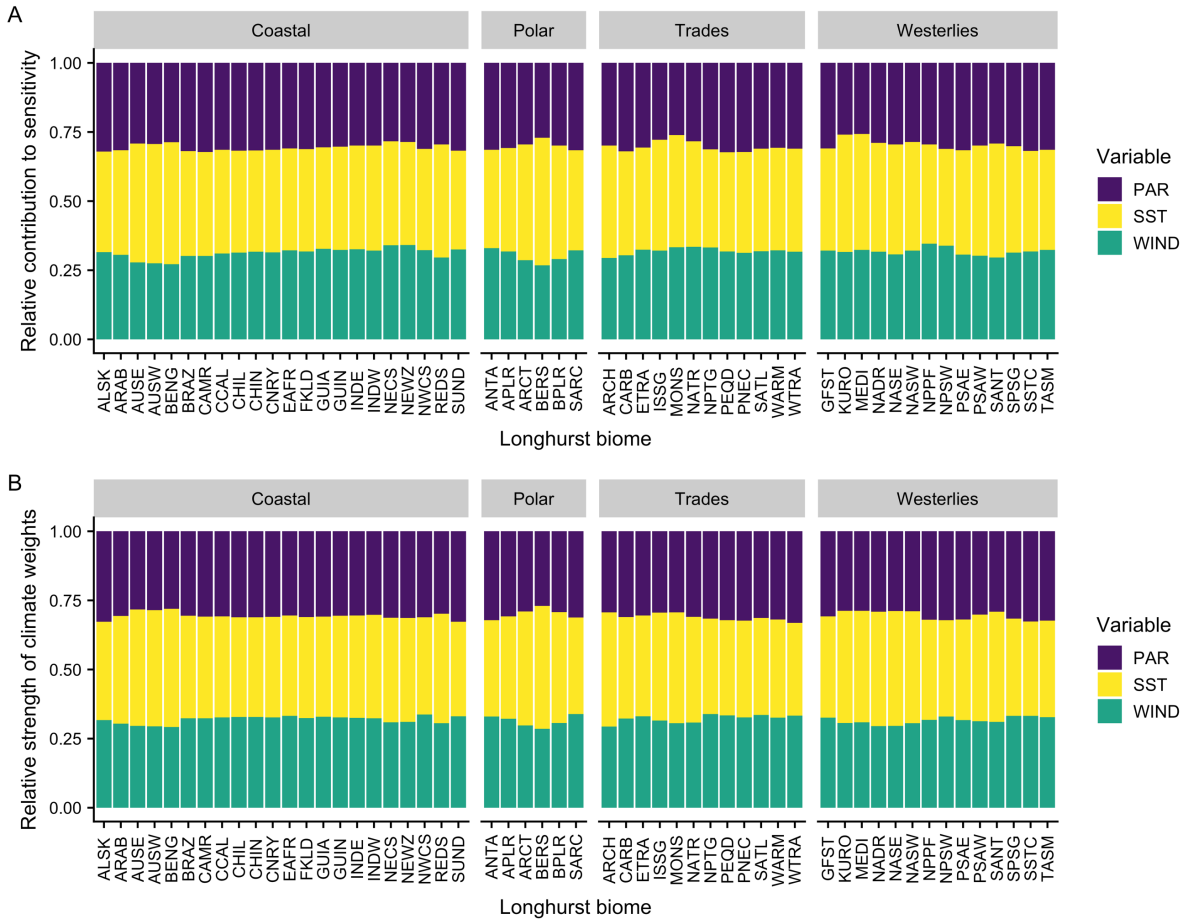

Figure B-10: Regional climatic driver influence and weights for the marine PSI. (A) The contribution of each climate variable to overall sensitivity, calculated as the ratio of Chl-a:climate variable variance multiplied by the variable's respective climate weight (climate variable-Chl-a regression coefficient), averaged per biome (plot corresponds to Figure 3.10). (B) Relative strength of the climate weight for each variable averaged per biome (plot corresponds to Figure B-7). The bars have been normalised to total 1.

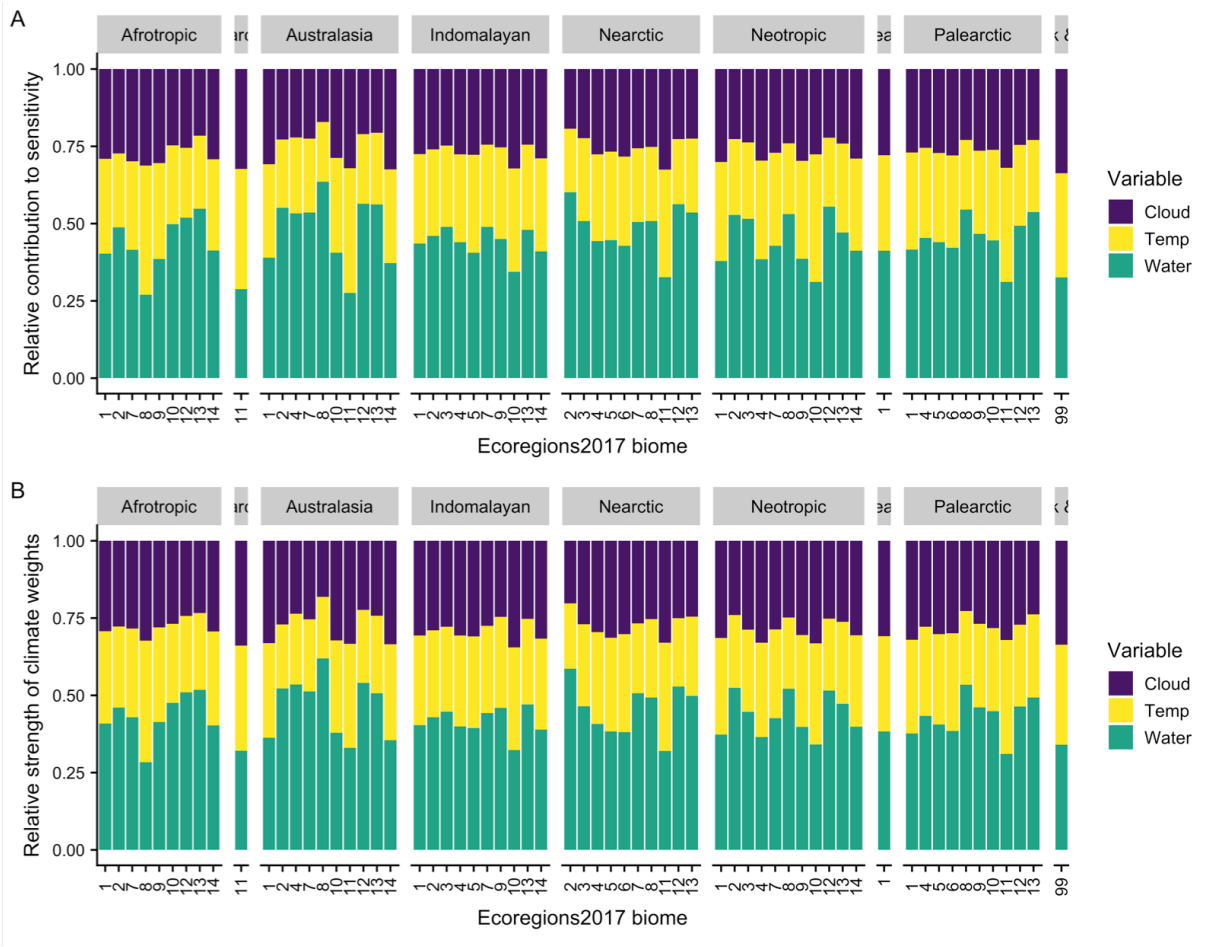

Figure B-11: Regional climatic driver influence and weights for the terrestrial VSI. (A) The contribution of each climate variable to overall sensitivity, calculated as the ratio of EVI:climate variable variance multiplied by the variable's respective climate weight (climate variable-EVI regression coefficient), averaged per biome (plot corresponds to Figure 3.10). (B) Relative strength of the climate weight for each variable averaged per biome (plot corresponds to Figure B-7). The bars have been normalised to total 1. Biomes in the VSI with only one province are from left to right, Antarctica, Oceania and Rock and Ice.

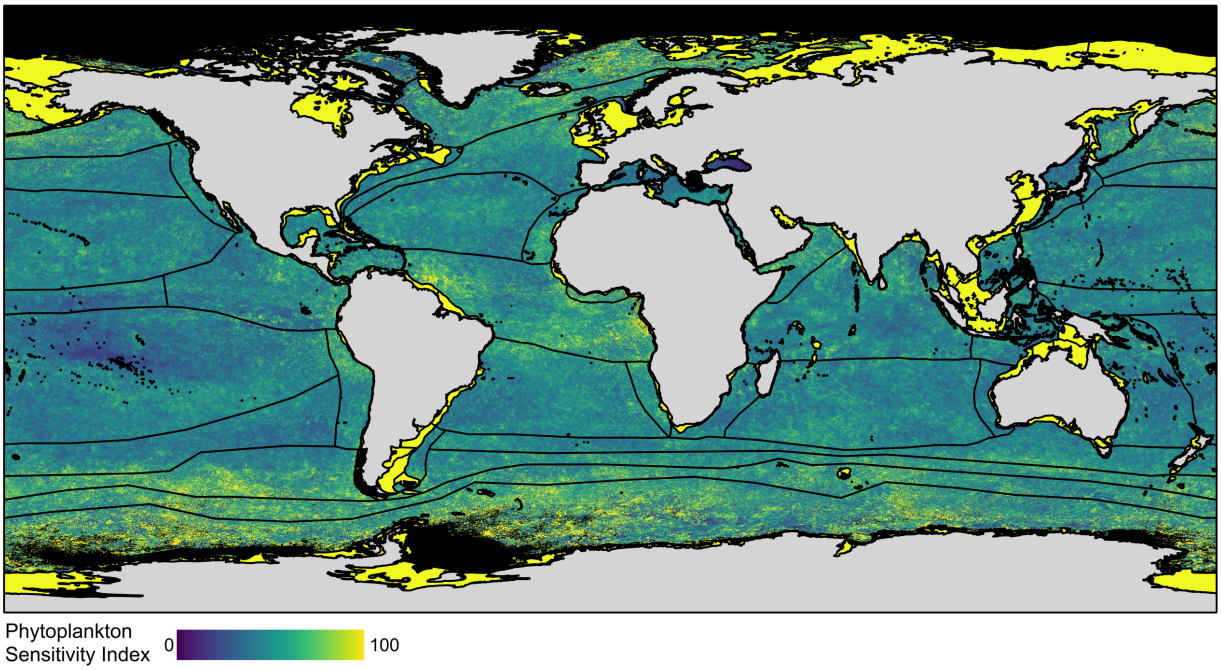

Figure B-12: Pelagic Provinces of the World (PPOW). The Pelagic Provinces of the World (PPOW) regionalisation (black lines) overlain on the Phytoplankton Sensitivity Index. Areas shaded in yellow are not covered by the PPOW.

Appendix C Chapter 4 BioTIME Metadata

Table C-1: Metadata for BioTIME datasets used in analyses. References corresponding to the 'Ref' column follow the table.

Realm	ID	Biome	Taxa	Title	No. species	No. samples	Summary methods	Ref.
Marine	45	Tropical seas	Fish	MCR LTER Coral Reef Long-term Population and Community Dynamics Fishes	338	1105	Transects	1, 2
Marine	71	Polar ecoregions	Marine plants	Phytoplankton from the White Sea. Barents Sea. Norwegian Sea and Arctic Basin 1993-2003	412	3250	Stations	3
Marine	72	Polar ecoregions	Marine invertebrates	White Sea Plankton	107	7569	Various	4
Marine	77	Temperate shelf and seas ecoregions	Birds	MEDITS Seabird surveys 1999 - 2000 - 2002	16	703	Transects	5, 6
Marine	78	Temperate shelf and seas ecoregions	Benthos	IOW Macrozoobenthos monitoring Baltic Sea (1980-2005) (EurOBIS)	212	19	Stations	7
Marine	108	Multiple ecoregions	Birds	Seabirds of the Southern and South Indian Ocean (Australian Antarctic Data Centre)	123	59928	Seabird Observations	8
Marine	112	Multiple ecoregions	Fish	NOAA Southeast Fishery Science Center (SEFSC) Commercial Pelagic Observer Program (POP) Data (SEFSC_POP)	540	136554	Stations	9
Marine	117	Temperate shelf and seas ecoregions	Marine invertebrates	South Western Pacific Regional OBIS Data Asteroid Subset (South Western Pacific OBIS)	156	1394	Transects	10
Marine	119	Temperate shelf and seas ecoregions	Fish	DFO Maritimes Research Vessel Trawl Surveys Fish Observations (OBIS Canada)	231	13945	Transects	11
Marine	121	Tropical coral	Fish	CRED Rapid Ecological Assessments of Fish Belt Transect Surveys and Fish Stationary Point Count Surveys in the Pacific Ocean 2000-2010 (OBIS-USA)	148	11408	Transects	12

Realm	ID	Biome	Taxa	Title	No. species	No. samples	Summary methods	Ref.
Marine	123	Temperate shelf and seas ecoregions	Fish	Maine Department of Marine Resources Inshore Trawl Survey 2000?2009 (OBIS-USA)	144	1750	Transects	13
Marine	125	Temperate shelf and seas ecoregions	Fish	MARMAP Chevron Trap Survey 1990-2009 (OBIS-USA)	101	1205	Chevron traps	14
Marine	142	Multiple ecoregions	Fish	Pelagic and Demersal Fish Database II. REVIZEE South Area (WSAOBIS)	189	276	Traps and longlines	15-17
Marine	143	Temperate shelf and seas ecoregions	Marine invertebrates	COPEPODA-ESPOBIS Data Base IMO-UdeC	106	60	Transects	18,19
Marine	152	Temperate shelf and seas ecoregions	Marine invertebrates	CMarZ (Census of Marine Zooplankton)-Asia Database	163	309	Stations	20
Marine	163	Temperate shelf and seas ecoregions	Benthos	North Pacific Groundfish Observer (North Pacific Research Board)	355	1827	Transects	21
Marine	169	Temperate shelf and seas ecoregions	All	CalCOFI and NMFS Seabird and Marine Mammal Observation Data. 1987-2006 (SEAMAP)	185	56832	Stations	22-25
Marine	171	Multiple ecoregions	Mammals	Bahamas Marine Mammal Research Organisation Opportunistic Sightings (SEAMAP)	28	2362	Sightings	26
Marine	172	Temperate shelf and seas ecoregions	All	POPA cetacean. seabird. and sea turtle sightings in the Azores area 1998-2009 (OBIS SEAMAP)	47	34883	Sightings	27-30
Marine	176	Temperate shelf and seas ecoregions	Marine invertebrates	Atlantic Zone Monitoring Program Maritimes Region (AZMP) plankton datasets. In Fisheries and Oceans Canada - BioChem archive (OBIS Canada)	320	1763	Stations	31
Marine	182	Temperate shelf and seas ecoregions	All	Snow crab research trawl survey database (Southern Gulf of St. Lawrence. Gulf region. Canada) from 1988 to 2010 (OBIS Canada)	33	5777	Bottom trawl	32

Realm	ID	Biome	Taxa	Title	No. species	No. samples	Summary methods	Ref.
Marine	183	Temperate shelf and seas ecoregions	Marine invertebrates	DFO Maritimes Research Vessel Trawl Surveys Invertebrate Observations (OBIS Canada)	16	4475	Stations	33
Marine	189	Tropical seas	Fish	St. John. USVI Fish Assessment and Monitoring Data (2002 - Present) (NOAA-CCMA)	254	1510	Stations	34
Marine	190	Tropical seas	Fish	St. Croix. USVI Fish Assessment and Monitoring Data (2002 - Present) (NOAA-CCMA)	247	2000	Traps	35
Marine	199	Tropical seas	Fish	Taiwan bottom trawl survey	631	48	Bottom trawl	36
Marine	204	Temperate shelf and seas ecoregions	Benthos	MACROBEL Long term trends in the macrobenthos of the Belgian Continental Shelf	344	1049	Grab	37
Marine	213	Temperate shelf and seas ecoregions	Benthos	Northeast Fisheries Science Center Bottom Trawl Survey Data (OBIS-USA)	1023	35644	Bottom trawl	38
Marine	271	Temperate shelf and seas ecoregions	Fish	Santa Barbara Coastal LTER	62	42	Transects	39
Marine	272	Temperate shelf and seas ecoregions	Marine invertebrates	Santa Barbara Coastal LTER	36	50	Quadrats	40
Marine	273	Temperate shelf and seas ecoregions	Marine invertebrates	Santa Barbara Coastal LTER	27	51	Transects	41
Marine	287	Temperate shelf and seas ecoregions	Fish	Maine Department of Marine Resources Inshore Trawl Survey 2000?2009 (OBIS-USA)	82	493	Transects	42
Marine	288	Temperate shelf and seas ecoregions	Fish	DFO Maritimes Research Vessel Trawl Surveys Fish Observations (OBIS Canada)	195	6774	Transects	43
Marine	295	Temperate shelf and seas ecoregions	Fish	Systematic global assessment of reef fish communities by the Reef Life Survey program	450	1078	Nets?	44

Realm	ID	Biome	Taxa	Title	No. species	No. samples	Summary methods	Ref.
Marine	296	Temperate shelf and seas ecoregions	Marine invertebrates	Systematic global assessment of reef fish communities by the Reef Life Survey program	412	1077	Nets?	45
Marine	297	Tropical coral	Marine invertebrates	MCR LTERCoral Reef Long-term Population and Community Dynamics Other Benthic Invertebrates. ongoing since 2005	13	1825	Quadrats	46
Marine	349	Temperate shelf and seas ecoregions	Benthos	St. M polychaete species time-series	141	89	Grabs	47,48
Marine	359	Temperate shelf and seas ecoregions	Fish	SBC LTER Reef Kelp Forest Community Dynamics Fish abundance	61	487	counts	49
Marine	365	Temperate shelf and seas ecoregions	Fish	Hahei marine dataset (1997-2002)	44	1477	transects	50
Marine	374	Temperate shelf and seas ecoregions	Birds	Monitoring site 1000 Shorebird Survey	70	13830	Pitfall traps	51
Marine	425	Temperate shelf and seas ecoregions	Benthos	Faunal communities and habitat characteristics of the Big Bend seagrass meadows 2009–2010	319	169	Tows	52
Marine	428	Temperate shelf and seas ecoregions	Fish	Long term monitoring of fish abundances from coastal SKagerrak	59	10725	Seine nets	53-56
Marine	435	Polar ecoregions	Marine invertebrates	Zooplankton collected with a 2-m 700-um net towed from surface to 120 m aboard Palmer Station Antarctica LTER annual cruises off the western antarctic peninsula 2009 - present	40	300	Tows	57
Marine	505	Temperate shelf and seas ecoregions	All	Fish and marine invertebrates from the Israeli Eastern Mediterranean sea 1990-4, 2000, 2008-2012	275	694	Trawl	58
Terrestrial	60	Tropical and subtropical moist broadleaf forests	Terrestrial plants	Forest Census Plot on Barro Colorado Island	325	8	Counts within defined area	59-64

Realm	ID	Biome	Taxa	Title	No. species	No. samples	Summary methods	Ref.
Terrestrial	67	Deserts and xeric shrublands	Birds	Animal Demography Unit - Coordinated Waterbird Counts (CWAC) (AfrOBIS)	68	417	Counts within defined area	65
Terrestrial	194	Temperate coniferous forest	Terrestrial invertebrates	Spatial and temporal distribution and abundance of moths in the Andrews Experimental Forest. 1994 to 2004	578	254	Transects	66
Terrestrial	214	Temperate coniferous forest	Terrestrial plants	Long-term growth mortality and regeneration of trees in permanent vegetation plots in the Pacific Northwest 1910 to present	39	14565	Plots	67
Terrestrial	217	Multiple ecoregions	Birds	Landbird Monitoring Program (UMT-LBMP)	268	43839	Point counts	68
Terrestrial	221	Boreal forests/Taiga	Terrestrial plants	Vegetation Plots of the Bonanza Creek LTER Control Plots Species Count (1975 - 2004)	52	195	Plots	69
Terrestrial	240	Deserts and xeric shrublands	Terrestrial plants	Pinon-Juniper (Core Site) Quadrat Data for the Net Primary Production Study at the Sevilleta National Wildlife Refuge New Mexico (2003-present)	167	2882	Habitats	70
Terrestrial	242	Temperate broadleaf and mixed forests	Terrestrial plants	Lac Croche understory vegetation data set (1998 to 2006)	12	298	Plots	71
Terrestrial	255	Temperate broadleaf and mixed forests	Terrestrial plants	Multi-decade. spatially explicit population studies of canopy dynamics in Michigan old-growth forests	22	508	Plots	72
Terrestrial	294	Tropical and subtropical moist broadleaf forests	Terrestrial invertebrates	Tam Dao Butterfly communities	277	45	Traps	73,74
Terrestrial	300	Temperate broadleaf and mixed forests	Terrestrial invertebrates	Insect Populations via Sticky Traps at KBS-LTER (Kellogg Biological Station. MI)	21	5888	Stations	75
Terrestrial	301	Temperate grasslands, savannas and shrublands	Terrestrial invertebrates	Konza LTER grasshopper monitoring. Konza Prairie LTER. KS	51	38	Sites	76,77

Realm	ID	Biome	Taxa	Title	No. species	No. samples	Summary methods	Ref.
Terrestrial	307	Temperate broadleaf and mixed forests	Terrestrial plants	Kellogg LTER seed bank	83	405	Stations	78
Terrestrial	313	Temperate broadleaf and mixed forests	Terrestrial invertebrates	Successional Dynamics on a Resampled Chronosequence Core Old Field Grasshopper Sampling	61	1409	Sweepnet	79
Terrestrial	316	Deserts and xeric shrublands	Reptiles	Lizard pitfall trap data (LTER-II LTER-III)	21	2620	Pitfall traps for lizards	80
Terrestrial	317	Flooded grasslands and savannas	Terrestrial plants	Mangrove Forest Growth from the Shark River Slough Everglades National Park (FCE) South Florida from January 1995 to Present	4	33	Tree measurements in permanent plots	81
Terrestrial	321	Deserts and xeric shrublands	Mammals	Small Mammal Exclosure Study. Jornada LTER. SMES rodent trapping data	19	11757	traps	82
Terrestrial	324	Tropical and subtropical grasslands, savannas and shrublands	Terrestrial plants	Temporal evaluation of natural regeneration in a semi-deciduous forest in Pirenopolis. Goias. Brazil	60	65	16 2x2m plots sampled in 5 years	83
Terrestrial	325	Tropical and subtropical grasslands, savannas and shrublands	Terrestrial plants	Temporal evaluation of natural regeneration in a semi-deciduous forest in Pirenopolis. Goias. Brazil	91	79	16 5x5m plots sampled in 5 years	84
Terrestrial	326	Tropical and subtropical grasslands, savannas and shrublands	Terrestrial plants	Temporal evaluation of natural regeneration in a semi-deciduous forest in Pirenopolis. Goias. Brazil	140	32	16 5x5m plots sampled in 2 years	85
Terrestrial	327	Mediterranean forests, woodlands and scrubs	Mammals	Fray Jorge Small Mammals 1989-2005	12	171843	Traps	86
Terrestrial	340	Deserts and xeric shrublands	Terrestrial plants	Small Mammal Exclosure Study (SMES) Vegetation Data from the Chihuahuan Desert	93	128	Transect plots	87

Realm	ID	Biome	Taxa	Title	No. species	No. samples	Summary methods	Ref.
Terrestrial	348	Tropical and subtropical moist broadleaf forests	Mammals	Bats (Mammalia Chiroptera) in restinga in the municipality of Jaguaruna south of Santa Catarina Brazil.	13	16	nets	88
Terrestrial	352	Tropical and subtropical moist broadleaf forests	Terrestrial plants	Flooded forest plot sampling in Peru	98	120	Plots	89
Terrestrial	353	Tropical and subtropical moist broadleaf forests	Terrestrial plants	La Planada Forest Dynamics Plots	180	2	Plots	90
Terrestrial	357	Temperate grasslands, savannas and shrublands	Mammals	Small Mammal Trapping Webs on the Central Plains Experimental Range	10	506	censuses	91
Terrestrial	362	Tropical and subtropical grasslands, savannas and shrublands	Mammals	Plant and small-mammal responses to large-herbivore exclusion in an African savanna	18	11052	transects	92,93
Terrestrial	366	Deserts and xeric shrublands	Mammals	Small Mammal Exclosure Study (SMES)	24	342	Pitfall traps	94
Terrestrial	369	Temperate broadleaf and mixed forests	Terrestrial invertebrates	Monitoring site 1000 Alpine research - Surface wandering beetles	29	29	Quadrats / Cores	95
Terrestrial	372	Temperate broadleaf and mixed forests	Birds	Monitoring site 1000 Village survey - Bird survey data	219	1435	Permanent quadrats	96
Terrestrial	373	Temperate broadleaf and mixed forests	Mammals	Village survey Medium and large mammal survey data	25	18189	Transects	97
Terrestrial	375	Temperate coniferous forest	Terrestrial invertebrates	Surface of the earth wandering beetles survey data	424	4553	Infrared video cameras	98
Terrestrial	376	Temperate broadleaf and mixed forests	Birds	Monitoring site 1000 forest and grassland research - Bird survey data -1st phase	240	1122	Spot census	99
Terrestrial	377	Temperate broadleaf and mixed forests	Birds	Monitoring site 1000 forest and grassland research - Bird survey data -2nd phase	251	8735	Aggregated timed surveys	100

Realm	ID	Biome	Taxa	Title	No. species	No. samples	Summary methods	Ref.
Terrestrial	420	Tundra	Birds	Species composition and population fluctuations of alpine bird communities during 38 years in the Scandinavian mountain range	47	99	sites	101
Terrestrial	421	Temperate grasslands, savannas and shrublands	Terrestrial invertebrates	Boulder County Open Space butterfly diversity and abundance	58	314	Transect?	102
Terrestrial	422	Temperate coniferous forest	Terrestrial invertebrates	Monitoring site 1000 Alpine research - Butterfly Survey	43	23	Fixed Point	103
Terrestrial	423	Temperate coniferous forest	Terrestrial invertebrates	Monitoring site 1000 Alpine research - Butterfly Survey	46	26	Transects	104
Terrestrial	424	Temperate coniferous forest	Terrestrial invertebrates	Monitoring site 1000 Alpine research - Bumblebee Survey	7	36	Transects	105
Terrestrial	458	Temperate broadleaf and mixed forests	Terrestrial invertebrates	Beetles from the Bavarian Forest	179	176	Plots	106-108
Terrestrial	459	Temperate broadleaf and mixed forests	Birds	Birds from the Bavarian Forest	52	126	Plots	109-111
Terrestrial	460	Temperate broadleaf and mixed forests	Terrestrial plants	Fungi from the Bavarian Forest	110	181	Plots	112-114
Terrestrial	461	Temperate broadleaf and mixed forests	Terrestrial plants	Lichens (obj) from the Bavarian Forest	26	188	Plots	115-117
Terrestrial	462	Temperate broadleaf and mixed forests	Terrestrial plants	Lichens (soil) from the Bavarian Forest	7	43	Plots	118-120
Terrestrial	463	Temperate broadleaf and mixed forests	Terrestrial plants	Mosses (obj) from the Bavarian Forest	34	188	Plots	121-123
Terrestrial	464	Temperate broadleaf and mixed forests	Terrestrial plants	Mosses (soil) from the Bavarian Forest	41	245	Plots	124-126
Terrestrial	465	Temperate broadleaf and mixed forests	Terrestrial plants	Plants from the Bavarian Forest	52	260	Plots	127-129

Realm	ID	Biome	Taxa	Title	No. species	No. samples	Summary methods	Ref.
Terrestrial	510	Temperate broadleaf and mixed forests	Terrestrial invertebrates	Butterfly fauna in Mount Gariwang-san Korea	105	55	Transects	130
Terrestrial	516	Tropical and Subtropical Moist Broadleaf Forests	Mammals	A large-scale fragmentation experiment for Neotropical bats	45	225	Mist-nets	130-135

References for BioTIME datasets

1 Brooks, A.J. "MCR LTER: Coral Reef: Long-term Population and Community Dynamics: Fishes". Moorea Coral Reef. Available at: http://mcr.lternet.edu/cgi-bin/showDataset.cgi?docid=knb-lter-mcr.6, accessed 2012.

2 Brooks, A.J. (2016) Moorea Coral Reef LTER: Coral Reef: Long-term Population and Community Dynamics: Fishes. Available at: knb-lter-mcr.6.54 doi:10.6073/pasta/d688610e536f54885a3c59d287f6c4c3, accessed 2016.

3 Ratkova, T. N. "Phytoplankton of the White Sea, Barents Sea, Amundsen & Nansen Basins". Institute of Oceanology, Academy of Sciences of Russia, Moscow, Russia; Arctic Ocean Diversity, University of Alaska Fairbanks, Fairbanks. Available at: http://www.arcodiv.org/Database/Plankton_datasets, accessed 2012.

4 Kosobokova, K. "White Sea Zooplankton". Shirshov Institute of Oceanology, Moscow; Arctic Ocean Diversity, University of Alaska Fairbanks, Fairbanks. Available at: http://www.iobis.org/mapper/?dataset=4488, accessed 2012.

5 "MEDITS seabird surveys 1999 / 2000 / 2002" (2011). Mediterranean Institute for Advanced Studies (IMEDEA) In: OBIS-SEAMAP. Available at: http://www.emodnet-biology.eu/component/imis/?module=dataset&dasid=1979, accessed 2012.

6 Louzao, M., Hyrenbach, K.D., Arcos, J.M., AbellÛ, P., Sola, L.G. & Oro, D. (2006) Oceanographic habitat of an endangered Mediterranean procellariiform: implications for marine protected areas. Ecological Applications, 16, 1683ñ1695.

7 Zettler, M.L. (2005) Macrozoobenthos baltic sea (1980-2005) as part of the IOW-Monitoring. Institut f¸r Ostseeforschung Warnem¸nde, Germany. Available at: http://www.iobis.org/mapper/?dataset=2289, accessed 2012.

8 Woehler, E. "Seabirds of the Southern and South Indian Ocean - Australian Antarctic Data Centre". Available at: http://www.iobis.org, accessed 2012.

9 "South Western Pacific Regional OBIS Data Asteroid Subset", NIWA (National Institute of Water and Atmospheric Research - New Zealand) MBIS (Marine Biodata Information System) accessed through South Western Pacific OBIS. Available at: http://www.iobis.org/mapper/?dataset=219, accessed 2012.

10 "South TX Outer Continental Shelf and MI, AL, and FL Outer Continental Shelf benthic organism sampling 1974-1978". US National Oceanographic Data Center, Silver Spring, Maryland, USA (2011). Available at http://www.usgs.gov/obis-usa/data_search_and_access/participants.html, accessed 2012.

11 Clark, D. & Branton, B. (2007) DFO Maritimes Research Vessel Trawl Surveys, OBIS Canada Digital Collections. Bedford Institute of Oceanography, Dartmouth, Nova Scotia, Canada, OBIS Canada,

12 "CRED Towed-Diver Fish Biomass Surveys in the Pacific Ocean 2000-2010". (2011) Coral Reef Ecosystem Division (CRED), Pacific Island Fisheries Sciences Center, National Marine Fisheries Service. Available at: http://www.iobis.org/mapper/?dataset=1581, accessed 2012.

13 Sherman, S. (2010) "Maine Department of Marine Resources Inshore Trawl Survey, 2000 ñ 2009". Maine Department of Marine Resources, Maine. Available at: http://www.usgs.gov/obis-usa/data_search_and_access/datasets.html, accessed 2012.

14 Reichert, M. (2009) "MARMAP Chevron Trap Survey 1990-2009". SCDNR/NOAA MARMAP Program, SCDNR MARMAP Aggregate Data Surveys, The Marine Resources Monitoring, Assessment, and Prediction (MARMAP) Program, Marine Resources Research Institute, South Carolina Department of Natural Resources U.S.A.. Available at: http://www.usgs.gov/obis-usa/data_search_and_access/participants.html, accessed 2012.

15 "REVIZEE South Score / Pelagic and Demersal Fish Database II". Available at: http://www.iobis.org/mapper/?dataset=105, accessed 2012.

16 Bernardes, R.¡. (2005) Peixes da Zona EconÙmica Exclusiva da regi„o sudeste-sul do Brasil: levantamento com armadilhas, pargueiras e rede de arrasto de fundo. Edusp.

17 Bernardes, R.A., Rodrigues, A.R., Rossi-Wongtschowski, C.L., dos Santos, A.P., Vieira, R.C. & Wahrlich, R. (2005) ProspecÁ„o pesqueira de recursos demersais com armadilhas e pargueiras na Zona EconÙmica Exclusiva da Regi„o Sudeste-Sul do Brasil. Instituto Oceanogr·fico.

18 Escribano, R., ManrÌquez, K. & Godoy, F. (2006) "Copepoda-COPAS Center (COPAS_CPD1) - Planktonic copepods from the Chilean Humboldt Current System - Eastern South Pacific Regional Node of OBIS (ESPOBIS)". Available at: http://www.iobis.org, accessed 2012.

19 Hidalgo, P., Escribano, R., Vergara, O., Jorquera, E., Donoso, K. & Mendoza, P. (2010) Patterns of copepod diversity in the Chilean coastal upwelling system. Deep Sea Research Part II: Topical Studies in Oceanography, 57, 2089ñ2097.

20 "CMarZ (Census of Marine Zooplankton)-Asia Database". Accessed through OBIS-SCAR-MarBIN. Available at: http://www.iobis.org/mapper/?dataset=1500, accessed 2012.

21 "The Observer Program database", accessed through the OBIS-USA North Pacific Groundfish Observer (North Pacific Research Board). Available at: http://www.iobis.org, accessed 2012.

22 Jahncke, J. & Rintoul, C. (2006) "CalCOFI and NMFS Seabird and Marine Mammal Observation Data, 1987-2006". California Cooperative Oceanic Fisheries Investigations (CalCOFI) and National Marine Fisheries Service (NMFS) cruises, 1987-2006 - OBIS SEAMAP. Available at: http://www.iobis.org, accessed 2012.

23 Rintoul, C., Schlagenhauf-Langabeer, B., Hyrenbach, K. D., Morgan, K. H. & Sydeman, W. J. (2006) Atlas of California Current Marine Birds and Mammals: Version 1. Unpublished report, PRBO Conservation Science, Petaluma, California.

24 Yen, P. P. W., Sydeman, W. J. & Hyrenbach, K. D. (2004) Marine bird and cetacean associations with bathymetric habitats and shallow-water topographies: Implications for trophic transfer and conservation. Journal of Marine Systems, 50, 79ñ99.

25 Yen, P. P. W., Sydeman, W. J., Bograd, S. J. & Hyrenbach, K. D. (2006) Spring-time distributions of migratory marine birds in the southern California Current: Oceanic eddy associations and coastal habitat hotspots over 17 years. Deep-Sea Research Part II: Topical Studies in Oceanography, 53, 399ñ418.

26 "Bahamas Marine Mammal Research Organisation Opportunistic Sightings - OBIS SEAMAP". Available at: http://www.iobis.org, accessed 2012.

27 "POPA cetacean, seabird, and sea turtle sightings in the Azores area 1998-2009 - OBIS SEAMAP". Available at: http://www.iobis.org/mapper/?dataset=4257, accessed 2012.

28 Amorim, P., Figueiredo, M., Machete, M., Morato, T., Martins, A. & Serr„o Santos, R. (2008) Spatial variability of seabird distribution associated with environmental factors: a case study of marine Important Bird Areas in the Azores. ICES Journal of Marine Science, 66, 29-40.

29 Machete, M. & Santos, R. (2007) Azores Fisheries Observer Program (POPA): a case study of the multidisciplinary use of observer data. Proceedings of the 5th International Fisheries Observer Conference, pp. 15-18.

30 Morato, T., Varkey, D.A., Damaso, C., Machete, M., Santos, M., Prieto, R., Santos, R.S. & Pitcher, T.J. (2008) Evidence of a seamount effect on aggregating visitors. Marine Ecology Progress Series, 357, 23-32.

31 Kennedy, M. & Spry, J. (2011) Atlantic Zone Monitoring Program Maritimes Region plankton datasets. Fisheries and Oceans Canada-BioChem archive. OBIS Canada, Bedford Institute of Oceanography, Dartmouth, Nova Scotia, Canada.

32 Wade, E. (2011) Snow crab research trawl survey database (Southern Gulf of St. Lawrence, Gulf region, Canada) from 1988 to 2010. OBIS Canada, Bedford Institute of Oceanography, Dartmouth, Nova Scotia, Canada,

33 Tremblay, J.M. & Branton, B. (2007) DFO Maritimes Research Vessel Trawl Surveys, OBIS Canada Digital Collections. Bedford Institute of Oceanography, Dartmouth, Nova Scotia, Canada, OBIS Canada.

34 "St. John, USVI Fish Assessment and Monitoring Data (2002 - Present)", (2007) Silver Spring, MD Publisher: NOAAs Ocean Service, National Centers for Coastal Ocean Science (NCCOS). National Oceanic and Atmospheric Association (NOAA)-National Ocean Service (NOS)-National Centers for Coastal Ocean Science (NCCOS)-Center for Coastal Monitoring and Assessment (CCMA)-Biogeography Team. Available at: http://www.iobis.org/mapper/?dataset=1672, accessed 2012.

35 "St. Croix, USVI Fish Assessment and Monitoring Data (2002 - Present)", (2007) Silver Spring, MD Publisher: NOAAs Ocean Service, National Centers for Coastal Ocean Science (NCCOS). National Oceanic and Atmospheric Association (NOAA)-National Ocean Service (NOS)-National Centers for Coastal Ocean Science (NCCOS)-Center for Coastal Monitoring and Assessment (CCMA)-Biogeography Team. Available at: http://www.iobis.org/mapper/?dataset=1673, accessed 2012.

36 Shao, K. T., Lin, J., Wu, C.-H., Yeh, H.-M. & Cheng, T.-Y. (2012) "A dataset from bottom trawl survey around Taiwan". Available at: http://www.iobis.org, accessed 2013.

37 Degraer, S., Wittoeck, J., Appeltans, W., Cooreman, K., Deprez, T., Hillewaert, H., Hostens, K., Mees, J., Vanden Berghe, E. & Vincx, M. (2006) ìMacrobel: Long term trends in the macrobenthos of the Belgian Continental Shelf.î Oostende, Belgium. Available at: http://www.emodnet-biology.eu/data-catalog?module=dataset&dasid=145, accessed 2013.

38 "Northeast Fisheries Science Center Bottom Trawl Survey Data (OBIS-USA)." (2005) NOAAís National Marine Fisheries Service (NMFS) Northeast Fisheries Science Center. Woods Hole, Massachusetts, USA. Available at: http://www.iobis.org/mapper/?dataset=1435, accessed 2013.

39 Reed, D. C. (2014a) ìSBC LTER: Reef: Kelp forest community dynamics: Abundance and size of giant kelp (Macrocystis pyrifera), ongoing since 2000î. Santa Barbara Coastal LTER. Available at: http://sbc.lternet.edu/cgi-bin/showDataset.cgi?docid=knb-lter-sbc.18, accessed 2016. doi:10.6073/pasta/d90872297e30026b263a119d4f5bca9f

40 Reed, D. C. (2014b) ìSBC LTER: Reef: Kelp forest community dynamics: Fish abundanceî. Santa Barbara Coastal LTER. Available at: http://sbc.lternet.edu/cgi-bin/showDataset.cgi?docid=knb-lter-sbc.17, accessed 2016. doi:10.6073/pasta/e37ed29111b2fddffc08355252b8b8c7.

41 Reed, D. C. (2014c) ìSBC LTER: Reef: Kelp forest community dynamics: Invertebrate and algal densityî. Santa Barbara Coastal LTER. Available at: http://sbc.lternet.edu/cgi-bin/showDataset.cgi?docid=knb-lter-sbc.19, accessed 2016. doi:10.6073/pasta/cd4cf864efecd69891dfe1d73b9ac9c3.

42 Sherman, S. (2010) "Maine Department of Marine Resources Inshore Trawl Survey, 2000 ñ 2009". Maine Department of Marine Resources, Maine. Available at: http://www.usgs.gov/obis-usa/data_search_and_access/datasets.html, accessed 2012.

43 Clark, D. & Branton, B. (2007) DFO Maritimes Research Vessel Trawl Surveys, OBIS Canada Digital Collections. Bedford Institute of Oceanography, Dartmouth, Nova Scotia, Canada, OBIS Canada,

44 Edgar, G. J. & Stuart-Smith, R. D. (2014) Systematic global assessment of reef fish communities by the Reef Life Survey program. Nature Scientific Data 1, 140007. doi:10.1038/sdata.2014.7.

45 Edgar, G. J. & Stuart-Smith, R. D. (2014) Systematic global assessment of reef fish communities by the Reef Life Survey program. Nature Scientific Data 1, 140007. doi:10.1038/sdata.2014.7.

46 Carpenter, R. (2015) ìMCR LTER: Coral Reef: Long-term Population and Community Dynamics: Other Benthic Invertebrates, ongoing since 2005î. Moorea Coral Reef LTER, knb-lter-mcr.7.28. Available at: doi:10.6073/pasta/8e7b3a0c7a8bf315739921861cc79d10, accessed 2016.

47 Laguionie-Marchais, C., Billett, D. S. M., Paterson, G. L. D., Ruhl, H. A., Soto, E. H., Smith, J. L. & Thatje, S. (2013) Inter-annual dynamics of abyssal polychaete communities in the North East Pacific and North East Atlantic-A family-level study. Deep-Sea Research Part I: Oceanographic Research Papers, 75, 175ñ186.

48 Laguionie-Marchais, C., Paterson, G. L. J., Bett, B. J., Smith, K. L. & Ruhl, H. A. (2016) Inter-annual species-level variations in an abyssal polychaete assemblage (Sta. M, NE Pacific, 4000 m). Progress in Oceanography, 140, 43ñ53.

49 Reed, D. C. (2014) ìSBC LTER: Reef: Kelp Forest Community Dynamics: Fish abundanceî. Santa Barbara Coastal LTER. Available at: doi:10.6073/pasta/e37ed29111b2fddffc08355252b8b8c7, accessed 2016.

50 Willis, T. ìHahei marine dataset (1997-2002), New Zealand fishî. Institute of Marine Sciences, University of Portsmouth. Accessed 2016.

51 Monitoring Site 1000 Project, Biodiversity Center, Ministry of Environment of Japan (2013) ìMonitoring site 1000 Shorebird Surveyî (ShorebirdsDatapackage2012.zip, downloaded from http://www.biodic.go.jp/moni1000/ findings/data/index.html). Accessed 2016.

52 Stallings, C. D., Mickle, A., Nelson, J. A., McManus, M. G. & Koenig, C. C. (2015) Faunal communities and habitat characteristics of the Big Bend seagrass meadows, 2009ñ2010. Ecology, 96, 304.

53 BarcelÛ, C., Ciannelli, L., Olsen, E.M., Johannessen, T. & Knutsen, H. (2016) Eight decades of sampling reveal a contemporary novel fish assemblage in coastal nursery habitats. Global change biology, 22, 1155-1167.

54 Olsen, E. M., Carlson, S. M., Gjøsaeter, J. & Stenseth, N. C. (2009) Nine decades of decreasing phenotypic variability in Atlantic cod. Ecology Letters, 12, 622ñ631. doi:10.1111/j.1461-0248.2009.01311.x

55 Rogers, L. A., Stige, L. C., Olsen, E. M., Knutsen, H., Chan, K.-S. & Stenseth, N. C. (2011) Climate and population density drive changes in cod body size throughout a century on the Norwegian coast. Proceedings of the National Academy of Sciences, 108(5), 1961ñ1966.

56 Stenseth, N. C., Bjørnstadf, O. N., Falck, W, Fromentin, J. M., Gjøsieter, J. & Gray, J. S. (1999) Dynamics of coastal cod populations: intra-and intercohort density

dependence and stochastic processes. Proceedings of the Royal Society of London B: Biological Sciences, 266(1429), 1645ñ1654.

57 Steinberg, D. (2017) Zooplankton collected with a 2-m, 700-um net towed from surface to 120 m, aboard Palmer Station Antarctica LTER annual cruises off the western antarctic peninsula, 2009 - 2016. Environmental Data Initiative. Available at: http://dx.doi.org/10.6073/pasta/fb658789188724be5f27c81a634647d5, accessed 2017.

58 Edelist, D., Rilov, G., Golani, D., Carlton, J.T. & Spanier, E. (2013) Restructuring the Sea: profound shifts in the world's most invaded marine ecosystem. Diversity and Distributions, 19, 69ñ77.

59 Condit, R., Lao, S., PÈrez, R., Dolins, S.B., Foster, R. & Hubbell, S. (2012) Dataset: Barro Colorado Forest Census Plot Data (Version 2012).

60 Condit, R. (1998) Tropical forest census plots: Methods and results from Barro Colorado Island, Panama and a Comparison with other plot. Springer Verlag and RG Landes Company, Berlin,

61 Condit, R., Ashton, P., Bunyavejchewin, S., Dattaraja, H., Davies, S., Esufali, S., Ewango, C., Foster, R., Gunatilleke, I. & Gunatilleke, C. (2006) The importance of demographic niches to tree diversity. Science, 313, 98-101.

62 Condit, R., Chisholm, R.A. & Hubbell, S.P. (2012) Thirty years of forest census at Barro Colorado and the importance of immigration in maintaining diversity. PloS one, 7, e49826.

63 Hubbell, S. P., Condit, R. & Foster, R. B. (2005) "Barro Colorado Forest Census Plot Data". Available at: https://ctfs.arnarb.harvard.edu/webatlas/datasets/bci, accessed 2012.

64 Condit, R., Pérez, R., Aguilar, S., Lao, S., Robin, F. & Hubbell, S. (2018) Tree species abundance through time in tropical forest census plots, Panama. DataONE Dash, Dataset, Available at: https://doi.org/10.15146/R3MM4V

65 "Animal Demography Unit - Coordinated Waterbird Counts (CWAC) - AfrOBIS". Available at http://www.iobis.org/, accessed 2012.

66 Jones, J. & Miller, J. "Spatial and temporal distribution and abundance of moths in the Andrews Experimental Forest, 1994 to 2008". H. J. Andrews Experimental Forest. Forest Science Data Bank, Corvallis. Available at: http://andrewsforest.oregonstate.edu/data/abstract.cfm?dbcode=SA015, accessed 2013.

67 Harmon, M. & Franklin, J. (2012) ìLong-term growth, mortality and regeneration of trees in permanent vegetation plots in the Pacific Northwest, 1910 to present.î Long-Term Ecological Research. Forest Science Data Bank, Corvallis. Available at: http://andrewsforest.oregonstate.edu/data/abstract.cfm?dbcode=TV010, accessed 2012.

68 USFS ìLandbird Monitoring Program (UMT-LBMP).î US Forest Service. Available at: http://www.avianknowledge.net/, accessed 2012.

69 Viereck, L.A., Van Cleve, K., Chapin, F.S., Ruess, R.W. & Hollingsworth, T.N. (2005) Vegetation Plots of the Bonanza Creek LTER Control Plots: Species Count (1975 - 2004). Environmental Data Initiative. Available at: http://dx.doi.org/10.6073/pasta/8dd0e1ac48e2f82b51adabfbd3c62ae2, accessed 2012.

70 Muldavin, E. ìPinon-Juniper (Core Site) Quadrat Data for the Net Primary Production Study at the Sevilleta National Wildlife Refuge, New Mexico (2003-Present).î Sevilleta Long Term Ecological Research Program. Available at: http://sev.lternet.edu/node/1718, accessed 2013.

71 Paquette, A., Laliberté, E., Bouchard, A., Blois, S. de, Legendre, P. & Brisson, J. (2007) Lac Croche understory vegetation data set (1998ñ2006). Ecology, 88, 3209. doi:10.1890/07-0513.1

72 Woods, K. D. (2009) Multi-decade, spatially explicit population studies of canopy dynamics in Michigan old-growth forests. Ecology, 90, 3587.

73 Bonebrake, T.C., Pickett, E.J., Tsang, T.P., Tak, C.Y., Vu, M.Q. & Van Vu, L. (2016) Warming threat compounds habitat degradation impacts on a tropical butterfly community in Vietnam. Global Ecology and Conservation, 8, 203-211.

74 Vu, L. V. (2009) Diversity and similarity of butterfly communities in five different habitat types at Tam Dao National Park, Vietnam. Journal of Zoology, 277, 15ñ22. doi:10.1111/j.1469-7998.2008.00498.x

75 Landis, D. & Gage, S. (2014) Insect Populations via Sticky Traps at KBS-LTER. Available at: http://lter.kbs.msu.edu/datatables/67, accessed 2016.

76 Joern, A. (2016) CGR02 Sweep Sampling of Grasshoppers on Konza Prairie LTER watersheds (1982-present). Environmental Data Initiative. Available at: http://dx.doi.org/10.6073/pasta/7060b2c244229a37e3bfc8c18f14ad02, accessed 2016.

77 Jonas, J.L. & Joern, A. (2007) Grasshopper (Orthoptera: Acrididae) communities respond to fire, bison grazing and weather in North American tallgrass prairie: a long-term study. Oecologia, 153, 699-711.

78 ìThe Main Cropping System Experiment (MCSE)î. KBS LTER, Kellogg Biological Station. Available at: http://lter.kbs.msu.edu/research/long-term-experiments/main-cropping-system-experiment/, accessed 2016.

79 Knops, J. & Tilman, D. Successional Dynamics on a Resampled Chronosequence - Experiment 014. Cedar Creek Ecosystem Science Reserve. Available at http://www.cedarcreek.umn.edu/research/data/dataset?ghe014, accessed 2016.

80 Lightfoot, D. ìSmall Mammal Exclosure Study (SMES)î. Sevilleta Long Term Ecological Research Program. Available at: http://sev.lternet.edu/content/small-mammal-exclosure-study-smes-0, accessed 2016.

81 Twilley, R., Rivera-Monroy, V. H. & Castaneda, E. (2005) ìMangrove Forest Growth from the Shark River Slough, Everglades National Park (FCE), South Florida from January 1995 to Presentî. Florida Coastal Everglades LTER. http://dx.doi.org/10.6073/pasta/bec6c029df692768f349106c69162df7. Available at: http://fcelter.fiu.edu/data/core/metadata/?datasetid=LT_PP_Rivera_002, accessed 2016.

82 Lightfoot, D. (2007) ìJornada Grasshopper Dataî. Jornada Basin LTER. Available at: http://jornada.nmsu.edu/lter/dataset/49712/view, accessed 2016.

83 Venturoli, F., Felfili, J. M. & Fagg, C. W. (2011) Temporal evaluation of natural regeneration in a semideciduous secondary forest in Pirenopolis, Goias, Brazil. Revista Arvore, 35(3), 473ñ483. https://dx.doi.org/10.1590/S0100-67622011000300010

84 Venturoli, F., Felfili, J. M. & Fagg, C. W. (2011) Temporal evaluation of natural regeneration in a semideciduous secondary forest in Pirenopolis, Goias, Brazil. Revista Arvore, 35(3), 473ñ483. https://dx.doi.org/10.1590/S0100-67622011000300010

85 Venturoli, F., Felfili, J. M. & Fagg, C. W. (2011) Temporal evaluation of natural regeneration in a semideciduous secondary forest in Pirenopolis, Goias, Brazil. Revista Arvore, 35(3), 473ñ483. https://dx.doi.org/10.1590/S0100-67622011000300010

86 Kelt, D. A., Meserve, P. L., GutiÈrrez, J. R., Milstead, W. B. & Previtali, M. A. (2013) Long-term monitoring of mammals in the face of biotic and abiotic influences at a semiarid site in north-central Chile. Ecology, 94, 977. doi:10.1890/12-1811.1.

87 Lightfoot, D. (2011) ìSmall Mammal Exclosure Study (SMES) Vegetation Data from the Chihuahuan Desert Grassland and Shrubland at the Sevilleta National Wildlife Refuge, New Mexico (2006-2009)î. Long Term Ecological Research Network. Available at: http://dx.doi.org/10.6073/pasta/d80d5e2196cd11ef79df23ebe5a77c19, accessed 2016.

88 Carvalho, F., Zocche, J.J. & MendonÁa, R.¡. (2009) Morcegos (Mammalia, Chiroptera) em restinga no municÌpio de Jaguaruna, sul de Santa Catarina, Brasil. Biotemas, 22, 193-201.

89 Myster, R.W. ìFlooded forest plot sampling in Peruî. Luquillo LTER. Available at: http://luq.lternet.edu/data/luqmetadata169, accessed 2016.

90 Norden, N., GarcÌa, H. & Salgado, B. ìLa Planada Forest Dynamics Plotî. The Center for Tropical Forest Science. Smithsonian Tropical Research Institute. Available at: http://www.ctfs.si.edu/site/La+Planada, accessed 2016.

91 Stapp, P. (2013) SGS-LTER Long-Term Monitoring Project: Small Mammals on Trapping Webs on the Central Plains Experimental Range, Nunn, Colorado, USA 1994 -2006, ARS Study Number 118. Environmental Data Initiative. Available at:

http://dx.doi.org/10.6073/pasta/2e311b4e40fea38e573890f473807ba9, accessed 2017.

92 Goheen, J.R., Palmer, T.M., Charles, G.K., Helgen, K.M., Kinyua, S.N., Maclean, J.E., Turner, B.L., Young, H.S. & Pringle, R.M. (2013) Piecewise disassembly of a large-herbivore community across a rainfall gradient: the UHURU experiment. PLoS One, 8, e55192.

93 Kartzinel, T.R., Goheen, J.R., Charles, G.K., DeFranco, E., Maclean, J.E., Otieno, T.O., Palmer, T.M. & Pringle, R.M. (2014) Plant and small?mammal responses to large?herbivore exclusion in an African savanna: five years of the UHURU experiment. Ecology, 95, 787-787.

94 Lightfoot, D. (2013) ìLizard pitfall trap data (LTER-II, LTER-III)î. Jornada Basin LTER. Available at: http://jornada.nmsu.edu/lter/dataset/49821/view, accessed 2016.

95 Monitoring Site 1000 Project, Biodiversity Center, Ministry of Environment of Japan (2015) ìMonitoring site 1000 Alpine research - Surface wandering beetlesî (KOZ07zip, downloaded from http://www.biodic.go.jp/moni1000/findings/data/index.html). Accessed 2016.

96 Monitoring Site 1000 Project, Biodiversity Center, Ministry of Environment of Japan (2014) ìMonitoring site 1000 Village survey - Bird survey data (2005-2012)î (SAT02.zip, downloaded from http://www.biodic.go.jp/moni1000/findings/data/index.html). Accessed 2016.

97 Monitoring Site 1000 Project, Biodiversity Center, Ministry of Environment of Japan (2014) ìMonitoring site 1000 Village survey - Medium and large mammal survey data (2006-2012)î (SAT03zip, downloaded from http://www.biodic.go.jp/moni1000/findings/data/index.html). Accessed 2016.

98 Monitoring Site 1000 Project, Biodiversity Center, Ministry of Environment of Japan (2014) ìMonitoring site 1000 Forest and grassland research - Surface wandering beetles survey dataî (GBDataPackage2014ver1.zip, downloaded from http://www.biodic.go.jp/moni1000/findings/data/index.html). Accessed 2016.

99 Monitoring Site 1000 Project, Biodiversity Center, Ministry of Environment of Japan (2014) ìMonitoring site 1000 Forest and grassland research - Bird survey dataî (BirdData2009-B_ver20120328.zip, downloaded from http://www.biodic.go.jp/moni1000/findings/data/index.html). Accessed 2016.

100 Monitoring Site 1000 Project, Biodiversity Center, Ministry of Environment of Japan (2014) ìMonitoring site 1000 Forest and grassland research - Surface wandering beetles survey dataî (GBDataPackage2014ver1.zip, downloaded from http://www.biodic.go.jp/moni1000/findings/data/index.html). Accessed 2016.

101 Svensson, S. (2006) Species composition and population fluctuations of alpine bird communities during 38 years in the Scandinavian mountain range. Ornis Svecica, 16(4), 183ñ210.

102 Oliver, J. C., Prudic, K. L. & Collinge, S. K. (2006) Boulder County Open Space butterfly diversity and abundance. Ecology, 87, 1066.

103 Monitoring Site 1000 Project, Biodiversity Center, Ministry of Environment of Japan (2015) ìMonitoring site 1000 Alpine research - Butterfly Surveyî (KOZ06.zip, downloaded from http://www.biodic.go.jp/moni1000/findings/data/index.html). Accessed 2016.

104 Monitoring Site 1000 Project, Biodiversity Center, Ministry of Environment of Japan (2015) ìMonitoring site 1000 Alpine research - Butterfly Surveyî (KOZ06.zip, downloaded from http://www.biodic.go.jp/moni1000/findings/data/index.html). Accessed 2016.

105 Monitoring Site 1000 Project, Biodiversity Center, Ministry of Environment of Japan (2015) ìMonitoring site 1000 Alpine research - Bumblebee Surveyî (KOZ08.zip, downloaded from http://www.biodic.go.jp/moni1000/findings/data/index.html). Accessed 2016.

106 Thorn, S., Bässler, C., Bernhardt-Rˆmermann, M., Cadotte, M., Heibl, C., Schäfer, H., Seibold, S. & M¸ller, J. (2016) Changes in the dominant assembly mechanism drive species loss caused by declining resources. Ecology Letters, 19, 163ñ170.

107 Thorn, S., Bässler, C., Gottschalk, T., Hothorn, T., Bussler, H., Raffa, K. & M¸ller, J. (2014) New insights into the consequences of post-windthrow salvage logging revealed by functional structure of saproxylic beetles assemblages. PLoS ONE, 9, e101757.

108 Thorn, S., Werner, S. A., Wohlfahrt, J., Bässler, C., Seibold, S., Quillfeldt, P. & M¸ller, J. (2016) Response of bird assemblages to windstorm and salvage logging - Insights from analyses of functional guild and indicator species. Ecological Indicators, 65, 142ñ148.

109 Thorn, S., Bässler, C., Bernhardt-Rˆmermann, M., Cadotte, M., Heibl, C., Schäfer, H., Seibold, S. & M¸ller, J. (2016) Changes in the dominant assembly mechanism drive species loss caused by declining resources. Ecology Letters, 19, 163ñ170.

110 Thorn, S., Bässler, C., Gottschalk, T., Hothorn, T., Bussler, H., Raffa, K. & M¸ller, J. (2014) New insights into the consequences of post-windthrow salvage logging revealed by functional structure of saproxylic beetles assemblages. PLoS ONE, 9, e101757.

111 Thorn, S., Werner, S. A., Wohlfahrt, J., Bässler, C., Seibold, S., Quillfeldt, P. & M¸ller, J. (2016) Response of bird assemblages to windstorm and salvage logging - Insights from analyses of functional guild and indicator species. Ecological Indicators, 65, 142ñ148.

112 Thorn, S., Bässler, C., Bernhardt-Rˆmermann, M., Cadotte, M., Heibl, C., Schäfer, H., Seibold, S. & M¸ller, J. (2016) Changes in the dominant assembly mechanism drive species loss caused by declining resources. Ecology Letters, 19, 163ñ170.

113 Thorn, S., Bässler, C., Gottschalk, T., Hothorn, T., Bussler, H., Raffa, K. & M¸ller, J. (2014) New insights into the consequences of post-windthrow salvage logging revealed by functional structure of saproxylic beetles assemblages. PLoS ONE, 9, e101757.

114 Thorn, S., Werner, S. A., Wohlfahrt, J., Bässler, C., Seibold, S., Quillfeldt, P. & M¸ller, J. (2016) Response of bird assemblages to windstorm and salvage logging - Insights from analyses of functional guild and indicator species. Ecological Indicators, 65, 142ñ148.

115 Thorn, S., Bässler, C., Bernhardt-Rˆmermann, M., Cadotte, M., Heibl, C., Schäfer, H., Seibold, S. & M¸ller, J. (2016) Changes in the dominant assembly mechanism drive species loss caused by declining resources. Ecology Letters, 19, 163ñ170.

116 Thorn, S., Bässler, C., Gottschalk, T., Hothorn, T., Bussler, H., Raffa, K. & M¸ller, J. (2014) New insights into the consequences of post-windthrow salvage logging revealed by functional structure of saproxylic beetles assemblages. PLoS ONE, 9, e101757.

117 Thorn, S., Werner, S. A., Wohlfahrt, J., Bässler, C., Seibold, S., Quillfeldt, P. & M¸ller, J. (2016) Response of bird assemblages to windstorm and salvage logging - Insights from analyses of functional guild and indicator species. Ecological Indicators, 65, 142ñ148.

118 Thorn, S., Bässler, C., Bernhardt-Rˆmermann, M., Cadotte, M., Heibl, C., Schäfer, H., Seibold, S. & M¸ller, J. (2016) Changes in the dominant assembly mechanism drive species loss caused by declining resources. Ecology Letters, 19, 163ñ170.

119 Thorn, S., Bässler, C., Gottschalk, T., Hothorn, T., Bussler, H., Raffa, K. & M¸ller, J. (2014) New insights into the consequences of post-windthrow salvage logging revealed by functional structure of saproxylic beetles assemblages. PLoS ONE, 9, e101757.

120 Thorn, S., Werner, S. A., Wohlfahrt, J., Bässler, C., Seibold, S., Quillfeldt, P. & M¸ller, J. (2016) Response of bird assemblages to windstorm and salvage logging - Insights from analyses of functional guild and indicator species. Ecological Indicators, 65, 142ñ148.

121 Thorn, S., Bässler, C., Bernhardt-Rˆmermann, M., Cadotte, M., Heibl, C., Schäfer, H., Seibold, S. & M¸ller, J. (2016) Changes in the dominant assembly mechanism drive species loss caused by declining resources. Ecology Letters, 19, 163ñ170.

122 Thorn, S., Bässler, C., Gottschalk, T., Hothorn, T., Bussler, H., Raffa, K. & M¸ller, J. (2014) New insights into the consequences of post-windthrow salvage logging revealed by functional structure of saproxylic beetles assemblages. PLoS ONE, 9, e101757.

123 Thorn, S., Werner, S. A., Wohlfahrt, J., Bässler, C., Seibold, S., Quillfeldt, P. & M¸ller, J. (2016) Response of bird assemblages to windstorm and salvage logging - Insights from analyses of functional guild and indicator species. Ecological Indicators, 65, 142ñ148.

124 Thorn, S., Bässler, C., Bernhardt-Rˆmermann, M., Cadotte, M., Heibl, C., Schäfer, H., Seibold, S. & M¸ller, J. (2016) Changes in the dominant assembly mechanism drive species loss caused by declining resources. Ecology Letters, 19, 163ñ170.

125 Thorn, S., Bässler, C., Gottschalk, T., Hothorn, T., Bussler, H., Raffa, K. & M¸ller, J. (2014) New insights into the consequences of post-windthrow salvage logging revealed by functional structure of saproxylic beetles assemblages. PLoS ONE, 9, e101757.

126 Thorn, S., Werner, S. A., Wohlfahrt, J., Bässler, C., Seibold, S., Quillfeldt, P. & M¸ller, J. (2016) Response of bird assemblages to windstorm and salvage logging - Insights from analyses of functional guild and indicator species. Ecological Indicators, 65, 142ñ148.

127 Thorn, S., Bässler, C., Bernhardt-Rˆmermann, M., Cadotte, M., Heibl, C., Schäfer, H., Seibold, S. & M¸ller, J. (2016) Changes in the dominant assembly mechanism drive species loss caused by declining resources. Ecology Letters, 19, 163ñ170.

128 Thorn, S., Bässler, C., Gottschalk, T., Hothorn, T., Bussler, H., Raffa, K. & M¸ller, J. (2014) New insights into the consequences of post-windthrow salvage logging revealed by functional structure of saproxylic beetles assemblages. PLoS ONE, 9, e101757.

129 Thorn, S., Werner, S. A., Wohlfahrt, J., Bässler, C., Seibold, S., Quillfeldt, P. & M¸ller, J. (2016) Response of bird assemblages to windstorm and salvage logging - Insights from analyses of functional guild and indicator species. Ecological Indicators, 65, 142ñ148.

130 Lee, C.M., Kim, S.-S. & Kwon, T.-S. (2016) Butterfly fauna in Mount Gariwang-san, Korea. Journal of Asia-Pacific Biodiversity, 9, 198-204.

131 Rocha, R. (2017) Tropical forest fragmentation: effects on the spatio-temporal dynamics of its bat communities. PhD Thesis, University of Lisbon, Lisbon, Portugal.

132 Rocha, R., López-Baucells, A., Farneda, F.Z., Groenenberg, M., Bobrowiec, P.E.D., Cabeza, M., Palmeirim, J.M. & Meyer, C.F.J. (2017) Consequences of a large-scale fragmentation experiment for Neotropical bats: disentangling the relative importance of local and landscape-scale effects. Landscape Ecology, 32, 31-45.

133 Sampaio, E.M., Kalko, E.K., Bernard, E., RodrÌguez-Herrera, B. & Handley, C.O. (2003) A biodiversity assessment of bats (Chiroptera) in a tropical lowland rainforest of Central Amazonia, including methodological and conservation considerations. Studies on Neotropical fauna and environment, 38, 17-31.

134 Farneda, F.Z., Rocha, R., López-Baucells, A., Sampaio, E.M., Palmeirim, J.M., Bobrowiec, P.E., Grelle, C.E. & Meyer, C.F. (2018) Functional recovery of Amazonian bat assemblages following secondary forest succession. Biological Conservation, 218, 192-199.

135 Rocha, R., Ovaskainen, O., López-Baucells, A., Farneda, F.Z., Sampaio, E.M., Bobrowiec, P.E.D., Cabeza, M., Palmeirim, J.M. & Meyer, C.F.J. (2018) Secondary

forest regeneration benefits old-growth specialist bats in a fragmented tropical landscape. Scientific Reports, 8, 3819.

Appendix D Chapter 4 Supplementary Figures

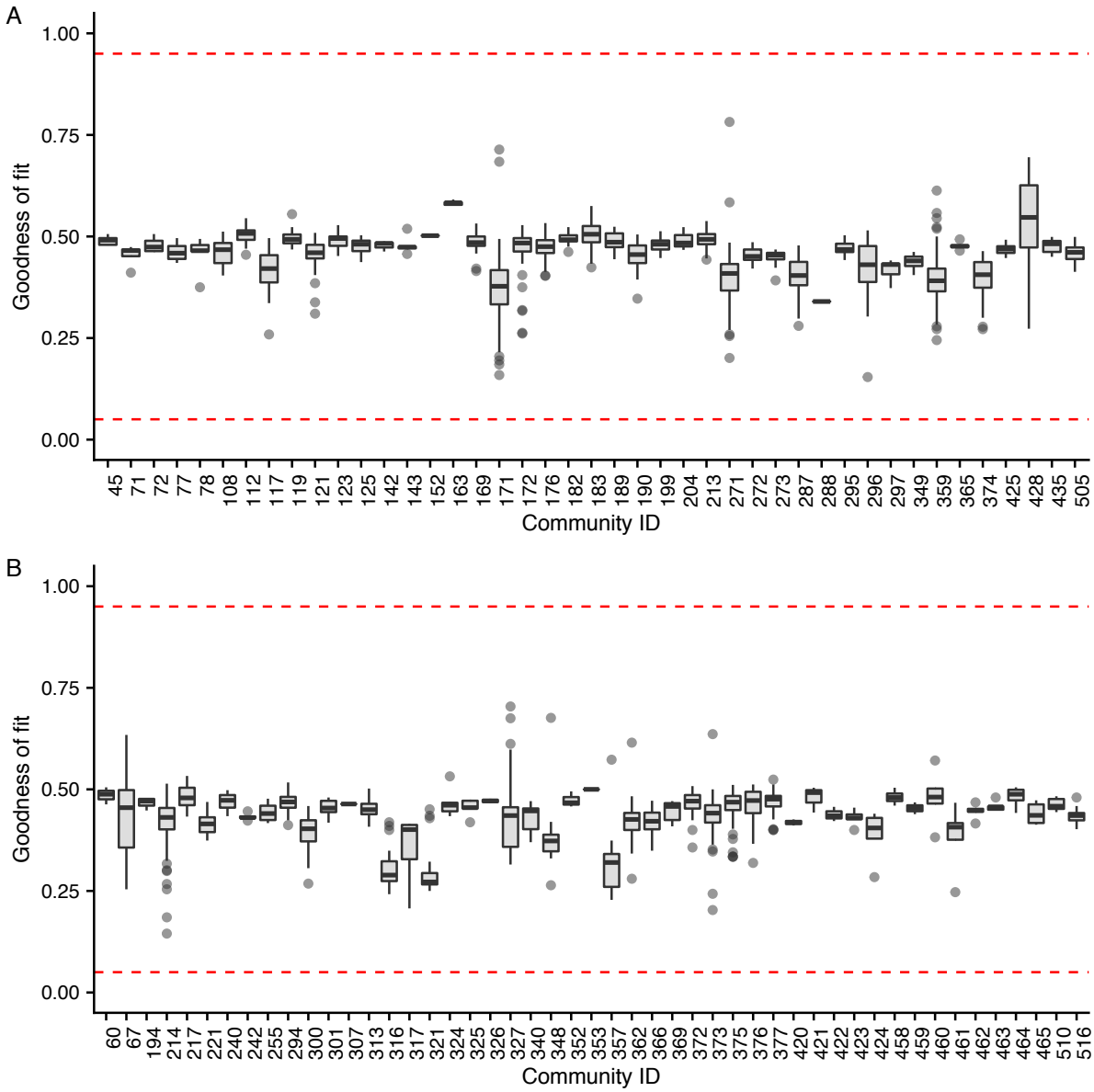

Figure D-1: The goodness of fit of species abundance distribution models fitted to BioTIME community data. Plots showing the goodness-of-fit of Poisson lognormal species abundance distribution models fitted to monthly (mm-yyyy) community assemblage data from the BioTIME database for the marine (A) and terrestrial (B) realm. The boxplots show the spread of goodness-of-fit values obtained for all monthly SADs fitted within each BioTIME study (community) ID. Goodness-of-fit is based on the log-likelihood model deviance between the estimated model and the empirical data compared to simulated data from 1,000 parametric bootstraps. Values below 0.5 and above 0.95 indicate lack of fit.

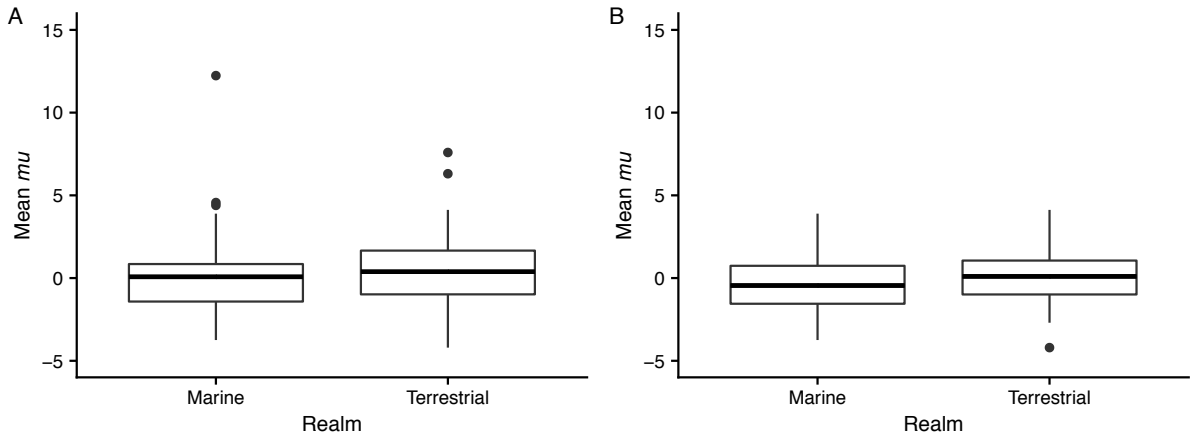

Figure D-2: Boxplots of the mean of community Species Abundance Distributions in the marine and terrestrial realm. Boxplots showing the distribution of the mean (mu) parameter of SAD distributions fitted to BioTIME communities for the marine terrestrial realm. No significant difference was found in mu between realms either before (A) or after (B) the removal of outliers. The central line shows the mean rather than the median.

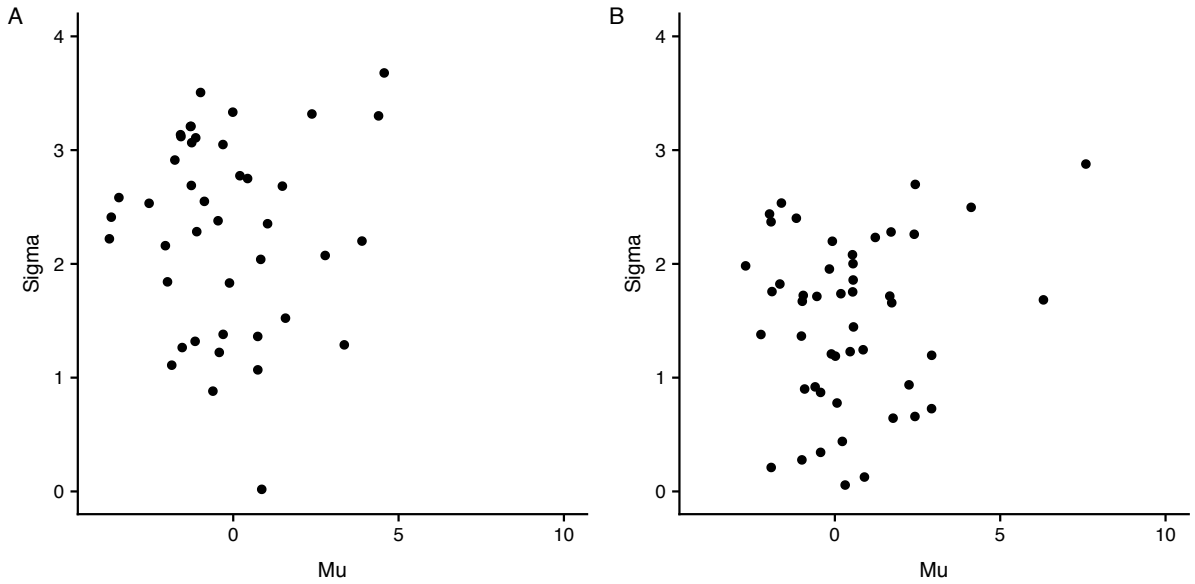

Figure D-3: Relationship between the average mu and sigma parameters for each BioTIME community Species Abundance Distribution across realms. Scatter plots showing the average mean (mu) and standard deviation (sigma) of SAD distributions fitted to BioTIME communities in the marine (A) and terrestrial (B) realm. No correlation was present between mu and sigma in either realm.

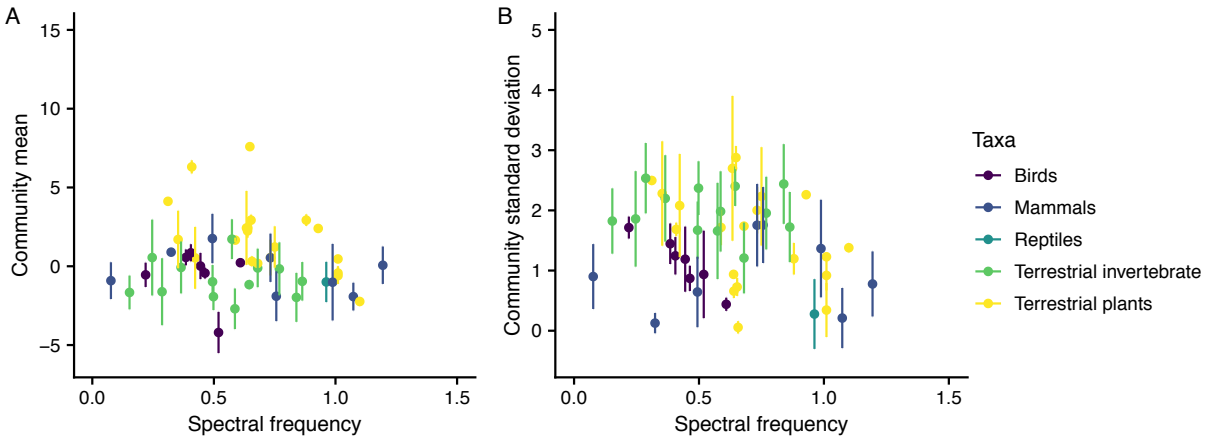

Figure D-4: Species Abundance Distributions along gradients of precipitation temporal autocorrelation. The average mean (mu parameter; A) and evenness (sigma parameter; B) with associated error (sd) of species abundances for each community, plotted against the spectral frequency of precipitation for each community in the terrestrial. SADs were calculated for each month-year combination of a community's time series within 2000-2013. Spectral frequencies were calculated for precipitation for the 2000-2013 time series for the corresponding coordinates of each community's abundance measurements. Communities are grouped by their BioTIME associated taxa.

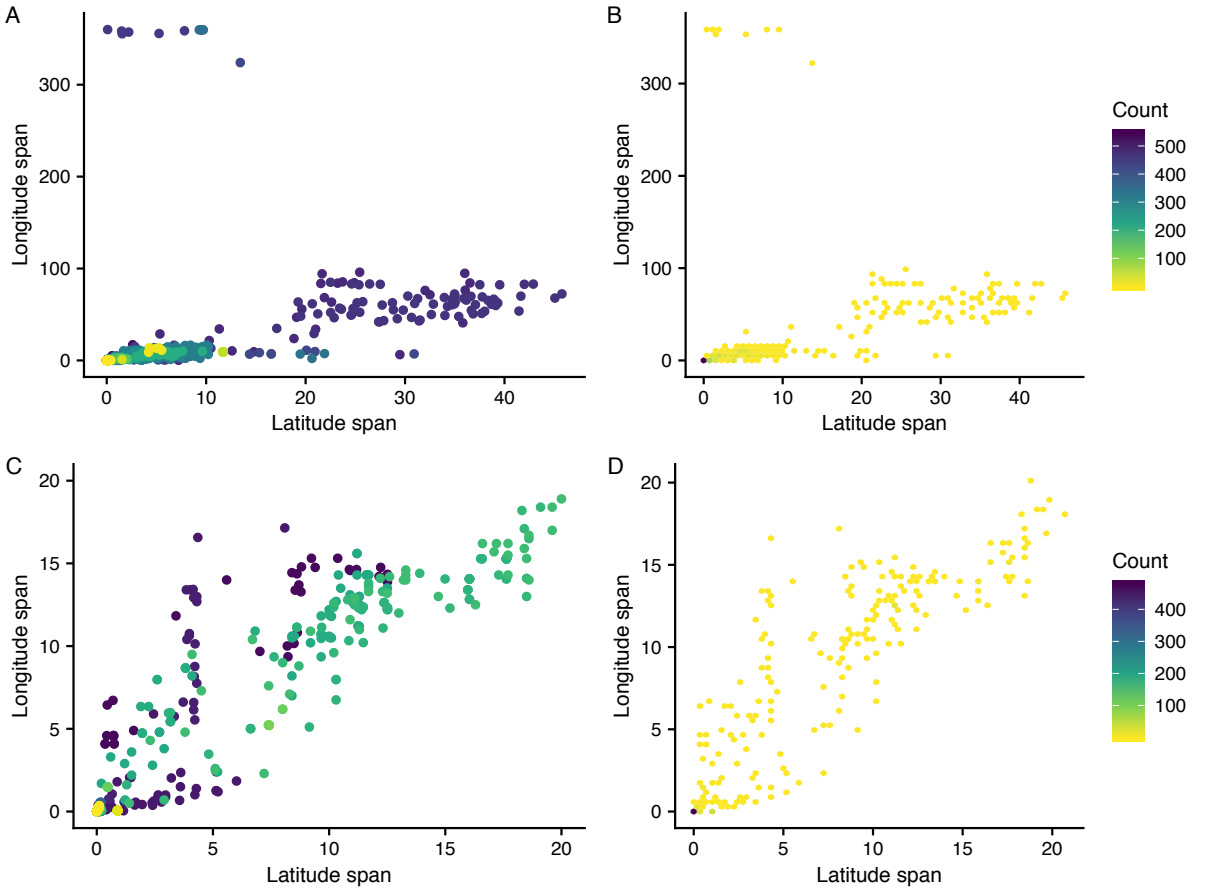

Figure D-5: Differences in the spatial extent of abundance observations within Species Abundance Distributions in the marine and terrestrial realm. Scatter plots showing the spatial extent of abundance observations within SADs in the marine (A,B) terrestrial (C,D) realm. Each pixel in A and C shows the difference between the minimum and maximum latitude and longitude of abundance observations within SADs fitted to

BioTIME study ID mm-yyyy combinations. The colours in A and C show the different study IDs, however given the volume (43 for Marine (A), 49 for terrestrial (C)) it wasn't possible to fit a colour scale that distinguished each of them, or feasible to include the legend. B and D show the same information as a density plot. Plots B and D show the density of fitted SADs within different spatial extents out of a total of 1,171 SADs for the marine realm and 877 for the terrestrial realm. 60 hexagonal bins were used in the horizontal and vertical directions to plot the data.

Table D-1: Proportion of SADs fitted covering different spatial extents. Proportion of SADs fitted to BioTIME study ID and mm-yyyy combinations with less than 1° or more than 10° between the minimum and maximum latitude and longitudes of abundance observations. Proportions are a percentage of 1,171 and 877 SADs fitted for the marine and terrestrial realms respectively.

	Latitude ≤ 1°	Longitude ≤ 1°	Latitude ≥ 10°	Longitude ≥ 10°
Marine	52.8%	52.6%	10.5%	15.4%
Terrestrial	66.7%	66.1%	17.8%	21.8%